DISSERTATION

PLURIPOTENCY FACTORS AND MIRNAS IN HUMAN OVARIAN CANCER CELLS AND THEIR SECRETED EXOSOMES REGULATE GENE EXPRESSION AND PHENOTYPE

Submitted by

Vanessa Ann Enriquez

Graduate Degree Program in Cell and Molecular Biology

In partial fulfillment of the requirements

For the Degree of Doctor of Philosophy

Colorado State University

Fort Collins, Colorado

Summer 2014

Doctoral Committee:

Advisor: Gerrit J. Bouma
Co-Advisor: Quinton A. Winger

Susan M. Bailey
Dawn L. Duval

ABSTRACT

PLURIPOTENCY FACTORS AND MIRNAS FROM HUMAN OVARIAN CANCER CELLS AND THEIR SECRETED EXOSOMES REGULATE GENE EXPRESSION AND PHENOTYPE

Ovarian cancer is the fifth most deadly cancer among women in the United States and the most lethal gynecological malignancy in the world. Recent studies reveal that human tumor cells release cell-secreted vesicles called exosomes. Exosomes are endosome-derived vesicles containing bioactive materials, including RNAs and miRNAs that can be detected in body fluids. Importantly, pluripotency factor LIN28, a regulator of *let-7* miRNAs, is present in ovarian cancer cells. High LIN28A and low *let-7* miRNA levels are associated with aggressive IGROV1 human ovarian cancer cells (Piskounova et al., 2011) so we compared this to low LIN28A and high *let-7* miRNA levels in less aggressive OV420 human ovarian cancer cells. Moreover, *let-7b, let-7c, let-7g*, and *let-7i* miRNA signatures were also present in their secreted exosomes. We hypothesized that ovarian cancer cell-secreted exosomes are taken up by target cells and induce changes in gene expression and cell behavior. Our data revealed that IGROV1 secreted exosomes taken up by HEK293 cells lead to significantly higher LIN28A mRNA levels, but not LIN28A protein levels and did not significantly change LIN28B mRNA or protein levels. However, IGROV1 exosome exposure to HEK293 cells did significantly increase invasion and migration. In addition, various genes involved in epithelial-mesenchymal transition, including *TIMP1* (25-fold higher), *NOTCH1* (11-fold-higher), *SNAI1 (SNAIL)*

(7-fold higher), *CDH1* (6-fold higher), *(MMP9* (4-fold higher), and *ZEB1* (3-fold higher), were significantly higher in HEK293 cells following uptake of IGROV1 secreted exosomes. We also postulated that ovarian cancer cell-secreted exosomes contain a distinct RNA signature capable of inducing phenotypic changes in target cells, as well as distinguishing aggressive, advanced ovarian exosomes from less aggressive ovarian exosomes. Since IGROV1 cells are a more aggressive epithelial ovarian cancer cell line, while OV420 cells are a less aggressive cell line, we performed RNAseq transcriptome analysis on exosomes from IGROV1 cells and exosomes from OV420 cells. The results yielded 312 differentially expressed RNAs. Future studies will allow us to detect the RNAs present in exosomes from urine in individuals with early stage versus late stage ovarian cancer. This may enable investigators to distinguish a poor prognosis group from a good prognosis group leading to a potential biomarker for ovarian cancer detection. Data from this study is important for elucidating the role ovarian cancer cell-secreted exosomes have on early metastasis and tumor progression, an area in ovarian cancer biology in critical need of advancement.

ACKNOWLEDGEMENTS

“If I have seen farther than others, it is because I stood on the shoulders of giants.”

Sir Isaac Newton

First and foremost, I would like to thank my advisor Dr. Gerrit J. Bouma for his constant guidance, patience, and mentorship. I remember meeting you at an ARBL tour (before I had even picked a lab) and thought to myself, “Wow, he seems so down to earth and smart. If I ever get to work with this person, I would be not only be gaining and extremely accomplished education, but I would be exceptionally fortunate to have such an incredible mentor.” I never would have thought that I would get the chance to work with you and feel very blessed to have such an unbelievable advisor. Jerry, you have shown me how to be the scientist I am today and I can only hope to one day inspire others in the lessons I’ve learned from you as I continue discovering my role in the scientific community.

I would also like to thank my co-advisor Dr. Quinton Winger for sharing his passion for placentation development with me and allowing me to gain some experience in this field. Also, I would like to thank you for showing me the importance for experimental design and always willing to speak with me about interpreting my data. To Drs. Dawn Duval and Susan Bailey, I would especially like to thank you for not only being wonderful insightful committee members, but for allowing me to work in your labs during my rotations when I was trying to find my “lab home”. I not only learned valuable

techniques from you and your students, but also was able to gain personal mentorship from you both and how to function as a woman in science. Your advice was invaluable and I will treasure your teachings for the rest of my life.

I am thankful for the McNair Scholars program that introduced me to the idea that I could pursue a higher education degree. This program sparked my interest in research and allowed me to work with my first mentor, Dr. Jodi Huggenvik who guided me toward a passion for scientific research. I am also incredibly thankful to the future Dr. Aspen D'Costa who was my nurse, friend, and supporter during my undergraduate degree. You will always be my lifelong friend! Mrs. Margaret Cech is also a person I would like to acknowledge, as she became an outside personal mentor who was my confidant. I would also like to thank the funding sources that have allowed me to continue my PhD dissertation work here at Colorado State University (CSU). I am thankful for the Bridge to the Doctorate Fellowship (Award #: 0603176) for funding my first two years in graduate school, the CSU CVMBS CRC grant, CSU Cancer Supercluster 2011, and the ACS-IRG #57-001-50 from the American Cancer Society.

I would like to extend my humblest appreciation toward my friends at ARBL, the place that was my home so for many years: Dr. Jillian Delehoy (formerly Guttormsen) whom was my close colleague during the first couple years of my PhD for showing me how to run a successful lab, Dr. Juliano C. da Silveria for showing me the ropes in the lab and always willing to talk about experiments and science, Dr. Dilka Murtazina for helping me through frustrating days and always being a listening ear and Brenda Martin for always

reassuring me that I could finish and do well in my future endeavors. I would like to extend a special thank you to the future Dr. Ellie Cleys, Lisa Nulton, and future Dr. Kathleen Eddy for being great lab mates and friends. You girls got me through days when I felt hopeless and alone. I could always depend on your to be a shoulder to cry on, sharing a sarcastic remark with me to make me smile, always reminding me “we can get through this”, celebrating the times when lab results worked or (more often then I would like to admit) telling me “you’ll figure it out” when my results didn’t work. I will always remember our days in the office/lab where you listened to me vent, gave me great advice and how you were always there to bounce ideas off. I am forever grateful for your friendship.

Lastly, it is with the deepest gratitude that I thank my entire familia! I can’t even begin to thank you for all that you’ve done and continue to do. You have all given me the strength to keep pushing forward, love that carried me through my toughest hours, and support and prayers to keep on fighting. You have believed in me accomplishing something great since I was a young girl. Mom and Dad, you have sacrificed so much to give your children an education. You always told me, “the key to the world lies in a degree” and I guess I took that literally. There were days when I felt broken down and your kind words lifted me up and reminded me that no matter what happened, you were proud of me. You both are an inspiration to me. God bless you for having the strength to put up with me and having the unwavering love and support, which allowed me to follow my dreams! In a million years with a million words I would never be able to express my gratitude to you; just know, that I love you from the depths of my heart and soul and am

forever grateful you are my parents! To my siblings, you have each played a significant part in helping me reach my goals. Victor, I remember how proud you looked when you saw me graduate with my Bachelors. You told me to fight for my dreams and I haven't given up yet, nor will I ever. I love you brother! Jessica, you were always around to listen my frustrations and give me hope and encouragement and for that I will be forever indebted to you. Your drive and resilience is inspirational and I continue to strive for the best because I see you doing this everyday. I love you little sister and know you will go on and accomplish great things! Christopher, my little big brother, you saved my life when you moved to Colorado. You took care of me when I didn't take care of myself. I remember when you would bring me lunch, sit with me, and watch me eat because you knew I was too busy and would "forget". You taught me to relax and take time for myself during a time when I gave everything to my work. I love you Cree! To my love, Sterling you have become my family away from home. You have seen me struggle through the toughest times (and still you stuck around), you encouraged me when all seemed unattainable or impossible to reach, and most importantly you have given me something to fight for, an additional family and a future here in Colorado where we can begin to set a foundation. I love you more with each passing day and am incredibly thankful and blessed to have such a wonderful man to share my adventures with. I love you Sterling!

DEDICATION

In dedication to my incredible family who never stopped believing in me and who was always there to pick me up. I am eternally thankful and blessed to have you in my life. Thank you for everything Enriquez, Neira and Krone Family, especially Cynthia (Mom), Victor (Dad), Victor, Jessica, Christopher, Kai, Kaden, Kole, and Sterling.

“I can do all things through Christ which strengthens me.” Philippians 4:13

TABLE OF CONTENTS

LIST OF TABLES

LIST OF FIGURES

LIST OF APPENDICIES

CHAPTER I: INTRODUCTION

Ovarian cancer is the fifth most deadly cancer among women in U.S. and is the most lethal gynecological malignancy in the Western World. Mostly diagnosed at late stages (III, IV), it often recurs and no treatment beyond palliative care is available. Very little is known about the molecular network and cellular communication that exists in late stage ovarian cancer cells that leads to metastasis. Therefore, our long-term goal was to discover novel molecular networks that regulate ovarian cancer metastasis, which can aid in discovering new treatments for recurrent cancer and lead to identification of potential diagnostic markers.

Tumor cells are known to release small cell-secreted vesicles called exosomes (Valadi et al., 2007; Al-Nedawi et al., 2008; Skog et al., 2008), which contain bioactive materials (including mRNAs and miRNAs) that can be detected in blood and urine (Taylor and Gercel-Taylor, 2008; Weber et al., 2010). Recent studies reveal that human ovarian cancer cells contain distinct miRNA signatures (Iorio et al., 2007) as well as miRNA signatures in tumor exosomes of ovarian cancer (Taylor and Gercel-Taylor, 2008). miRNAs are evolutionally conserved short non-coding RNAs capable of regulating post-translation by binding to 3'UTRs of mRNAs. Upon binding, mRNA is cleaved and degraded or silenced (Guo et al., 2010). It is important to study miRNAs and their targets because they are involved in regulating all aspects of the hallmarks of cancer (Ruan, Fang and Ouyang, 2009). A particular family of miRNAs (*let-7s*) is a regulator of LIN28, an RNA binding protein and a pluripotency factor, and is a well-conserved tumor

suppressor. As cancer progresses, LIN28A increases and the *let-7* tumor suppressor is lost. When *let-7* intranasal *let-7* is administered to mice models of lung cancer, tumor growth reduces (Esquela-Kerscher et al., 2008). Intriguingly, high LIN28A levels are associated with advanced human malignancies (Viswanathan et al., 2009). Stem cell factor LIN28 is a regulator of miRNA function expressed in cancer tumors (Zhong et al., 2010; Peng et al., 2010). LIN28A negatively regulates mature *let-7* miRNA biogenesis, thereby preventing cell differentiation; but the role of LIN28A and *let-7* in exosomes from ovarian cancer cells is not understood. Since miRNAs have been identified as regulators of cancer cell functions (Calin et al., 2002), elucidating critical miRNAs and their target genes will provide new information regarding the processes that lead to ovarian cancer development and progression.

My PhD dissertation presents new data that: 1) identified the presence of pluripotency factors and miRNAs in more aggressive ovarian cancer cells versus less aggressive ovarian cancer cells, 2) determined the presence of *LIN28* and *let-7* miRNAs in aggressive and less aggressive ovarian cancer cell-secreted exosomes, and confirmed that exosomes secreted from high LIN28A expressing cells taken up by HEK293 recipient cells can induce changes in gene expression and cell phenotype, and 3) identified RNA signatures in ovarian cancer cell-secreted exosomes from high LIN28A expressing, aggressive cancer cells (IGROV1) versus low LIN28A expressing, less aggressive cancer cells (OV420). These RNA signatures could potentially serve as biomarkers to detect ovarian cancer at early stages. Furthermore, these exosomal RNA signatures secreted from high LIN28 expressing cells could be assessed in urinary

exosomes to distinguish stage I-II and stage III-IV ovarian cancer patients, respectively. Ultimately, such information may result in better treatment of ovarian cancer in patients with recurrent and/or metastatic disease, and potentially aid in identification of an ovarian cancer biomarker.

CHAPTER II: REVIEW OF LITERATURE

BACKGROUND AND SIGNIFICANCE

Ovarian cancer is the fifth most deadly cancer among women in the nation and the most lethal gynecological malignancy among women in the United States, primarily due to the lack of early detection markers, vague symptoms, and the persistence of dormant, drug-resistant cancer cells that contribute to late diagnoses. Approximately 75% are diagnosed in late stages (III, IV), with a 5-year survival rate of less than 20% (Zhang et al., 2008c). The incidence and mortality rates for women in the United States with ovarian cancer has not changed over the past few decades (Altekruse et al., 2010) due to the inability to detect ovarian cancer at an early stage. Early disease is often overlooked; leading to widely disseminated peritoneal disease and increased risk of relapse even after post treatment with chemotherapy and cytoreductive surgery (du Bois et al., 2003). Clinical treatment of patients with recurring ovarian cancer now focuses on prolonging life with the least amount of pain via analgesics and through toxicity management of drug-based therapy (Armstrong, 2002).

Since 90% of all ovarian cancer tumors arise from the ovarian surface epithelium that covers the surface of the ovary (Nicosia and Johnson, 1984; Nicosia and Nicosia, 1988; Auersperg et al., 1988; Fox, 1993), epithelial ovarian cancer (EOC) is the most aggressive and deadly form of ovarian cancer. LIN28A, a negative regulator of *let-7* miRNAs, is high in advanced human malignancies (Viswanathan et al., 2009), but it is unknown if LIN28 regulatory miRNAs are regulated are also elevated in EOCs. More

importantly, the way in which genes and miRNAs communicate their message from a tumor cell to a target cell is unclear. It is known that exosomes contain bioactive materials (including mRNAs and miRNAs) are present in blood and urine, (Taylor and Gercel-Taylor, 2008; and Weber et al., 2010) transferring their contents from one cell to another. Interestingly, tumor cells release exosomes containing tumorigenic factors such as mRNAs and miRNAs in ovarian cancer (Taylor and Gercel-Taylor, 2008). Therefore, current research efforts are centered on identifying the molecular factors contained in secreted exosomes from tumors to assess their potential metastatic effect. These studies can lead to a better understanding of the function of exosomes and miRNAs in advanced ovarian cancer and potentially lead to discovery of novel molecular factors that influence metastatic disease development.

OVARIAN BIOLOGY

FEMALE REPRODUCTIVE PHYSIOLOGY

Sex determination and fetal ovarian development

During embryogenesis, individual somatic cells respond to highly evolutionary conserved bone morphogenetic protein 4 signals, which are involved in early embryonic development, leading to the downstream activation of Sma and Mad related proteins (SMAD) that are mediators of transcriptional activation (Fujiwara, Ying and Hogan, 2001; Ying et al., 2000; Shi and Massague, 2003; Massague et al., 2005). SMADs activate PR domain zinc finger protein 1, also known as BLIMP1, which is a master regulator of expression in a developing embryo resulting in the specification of primordial germ cells (PGCs), which form all gametes, (sperm or oocytes) (Durcova-

Hills et al., 2008). PGCs develop from the somatic cells of the proximal epiblast within the inner cell mass (ICM) that give rise to the structures of the fetus. PGCs then migrate to the genital ridges of the bipotential gonad at approximately week 6 in human development (Coticchio, Albertini, De Santis, 2013). There are two main processes that take place for determining the sex of individuals after PCG migration, primary sex determination and phenotypic sex development.

In primary sex determination, germ cells do not determine gonadal sex (Gilbert, 2000). Gonadal development is dependent on signals the biopotential gonads receive from the surrounding environment. In female (XX) individuals, R-spondin-1 protein (RSPO1), a protein involved in development of early gonads, is activated and leads to upregulation of wingless-type MMTV integration site family member 4 (WNT4), which is required in sex development to regulate cell fate and patterning during embryogenesis. When WNT4 signals bind to Frizzled receptors, β-catenin, a cadherin-associated protein, is de-phosphorylated leading to transcription of downstream targets that are necessary to enable fetal ovarian development making WNT4 and β-catenin essential for fetal gonad development (Boyer et al., 2010). If RSPO1 is lost, this causes the XX individual to undergo gonadal sex reversal (Tomizuka et al., 2008; Chassot et al., 2011) indicating the importance of RSPO1 in female gonadal development and the importance of activating downstream signals for gonadal development.

Elegant experiments provided evidence for the role of hormones in phenotypic sex development by use of rabbits (Jost, 1947). Gonads were removed, leading to the

maintenance of the internal Müllerian duct and female external genitalia in both XX and XY rabbits. This demonstrated that a signal from the gonads was necessary for Wolffian duct formation. Next, the gonads of XX and XY rabbits were removed and testosterone, a steroid hormone, was added via implants. Female and male rabbits retained the Müllerian duct as well as the Wolffian ducts and male external genitalia. This demonstrated the Wolffian duct required testosterone and a signal from the male gonads to cause the Müllerian duct to regress. The last experiment Jost performed was dissection and removal of the gonads, but testis fragments were added back to females. Females developed only Wolffian ducts as well as external male genitalia, meaning some factor from the testis inhibited Müllerian duct progression. These experiments were integral on understanding male and female phenotypic development. The female internal reproductive tract is formed by the mesonephros, which is a tissue that borders the fetal ovary. The Müllerian duct will differentiate into the fallopian tubes, uterus and the upper one-third portion of the vagina.

Oogenesis, follicle development, and hormonal regulation

Oogenesis begins in the early stages of germ cell development. PCG migration occurs and germ cells begin to proliferate and undergo mitotic divisions with incomplete cytokinesis between the 4^{th} and 5^{th} week in human development (Pepling and Spradling, 1998; Pepling and Spradling, 2001; Pepling, 2006; Tingen, Kim and Woodruff, 2009). Once the PGCs reach the biopotential gonad, they differentiate into oogonia and continue mitotic divisions. Only a finite number of oogonia are made before birth (approximately 7 million), but directly prior to parturition there is massive germ cell

loss leaving only approximately 2 million primary oocytes at birth. Recently the idea of finite number of oocytes has been challenged by evidence that germline stem cells exist in the ovary (Johnson et al., 2004; Johnson et at, 2005; Eggan et al., 2006), but more evidence is needed to support the presence or function of germline stem cells.

After ovarian determination occurs, oogonia enter meiosis I at approximately 6 weeks of development; at birth primary oocytes are arrested in prophase of meiosis I. This happens through cell-cell communication between cumulus cells that surround the primary oocyte and granulosa cells via gap junctions (Dekel et al., 1981; Wassarman and Albertini, 1994; Chaube, 2001; Webb et al., 2002). Cyclic AMP (cAMP), a secondary messenger, is activated to mediate signals sustaining the oocyte arrested in meiosis I (Vaccari et al., 2008). Increases in cAMP within the oocyte lead to activation of protein kinase A (PKA) enzyme to phosphorylate two CDKI regulators Wee1/Myt1 kinase (Standford and Rudermand, 2005) and Cdc25B phosphatase (Pirino, Wescott and Donovan, 2009) to repress mitosis-promoting factor (MPF), leading to arrest of the oocyte (Tripathi et al., 2010). Following the luteinizing hormone (LH) surge during ovulation of the oocyte, there is an asymmetric distribution of cytoplasm during metaphase I leading to the generation of a small polar body. The first polar body will be extruded while the secondary oocyte will complete meiosis I at ovulation. After ovulation occurs, the oocyte will arrest in metaphase of meiosis II. The mechanism by which the oocyte becomes arrested revolves around stabilizing MPF by triggering the Mos/mitogen-activated protein kinase pathway (Mos/MAPK) (Yoshida, Mita and Yamashita, 2000). The Mos/MAPK pathway is activated during vertebrate oocyte

maturation, by activating cytostatic factors (Tripathi et al., 2010) to arrest ovulated oocytes in metaphase of meiosis II.

Before folliculogenesis can occur, oogonia cluster together to form germ cell cysts. These form due to the incomplete cytokinesis in mitosis allowing daughter cells to be connected by intercellular bridges (Pepling and Spradling, 1998; Pepling and Spradling, 2001; Pepling, 2006; Tingen et al., 2009). Somatic cells communicate with the cysts leading to the degradation of the intercellular bridges; FIGα, a bHLH transcription factor associated with postnatal oocyte-specific gene expression, signals are activated from the oocyte to recruit flattened pre-granulosa cells to surround the oocyte (Soyal et al., 2000) forming a primordial follicle. The primordial follicle arrests at prophase of meiosis I prior to birth and stays in this phase until ovulation. The pre-granulosa cells that surround the oocyte become cuboidal, (Peters et al., 1973; Cran and Moor, 1980; Hirshfield, 1991; Rajah et al. 1992) initiating the switch from primordial follicle to a primary follicle. The primary follicle also begins to form the zona pellucida by activating zona glycoprotein genes ZP1, ZP2 and ZP3, which function as receptors for spermatozoa (Hinsch and Hinsch, 1999). The primary oocyte secretes GDF-9, a TGFβ growth factor, and initiates the growth of cuboidal granulosa cells (Nilsson and Skinner, 2002). The secondary follicle is formed and theca cells begin to surround the follicle. In a tertiary follicle, theca interna and theca externa surround the granulosa cells and the antrum begins to form by the movement of granulosa cells (Rodgers and Irving-Rodgers, 2010). The theca interna have receptors for LH, a hormone that triggers ovulation, and produce testosterone that signals to the granulosa cells. The granulosa

cells produce CYP19 aromatase, a p450 aromatase that is involved in estrogen biosynthesis, to convert testosterone into estrogen. The cells that surround the oocyte are now called cumulus cells, which are differentiated granulosa cells. Starting at puberty, following an LH surge, the oocyte surrounded by cumulus cells ovulates by breaking through the ovarian surface epithelial layer into the fallopian tube, completes meiosis I, and arrests in metaphase of meiosis II. As LH levels increase, the follicle secretes luteolytic hormone prostaglandin F2alpha (PGF2α), which induces contraction of the theca externa, causing pressure on the follicle and aiding in rupture of the oocyte at the LH surge. After ovulation, the remnants of the follicle form the corpus luteum (CL), which secretes estrogen and progesterone to inhibit gonadotropin-releasing hormone (GnRH) from the hypothalamus and secretion of LH and follicle stimulating hormone (FSH) from the pituitary. This leads to thickening of the lining of the uterus, which is essential for proper implantation. If pregnancy does not occur, the corpus luteum will regress into a corpus albican and luteolysis occurs.

Hormonal regulation of the female reproductive system is summarized in Figure 1. Briefly, the hypothalamus secretes GnRH, which is responsible for the synthesis and secretion of FSH and LH from the anterior pituitary. FSH signals to the granulosa cells enabling production of estradiol, while LH acts on the theca cells to produce testosterone, which then acts on granulosa cells. Granulosa cells convert testosterone to estrogen using CYP19 aromatase leading to follicular growth. As the follicles grow, they begin to secrete estrogens leading to a negative feedback to the anterior pituitary

and to the hypothalamus. Granulosa cells also secrete inhibin, which acts on the anterior pituitary to inhibit secretion of FSH.

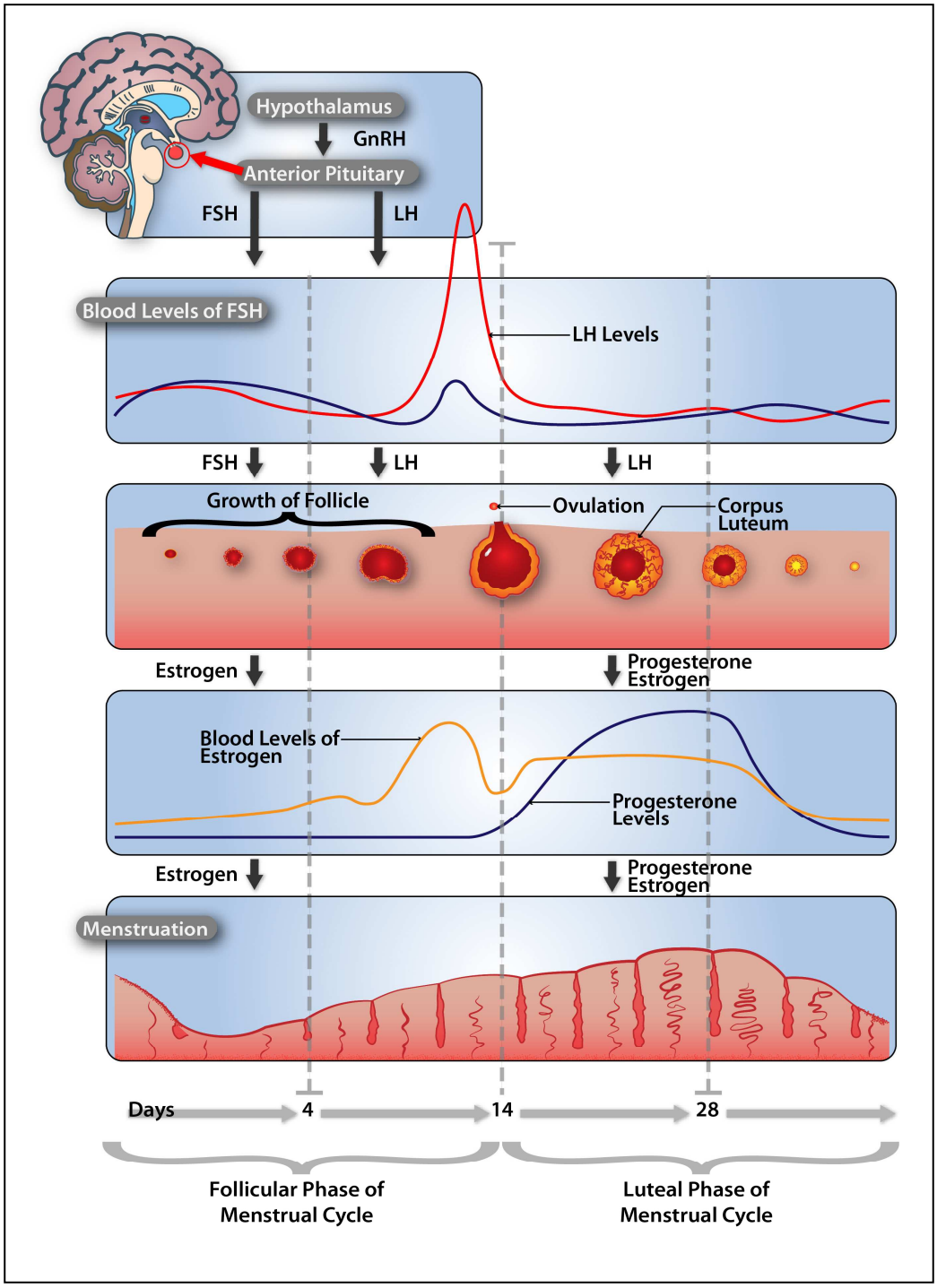

Figure 1: The menstrual cycle and hormonal regulation

High levels of estrogen in the late follicular phase create a positive feedback to the hypothalamus and pituitary leading to upregulation of LH. This leads to the LH surge and the oocyte completes meiosis I, ovulates and formation of the corpus luteum occurs, which then secretes progesterone and estrogen.

In the luteal phase (days 14-28 of menses), LH levels fall because progesterone and estrogen from the corpus luteum negatively feedback to the hypothalamus and anterior pituitary. FSH level also drop because inhibin is secreted from the corpus luteum. If there is no pregnancy, corpus luteum regresses and progesterone and estrogen levels will continue to fall leading to the generation of new follicles and continuation of the menstrual cycle. Understanding the normal physiology of ovarian development can aid in elucidating the aberrant molecular mechanisms that lead to abnormal ovarian phenotypes and ultimately cancer.

CANCER BIOLOGY

HISTORY OF CANCER DEVELOPMENT "HALLMARKS OF CANCER"

Cancer is uncontrolled proliferation of cells in the body. There are various types of cancer with specific mechanisms, but there are similar events that are indicative of all neoplasia. There are six biological capabilities that are acquired during tumorigenesis leading to an additional four transformations that must occur to produce a solid tumor (Hanahan and Weinberg, 2011). The necessary steps are as follows: 1) the ability to sustain proliferative signals, 2) evasion of growth suppressors, 3) faculty to avoid immune destruction, 4) resist cell death, 5) ability to replicate indefinitely leading to

immortality, 6) survival even with genomic instability and mutations, 7) activation of invasion and metastasis, 8) induction of angiogenesis, 9) capacity to promote inflammation, and 10) capability to deregulate cellular energetics.

Tumors must be able to sustain proliferation signals, evade growth suppressors, avoid immune destruction and resist cell death. They have the ability to reduce their requirements for growth factors unlike normal cells, which need specific growth factors to grow and divide. The reason tumor cells can survive in low serum is because they: 1) acquire mutations in cellular genes that can stimulate inappropriate production of growth factors and may even be able to generate their own; 2) mutate growth factor receptor genes to stimulate deregulation either in favor of constitutive activation or competitive inhibition depending on the target; 3) deregulate cellular growth signal transduction pathways to produce growth factors with or without signal or receptor activation.

The first adaptation of cancerous cells is that cells begins to acquire altered morphology. Normal cells maintain contact inhibition, meaning they will stop growing once they have come in contact with another cell by increasing signals that arrest cell growth. When cancer tumor cells come in contact with another cell they begin rounding, and pile up to create colonies in a process called focus formation. Another morphological change that occurs, during foci formation, is deregulation of actin stress fibers and focal adhesion molecules. This occurs when Rac1/Cdc42-specific GAP with a predicted molecular mass of 72 kDa protein (RC-GAP72) works to activate cyclin dependent kinase 42, used in cell cycle regulation, and Rac1GTPases, used in

regulation of actin dynamics, to interact with actin stress fibers through creation of rounding and aberrant morphology when overexpressed (Lo, 2006). Actin stress fibers and focal adhesion molecules can mediate cell migration, attachment, differentiation and gene expression; when they are altered the morphology of the cell changes. Lastly, the signal transduction pathways of adhesion and motility are deregulated leading to an altered cell. Focal adhesion kinases (FAK), which are associated with cellular adhesion and spreading processes of the cells, have a direct interaction with the tumor suppressor p53 (Golubovskaya Finch and Cance, 2005) and can deregulate the PI3K/AKT/mTOR pathway, which is important in apoptosis (Xie et al., 2011) and is based on cellular changes in adherence.

Tumors must also sustain immortality, thrive in the midst of genomic instability, and activate invasion and metastasis. Normal cells have a set number of cell divisions that can occur (<50) due to progressive telomere shortening triggering senescence (Huffman et al., 2000). However, tumor cells can overcome this barrier/tumor suppressor mechanism as they can activate telomerase activity or utilize alternate mechanisms to maintain telomere length (Bryan et al., 1995), conferring replicative immortality. Normal cells can grow to a certain density until they reach a saturation point, called contact inhibition, where they can no longer sustain the space they are in whereas tumor cells do not reach a saturation point and can grow to vast numbers such as 100 X 10^6 cells. In a study, volatile organic compounds were measured after 100 X 10^6 lung cancer cells were incubated overnight in a sealed fermenter (Sponring et al., 2009). Normal cells would have died under these conditions, but cancer cells survived.

Genomic instability is often an indicator of tumor cells, as they can have numerous changes in their chromosomes and still survive. Tumor cells can also acquire anchorage independence, which is the ability of single cells to form colonies in an agar/nitrocellulose matrix with traditional growth media. This is unique because in soft agar environments in which normal cells cannot adhere to a solid surface they undergo anoikas, which is programmed cell death by anchorage-dependent cells, but tumor cells have the ability to grow in the absence of attachment and survive. Additionally, tumor cells acquire the capability to metastasize through increased motility and the ability to invade surrounding tissues.

To sustain angiogenesis, tumor cells cause quiescent endothelial cells to reactivate, enabling them to sustain their own vasculature (Hanahan and Folkman, 1996). Tumors also activate many pro-angiogenic signals such as vascular endothelial growth factor (VEGF)-A, as well as VEGF receptors (Shibuya, 2006). Tumors were originally thought to induce inflammation, but when mice were treated with thioglycollate medium, a media that induces inflammation (Li et al., 1997), the inflammation caused tumor formation by upregulation of *IL-6* in malignant epithelial ovarian cancer (Rath et al., 2010).

The last determining factor for tumorigenesis was the reprogramming of energy metabolism. Ovarian cancer cells were found to be sensitive to glucose (Priebe et al., 2011). When cells were deprived of glucose, 5’ adenosine monophosphate-activated protein kinase (AMPK) was activated and caused inhibition of serine/threonine-specific protein kinase (Akt) phosphorylation leading to glucose deprivation and cell death of

ovarian cancer cells (Priebe et al., 2011). This study demonstrated the importance for further understanding of how cellular energetics function in tumorigenesis.

A way to test whether cells are tumorigenic is to sample cells from tumors or cancer cell lines, inject them into severe combined immunodeficiency (SCID) mice, (mice that have immune systems so highly compromised that they do not function), via xenotransplantation and monitor the mice for tumor formation (Fogh, Fogh and Orfeo, 1977). This particular type of experimentation is widely used in the cancer field to demonstrate the effect of drug treatments. Another method to manipulate gene expression is by gene overexpression or RNA interference, where RNA molecules inhibit gene expression, to understand the affect on tumorigenesis (Wei et al., 2010) *in vitro* and *in vivo*. The nature of tumors differ with each cancer type as well as the regulation pathways that produce them. One of the latest areas of regulation that was posed as a new capability was genomic instability (Hanahan and Weinberg, 2011).

MAINTENANCE OF GENOMIC STABILITY

DNA repair

There are many DNA repair mechanisms that normal cells utilize to combat mutations. Mutations are formed when DNA sequence modifications occur upon DNA damage. Endogenous damage can occur through replication errors or via reactive oxygen species production through normal metabolic by-products. Exogenous DNA damaging agents include chemicals, environmental toxins, ionizing radiation, ultraviolet rays (causing thymidine dimers), and heat which can lead to base degradation. Single

stranded DNA (ssDNA) damage is repaired by base excision repair, mismatch repair or nucleotide excision repair, while double-strand breaks (DSBs) are repaired by non-homologous end joining (NHEJ) or by homologous recombination (HR).

Base excision repair (BER) is a type of DNA repair that is an error-free method; i.e., it does not alter the DNA sequence. Specific DNA glycosylases recognize the damaged base and endonucleases remove it, producing an abasic site. DNA polymerase-β replaces the removed base with the correct nucleotide, then two ATP-dependent enzymes act on the lesion to ligate the break. If it is a small lesion, short-patch BER (Fromme and Verdine, 2004) will recruit the DNA polymerase-β AP lyase to cleave the 5'-sugar OH^- residue. The DNA polymerase-β, along with X-ray repairs cross-complementing protein 1 (XRCC1), will insert the appropriate nucleotide using the complementary strand. XRCC1 recruits ligase III to seal the 3'-sugar PO_4 bond, completing the repair. If the lesion is large, the long-patch BER (Fromme and Verdine, 2004) will be used. The strand is displaced in the 5'-3' direction by 2-10 nucleotides using DNA polymerase δ or ε with proliferating cell nuclear antigen (PCNA). An endonuclease, FEN1, removes the flap and PCNA recruits DNA ligase I to ligate the 3'sugar PO_4 bond completing the repair (Fromme and Verdine, 2004). This process is most frequently used during replication when an incorrect base is inserted in the DNA.

Mismatch repair corrects mismatches of the normal A-T and C-G base pairing and is also another error-free method. Either the MSH2/MSH6 dimer (MutSα) or the MSH2/MSH3 dimer (MutSβ) recognizes a mismatch in the DNA. MutSβ recognizes

base-base mismatches as well as small loop insertions, while the MutSα only recognize small loop insertions. When MutSβ or MutSα binds to a mismatched base, as well as DNA mismatch repair protein PMS2 (PMS2) and mutL homolog 1 (MLH1) they recruit exonuclease 1 (EXO1), an enzyme that interacts with MutSα. Upon EXO1 binding, excision of the mutant strand (Tishkoff et al., 1998) occurs and DNA polymerase δ or ε, DNA ligase is recruited to ligate the stand.

Nucleotide excision repair (NER) responds to larger, bulkier distortions of the DNA helix. The DNA helix distortion is first recognized by a heterotrimeric complex comprised of Xeroderma Pigmentosum group C protein (XPC), human Rad23 homolog protein (hHR23B) and centrin 2 (CETN2) (Stauffer and Chazin, 2004). Once the bend of the DNA helix is detected, transcription factor II H (TFIIH) is recruited. TFIIH is a factor within the RNA polymerase II preinitiation complex that contains ten subunits including helicases Xeroderma Pigmentosum complementation group B (XPB) and Xeroderma Pigmentosum group D (XPD). Once TFIIH is recruited and unwinds the helix with XPB helicase in the 3'-5' direction and XPD helicase in the 5'-3' direction, replication protein A (RPA) is recruited to prevent ssDNA from winding back on itself and DNA repair protein complementing Xeroderma pigmentosum complementation group A protein (XPA) binds to the TFIIH complex. RPA and XPA recruit Xeroderma Pigmentosum complementation group G protein (XPG) and excision repair cross-complementation group 1/Xeroderma Pigmentosum complementation group A protein (ERCC1/XPF) endonucleases to incise the 3' and 5' strand, respectively (Fisher et al., 2011). After release of the damaged oligonucleotide, the approximate 24-32 nucleotide gap is filled

in a PCNA-dependent manner by DNA polymerase δ or ε, and PCNA recruits DNA ligase I to ligate the final nick.

Non-homologous end joining is a process normally utilized when ionizing radiation and certain chemicals produce DSBs. This process is prone to error because there is no template to utilize for reparation of the site. The process begins with the Ku70/Ku80 heterodimer binding to the broken DNA ends (Featherstone and Jackson, 1999), recruiting DNA-dependent protein kinase catalytic subunit (DNA-PKCs), X-ray repair cross-complementing protein 4 (XRCC4), and DNA Ligase IV (Jackson, 2002). Once DNA-PKCs bind to the damaged DNA, it phosphorylates Ku70/Ku80 proteins, which increases its affinity for the DNA. Recruitment of processing factors XRCC4 and Ligase IV repair the damaged DNA and Ligase IV ligates the ends together.

The other pathway for repair of DSBs is HR, which is an error free process thought to generate genetic diversity because it can cause genetic recombination as it uses homologues to repair damage. Briefly, DSBs occur, activating the ataxia-telangiectasia mutated (ATM) kinases to phosphorylate downstream effectors and recruit the Mre11-Rad50-Nbs1 (MRN) complex, replication protein A (RPA), Rad52 and Rad51 to the site of the DSB. The MRN complex promotes DNA resection of the broken DNA using exonuclease activity to create 3’ single-stranded overhangs. RPA binds the DSB and prevents ssDNA from winding back on itself and assembly of the BRCA1-PALB2-BRCA2 complex forms to recruit Rad51 binding to the BRAC2 DNA-binding domain. Rad51 searches for the homologous template strand to initiate pairing. If BRAC2 is

impaired and cannot bind Rad51, Rad52 may provide a back-up system for Rad51 function by recruiting Rad51 for loading onto ssDNA, displacing RPA (Lok and Powell, 2012). Once these proteins are bound to the DSB, the 3' single stand overhang end invades the homologous duplex DNA sequence on the sister chromatid guided by Rad51. DNA polymerases elongate the 3' end of the damaged DNA making a D-loop or Holliday Junction; a nuclease can then cut the D-loop horizontally or vertically and ligase can seal the ends, leading to error-free repair of the DSBs.

Mutations

Mutations are any changes to the linear sequence of DNA; there are many types of mutations associated with cancer. A point mutation occurs when the incorrect nucleotide is inserted into the DNA sequence. Normal base pairing places a pyrimidine (C, T) with a purine (G, A); C pairs to G, and T pairs with A. A transition point mutation inserts a pyrimidine with a pyrimidine (C-T) or a purine with a purine (G-A). If not repaired, this mutation can be detrimental as it leads to the translation of one incorrect amino acid. A transversion point mutation occurs when a pyrimidine is paired with the wrong purine (C-A or T-G). There are also silent mutations, which place the wrong nucleotide into the sequence, but do not lead to a change in the amino acid. Additionally, missense mutations happen when one point mutation results in coding for a different amino acid, and nonsense mutations transpire when one point mutation leads to a stop codon and the protein is truncated. There are also frameshift mutations that alter the entire code by either insertion or deletion of a nucleotide, and therefore these are one of the more detrimental types of mutations. Another type of mutation, loss

of heterozygosity (LOH), leads to a loss of one allele. Individuals who have an initial germline or somatic mutation in the tumor suppressor retinoblastoma 1 gene (RB1) on the q arm of chromosome 13 at the position 14.2 are more susceptible to retinoblastoma (Dryja et al., 1986). Replacement of the normal allele with the mutant allele through loss of heterozygosity leads to rapid development of cancer in the retina called retinoblastoma.

Chromosomal re-arrangements affect large areas of DNA, representing inter-chromosomal exchange of material between chromosomes. The most recognized translocation is the Philadelphia chromosome, discovered in 1960 when abnormalities were detected in chromosomes of patients with chronic myelogenous leukemia (CML) (Nowell and Hungerford, 1960). Further studies of this translocation revealed the abelson murine leukemia viral oncogene homolog 1 (ABL1) gene, a proto-oncogene on chromosome 9 (region q34), with the breakpoint cluster region (BCR) on chromosome 22 (region q11) (Rowley, 1973; de Klein et al., 1982) leading to the discovery that this translocation can lead to CML development. This ABL1-BCR fusion is expressed in patients with chronic myeloid leukemia and acute lymphoblastic leukemia (Hagemeijer et al., 1990).

Inversions are intra-chromosomal rearrangements that result when a segment of the chromosome reverses its orientation. Often, cytogeneticists use FISH (fluorescent *in situ* hybridization) to detect the chromosome aberrations (Jobanputra et al., 1998). A new technique called chromosome orientation fluorescence *in situ* hybridization (CO-

FISH) was established to visually determine 5’ to 3’ orientation (Bailey et al., 1996). These techniques are used to study chromosomal aberrations, and have been applied to fusion of dysfunctional telomeres to DSBs (Bailey et al., 2010).

Telomeres/Telomerase

Telomeres are the natural ends of chromosomes and must evade DNA damage responses in order to maintain genomic stability in the prevention of cancer. Telomeres end in a 3’ single-stranded overhang of approximately 150-500kb in length (Huffman et al., 2000), and experience an end-replication problem (Watson, 1972; Levy et al., 1992) as the lagging-strand telomere requires an RNA primer (approximately 8-12 nucleotides in length) and so it shortens with every round of replication. Once telomeres become critically short, a permanent cell cycle arrest known as senescence is triggered and the cell enters a non-replicative state that contributes to aging phenotypes. The majority of cancers bypass this tumor suppressor barrier by activating telomerase (Wright and Shay, 2005) making it an attractive therapeutic agent.

Telomerase is a ribonucleoprotein that uses its RNA template to synthesize telomeric DNA. It consists of a telomerase reverse transcriptase (TERT) and telomere RNA template (TR) subunits. TERT mutations can alter telomerase enzymatic activity (Prescott, Blackburn and Prescott, 1997), but it was unknown until recently how the catalytic cycle of telomerase worked (Liu and Li, 2010). It was determined that telomeric DNA on the 3’ single-stranded overhang serves as the substrate for binding the 5’ region of TR, stimulating the active site to begin transcription. The mechanism for the

RNA/DNA hybrid strands separation and realignment process is still unknown, as any mutations that affect TR and TERT can negatively affect telomerase function. Investigation of the functional roles telomerase plays in ovarian cancer are beginning to be elucidated, and thus far it has been found upregulated in 90-97% of ovarian carcinomas (Gorham et al., 1997, Yokoyam et al., 1998; Wright and Shay, 2007), supporting telomerase as a potential player in ovarian cancer progression, as well as an attractive target for therapeutic intervention.

Oncogenes/Tumor Suppressors

Proto-oncogenes are normal cellular genes, often in signal transduction pathways, that when altered can act as an oncogene (i.e. gain of function), and contribute to tumorigenesis. Peyton Rous discovered the first oncogene, now known as v-src, using chickens as a model to study sarcomas in breast cancer formation (Rous, 1910). The chickens were injected with human sarcoma in the breast muscle tissue, forming sarcomas; he dissected tumors and exposed young chickens to cell-free filtrate. These chickens formed sarcomas, demonstrating sarcomas can be transmitted via what is now known as the Rous sarcoma virus (RSV), an oncogenic retrovirus (Rous, 1910).

Tumor suppressors are an altered form of a normal cellular gene that leads to loss of function. They are also known to protect the cell, but when mutated lead to uncontrolled regulation of their downstream signaling targets. The most noted tumor suppressor, nicknamed the guardian of the genome, (Lane, 1992) is p53. p53 was first thought to be an oncogene (Eliyahu et al., 1984), but it was found to be a tumor suppressor when

p53, located on the deleted portion of chromosome 17 in colorectal neoplasia, could no longer suppress growth in colorectal neoplasia (Baker et al., 1989). p53 is responsible for cell maintenance and mutations are present in half of all human tumors (Hollstein et al., 1991). In cancer, p53 mutated tumors can tolerate DNA damage and deregulation of control systems without experiencing apoptosis (Ryan and Vousden, 1998). Mutations of p53 can cause p53 protein to lose transcription activation function, leading to increased p53 levels in accumulated cancer cells without triggering apoptosis.

It is interesting that microRNAs (miRNAs) can also have oncogenic or tumor suppressor functions (Zhang et at., 2007). Oncogenic miRNAs called “oncomirs” are altered miRNAs that lead to miRNA gain of function and tumor suppressor miRNAs “tsmirs” are altered miRNAs that lead to miRNA loss of function. Tumor suppressor miRNAs suppress oncogenes in healthy cells, but when lost, oncogenes can be upregulated. Conversely, oncogenic miRNAs inhibit tumor suppressors leading to cancer. Another way miRNAs regulate cancer is by targeting cellular mRNA targets involved in oncogenic regulation. miRNAs will bind to mRNA targets and either silence or cleave mRNA leading to deregulation of gene expression that can lead to cancer progression. Both oncogenes and tumor suppressors mediate numerous pathways that are involved in cancer.

Signaling pathways altered in cancer processes

Normal cells have synergistic communication in regulation of cellular pathways; in cells that have lost such regulation of pathways that repair DNA damage or control cell cycle

checkpoints, tumor formation can occur. Recently ten biological capabilities that initiate the development of tumors were described (Hanahan and Weinberg, 2011), and the Kegg pathway identifies eleven key pathways in cancer that regulate tumor survival (Kanehisa and Goto, 2000): 1) Wnt signaling, 2) Janus kinase-signal transducer and activator of transcription (Jak-STAT) signaling, 3) Erythroblastic Leukemia Viral Oncogene Homolog (ErbB) signaling, 4) Mitogen-activated protein kinase (MAPK) signaling, 5) Mammalian target of rapamycin (mTOR) signaling, 6) Vascular endothelial growth factor (VEGF) signaling, 7) Peroxisome proliferator-activated receptors (PPAR) signaling, 8) cell cycle regulation, 9) apoptosis, programmed cell death, 10) transforming growth factor β (TGFβ) signaling, and 11) the p53, tumor suppressor. The main functions in each of these pathways vary, but they work synchronously to regulate the hallmarks of cancer.

The main pathways in ovarian cancer are as follows: 1) p53, since 50-80% of tumors from ovarian cancer patients have mutations in the tumor suppressor p53; 2) cell cycle regulation, because cyclin-dependent kinase inhibitor 2A CDKN2A (p16INK4A), regulators of cell cycle progression at G1 and S-phase, are either deleted or mutated in ovarian epithelial tumors; 3) ErbB, as Kristin rat sacrcoma viral oncogene homolog (KRAS) mutations are found in 30% of ovarian carcinomas; 4) Wnt signaling, as 10-20% of ovarian cancers have amplification of v-myc avian myelocytomatosis viral oncogene homolog (MYC), and finally 5) mTOR, which is a major pathway in epithelial ovarian cancer by regulating the phosphatidylinositol-4,5-bisphosphate 3-kinase (PI3K) pathway that signals through the mTOR pathway (Huret, 2013).

OVARIAN CANCER

STAGES, GRADES, AND HISTOLOGICAL TYPES

Due to the heterogeneous nature of tumors, it is vital to assess each tumor to determine the best treatment for individual patients with ovarian cancer. Upon removal of a tumor, it is examined to determine whether it is benign or malignant. This is done through specific criterion based on morphology, size, and analysis of the peritoneal cavity from which the ovary resides in order to assess stage, grade and the histological cell type of the tumor removed.

The International Federation of Gynecology and Obstetrics (FIGO) have established guidelines based on years of examining the clinical research on ovarian cancer. There are three staging databases used in the United States: The National Cancer Institute Surveillance, Epidemiology, and End Results (SEER) program, American Joint Committee on Cancer (AJCC), and the International Union for Cancer Control (UICC) (Edge et al., 2010). The most widely used and accepted method for staging is the TNM classification of malignant tumors system (TNM system), a coding system based on the extent of the primary tumor (T), regional lymph nodes (N), and distant metastases (M) (Edge et al., 2010). TNM system helps determine the sub stages of ovarian cancer leading to diagnosis and ultimately a treatment plan.

There are four stages of ovarian cancer: Stage I, Stage II, Stage III and Stage IV, and within each stage are multiple TMN system subcategories. Stage I occurs when the disease is isolated to one or both of the ovaries. The three subcategories of Stage I

include: Stage IA, Stage IB and Stage IC. Stage I is determined if only one ovary is affected the tumor does not penetrate the tissue covering the ovary, and no tumor cells are present in peritoneal washings. Stage IB is similar to stage IA, except diseased tissue is found in both ovaries and stage IC is determined when the cyst on either ovary has ruptured and tumor cells are present, indicated by positive score when peritoneal washes performed. According to the SEER program, the 5-year survival rate for individuals with Stage I epithelial ovarian cancer is 89% (SEER, 2012).

Stage II determination occurs when the disease is confined to the pelvic region; this is the first stage in which the disease metastasizes. It is also subdivided into three categories, IIA, IIB, and IIC. Stage IIA ensues when the disease has spread to the uterus, fallopian tubes or both; by stage IIB the disease has reached the pelvic structures and at stage IIC the disease is not only found in the pelvic structures, but also in the abdominal fluid. Women with Stage II ovarian cancer have a 66% 5-year survival rate when cancer is normally detected at this stage (SEER, 2012).

Stage III ovarian cancer is classified as tumors present in the pelvis, and secondary tumors can be confirmed histologically in the liver and/or omentum. Stage III is subdivided into 3 categories: Stage IIIA is when the tumor is confined to the pelvis and has metastasized to the small bowel and mesentery, but has not entered the lymph nodes. Stage IIIB has metastases on peritoneal surfaces smaller than 2cm, but still has no lymph node positive spread, and Stage IIIC metastases on peritoneal surfaces are

greater than 2cm with spread into the lymph nodes. Thirty-four percent of women have a 5-year survival rate when stage III ovarian cancer is detected (SEER, 2012).

The final stage of ovarian cancer is Stage IV and consists of distant metastases that include the liver and a positive cytology result. The 5-year-survival rate is 26.9% for women staged in this final stage of ovarian cancer and women who go un-staged have a 18% 5-year survival rate (SEER, 2012). In all stages of ovarian cancer tumor grade is also gauged.

Tumor grade is another means of assessing the degree of tumor differentiation shown to be an important prognostic tool in determining diagnosis (Clark et al., 2001), which in turn improves treatment and survival of the patient. Ovarian carcinoma has three grades, Grade 1, 2, and 3. Grade 1 (low-grade) is when cancer cells are well differentiated and resemble those of normal cells. Grade 2 (moderate-grade) is when cancer cells begin to look abnormal and have begun to proliferate more rapidly. Grade 3 (high-grade) cancer cells have de-differentiated and are fast growing (FIGO, 2009). Patients diagnosed with high-grade tumors have a poorer prognosis than individuals with low-grade tumors (Heintz, 1988). A universal system of assessing ovarian cancer was established, integrating the FIGO grading system based on architecture of the tumor as well as nuclear grade, and mitotic count (Shimizu et al., 1998; FIGO, 2009). Grading also is used in assessing in the histological type of cancer.

Since 90% of all ovarian cancer tumors are comprised of the ovarian surface epithelium (peritoneal mesothelium), which covers the surface of the ovary (Nicosia and Johnson, 1984; Nicosia and Nicosia, 1988; Auersperg et al., 1988; Fox, 1993) it is vital to determine the histological type of an individual tumor, as serous epithelial ovarian cancer (EOC) is the most aggressive form of ovarian cancer. There are eight EOC histological types: serous, endometrioid, mucinous, clear cell, transitional cell, squamous cell, mixed epithelial, and undifferentiated (Tavassoli et al., 2003). The more common are serous, endometrioid, and mucinous (Tavassoli et al., 2003). Serous EOC cells are the most common and the most widespread forms of ovarian cancer, resembling normal cells of the fallopian tubes. Mucinous EOC cells mimic endocervix cells and comprise 1% of all common epithelial tumors. Clear cell EOC cells resemble nests that form in the vagina and comprise 6% of common epithelial tumors, of which nearly all are malignant. Endometrioid EOC cells resemble cells from the endometrium and comprise 20% of common epithelial tumors. As there are numerous stages, grades, and histological types within EOC tumors, it is crucial to determine the origin of the tumor.

TUMORS

In ovarian cancer there are three different cell types of origin: 1) malignant germ cell tumors (GCTs), 2) ovarian sex cord tumors, and 3) epithelial tumors. GCTs arise from the germ cells of the ovary and are thought to occur during aberrant migration of primordial germ cells (PGCs) during development. During early development, primordial germ cells migrate to the genital ridge through the midline of the body and hindgut

(Schmoll, 2002; Oosterhuis et al., 2007). During this time, it is thought that some germ cells fail to migrate to the genital ridge and develop into either testicular germ cell tumors or ovarian germ cell tumors. GCTs from the ovary are found in girls and young women and account for approximately 1-2% of ovarian malignancies (Pectasides, Kassanos and Pectasides, 2008; Conic et al., 2011). The second type of ovarian tumors is ovarian sex cord stromal tumors, which account for approximately 7% of ovarian malignancies and can be found in young girls as well as adults (Crum, 1999; Colombo et al., 2007; Conic et al., 2011). They are derived from mesonephros mesenchymal stromal cells in the undifferentiated gonad, including theca, and a second group of cells that differentiates in to the granulosa cells (Satoh, 1991; Robboy et al., 1994). These cells are found in the cortex of the adult ovary and are involved in folliculogenesis. The final type of ovarian tumors are epithelial tumors, which constitute approximately 75% of all ovarian cancer tumors and result in approximately 90% of all ovarian cancer deaths (Seidman et al., 2004; Bell, 2005; Güth et al., 2007) usually occurring in women >63 years in age. These tumors are also known to occur earlier in women with familial risk factors for ovarian cancer, such as BRCA1 or BRCA2 mutations (King et al., 2003). EOC tumors arise from ovarian surface epithelium (peritoneal mesothelium) and there are many different theories as to how they are derived (see origins section). There are two types of EOC tumors (Kurman and Shih, 2010; Romero and Bast, 2012). Type I is comprised of low-grade serous, mucinous, endometrioid, or clear cell histological type, which rarely leave the basement membrane of the ovary, and are less proliferative then Type II tumors (Smith Sehdev, Sehdev and Kurman, 2003), which are most commonly found in Stage III and IV EOC patients. These tumors are found outside of the ovary in

the omentum and peritoneal cavity of the female reproductive system, are high-grade serous carcinomas that are aggressive, invasive, and highly proliferative, commonly containing p53 mutations (Bell, 2005; Cho and Shih, 2009), as well as display of chromosomal instability.

Each EOC patient is staged according to FIGO and TMN guidelines, but can contain different cell morphologies due to heterogeneity, suggesting that tumors are derived from various types of cells. In order to study how EOC tumors function, various cell lines have been established (Fogh, Fogh and Orfeo, 1977) and more are being documented and validated each year. While ovarian cancer has numerous morphological states (Figure 2), each has different functions and behaviors. The IGROV1 cell line was isolated from a 47-year-old women with Stage III epithelial ovarian cancer, and resembles cells in the primary tumor. Interestingly, the IGROV1 cell line can induce peritoneal carcinomatosis in SCID mice after xenotransplantation leading to rapid tumor formation and cell growth (Benard et al., 1985), which makes it an attractive cell line to study for metastasis occurrence in human EOC patients. The EOC cell line OV420, also known as OVCA 420 cells, was originally isolated from ascites and tumors from late stage ovarian cancer patients (Tsao et al., 1995) and does not form tumors in SCID mice post injection subcutaneously (Lee et al., 2000). In order to better assess progression into metastatic tumors, particular steps are taken to correctly diagnose and treat cancers, but little understanding of how EOCs originate has led to high mortality and incidence rates that have not changed in the past few decades (SEER, 2012).

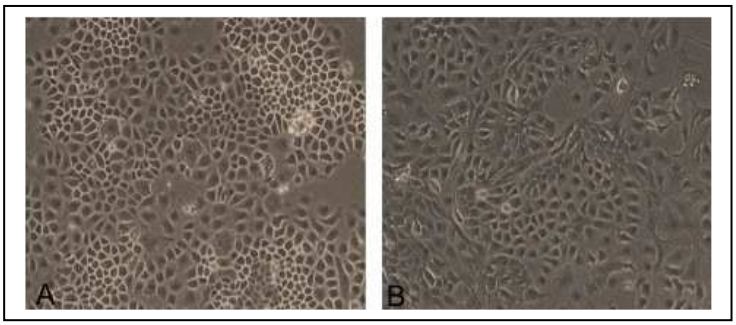

Figure 2: Morphology of EOC cell lines. A) IGROV1 cell lines are a mix of endometrioid and serous cell types and B) OV420 cells lines are mostly serous.

ORIGINS

A clear understanding of the tissue origins of ovarian cancer could improve our ability to prevent and treat this disease. Unfortunately, the origins of ovarian cancer are still an enigma and have been a much-debated topic over the years. The three most explored ovarian cancer theories are: 1) inclusion cyst, where ovarian cancer arises from ovarian epithelial (OSE) cells, 2) Müllerian theory, which states all tumors in the pelvis that exhibit the Müllerian-derived phenotypes are derived from Müllerian-type epithelia, including OSEs, and 3) the tubal theory, where high grade serous carcinomas are produced by the fallopian tubes.

The most traditional and well-researched theory is that ovarian cancer arises from ovarian surface epithelial cells or ovarian epithelial inclusions (Fathalla 1972; Auersperg et al. 1998). Since the ovary consists of germ cells, stromal cells, and OSE, it is thought that ovarian cancer arises from the OSE when it invaginates into the cortex of the ovary leading to the formation of cortical inclusion cysts (Nicosia and Johnson, 1984; Nicosia and Nicosia, 1988; Auersperg et al., 1988). This is called the incessant ovulation model (Fathalla 1972; Auersperg et al. 1998) and is based on the monthly repair the ovary

must undertake upon ovulation of the oocyte. During this process, OSE become trapped in the cortex of the ovary leading to transformation of cells into malignant tumors. One study used the HOX transcription factor genes, master regulators of the morphogenesis in the female reproductive system, to transform undifferentiated mouse ovarian surface epithelium cells into tumors that histologically resembled serous carcinomas, endometrioid carcinomas, and mucinous carcinomas (Naora, 2005). A drawback to this study was that no ovarian lesions formed.

The second theory to explain EOCs origin is the Müllerian theory (Lauchlan, 1972). It was postulated that all tumors in the pelvis exhibiting Müllerian-type phenotypes were derived from the Müllerian-type epithelia, including OSEs. This theory explains how ovarian cancer cells are found outside of the ovary in the Müllerian system and is supported by pathology experiments that demonstrated direct metaplasia in endometriosis patients occurred from ovarian surface inclusions, not from ovarian epithelium cells (Zheng et al., 2005). This theory would indicate an extaovarian origin, rather than an ovarian origin.

An alternative origin hypothesis is that high-grade serous carcinomas are produced by the fallopian tubes (Diniz et al., 2011) via metastasis of the fallopian tubes to form high-grade serous carcinomas in the ovary. This notion started when approximately 50% of familial ovarian cancer patients with a BRCA1/2 mutation underwent prophylactic oophorectomies, yet still developed high-grade serous carcinomas in the fallopian tubes (Piek et al., 2001) called serous tubal intraepithelial carcinoma (STICs). To further

support this theory, several researchers have examined patients with the BRCA 1/2 mutation in relation to high-grade serous carcinoma and found early ovarian cancer originates from the fallopian tube (Leeper et al., 2002; Olivier et al., 2004; Finch et al., 2006a; Finch et al., 2006b; Lamb et al., 2006; Hermsen et al. 2006; Callahan et al., 2007). Other evidence to support this theory was provided by a double knockout mouse model with conditional knock-out of Dicer and PTEN (Kim et al., 2012). Dicer is an RNA III endoribonuclease involved in miRNA processing, and PTEN, a tumor suppressor that inhibits the PI3K pathway. When both Dicer and PTEN were depleted in mice ranging from ages 6.5 to 13 months, 100% of the mice died from metastasis of tumors to the ovary and the abdominal cavity (Kim et al., 2012). Moreover, when the fallopian tubes were unilaterally removed from mice between the ages of 6-11 months, ovarian cancer failed to develop even when the ovary was left intact (Kim et al., 2012). These studies substantiate the theory of ovarian cancer originating from the fallopian tube, at least in some cases, but additional research is needed to confirm this hypothesis.

As the origin is unknown, it is inferred that this is a main reason the incidence and mortality of ovarian cancer has not declined in the past decades (SEER, 2012). Once more is understood about how ovarian cancer originates, better evaluation of ovarian tumors can be made, possibly leading to earlier diagnosis and better understanding of how the tumor metastasizes.

METASTASIS

Metastasis is the ability of cells within a malignant tumor to escape from the surrounding basal lamina of the tumor in a complex sequence of steps known as the invasion-metastasis cascade, which acts through many different cellular and signaling proteins. Briefly, the invasion-metastasis cascade consists of six steps: 1) primary tumor formation, 2) localized invasion, 3) intravasation to gain access to the blood vessels 4) transport through circulation, 5) extravasation onto a distant tissue, and 6) colonization to form a macrometastasis at a distant site.

There are many theories regarding the etiology of ovarian cancer (origins). The one best explained is the inclusion cyst theory based on the incessant ovulation model in type II ovarian tumors. OSE cells must first transform to become a primary tumor. Ovarian tumor formation of high-grade carcinomas versus low-grade carcinomas (Kurman and Shih, 2004) demonstrated how a primary tumor can be generated from OSE cells (Figure 3).

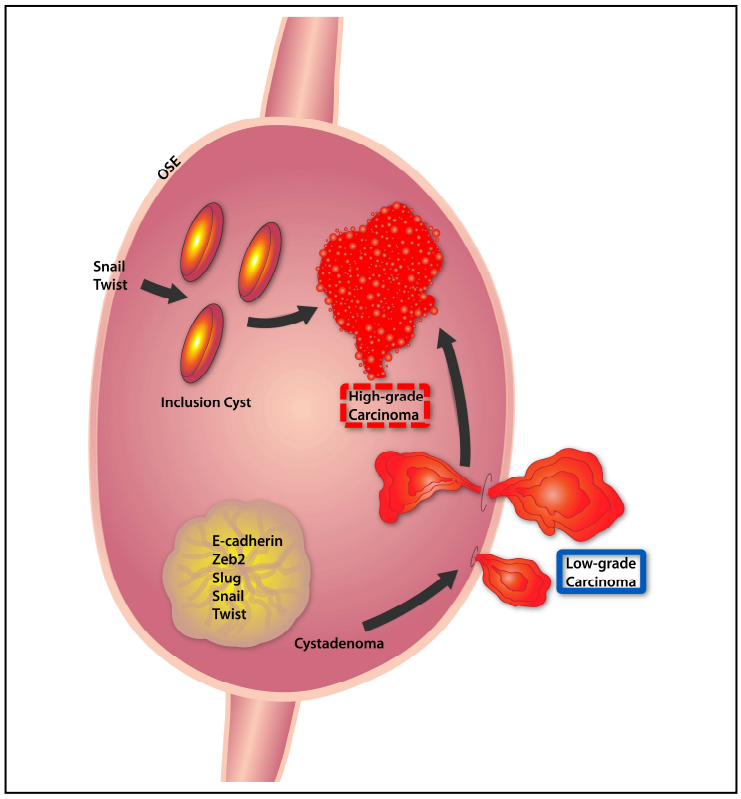

Figure 3: EOC tumor formation. Red dashed lines are type II tumors and blue solid lines are Type I tumors.

OSEs do not express high levels of E-cadherin, a transmembrane glycoprotein that functions in maintaining cellular adhesions, but express a zinc finger transcription factor protein snail homology 1 (Snail), and basic helix-loop-helix twist-related protein 1 (Twist) (Imai et al., 2003; Hosono et al., 2007; Yoshisa et al., 2009). As they gain contact with the cortex of the ovary they generate inclusion cysts. Both Snail and Twist repress the expression of E-cadherin transition through various mechanisms. p70 S6 kinase is a downstream effector in the activated PI3K pathway in cancer and can upregulate Snail (Pon et al., 2008). Snail can repress E-cadherin (Pon et al., 2008; Batlle et al., 2000; Cano et al., 2000; Bolos et al., 2003) and lead to formation of a type II high-grade carcinoma tumor (Figure 3). Twist is found to be upregulated in type II high-grade carcinoma tumors (Yoshisa et al., 2009), but a mechanism has yet to be established.

Some type I low-grade carcinomas can generate type II high-grade carcinomas by increasing the expression of zinc finger E box binding protein 2 (Zeb2), Snail, zinc finger protein snail homolog 2 (Slug), and Twist (Yoshisa et al., 2009). Although this is one way to show generation of ovarian cancer in primary tumor formation, many additional pathways can be involved due to the numerous histological cell types that can be formed from the heterogeneous metastatic tumor.

Once a type II tumor is established, it begins acquiring various signals that allow it to break through the basement membrane of the ovary and begin localized invasion. In a process known as epithelial-mesenchymal transition (EMT), signals that control cell attachment, polarity, and motility are altered making the epithelial cell more mesenchymal and more invasive. Metastatic cancer cells acquire proteolytic mechanisms to degrade the basement membrane called matrix metalloproteases (MMPs) (Stack et al., 1998; Ghosh et al., 2002), which allows for invasion to other tissues. Additionally, the Cadherin switch (Tomita et al., 2000; Wheelock et al., 2008) is activated when E-cadherin, a marker for epithelial cells, is downregulated and N-Cadherin, a maker for mesenchymal cells, is upregulated, enabling detachment of cells and cellular movement outside of the basement membrane to occur. As the tumor grows, the polarity of the epithelial cells changes. Epithelial cells are normally polarized, consisting of an apical and basal side; during uncontrolled proliferation of metastatic cancer cells, epithelial cells lose their polarity (Tanos and Rodriguez-Boluan, 2008). Polar cells cannot move toward chemoattractants by means of cytoskeletal elements like actin and microtubules, while non-polar cells can. This is key because non-polarized

cells are more metastatic (Goswami et al., 2005). Mammary tumors have extremely non-polar tumor-associated macrophages (TAMs) that aid in sustaining angiogenesis (Goswami et al., 2005). TAMs secrete growth factors, such as epithelial growth factor, which leads to increased motility of the tumor cells. Additionally, CSF-1, a macrophage cytokine secreted by TAMs in the non-polar tumor cells, follows the macrophage out of the basement membrane (Lin et al., 2001), increasing metastasis since MMPs have opened the membrane. Therefore when metastasizing cells lose their polarity, they can leave the site of the primary tumor and intravaste into blood vessels.

Metastasizing tumor cells that enter the blood stream go through a number of steps leading to extravasation, called the seed and soil hypothesis (Fokas et al., 2007). This is described as tumors having adequate mutations to invade and metastasize or “the seed”, while the target cells have to be able to accept the metastasizing cell, “ the soil”. Tumor cells circulating in the blood stream become physically trapped in the capillary and form a microthrombosis as platelets attach to the tumor cell. The tumor cell then interacts with the capillary basement membrane by moving the endothelial cells. Extravasation leads to the production of tumor fibrin and proteases, such as prothrombinase. These are secreted from the tumor cell to help degrade the microthrombosis (Hoeben et al., 2004), which leads to proliferation of the tumor cell. As the tumor grows, macrophages are thought to aid in tumor cell invasion, leading the cells into the target region (Qian et al., 2009). Once the macrometastasis has formed, it is believed that cell signals are again altered leading to a more epithelial-like tumor cell rather then mesenchymal tumor cell, as seen in invasion, but this process is still

unclear. As a micrometastasis establishes its own vascularization, further metastasis occurs. Ovarian cancer is normally detected after the tumor has metastasized. It is often diagnosed in late stages (III, and IV) leading to approximately 18% 5-year survival rate (SEER, 2012); therefore current research is focusing on identifying an early diagnostic biomarker to better treat ovarian cancer patients.

DIAGNOSIS

Currently, no effective screening method to detect the early onset ovarian cancer or recurrent ovarian cancer exists. Prior to 2000, cancer antigen 125 (CA-125), a cell surface glycoprotein, was used as a diagnostic marker indicator of the presence of ovarian cancer. A CA-125 positive ovarian cancer patient would undergo cytoreductive surgery to remove part of the malignant tumor (Chi et al., 2000). Unfortunately, after the beginning of ultra-radical cytoreductive surgery, the removal of microscopic ovarian cancer cells was implemented; this test was no longer accurate as a positive predictive outcome marker (Memarzadeh et al., 2003; Obeidat et al., 2004; Gemer et al., 2005). Studies focused on using CA-125 and transvaginal sonography to identify approximately 89% advanced stage (III, IV) ovarian cancer patients, but of these patients, only 21% were in early stage (I, II) (Partridge et al., 2009); therefore the detection of early ovarian cancer is still ellusive.

Recently, CA-125 and urine collected from individuals with and without ovarian cancer was used to determine if matrix metalloproteinases (MMPs), involved in migration of cells through the body, could be used to detect early onset of ovarian cancer (Coticchia

et al., 2011). Individuals were screened for CA-125 and those with a CA-125 level <35 U/mL were additionally screened for MMP2 and MMP9 utilizing the ELISA technique (Coticchia et al., 2011). They found they could discriminate between normal and ovarian cancer patients. The matrix metalloproteinases, MMP-2 and MMP-9, have also been implicated as potential prognostic detectors of ovarian cancer rather than CA-125 in advanced or recurrent ovarian cancer patients (Coticchia et al., 2011). This lead to examination of whether MMP-2, MMP-7, MMP-9, MT1-MMP and their inhibitors, tissue inhibitor matrix metalloproteinases (TIMP-1 and TIMP-2), were prognostic for advanced ovarian cancer patients, but unfortunately none were predictive of cytoreductive outcome or survival (Brun et al., 2012). Additional studies are focused on confirming these results, as well as identifying additional potential biomarkers for detecting recurrence and early onset.

TREATMENTS

Current treatment strategies for ovarian cancer vary depending on stage, grade, and histological type. There are three broad treatments for ovarian cancer patients. The first is surgery to assess the tumor and range of metastasis, as well as determining stage, grade, and identification of histological type. Therapy is then designed, which may consist of adjuvant chemotherapy and radiation treatment. Sometimes it is difficult to perform surgery on the patient first; therefore, neo-adjuvant chemotherapy is administered before debulking of the tumor. Debulking, also known as cytoreduction surgery, is often a significant prognostic factor for women with stage IIIC ovarian cancer (Chi et al., 2006). It has been described by various groups that optimal debulking versus

sub-optimal debulking leads to increased survival rates and prognosis (Duska et al., 2002; Rutledge et al., 2006; Silasi et al., 2008; Rauh-Hain et al., 2011). After the tumor and affected areas have been removed, chemotherapy is administered. Chemotherapy regimens differ for each patient depending of the level and extent of disease, but normally include some form of platinum-based drug given alone or in combination. The final treatment is the use of ionizing radiation. For advanced stages of ovarian cancer this method is not often utilized as diagnosis of this cancer generally occurs at late stages and the effect of radiation on EOC patients in late stages is unknown (Mano et al., 2007.) Recently, it was postulated that current treatments for ovarian cancer patients were ineffective due to the possibility that while chemotherapy can kill off malignant cancer cells, it can intensify cancer stem cell proliferation (Abubaker et al., 2013). Emerging evidence suggests that subpopulations of cells expressing the surface marker $CD44^+$ are chemoresistant to Paclitaxel and Carboplatin (Alvero et al., 2009), common drugs used in the treatment of patients with ovarian cancer. Elucidating potential cancer stem cell populations are key to better understanding and treatment of recurrent ovarian cancer.

WHAT ARE STEM CELLS?

STEM CELLS

Stem cells have generated considerable attention due to their unique abilities for self-renewal, differentiation into specialized cells, and giving rise to the ectoderm, mesoderm, and endoderm of the embryo. To fully understand what stem cells are, we must understand how they are derived. Embryogenesis is a process that ends in the

production of a fully formed fetus; undifferentiated cells give rise to all cell types in the embryo. Many cellular divisions occur from the fertilized totipotent egg that lead to the production of pluripotent cells, which are cells capable of self-renewal and creation of various cell types. During embryogenesis, cells undergo rapid cell division and various cellular functions are initiated to activate the differentiation of cells.

At the morula stage, the cleavage process begins, and cells form tight junctions, changing cell shape and making cell numbers indiscernible. During this compaction state the cells are called blastomeres. In the 1950s and 1960s while scientists were working on pre-implantation embryology in order to develop *in vitro* fertilization techniques (Chang, 1955; Edwards and Gates, 1959), they discovered cells with numerous capabilities. Several years later a curious discovery about the nature of blastomeres was revealed upon fusion of mouse 8-cell and 16-cell embryos to blastocysts to create viable chimeras (Tarkowski et al., 1961). These findings indicated that mammalian blastomeres had pluripotency capabilities, which led to uncovering embryonic stem cells (ESC) ability to sustain growth indefinitely (Evans and Kaufman, 1981).

It is during the blastocyst stage that two distinct pluripotent cell populations form: the inner cell mass (ICM) and the trophectoderm. The ICM gives rise to the extraembryonic endoderm and the epiblast, which in turn gives rise to extraembryonic tissues and primitive ectoderm, respectively (Niwa, 2007). The ICM cells are also able to form embryonic stem cells (ESCs), but are unable to give rise to placental elements. The

cells nearest to the ICM are the trophoblast stem cells of the trophectoderm. The trophectoderm gives rise to extraembryonic ectoderm and placental elements (Rossant and Tam, 2009). The trophectoderm and ICM cells can be harvested and cultured indefinitely (Oda, Shiota, and Tanaka, 2006;). Currently, numerous studies are preformed in order to understand similarities and differences between trophoblast stem cells and ESCs. Since stem cells have the ability to maintain pluripotency and drive differentiation, stem cell populations are of great interest to researchers. The fact that stem cell populations exist in cancer cells may underlie ovarian cancer recurrence and metastases.

CANCER STEM CELLS

Cancer stem cells (CSCs) are small subpopulations of cells within a tumor capable of self-renewal, and unlike ESCs, able to generate all cell lineages of the tumor from which they were derived (Clarke et al., 2006; Ichim and Wells, 2006); therefore, CSCs can give rise to new cancer cells. CSCs are also thought to survive in the microenvironment after abscission of the primary tumor, chemotherapy and radiation treatment leading to repopulation of the primary tumor (Kim and Tannock, 2005). CSCs were first successfully identified in acute myeloid leukemia (AML) patients through isolation of subpopulations of cells and injecting them into immunosuppressed SCID mice, which led to a formation of a tumor (Lapidot et al., 1994). Two hypotheses are currently being explored regarding the nature of CSCs: the CSC hypothesis and clonal evolution hypothesis.

The CSC hypothesis states that only a rare subset of cells within a tumor possess indefinite proliferation potential to drive the formation and growth of tumors (Reya et al., 2001). This hypothesis was first described when cells expressing surface markers CD34+ and CD38- in acute myeloid leukemia (AML) patients were identified to self-renew, proliferate and differentiate (Bonnet and Dick, 1997). Additionally, AML cells that expressed cell surface makers CD34+ CD38- were able to produce tumors using xenotransplantation in support of the CSC hypothesis (Lapidot et al., 1994). Furthermore, a different method termed Aldefluor enzymatic assay was used to isolate stem cell side populations from normal and malignant breast cancer cells by virtue of increase aldehyde dehydrogenase (ALDH) activity (Ginestier et al., 2007), shown to increase in stem cell populations of AML patients (Pearce et al., 2005).

The clonal evolution hypothesis embraces the idea that any cancer cell can become invasive, metastatic, and/or develops resistance to cancer therapies and cause recurrence. The most noteworthy evidence supporting the clonal evolution theory was from breast tumor cells in mice (Dexter et al., 1978). In this study, four samples from a mammary tumor and created four cell lines (Dexter et al., 1978). Interestingly, each of those lines had distinct tumor subpopulations they believe arose from a single mouse mammary tumor suggesting support for the clonal evolution theory (Dexter et al., 1978). Both hypotheses have evidentiary support, so either has the potential of describing CSCs depending on the cell type. It is widely accepted in the cancer field that both hypotheses are possible, although more exploration of the origin of CSCs has yet to be established.

Additionally, CSCs are thought to survive in the microenvironment after abscission of the primary tumor and/or chemotherapy and radiation treatment leading to repopulation of the primary tumor. Mammary CSC fractions have fewer reactive oxygen species (i.e. hypoxic) than normal mammary epithelial stem cells after exposure to ionizing radiation (Diehn et al., 2009). A study determined there was less DNA damage in CSC fractions then epithelial stem cells leading to the conclusion that CSCs can survive radiation treatment (Diehn et al., 2009). Interestingly, a subpopulation of ovarian cancer cells expressing the surface markers $CD24^+$, $CD44^+$, and $EpCam^+$, were found to enhance invasiveness of CSCs even after treatment with doxorubicin, cisplatin, and paclitaxel, drugs normally given to ovarian cancer patients (Wei et al., 2010). It has also been demonstrated that CSCs increased within this enriched population (Wei et al., 2010) providing further evidence that CSCs exist. More studies are needed to better understand how CSCs function in tumor repopulation and/or serve as potential biomarkers following therapeutic treatments.

PLURIPOTENCY FACTORS

Initially the pluripotent nature of ECS was studied using cells isolated from the ICM of mouse embryos (Evans and Kaufman, 1981) and by somatic cell nuclear transfer. The transfer of nuclei of somatic cells into oocytes after the second meiotic division allowed many groups to generate ESC-like cells (Wilmut et al., 1997; Wakayama et al., 1998; Campbell et al., 1996). Due to ethical issues, it currently is not possible to derive and establish new human ESCs in the United States.

Many researchers began to study transcription factors that may be important in regulating formation of ESCs. Recently, the transcription factors Pou5f1, Sox2, Kif4, and c-Myc where found to be essential in reprogramming mouse fibroblast cells to a pluripotent state (Takahashi and Yamanaka., 2006); Additionally, identification of the molecular factors necessary for making human ESCs (POU5F1, NANOG, SOX2, and LIN28A) from the human fetal fibroblast cell line IMR90 (Yu et al., 2007) was discovered. When these factors are introduced into differentiated cells, somatic cells were reprogrammed into ESC-like cells called induced-pluripotent stem (iPS) cells. Understanding the gene regulation and pathways involved in NANOG, SOX2, POU5F1 and LIN28A activation can expedite understanding how cancer progression occurs as it shares many similarities to iPS cells and ESCs.

The homeobox transcription factor, NANOG, is best known for its role in sustaining pluripotency during development of ESC lines while in the absence of LIF, a cytokine implicated in inhibiting differentiation (Chambers et al., 2003; Mitsui et al., 2003; Pan and Pei, 2003; Pan and Pei, 2005). NANOG is regulated by the interaction of POU5F1 and SOX2, a member of the high-mobility group (HMG) superfamily (Rodda et at., 2005; Kuroda et al., 2005). It has also been suggested that NANOG can be regulated by POU5F1 and SOX2 independently (Kuroda et al., 2005). POU5F1 is a POU-family transcription factor found in pluripotent cells of the ICM and primordial germ cells (PGCs) during development of an embryo (Pesce and Scholer, 2001), and was discovered in 1990 (Scholer et al., 1990). POU5F1 belongs to the octomer-binding protein family. NANOG and SOX2 can activate POU5F1 transcription in ES cells (Pan

et al., 2006; Ambrosetti, Basilico, and Dailey 1997; Rodda et al., 2005). Recently, LIN28A was shown to bind directly with POU5F1 mRNA through high affinity sites within its coding region (Qiu et al., 2010).

Pluripotency factor LIN28A is found on chromosome 1p36.11 in humans and is an evolutionarily conserved RNA binding protein that negatively regulates mature *let-7* miRNA expression in embryonic stem cells (Newman, Thomson and Hammond, 2008), trophoblast stem (TS) cells (Seabrook et al., 2013), and cancer tumors (Zhong et al., 2010; Peng et al., 2010). LIN28A is thought to contribute to the pluripotent state of iPS cells by inhibiting *let-7* miRNA processing (Viswanathan, Daley, and Gregory, 2008). LIN28A and LIN28B can block the maturation of *let-7a* in ovarian cancer tumor samples (Lu et al., 2009). When LIN28B is highly expressed it often leads to poor prognosis and could be an indicator of higher risk in patients developing ovarian cancer. Additionally, LIN28A and POU5F1 are co-expressed and upregulated in advanced stage ovarian cancer (Peng et al., 2010); furthermore, *let-7* is downregulated when cells undergo EMT (Mezzanzanica et al., 2010). The exact roles of pluripotency genes in ovarian cancer are still unknown. The influence of human pluripotency genes on miRNA function in cancer is also unclear. Therefore, it is vital to study the molecular pathways that regulate these genes in order to identify stem cells characteristics in cancer and how they relate to cancer invasiveness.

MICRORNAs (miRNAs)

Past ovarian cancer studies have focused on understanding the function of protein-coding genes, but examination of functional non-coding sequences in cancer, such as miRNAs, is poorly understood. MicroRNAs *lin-4* and *let-7* were first discovered in *Caenorhabditis elegans* (Lee, Feinbaum and Ambros, 1993, Reinhart et al., 2000) and were found to be instrumental for proper developmental timing in worms. MicroRNAs are approximately 22 nucleotide non-coding RNAs that regulate gene expression in a post-transcriptional manner (Landi et al., 2011). They are phylogenetically conserved non-coding RNAs found in all eukaryotic cells (plants, animals, and some viruses) that function in silencing target genes by binding to the 3' untranslated region (3'UTR) of target mRNAs and inhibit translation of the mRNA or promote mRNA degradation. It was originally thought that many regions of the genome were "junk", but they actually encode miRNAs.

The biogenesis of miRNA can be broken down into six steps: 1) transcription, 2) cleavage, 3) export, 4) dicing, 5) RNA-induced silencing complex (RISC) formation, and 6) mature miRNA function. RNA Pol II usually transcribes miRNAs, but emerging data suggests that RNA Pol III can also transcribe miRNAs, which is the same polymerase that transcribes tRNA (Borchert, Lanier and Davidson, 2006). Initially, miRNAs are transcribed as a long primary transcript called primary miRNAs (pri-miRNA). pri-miRNA can be 100s or 1000s nucleotides long, have a 5' cap and a poly-A tail, and contain a hairpin stem loop. Cleavage occurs when the nuclear microprocessor complex recognizes the stem-loop of the pri-miRNA and cleaves it into a precursor miRNA (pre-

miRNA). The nuclear microprocessor complex consists of Drosha (RNase III enzyme) and DGCR8 (also known as Pasha “Partner of Drosha”). Drosha cleaves the 5’ and 3’ arms of the pri-miRNA and Pasha determines the precise location of cleavage leaving behind a hairpin stem loop that is approximately 33 base pairs long in humans. Export of the pre-miRNA occurs when exportin-5 and Ran-GTP export pre-miRNA into the cytoplasm. Exportin-5 recognizes the 3’ single stranded overhang on the pre-miRNA and ensures that only correctly processed pre-miRNAs are exported. Ran-GTP is needed for Exportin-5 to move across the nuclear membrane where Dicer (endoribonuclease) recognizes the pre-miRNA hairpin stem loop and cleaves it leaving another 3’ single stranded overhang and a microRNA duplex (approximately 22nts long). Dicer also initiates the formation of RNA-induced silencing complex (RISC) and Tar RNA binding protein (TRBP) stabilizes Dicer. TRBP is not essential for correct cleavage to occur and can occur even in its absence. RISC formation is composed of Dicer, TRBP, PACT (protein activator of PKR), and Ago2 and is responsible for selecting the miRNA stand and slicing the target gene. RISC binds to one strand, (guide strand), while the passenger strand is targeted for degradation. The miRNA strand with the less thermodynamically stable base pair at its 5′ end in the duplex is preferentially loaded into RISC. Once the strand used for degradation or silencing is selected, Ago2 (endonuclease) slices the guide strand away from the passenger strand. Ago2 is also the major component of cutting the mRNA upon miRNA binding to the target mRNA. The final stage in biogenesis of miRNAs is the production of the mature miRNA.

Two important functions of miRNAs include 1) miRNAs binding to mRNA targets with perfect complementarity, leading to the degradation of the mRNA; and 2) translational repression of the mRNA occurring when miRNAs bind their target mRNAs and repress protein translation. miRNA specificity is determined by the 2-8 nucleotides at the 5' end called the seed sequence (Huntzinger and Izaurralde, 2011). Seed sequences bind with varying strength of complementarity with the target mRNA using Watson-Crick base pairing and non-Watson-Crick base paring can occur, leading to imperfect complementarity binding (Lee, Chen and Au, 2011).

In 2002, the first described miRNAs, *miR-15* and *miR-16,* were found in chronic lymphocytic leukemia, thus beginning the exploration of miRNAs as potential targets that regulate cancer in humans (Calin et al., 2002). Recent studies reveal that human ovarian cancers express distinct miRNA signatures (Iorio et al., 2007) making them attractive candidates as potential diagnostic markers for ovarian cancer progression. In ovarian cancer, *let-7* miRNAs act as tumor suppressors by targeting KRAS, MYC and HMGA2 (Bussing, Slack and Grosshans, 2008), and by regulating cell proliferation, differentiation, and apoptosis (Johnson et al., 2007; Selbach et al., 2008). Another set of miRNAs that may serve as potential biomarkers are the *miR-200* cluster. The *mir-200* cluster is highly expressed in advanced ovarian cancer (Hu et al., 2009) and negatively regulates the zinc finger E-box binding homeobox 1/2 (ZEB1/2), which is highly expressed in cells undergoing EMT (Bendoraite et al., 2009).

Many circulating miRNAs have been discovered in vesicles and recent studies using serum from prostate cancer patients identified miRNA differences in prostate cancer patient's versus normal patients (Mitchell et al., 2008; Brase et al., 2011). This form of communication, involving vesicles, may affect transcription and translation of genes in target cells. Understanding how cells communicate with one another, and how cell secreted vesicles act also can provide insight into tumor development.

CELL SIGNALING AND TRAFFICKING

ENDOSOMAL TRAFFICKING

The purpose of endocytosis is to maintain homeostasis of the plasma membrane through regulation of the secretory activity of proteins and lipid compartments and recycling or degradation of membrane factors (e.g. receptors). In eukaryotic cells, there are numerous modes of internalization such as macropinocytosis, phagocytosis, receptor-mediated endocytosis, and non-clathrin mediated endocytosis, but the most general mode is clathrin-dependent endocytosis.

Clathrin-dependent endocytosis occurs when clathrin-coated vesicles form on the cytoplasmic side of the plasma membrane, leading to the invagination of transmembrane cargo into an endosome. Adaptor protein complexes (AP-2) are targeted to the cytoplasmic face of plasma membrane through interactions between tyrosine-based motifs (Bonifacino and Dell'Angelica, 1999; Kirchhausen, 1999), which initiate clatherin nucleation into a polygonal ring (Ehrlich et al., 2004). Clatherin is comprised of 3 heavy chains and 3 light chains and can bind to the clustered μ-subunits

of AP-2 (Ohno et al.,1995; Boll et al., 1996; Bonifacino and Dell'Angelica, 1999; Schmid et al., 2006), leading to clathrin lattice formation and curvature of the membrane. Amphiphysin dimerizes through its N-terminal region with the heavy chain of clathrin and the central region of AP-2. (Takei et al., 1999) Dimerization causes recruitment of dynamin (GTPase) to the SH3 domain of amphiphysin via its proline-rich domain (Takei et al., 1999; Sever, 2002; Praefcke and McMahon, 2004; Kruchten and McNiven, 2006), and constriction of the clathrin-coated vesicle from the plasma membrane. It has also been shown that PI(4,5)P_2-to-PI4P conversion via Synaptojanin-1, a phosphoinositide phosphatase, may interact with dynamin when the curvature of the membrane is at its highest constriction (Ferguson et al.,2009; Mettlen et al., 2009; Praefcke and McMahon, 2004), which may aid in detachment (Chang-Ileto et al., 2011). Once the clathrin-coated vesicle is free of the plasma membrane, Hsp70 and its co-chaperone auxilin aid in removal of the clathrin-coat (Schlossman et al., 1984; Chappell et al., 1986; Sousa and Lafer, 2006). Auxillin binds to clatherin-coated lattice at vertex points where the 3 triskelions meet, at the α-appendage domain of AP-2, and with Hsp70 in its ATP-dependent conformation (Scheele, Kalthoff and Ungewickell, 2001) at the auxilin J domain (Holstein, Ungewickell, and Ungewickell, 1996). Upon hydrolysis of adenosine triphosphate (ATP) to adenosine diphosphate (ADP), the heat-shock protein 70 (Hsp70) and the co-chaperone auxilin catalyze clatherin-coat disassembly (Rapoport et al., 2008) exposing a primary endocytotic vesicle to the cytoplasm.

It is not clear how early endosomes (EE) are formed *de novo*, but it is postulated that the primary endocytotic vesicles from receptor-mediated endocytosis and non-clathrin

mediated endocytosis (Mayor and Pagano, 2007) fuse to form EE (Helenius and Marsh, 1982). An EE is comprised of tubular and vacuolar domains that function to sort incoming cargo that may be targeted for degradation, shuttle cargo to the recycling endosome via tubular domains, or take up cargo from the trans-golgi network (Donaldson and McPherson, 2009; Naslavsky et al., 2004). The EE has a slightly acidic environment (pH approximately 6.3-6.8) (Yamashiro and Maxwell, 1987), which is aided by ATP H^+ pumps (Al-Awqati, 1986) on the limiting membrane. Initial degradation can begin in the EE due to its slight acidity, which leads to the disassociation of the low-density lipoprotein (LDL) (Kornfeld & Mellman, 1989). The limiting membrane of an EE is composed of numerous elements that have specific functional attributes, (e.g. GTP Rab5), necessary in development of the EE to late endosome (LE) maturation, PI3P a phosphatidylinositol 3-kinase, and VPS34/p150 the effector for Rab5. Intraluminal vesicles (ILVs) also begin to form in the vacuolar domain of the LE by limiting membrane invagination. The surface of the limiting membrane facing the cytoplasm contains the endosomal-sorting complex required for transport (ESCRT), which recognizes ubiquitinated proteins inside of EE ILVs (Raiborg et al., 2008). As the EE continues to collect cargo from the plasma membrane, microtubules move the EEs to the perinuclear endosome where they can fuse to the LE. During movement along the microtubules, EE can also take-up material from the trans-golgi network, such as lysosomal hydrolases and integral lysosomal membrane proteins (LMPs), which get packaged into ILVs.

LEs are formed when Rab5 is converted to Rab7 (Rink et al., 2005), Rab GTPases are master regulators of endosome biogenesis, and are derived by the vacuolar domains of EEs. Upon fusion of the EE with LEs, the tubular domains are lost, but it is unclear as to how this occurs. Numerous processes must then be initiated to form a mature LE, including the Rab5 to Rab7 switch, ILV formations, lysosomal enzymes and membrane proteins accumulation, the pH of LE becomes more acidic (pH 6.0-4.9), phosphatidylinositol conversion of PI3P to $PI(3,5)P_2$, more circular morphology due to loss of tubular extensions, inhibition of fusion with the EE and recycling of receptors with the plasma membrane, microtubule restrictions leading to perinuclear sequestration, changes in ion environment and temperature, and density alteration (Huotari and Helenius, 2011). ILVs are known to contain cargo that will either enter the lysosome to be degraded and accumulate ESCRTs, or contain ubiquitinated cargo destined for lysosomal degradation. Once LEs mature, they fuse with the lysosome to form an endolysosome. As a lysosome has a pH below 5, lysosomal hydrolases contained in the ILVs are released and the degradation of cargo commences. During the endosomal maturation process many different vesicles are created, each maintaining a distinct function. Recently, more emphasis is being placed on understanding the function these vesicles have in intracellular and extracellular environments.

CELL SECRETED VESICLES

LE is also known as multivesicular bodies (MVBs) (Sotelo et al., 1959; Novikoff, Essner and Quintana, 1964). MVBs range in size from 50nm-1000nm in size and their morphology is similar to LE, except tubular extensions of the EE are removed and they

are circular in shape. MVBs are either targeted to the lysosome for degradation of ILV cargo, or some fuse with the plasma membrane and dispel their contents into the extracellular environment. The latter MVB mode of secretion was discovered via studying transferrin receptor fate in sheep and rat reticulocytes as they matured (Pan, Teng and Wu., 1985; Harding, Heuser J and Stahl, 1983), and has been implicated in various cell types including but not limited to, B lymphocytes, dendritic cells, T cells, epithelial cells reticulocytes, glioblastoma cancer cells, and ovarian tumor environments. (Raposo et al., 1996; Skokos et al., 2001; Escola 1998; Thery et al., 1999, Zitvogel et al., 1998; Thery et al., 2001; van Niel 2001; Skog et al., 2008; Keller et al., 2009). Unfortunately, the molecular signature defining the fate of these two populations of MVB has yet to be discovered.

Another important secretory vesicle that resides in the MVB is the accumulated ILV. ILVs are a vital part of endosomal maturation and have a different membrane composition than the limiting membrane of the LE. ILVs do not contain lysosomal-associated membrane proteins (LAMPs), therefore they cannot aid in receptor signaling with ligands restricting activation of receptors within ILVs. ILVs that enter the extracellular environment as MVBs and fuse with the plasma membrane are called exosomes. Exosomes are endosome-derived organelles 30-100nm in size. They are derived from MVBs that are destined to fuse with the plasma membrane and have a unique membrane that differs from the MVB, but mirrors the ILV membrane molecular composition (Raposo et al., 1996; Escola et al., 1998; Thery et al., 1999). Evidence for similarity between membranes of ILVs and exosomes was provided by studies of the

trafficking of MHC class II molecules in which live cell fusion of green fluorescent protein labeled MHC class II molecules were loaded into the ILVs of MVB (Wubbolts et al., 1996); MHC class II molecules were also gold-labeled and found internalized within exosomes (Raposo et al., 1996).

Some common proteins found in exosome membranes include annexins and Rab GTPases, which interact with the membranes of target cells to initiate fusion events (Valapala and Vishwanatha, 2011), ESCRT (endosomal sorting complex required for transport) proteins (Stoorvogel et al., 2002; Trajkovic et al., 2008), tetraspanins (CD81, CD63, CD9) (Pols and Klumperman, 2008; Rana and Zöller, 2011), and heat shock proteins (HSP60, HSP70, HSP90) (Johnson and Fleshner, 2006; Evdonin et al., 2006; Johnstone, 2006). It is noteworthy that CD63 is enriched approximately 7-fold in ILVs as compared to the limiting membrane of the MVB (Escola et al., 1998), making CD63 a valuable biomarker of exosomes (Pols and Klumperman, 2008).

Although ILVs mirror exosomes, the exact biogenesis process of exosomes has yet to be discovered. Exosomes contain ESCRTs (Stoorvogel et al., 2002; Trajkovic et al., 2008) that function in numerous ways during endosome maturation and ESCRT-0, -I, -II, and –III can all recognize ubiquitinated cargo. ESCRT-0 has two ubiquitin binding sites, Hrs and STAM proteins that will covalently bind ubiquitinated cargo (McCullough et al., 2006; Raiborg et al., 2008; Berlin, Schwartz and Nash, 2010; Morita, 2012), ESCRT-I and –II are involved in endosomal ILV intravasation (Boura et al., 2012; Morita, 2012), and ESCRT-III is involved in the abscission of the ILV from the MVB

(Wollert et al, 2009; Morita, 2012). Exosomes also contain cholesterol, sphingolipids, PI3P, and bis(monoacylglyceryl)phosphate/ lysobisphosphatidic acid (BMP/LBPA) (Kobayashi et al., 1998) in their membrane, and they promote acid sphinogomyelinase to convert sphinogomyelin to ceramide, a lipid molecule (Kolter and Sanhoff, 2005). Ceramide is necessary for budding of ILVs within the MVB (Trajkovic et al., 2008); therefore, it was postulated that ceramide might be important in the biogenesis of exosomes (Marsh and van Meer, 2008). They also report that ceramide generated on the cytosolic side of the membrane accumulated lipid microdomains, leading to invagination of ILVs, independent of the ESCRT machinery. In 2012, an alternate ESCRT dependent pathway that utilized ESCRT machinery to target certain MVB for fusion with the plasma membrane or the lysosome (Baietti et al., 2012). As the EE matures into a LE (also known as a MVB), syndecan (transmembrane receptor that preferably target G-protein coupled receptors) can be incorporated into the limiting membrane. Syntenin contain a PDZ (postsynaptic density 95, PSD-85; discs large, Dlg; zonula occludens-1, ZO-1) domain and can bind to transmembrane domains of syndecan allowing ALD-2-interacting protein X (ALIX), a protein involved in the endosomal lysosomal system, to bind to Syntenin via LYPX(n)L amino acid motifs thereby recruiting ESCRT-III to form an ILV (Baietti et al., 2012).

Exosomes contain bioactive materials, including mRNAs, miRNAs, and proteins (Valadi et al., 2007). Numerous cell types secrete exosomes, which can be isolated from culture medium via differential ultracentrifugation methods (Rani et al., 2011). Exosomes have been shown to circulate in biological fluids such as urine (Pisitkun et al., 2004), saliva

(Gonzalez-Begne et al., 2009) plasma (Caby et al., 2005), epididymal fluid (Gatti et al., 2005), amniotic fluid (Keller et al., 2007), follicular fluid (da Silveria et al., 2012), malignant and pleural effusions of ascites (Andre et al., 2002), bronchoalveolar lavage fluid (Torregrosa et al., 2012), synovial fluid (Sternjak et al., 2002) and breast milk (Admyre et al., 2007). Recently, tumors have been shown to release exosomes containing tumorigenic factors (Taylor and Gercel-Taylor, 2008). Further exploration of cancer specific exosomes has the potential to identify cancer-specific biomarkers. Exosomes make attractive candidates for understanding transcriptional and translational effects of genes and miRNAs, as well as elucidating how tumor cells communicate with non-tumor cells thereby contributing to metastatic disease.

CONCLUSION

In summary, ovarian cancer is a deadly disease in women, especially for those who relapse after treatment, a sobering reality due to a lack of diagnostic markers for uncontrolled proliferation and metastatic progression. In this regard, it is essential to study the regulatory mechanisms of how genes and miRNAs communicate their message from a tumor cell to a non-tumor cell. LIN28A, a negative regulator of *let-7* miRNAs, is highly expressed in ovarian cancer patients and is associated with advanced human malignancies (Viswanathan et al., 2009). Further, ovarian cancer has been shown to release exosomes containing tumorigenic factors (Taylor and Gercel-Taylor, 2008). The current study tests the central hypothesis that ovarian cancer secreted exosomes contain mRNAs and miRNAs that induce changes in gene expression and phenotype of target cells. I postulate that LIN28A plays an important

role in ovarian tumorigenesis by relaying factors via secreted exosomes. Results reported here will inform future investigations into how to prevent tumor exosomes from targeting cells, and/or how to use exosomes as delivery vehicles of cancer drugs to targeted cells.

CENTRAL HYPOTHESIS

Ovarian cancer cell-secreted exosomes contain factors that can induce changes in gene expression and cell phenotype in target cells (Figure 4).

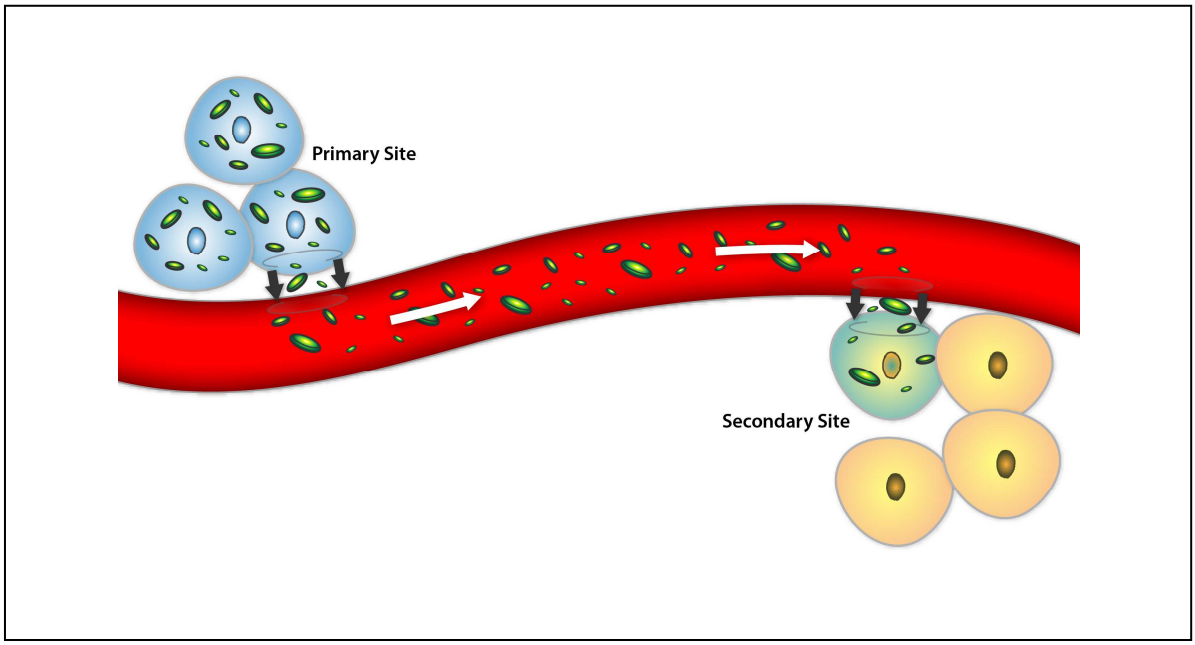

Figure 4: Central Hypothesis

AIM 1: Determine the presence of pluripotency factors and miRNAs in more aggressive ovarian cancer cells versus less aggressive ovarian cancer cells.

AIM 2: Determine the presence of LIN28 and let-7 miRNAs in aggressive and less aggressive ovarian cancer cell-secreted exosomes, and if exosomes taken up by HEK293 cells induce changes in gene expression and cell phenotype.

AIM 3: Identify RNA signatures in ovarian cancer cell-secreted exosomes from more aggressive cancer cells (IGROV1) versus less aggressive cancer cells (OV420).

CHAPTER III: IDENTIFICATION OF ENDOGENOUS PLURIPOTENCY FACTORS AND MICRORNAS IN OVARIAN CANCER CELLS

SYNOPSIS

Epithelial ovarian cancer (EOC) is the most lethal gynecological malignancy worldwide primarily due to the lack of early biomarkers, vague symptoms resulting in a late diagnosis, and persistence of dormant, drug-resistant cancer cells. A select set of pluripotency factors, necessary to create induced-pluripotent cells, are studied in many cancers. However, little is known about these factors in ovarian cancer cells. In this study we examined the presence of pluripotency factors and miRNAs in a more aggressive ovarian cancer cell line (IGROV1) versus a less aggressive ovarian cancer cell line OVCA 420 (OV420). We identified *LIN28A, POU5F1*, and *HMGA2* levels that were increased ($p<0.03$) in IGROV1 cells compared to OV420 cells. We found MYC was higher ($p<0.03$) in OV420 cells compared to IGROV1 cells. Additionally, the MYC-regulated miRNA-*17/92 cluster (miR-17, miR-19a, miR-19b, miR-20a,* and *miR-92a)* was significantly higher in OV420 cells. Immunofluorescence demonstrated LIN28A was present in the cytoplasm and nucleus of IGROV1 cells, and faintly detected in the cytoplasm in OV420 cells. Finally, using chromatin immunoprecipitation assay, we demonstrated TFAP2C binding sites are present in the LIN28A promoter region and revealed it could bind these sites. This study can lead to future exploration of pluripotency factors and miRNAs and their role in metastasis.

INTRODUCTION

Pluripotency factors LIN28A, POU5F1 and SOX2 are involved in reprogramming somatic cells into pluripotency cells in ES cells (Takahashi and Yamanaka, 2006). Additionally, LIN28A and POU5F1 are co-expressed and upregulated in ovarian tumors (Peng et al., 2010) suggesting aggressive cancer cells have increased levels of LIN28A and POU5F1. Also TFAP2C, POU5F1, and serum CA-125 can be used to distinguish malignant ovarian germ cell tumors from normal ovarian tissue (Salonen et al., 2008), but the role of TFAP2C in epithelial ovarian cancer is not understood. Furthermore, the role and regulatory effect of these pluripotency factors and miRNAs in ovarian cancer is still unclear.

In the past decade, investigations focused on determining the function of protein-coding genes in human cancers (Calin et al., 2006; Lu et al., 2005), but more recently small non-coding RNAs called miRNAs, are beginning to be studied. MicroRNAs are approximately 22 nucleotides (nts) in length and regulate gene expression in a post-transcriptional manner by binding to target regions in the 3' UTR of mRNA (Landi et al., 2011). In 2002, *miR-15* and *miR-16* was found down-regulated in chronic lymphocytic leukemia (Calin et al., 2002), which led researchers to begin to explore the role of miRNA regulation in cancer.

In ovarian cancer, *let-7s* are tumor suppressor miRNAs that target KRAS, MYC and HMGA2 (Bussing, Slack and Grosshans, 2008) and regulate cell proliferation, differentiation, and apoptosis (Johnson et al., 2007; Selbach et al., 2008). Assessing the

relative levels of these and other miRNAs in ovarian cancer cells that may be associated with pluripotency factors LIN28A, HMGA2, TFAP2C, MYC and POU5F1 can give us insight in the development of epithelial ovarian cancer.

LIN28A, found on chromosome 1 in humans, is an evolutionary conserved RNA binding protein, which negatively regulates mature *let-7* miRNA expression in embryonic stem cells (Newman, Thomson and Hammond, 2008), trophoblast stem (TS) cells (Seabrook et al., 2013), and cancer tumors (Zhong et al., 2010; Peng et al., 2010). LIN28A is also increased in advanced ovarian malignancies (Viswanathan et al., 2009). Many different miRNAs are aberrantly expressed in ovarian cancer and recently human ovarian cancer cells were found to contain distinct miRNA signatures (Iorio et al., 2007). Therefore, elucidating the role of LIN28A and miRNAs in cancer cells is necessary to understand EOC development and progression.

TFAP2C is a transcription factor implicated in ovarian cancer, which binds the palindromic consensus sequence, 5-GCC(N3)GGC-3 (Williamson et al., 1996), and is upregulated in advanced ovarian cancers (Odegaard et al., 2006). It is unknown if these conserved target binding sites are present in the promoter region of LIN28A.

Recently, transcription factor HMGA2 was found overexpressed in individuals with high-grade serous carcinoma (Mahajan et al., 2010), and *let-7/miR-98* family is a negative regulator of HMGA2 (Malek et al., 20008). *MiR-200c* and *miR-141* are localized to the same region of HMGA2 on chromosome 12p13.31 (Iorio et al., 2007), and their

expression is also upregulated in ovarian cancer. MicroRNA *let-7* targeting HMGA2 in ovarian cancer is a promising target in ovarian cancer treatment.

Finally, POU5F1 is a POU-family transcription factor that is found in pluripotent cells of the ICM and primordial germ cells (PGCs) during development of an embryo (Pesce and Scholer, 2001) belonging to the octomer-binding protein family. Recently, LIN28A was shown to bind directly to POU5F1 mRNA (Qiu et al., 2010). Additionally, in a subpopulation of ovarian cancer tumor cells LIN28A and POU5F1 were co-expressed in tumors that correlated with advanced ovarian tumor grade (Peng et al., 2010). With suppression of these two transcription factors, cell viability is decreased. Together these studies indicate POU5F1 and LIN28A may have a synergistic role in ovarian cancer development. Therefore, assessing the relative levels of both these factors in a more aggressive versus a less aggressive cancer line may provide insight in determining what factors are involved in high-grade EOC tumorigenesis.

The purpose of this study was to assess expression of LIN28A, HMGA2, TFAP2C, MYC and POU5F1 and miRNAs found in IGROV1 (more aggressive) and OV420 (less aggressive) EOC cell lines. IGROV1 cell lines are a mix of endometrioid and serous cell types and OV420 are mostly serous. The IGROV1 cell line was isolated from a 47-year-old woman with Stage III epithelial ovarian cancer and resembles cells in the primary tumor. Interestingly, IGROV1 cells can induce peritoneal carcinomatosis in SCID mice after xenotransplantation leading to rapid tumor formation and cell growth (Benard et al., 1985), making it an attractive cell line to study metastasis. OV420 cells, also known as

OVCA 420 cells, were originally isolated from ascites and tumors from a late stage ovarian cancer patient (Tsao et al., 1995) and do not form tumors in (Lee et al., 2000). We sought to compare relative levels of these pluripotency factors and miRNAs in these EOC cell lines in order to identify differences between less aggressive and more aggressive EOC cells.

MATERIALS AND METHODS

Cell lines and culture conditions

IGROV1 and OV420 human epithelial cell lines were generously provided by Dr. Monique Spillman (University of Colorado Denver) and were cultured in Roswell Park Memorial Institute (RPMI 1640) medium with L-glutamine 1X (Cellgro, 10-040-CV) and supplemented with 10% fetal bovine serum (FBS) (Atlas Biologicals, F-0500-D) and 1% antibiotic-antiomycotic solution (Cellgro, 30-0004-Cl). All cell lines were cultured in a standard humidified incubator at 37°C in a 5% CO_2 atmosphere.

Chromatin immunoprecipitation assay (ChIP)

Chromatin immunoprecipitation (ChIP) was performed as described in Dahl and Collas (2008) with minor modifications. Briefly, cells were grown on 10cm plates to approximately 80-90% confluence and washed with ice-cold 1X DPBS and proteins cross-linked to DNA in 37% formaldehyde on ice for 8 minutes. Fixation was stopped by quenching samples in 125mM Glycine for 5 minutes. Samples were washed in 1X DPBS and then lysed in 120μL buffer (50mM Tris-HCl pH 8.0, 10mM EDTA, 1% SDS, 1X protease inhibitor mix and 1mM PMSF) for 30 minutes on ice. Lysed cells were

sonicated for 10 minutes on high (30 seconds off and 30 seconds on) using a Bioruptor (Diagenode, NJ) to get approximately 500bp DNA sized fragments. RIPA ChIP buffer was added (10mM Tris-HCl pH7.5, 140mM NaCl, 1mM EDTA, 0.5mM EGTA, 1%(v/v) Triton X-100, 0.1%(w/v) SDS, 1x protease inhibitor mix and 1mM PMSF) and samples centrifuged for 10 minutes at 12,000 xg at 4°C. Supernatant was collected and RIPA ChIP buffer added. Input DNA was separated from the sample prior to immunoprecipitation. Immunoprecipitation was performed using 2μg of TFAP2A antibody (Santa Cruz Biotechnologies, sc-6312), 2μg of TFAP2C antibody (Santa Cruz Biotechnologies sc-31935), and 2μg of mouse IgG (Vector Laboratories, I-2000) and the Active Motif ChIP-IT Express Chromatin Immunoprecipitation Kit (Active Motif, 53018). PCR analysis was performed using primers that targeted potential TFAP2C binding sites (GCC(N_3)GGC) in LIN28A promoter region in the 5"UTR located at -186 to -51 (151bp size), Forward primer: 5'-caccccagaggtgtcagaga-3', Reverse primer, 5'-cttttcaaaggctcccaaattc-3'). Input DNA was analyzed for the presence of the LIN28A promoter sequences, as a positive control using the same primers, and a nonspecific mouse IgG antibody was used as a negative control.

RNA isolation

Total RNA was extracted from confluent cells and lysed with 300uL of MirVana lysis binding buffer and 30uL of miRNA homogenate additive. RNA was isolated as per manufacturer's instructions using MirVana miRNA isolation kit (Ambion, AM1561) and resuspended in 30μL of RNase/DNase-free water. Once total RNA was isolated from cells, DNase-free™ DNase Treatment and Removal kit (Ambion, AM1906) was used on

all samples to eliminate genomic DNA contamination. RNA quality and concentration were assessed using the NanoDrop® ND-1000 spectrophotometer (NanoDrop Technologies, USA). Total RNA absorbance of 260/280 was measured and samples with RNA purity between 1.7-2.2 were used for experiments. Samples were stored at -80°C until qRT-PCR was performed.

*Quantitative real-time PCR (*qRT-PCR)

Taqman qRT-PCR was performed from total RNA (see above) where 1μg of cDNA was made for cells using qScript™cDNA supermix (Quanta Biosciences, 95047-100) as per manufacturer's instructions. cDNA was diluted to a final concentration of 10ng/rxn for cells and 20ng/rxn for exosomes and combined with 2x Ssofast™ Probe Supermix (Bio-Rad, 172-5230) and 20x Taqman Assay Mix (Applied Biosystems). The 20X Taqman Assay mix Probes (Applied Biosystems) used for this study were as follows: LIN28A (Hs00702808_s1), cMYC (Hs00905030_m1), POU5F1 (Hs00999632_g1), TFAP2C (Hs00231476_m1), HMGA2 (hs00971725_m1), GAPDH (H99999905_m1). qRT-PCR was performed using the Lightcycler 480 Real Time PCR System (Roche Applied Science). The cycling parameters were initial denaturation for 30 seconds at 95°C followed by 45 cycles of repeating denaturing at 15 seconds at 95°C and annealing for 30 seconds at 60°C with a final cooling cycle for 5 minutes at 37°C. Data was normalized using the housekeeping gene GAPDH and relative levels were calculated using the comparative Ct method to obtain $2^{-\Delta Ct}$ values. Each of the four samples was

run in duplicate with reverse transcriptase negative controls, non-template controls, and experiments were repeated at least twice. Statistical analysis was determined by a two-sided unpaired Student's t-test with p-value <0.05.

miRNA qRT-PCR was performed from total RNA (see above) where 1μg of cDNA was made for cells using the miScript RT Kit supermix (Qiagen, 218161) as per manufacturer's instructions. cDNA was diluted to a final concentration of 1.5ng/rxn for cells and exosomes and combined with 2x QuantiTech® SYBR green PCR master mix, 10X miScript Universal Primer (miScript PCR Green PCR Kit, Qiagen, 218075) and 10uM of primer of interest (Table 1, List of primers and sequences). qRT-PCR was performed using the Lightcycler 480 Real Time PCR System (Roche Applied Science). The cycling parameters were initial denaturation for 15 minutes at 95°C followed by 45 cycles of repeating denaturing at 15 seconds at 95°C, annealing for 30 seconds at 55°C, elongation for 30 seconds at 72°C with a final cooling cycle of 30 minutes at 40°C. Melt curves were also calculated to ensure single miRNA amplicons were produced using the following cycling parameters: 95°C for 5 seconds and 65°C for 1 minute. Data was normalized using the snRNA (U6), and relative levels were calculated using the comparative Cp method. Four samples from each cell line were run in duplicate with reverse transcriptase negative controls, non-template controls, and experiments were repeated. Statistical analysis was determined by a two-sided unpaired Student's t-test with P<0.05.

Table 1: List of miRNA sequences. This table represents the human miRNA sequences used for qRT-PCR experiments. These sequences were obtained from miRBase program.

miRNA primers	Sequence (5'-3')
hsa-let-7a-3p	CUAUACAAUCUACUGUCUUUC
hsa-let-7-f1-3p	CUAUACAAUCUAUUGCCUUCCC
hsa-miR-9	UCUUUGGUUAUCUAGCUGUAUGA
hsa-miR-17	CAAAGUGCUUACAGUGCAGGUAG
hsa-miR-18a	UAAGGUGCAUCUAGUGCAGAUAG
hsa-miR-19a	UGUGCAAAUCUAUGCAAAACUGA
hsa-miR-19b	UGUGCAAAUCCAUGCAAAACUGA
hsa-miR-20a	UAAAGUGCUUAUAGUGCAGGUAG
hsa-miR-22	AAGCUGCCAGUUGAAGAACUGU
hsa-miR-30a	UGUAAACAUCCUCGACUGGAAG
hsa-miR-30b	UGUAAACAUCCUACACUCAGCU
hsa-miR-30c	UGUAAACAUCCUACACUCUCAGC
hsa-miR-30d	UGUAAACAUCCCCGACUGGAAG
hsa-miR-30e	UGUAAACAUCCUUGACUGGAAG
hsa-miR-31	AGGCAAGAUGCUGGCAUAGCU
hsa-miR-92a	UAUUGCACUUGUCCCGGCCUGU
hsa -miR-200a	UAACACUGUCUGGUAACGAUGU
hsa-miR-200b	UAAUACUGCCUGGUAAUGAUGA
hsa-miR-200c	UAAUACUGCCGGGUAAUGAUGGA
hsa-miR-125a-3p	ACAGGUGAGGUUCUUGGGAGCC
hsa-miR-125a-5p	UCCCUGAGACCCUUUAACCUGUGA
hsa-miR-125b	UCCCUGAGACCCUAACUUGUGA
snRNA (U6)	CGCAAGGAUGACACGCAAAUUC

Immunofluorescence assay

IGROV1 and OV420 cells were grown to approximately 80-90% confluence. Cells were trypsinized from 10cm cell plates (Thermo Scientific Nunc) and 1,000 cells were seeded on glass chamber slides (Thermo Scientific Nunc) and grown for 24 hrs. Cells were fixed using 4% PFA (USB Corporation) for 15 min and then treated with Liberate Antibody Binding (L.A.B.) solution (Polysciences Inc., 24310-500) for 15 min to expose the epitopes. After three 3 min washes with 1X DPBS (Thermo Scientific, SH30028FS) cells were blocked with 10% goat serum (Vectastain ABC Kit, PK-4000). Rabbit LIN28A

(1:100) (Abcam 63740) primary antibody was added and cells were stored overnight at 4°C. After 24 hours, cells were washed 3 times with 1X DPBS (Thermo Scientific, SH30028FS) and incubated with the secondary antibody goat anti-rabbit Rhodamin IgG Alexa Fluor® 594 (1:100) (Invitrogen, A11037) for 45 min at room temperature in the dark. After three 3 min washes with DPBS (1x) (Thermo Scientific) cells were treated with 1mg/mL of DAPI for 10 min in the dark and then washes were repeated. Controls for this experiment were treated using the same protocol, but omitting the primary antibody. Slides were stored at 4°C, and imaged 24 hours later on the Olympus FSX100 Bio Imaging Navigator using the FSX100 software. Each picture is taken at 40X magnification.

RESULTS

LIN28A, TFAP2C, HMGA2, POU5F1, and MYC levels in ovarian cancer cell lines

In order to examine the presence of pluripotency factors in ovarian cancer cell lines we first determined the relative levels of *LIN28A, TFAP2C, HMGA2, POU5F1,* and *MYC* mRNA in these cell lines. IGROV1 cells had significantly higher levels ($p<0.03$) of *LIN28A, POU5F1, and HMGA2* compared to OV420 cells (Figure 5). In contrast, OV420 cells had significantly higher levels ($p<0.03$) of *MYC* (Figure 5) compared to IGROV1 cells. There was no significant difference between the cells lines for *TFAP2C* and it was generally present at low levels.

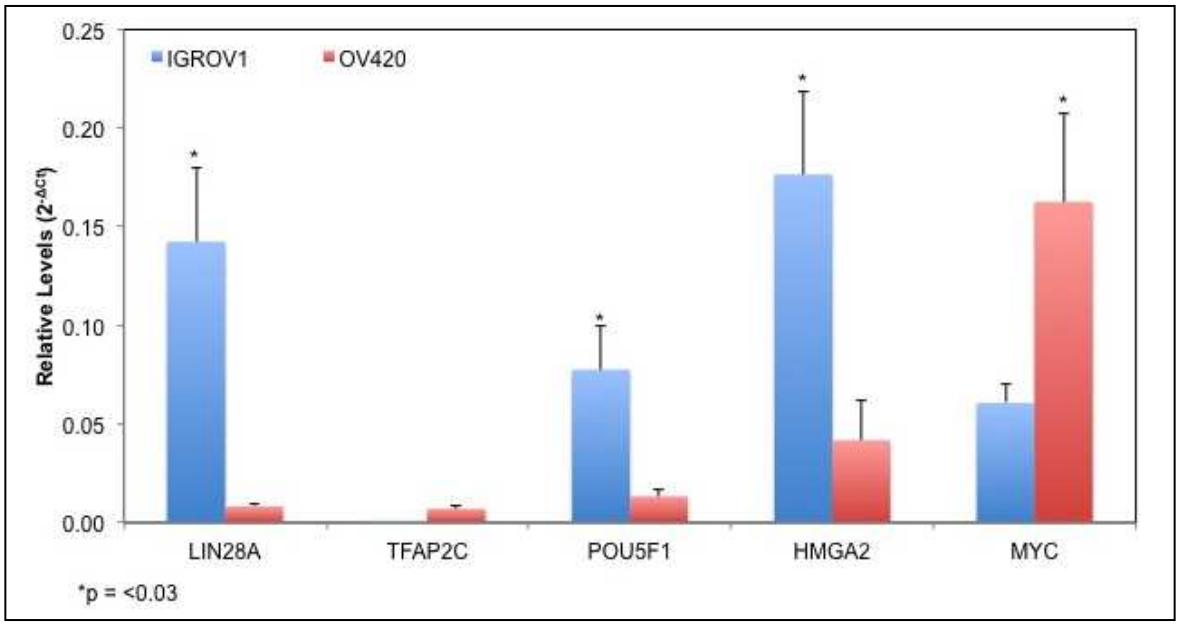

Figure 5: *LIN28A, TFAP2C, POU5F1, HMGA2, and MYC* levels in ovarian cancer cell lines. Data was normalized against the housekeeping gene GAPDH. Asterisk indicates a p-value <0.03.

miRNA levels in ovarian cancer cell lines

To evaluate the expression levels of various miRNAs in IGROV1 and OV420 cells, qRT-PCR was used. Data revealed significantly lower levels ($p<0.05$) in the isoforms of the miRNAs let-*7a-3p* and *let-7f-1-3p* isoforms in IGROV1 cells compared to the OV420 cells (Figure 6).

MicroRNAs *miR-17, miR-19a, miR-19b, miR-20a, miR92a,* which are part of the *miR-17-92* cluster, are lower ($p<0.05$) in IGROV1 cells compared to OV420 cells (Figure 6). Additionally, the *miR-200a, miR200b* and *miR-200c* isoforms, from the *miR-200* family of miRNAs, are lower ($p<0.05$) in IGROV1 cells compared to OV420 cells (Figure 6). *MicroRNA-9* was lower ($p<0.05$) in IGROV1 cells compared to OV420 cells (Figure 6) as well as m*iR-22, miR-31, miR-125a-3p, miR-125a-5p* (Figure 6).

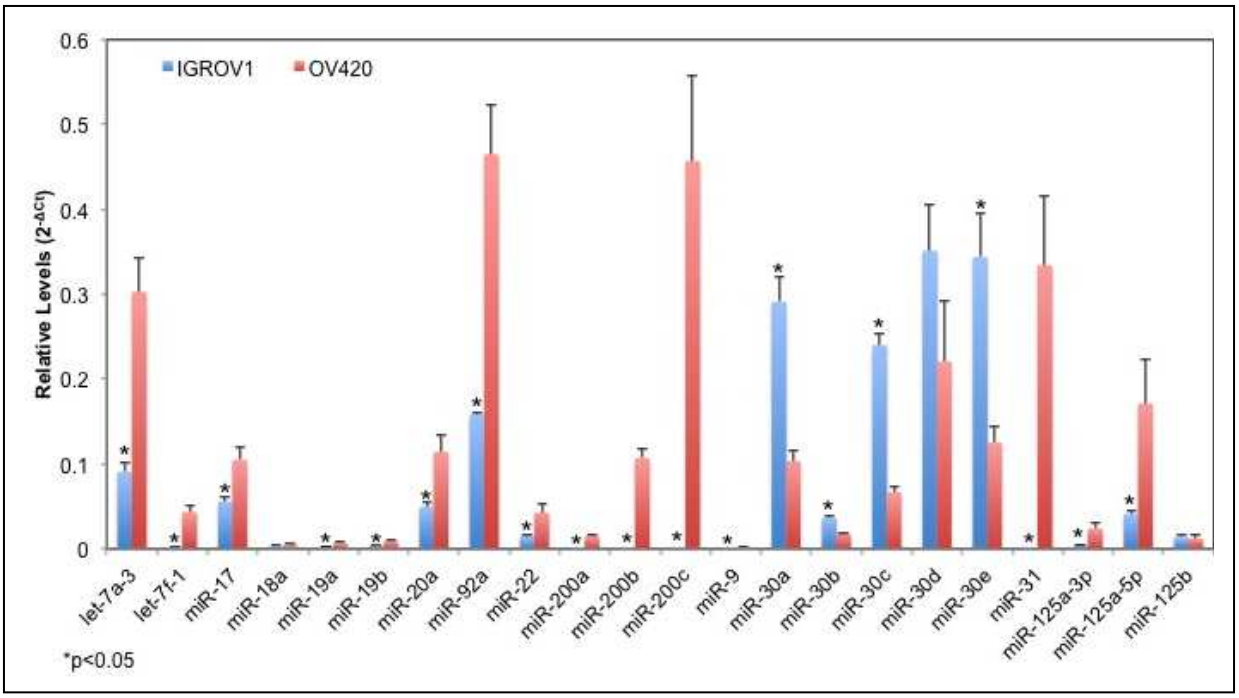

Figure 6: miRNAs levels in ovarian cancer cell lines. qRT-PCR Data was normalized against the U6 snRNA. Asterisk indicates a p-value <0.05.

Protein localization of LIN28A in ovarian cancer cells

Immunofluorescence was performed using IGROV1 and OV420 cells to determine LIN28A protein localization. The cytoplasm of OV420 cells was very faintly positive for LIN28A (Figure 7), while the cytoplasm and nuclear area of IGROV1 cells were positive for LIN28A (Figure 7).

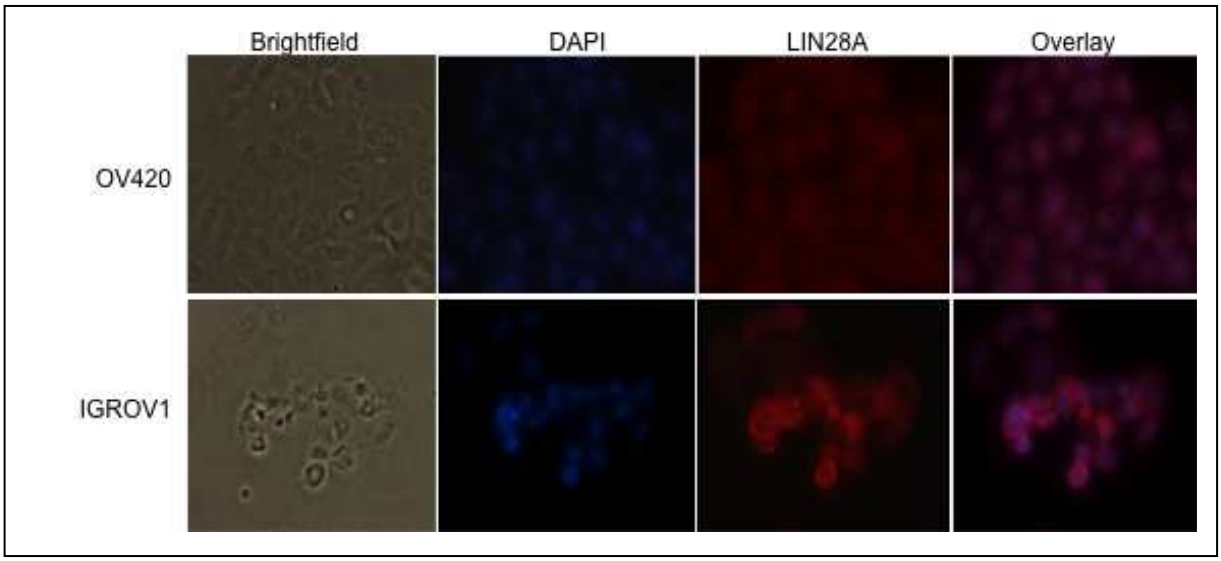

Figure 7: LIN28A in IGROV1 and OV420 ovarian cancer cells. Very low level of LIN28A protein localize to the cytoplasm in OV420 cells, while IGROV1 ovarian cancer cells have LIN28A protein localized to the nucleus and cytoplasm. Images were taken at 40X magnification. DAPI was used to stain the nucleus of the cells (blue) and red color indicate LIN28A.

Binding of TFAP2C to LIN28A promoter

Chromatin immunoprecipitation assay was performed on IGROV1 and OV420 cells to determine if TFAP2C can bind to binding sites (5'-GCC(N_3)GGC-3') in the promoter region of LIN28A. TFAP2A and TFAP2C can recognize the same target binding sequences. Antibodies against TFAP2A and TFAP2C were able to precipitate LIN28A chromatin fragments in IGROV1 and OV420 cells (Figure 8) indicating TFAP2A/TFAP2C binds to promoter region of LIN28A in IGROV1 and OV420 cells.

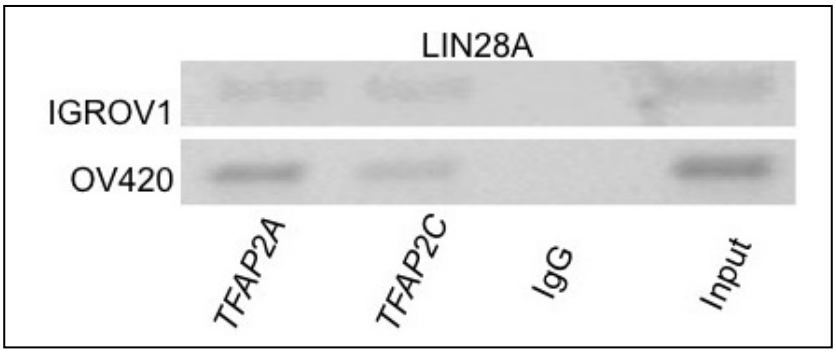

Figure 8: TFAP2A and TFAP2C bind recognition sites in the promoter regions of LIN28A in IGROV1 and OV420 cells.

DISCUSSION

In this study we sought to characterize the presence of pluripotency factors and a select group of miRNAs, (*let-7a-3p, let-7f-1, miR-9, miR-17-92 cluster, miR-22, miR-30 family, miR-31, miR-200 family, miR-125a-3p, miR-125a-5p,* and *miR-125b*) in IGROV1 (more aggressive) and OV420 (less aggressive) EOC cell lines. We performed mRNA profiling in IGROV1 and OV420 cells and showed higher levels of *LIN28A*, *POU5F1* and *HMGA2* in IGROV1 cells, suggesting the more aggressive tumorigenic nature of these cells, when injected into SCID mice are possibly due to high levels of these factors. It was previously described that LIN28A is found in high-grade ovarian carcinoma tumors (Viswanathan et al., 2009), and more recently that IGROV1 cells have high levels of LIN28A, which interacts directly with *let-7s* to inhibit mature *let-7* formation (Piskounova et al., 2011). These findings are consistent with our data. Furthermore, LIN28A co-expression with POU5F1 is associated with cancer stem cell subpopulations of patient tumor samples (Peng et al., 2010). Our data revealed IGROV1 cells have increased levels of both *LIN28A* and *POU5F1* suggesting that aggressive EOC cancer cells may have a subpopulation of cancer stem cells that are less differentiated. Moreover,

approximately 75% of high-grade serous ovarian carcinomas have high levels of *HMGA2* (Wu and Wei, 2013). Interestingly, we demonstrated OV420 cells have significantly higher levels of *MYC* compared to IGROV1 cells. A recent study evaluated the prognostic value of p53, p27, and C-MYC expression and found that 30% of patients with stages I-II had tumors displaying p53 negative, p27 negative and high levels of MYC (Skirnisdottir et al., 2011). Patients with these three expression results led to disease-free survival of 92% using tissue microarray and immuohistochemistry (Skirnisdottir et al., 2011). Although we did not test for p53 or p27 levels in IGROV1 or OV420 cells, our study confirms that *MYC* levels are significantly higher in the less aggressive EOC cell line OV420. Additionally, MYC was found significantly higher in the non-C5 tumors (Helland et al., 2011) suggesting MYC is specifically upregulated in a subtype of ovarian cancers. Overall, these data support previous findings that *LIN28A, POU5F1, HMGA2* are higher in more aggressive cancer cells and, to our knowledge, are the first to show *MYC* is higher in less aggressive OV420 cells.

MiRNA profiling was performed for *let-7a-3p, let-7f-1, miR-9, miR-17-92 cluster, miR-22, miR-30 family, miR-31, miR-200 family, miR-125a-3p, miR-125a-5p,* and *miR-125b*. The *let-7* family of miRNAs was selected because LIN28A interacts directly with the *let-7* family (Piskounova et al., 2011; Viswanathan et al., 2008; Peng et al., 2010; Lu et al., 2009), and all three pluripotency genes are targeted by the tumor suppressor *let-7* (Park et al., 2007; Helland et al., 2011; Sampson et al., 2007). We reported a significant decrease in miRNAs *let-7a-3p* and *let-7f-1* in the IGROV1 cells, which is consistent with a study that found *let-7a* was downregulated in ovarian cancer tissues compared to

human immortalized surface epithelial cells (Yang et al., 2008a). Also, *let-7f* was reported to be downregulated in ovarian cancer tissues compared to human ovarian epithelial cells (Dahiya et al., 2008) providing further support that *let-7* is lower in ovarian tumors. Moreover, HMGA2 and MYC interact with *let-7s* to inhibit mature *let-7* formation (Helland et al., 2011) indicating MYC and HMGA2 negatively regulate *let-7*. These results suggest high levels of *LIN28A* and *HMGA2* target *let-7* miRNAs leading to in lower levels of *let-7a* and *let-7f* in IGROV1 cells as well as low levels a *MYC* have high levels of *let-7a* and *let-7f.*

Another family of miRNAs that were significantly lower in IGROV1 cells was members of the miRNA-*17/92 cluster: miR-17, miR-19a, miR-19b, miR-20a,* and *miR92a.* The *miR-17/92* cluster is deregulated in human breast cancers (Hossain et al., 2006; Yu et al., 2008), is upregulated in 65% of lymphoma tumor samples and is known as an “oncomir” (He et al., 2005). We have demonstrated that IGROV1 cells have lower levels of miRNAs in this family, which seem contradictory to what has been demonstrated in other cancers (He et al., 2005; Volinia et al., 2006; Petrocca et al., 2008), however *miR-17/92* cluster exhibits a pleiotropic role. This cluster of miRNAs is differentially expressed depending on the cell type and its role has not been thoroughly explored in ovarian cancer. In our study, we found MYC to be significantly higher in OV420 cells as well as *miR-17, miR-19a, miR-19b, miR-20a, miR92a*. More importantly, it was found that C-MYC binds to the *miR-17/92* cluster (O’Donnell et al., 2005), indicating this cluster can be modified by MYC. Since IGROV1 cells do not have high levels of *MYC*, it

is possible that *miR-17, miR-19a, miR-19b, miR-20a, miR92a* are lower in IGROV1 cells because MYC is too low to regulate these miRNAs.

MiR-22 was lower in IGROV1 cells compared to OV420 cells. It has previously been reported that *miR-22* is downregulated in ovarian cancer tumor tissues (Wyman et al., 2009) and in late-stage ovarian cancer (Zhang et al., 2008b). Moreover, *miR-22* is downregulated in high metastatic ovarian cancer cells (SKOV3-ip) (Li et al., 2010).

Recent data suggests that *miR-30a/b/c* are significantly elevated in plasma samples from 42 women with serous epithelial ovarian cancer, and can be used to distinguish ovarian cancer patients healthy control subjects (Shapira et al., 2014). Also, *miR-30* is higher in stage III ovarian cancers that are resistant to platinum-based chemotherapy (Eitan et al., 2009). In this study, we demonstrated *miR-30a/b/c/e* is significantly higher in IGROV1 cells. Together these studies provide evidence that elevated levels of *miR-30* can be detected in late stage ovarian cancer cells and suggest a potential role of *miR-30* in ovarian cancer, although further examination is needed to confirm these results.

Another set of miRNAs examined were *miR-9, miR-22, miR-125a-3p, miR-125a-5p,* and *miR-31,* and they were significantly lower in IGROV1 cells. Additionally, p53 mutations are detected in malignant epithelial ovarian cancer of approximately 50% of patients (Wen et al., 1999) and loss of *miR-31* is associated with p53 pathway activation in serous ovarian cancer (Creighton et al., 2010). We also reported significantly lower

levels of *miR-125a* in IGROV1 cells. These two miRNAs (*miR-31* and *miR-125a*) were also detected at lower levels in ovarian cancer tumors (Iorio et al., 2007) and serous ovarian carcinoma (Nam et al., 2008), which is similar to our findings.

The final set of miRNAs assessed was the *miR-200* family. Higher levels of *miR-200c* were previously described as a positive indicator of overall survival in serous ovarian cancer patients (Nam et al., 2008). However, conflicting results exist as low levels of *miR-200c* and correlate with increased survival in miRNA profiles of epithelial ovarian cancer patients (Marchini et al., 2011). These data indicate a pleiotropic role for *miR-200c* in EOC. Our study found that *miR-200* family (miR-200a/b/c) was significantly lower ($p<0.05$) in IGROV1, which is similar to what Nam and colleagues described (2008). Additionally, the *miR-200* family is associated with regulating epithelial to mesenchymal transition (EMT) (Bendoraite et al., 2009; Koutsaki, Spandidos, and Zaravinos, 2014) suggesting *miR-200* found in IGROV1 cells may have a role in metastasis by regulating EMT.

In addition to characterizing pluripotency stem cell factors and miRNAs, we assessed subcellular localization of LIN28A in IGROV1 and OV420 cells due to increasing evidence that LIN28A may regulate let-7 miRNAs differently in human embryonic stem cells (Van Wynsberghe et al., 2011) and certain ovarian cancer cell lines, including IGROV1 cells (Piskounova et al., 2011). The mechanism by which LIN28A, and its homolog LIN28B, function in regulating *let-7* miRNAs was thought to work the same. However, recently it was discovered that LIN28A functions to inhibit precursor *let-7*

miRNAs in the cytoplasm, and LIN28B inhibits primary *let-7* miRNAs in the nucleus (Piskounova et al., 2011). IGROV1 cells have LIN28A localized predominantly to the cytoplasm, but are also found in the nucleus (Piskounova et al., 2011), which was confirmed in our study. Conversely, we also demonstrated that OV420 cells do not have LIN28A in the nucleus and very low levels are only found in the cytoplasm. LIN28A also was localized in the nucleus of human embryonic stem cells (Van Wynsberghe et al., 2011) and could bind primary miRNAs to inhibit their processing, (i.e. pre-miRNAs). This suggests LIN28A protein found in the more aggressive IGROV1 cells could play a dualistic role in regulating *let-7* miRNAs, as LIN28A is found in the cytoplasm as well as the nucleus. LIN28A upregulation could lead to further increases in LIN28A and *let-7* regulated targets (i.e., HMGA2), accelerating ovarian cancer development.

TFAP2A and TFAP2C are transcription factors required for embryonic development (Hilger-Eversheim et al., 2000) and are evolutionary conserved proteins. When Tcfap2a is mutated in mice models, it is embryonic lethal as the embryo fails to develop heart structures properly (Brewer et al., 2002); if Tcfap2c is knocked down in mice, the embryos fail to expand and hatch in the blastocyst stage resulting in embryonic death. (Choi et al., 2012a). Also, when Tcfap2a and Tcfap2c double null embryos were produced in mice, embryonic death occurred earlier (Winger et al., 2006). These studies indicate the TFAP2 family is important for mammalian development. Moreover, the role of TFAP2C in cancer progression is explored. For example, overexpression of TFAP2C has been correlated with invasive breast cancer (Gee et al., 2008) and more importantly, TFAP2C is upregulated in advanced stage ovarian carcinoma (Odegaard et

al., 2006). However, the role of TFAP2A and TFAP2C in epithelial ovarian cancer has yet to be elucidated. Upon analysis of the 5' UTR of the LIN28A promoter region, TFAP2A and TFAP2C binding sites (5'-GCC(N_3)GGC-3') were found; we postulated that TFAP2A and TFAP2C may bind to LIN28A in ovarian cancer cell lines. Our ChIP analysis revealed TFAP2A and TFAP2C can bind to the promoter region of LIN28A in IGROV1 and OV420 cells. To our knowledge this is the first time TFAP2A and TFAP2C have been studied in EOC cell lines, and our data suggest it is possible that TFAP2A and TFAP2C regulate LIN28A in IGROV1 and OV420 cells, but functional analysis has yet to be performed.

In conclusion, this study revealed pluripotency factors and miRNAs can be used to distinguish more aggressive (IGROV1) cells versus less aggressive (OV420) cells. Specifically, we identified IGROV1 cells have high LIN28A levels and OV420 cells have low LIN28A levels in ovarian cancer cells. We also found *MYC* displayed higher levels in OV420 cells and also that *miR-17, miR-19a, miR-19b,* and *miR-92a* levels were higher in OV420 cells. Furthermore, we demonstrated aggressive IGROV1 cells containing high LIN28A could play a dualistic role in regulating *let-7* miRNA maturation in the cytoplasm as well as the nucleus. Additionally, we determined TFAP2A and TFAP2C can bind to LIN28A promoter regions in IGROV1 and OV420 cells indicating an additional form of LIN28A regulation may exist through TFAP2A and TFAP2C binding. This study may lead to a better understanding of pluripotency factors and miRNAs in advanced ovarian cancer and potentially lead to functional analysis to determine the role pluripotency factors play in metastatic disease development.

CHAPTER IV: OVARIAN CANCER CELL-SECRETED EXOSOMES INDUCE INVASION AND MIGRATION

SYNOPSIS

Epithelial ovarian cancer is the most aggressive and deadly form of ovarian cancer, and is the most lethal gynecological malignancy worldwide therefore efforts to elucidate the molecular factors that lead to EOC are essential to better understanding metastatic disease. Recent studies reveal that tumor cells release cell-secreted vesicles called exosomes. Exosomes are endosome-derived vesicles (30-100nm) containing bioactive materials, including miRNAs that can be detected in the bloodstream and urine. Importantly, stem cell factor LIN28, a regulator of *let-7* miRNAs, is present in ovarian cancer cells. Moreover, the effect of EOC cancer cell-secreted exosomes on cells is not understood. Our preliminary data (Chapter III) revealed high LIN28 and low *let-7* miRNAs levels in aggressive IGROV1 human ovarian cancer cells compared to low LIN28 and high *let-7* miRNAs in less aggressive OV420 human ovarian cancer cells. LIN28 is a pluripotency stem cell factor that regulates let-7 miRNAs. We hypothesized that exosomes from more aggressive cancer cells (IGROV1) containing high LIN28 can be taken up by HEK293 leading to changes in gene expression and cell phenotype. Real-time PCR and Western blot analysis confirmed LIN28A expression levels were significantly higher ($p<0.05$), whereas isoforms of the *let-7* miRNA family were significantly lower ($p<0.02$) in aggressive IGROV1 cells. Furthermore, RT-PCR and real-time PCR demonstrated IGROV1 exosomes contain *LIN28A* and lower levels of *let-7b, let-7f,* and *let-7i* ($p<0.05$) compared to OV420 exosomes, respectively. IGROV1 cell-secreted exosomes are taken up by HEK293 cells and increased the relative levels of

45 genes related to epithelial to mesenchymal transition (EMT), including *TIMP1* (25-fold), *NOTCH1* (11-fold), *SNAI1 (SNAIL)* (7-fold), *(MMP9* (4-fold), and *ZEB1* (3-fold) and increased *miR-9*, a regulator of LIN28A. Also, we demonstrated increased invasion and migration ($p<0.04$) in HEK293 cells that have taken up IGROV1 secreted exosomes. Our study revealed exosomes secreted by IGROV1 cells that contain high LIN28A are taken up by HEK293 cells and induce changes in EMT as well as invasion and migration. Elucidating the molecular and phenotypic effects ovarian cancer cell-secreted exosomes have on target cells will lead to greater understanding and insight into cancer metastasis and tumor development.

INTRODUCTION

Epithelial ovarian cancer (EOC) is the most lethal gynecological malignancy worldwide due to its asymptomatic nature and is often detected in late stages when metastasis has occurred (Jemal et al., 2006). In ovarian cancer, tumor cells release small cell-secreted vesicles called exosomes (Valadi et al., 2007; Al-Nedawi et al., 2008; Skog et al., 2008). Exosomes are endosome-derived vesicles (30-100nm) that contain bioactive materials (including mRNAs and miRNAs) are present in the bloodstream (Taylor and Gercel-Taylor, 2008) as well as urine (Pisitkun et al., 2004), saliva (Gonzalez-Begne et al., 2009) plasma (Caby et al., 2005), epididymal fluid (Gatti et al., 2005), amniotic fluid (Keller et al., 2007), follicular fluid (da Silveria et al., 2012), malignant and pleural effusions of ascites (Andre et al., 2002), bronchoalveolar lavage fluid (Torregrosa et al., 2012), syovial fluid (Sternjak et al., 2002) and breast milk (Admyre et al., 2007). Tumor

cell secreted exosomes have also been implicated in increased proliferation (Skog et al., 2008) and invasion (Ginestra et al., 1998; Clayton et al., 2007; Friel, 2010).

MicroRNAs are abundantly expressed in human cancers (Zhong, Coukos and Zhang, 2012; Farazi et al., 2013) and are non-protein coding RNAs that function as post-translational regulators by binding to the 3'UTR of target mRNAs (Cai et al., 2009). They are evolutionally conserved and are approximately 22 nucleotides in length. Upon binding to the 3'UTRs of target mRNAs, translational inhibition occurs in the form of mRNA target cleavage or translational repression. There are unique miRNA signatures in human cancers (Calin and Croce., 2006), including ovarian cancer (Iorio et al., 2007). Furthermore, miRNAs can alter signaling pathways involved in the hallmarks of cancer (Ruan, Fang and Ouyang, 2009).

High LIN28A levels are associated with advanced human malignancies (Viswanathan et al., 2009) and LIN28A is often expressed in ovarian tumors (Zhong et al., 2010; Peng et al., 2010). There are two paralogs of LIN28, LIN28A and LIN28B. Both contain a cold shock domain (CSD) and a CCHC-zinc finger RNA binding domain and regulate *let-7* inhibition by CSD binding to the NGNGAYNNN (N=any base and Y=pyrimidine) sequence on the terminal loop of *let-7* and the CCHC-zinc finger RNA binding domain binding to the GGAG sequence on the *let-7* terminal loop (Nam et al., 2011). The linker between the CSD and the CCHC-zinc finger allow for binding of all twelve *let-7* miRNA family members.

The overall goal of this study was to test the hypothesis that exosomes from high LIN28 expressing, aggressive ovarian cancer cells (IGROV1) can be taken up by HEK293 cells leading to changes in gene expression that confer a more aggressive cell phenotype, while exosomes from low LIN28 expressing, less aggressive ovarian cancer cells (OV420) cannot.

MATERIALS AND METHODS

Cell Lines and Culture Conditions

IGROV1 and OV420 human epithelial cell lines were generously provided by Dr. Monique Spillman (University of Colorado Denver) and were cultured in Roswell Park Memorial Institute (RPMI 1640) medium with L-glutamine 1X (Cellgro, 10-040-CV) and supplemented with 10% fetal bovine serum (FBS) (Atlas Biologicals, F-0500-D) and 1% antibiotic-antiomycotic solution (Cellgro, 30-0004-Cl). HEK293 cells were kindly provided by Dr. Russell Anthony (Colorado State University) and were cultured in Dulbecco's Modified Eagle Medium (DMEM) (Cellgro, 10-017-CV) and supplemented with 10% fetal bovine serum (Atlas Biologicals, F-0500-D) and 1% antibiotic-antiomycotic solution (Cellgro, 30-0004-Cl). All cell lines were cultured in a standard humidified incubator at 37°C in a 5%CO2 atmosphere.

Lentiviral transductions for exosome tracking

IGROV1 cells line were stably transduced with pCT-CD63-GFP Cyto-tracers^{TM} (System Biosciences, CYTO120-VA-1) to create an IGROV1-CD63-GFP cell line (Figure S1) used for exosome tracking. The Cyto-tracers^{TM} utilizes an HIV-based lentivirus system with the pCT-CMV-GFP-Fusion-EF1-Puro vector where the cytomegalovirus promoter

(CMV) drives expression of the GFP-fusion protein, while the EF1 promoter drives the puromyocin (Puro) resistance gene. Briefly, $1x10^3$ IGROV1 cells were seeded onto 24-well plates 24 hours before transfection to allow adhesion and were grown to approximately 60-80% confluency. The cells were transfected with pCT-CD63-GFP at a multiplicity of infection (MOI) of 2000 virus particles per cell with addition of Polybrene (Millipore, TR-1003-G) at a final concentration of 2μg/mL to increase the efficiency of lipofection transfection. Cells were incubated for 24 hours to allow random virus insertion and 1-day later fresh medium was added without puromyocin for another 24 hours. Infected IGROV1 cells were selected by adding puromyocin at a final concentration of 4μg/mL to transfected cells and untreated control IGROV1 cells until control (uninfected) cells died.

Exosome isolation

Complete RPMI 1640 and DMEM medium was ultracentrifuged (Beckman L8-80) at 100,000*g* for 16hrs at 4°C to pellet secreted membrane vesicles less than 1000nm to obtain vesicle-depleted medium. Sterile filtration was performed on vesicle-depleted medium via 0.2uM PES membrane (Thermo Scientific, 565-0020) and stored at 4°C until exosome collection.

For exosome isolation, $1x10^6$ cells were seeded onto four 10cm cell plates (Celltreat, 229690) and cultured in either RPMI 1640 vesicle-depleted medium or DMEM vesicle-depleted medium for three days. Supernatant was collected and centrifuged at 3,000g for 15min at 4°C to remove cells and cell debris. Supernatant and ExoQuick-TC™

Exosome precipitation solution (System Biosciences, EXOTC50A-1) were combined in a 5:1 dilution (respectively) and exosomes were collected as per manufacturer's instructions. Briefly, supernatant/ExoQuick-TC™ biofluid was centrifuged at 1,500g for 30 minutes at 4°C, biofluid was aspirated, and recentrifuged at 1,500g for 5 minutes at 4°C to remove excess biofluid without disturbance of exosome pellet. Four exosome pellets were combined and either resuspended in 200μL of TRIzol LS Reagent (Life Technologies, 10296028) for qRT-PCR, or 300μL M-PER (Thermo Scientific, 78501) supplemented with Halt proteinase inhibitor cocktail (Thermo Scientific, 1:100, 87786) and phenylmethanesulfonyl fluoride solution (Boston BioProducts, 1:100, PI-120) for Western Blot. Exosomes were stored at -80°C until RNA isolation or protein isolation occurred.

RNA isolation

Total RNA was extracted from confluent cells and lysed with 300uL of MirVana lysis binding buffer and 30uL of miRNA homogenate additive. RNA was isolated as per manufacturer's instructions using MirVana miRNA isolation kit (Ambion, AM1561) and resuspended in 30μL of RNase/DNase-free water.

Total RNA was isolated from exosome isolates using TRIzol® LS Reagent (Life technologies, 10296-028). RNA isolation method was completed as per manufacturer's instructions with minor modifications. Briefly, exosomes were lysed in 200μL of TRIzol LS Reagent (Life technologies, 10296-028) and homogenized for 5 minutes to ensure complete lysis occurred. Phase separation was conducted by adding 128μL of

chloroform to the RNA/DNA/protein phase and homogenization for 5 minutes. Samples were centrifuged for 15min at 4°C to separate the RNA, DNA, and protein phases. The RNA aqueous phase was added to 400μL of cold 100% isopropanol and stored at -80°C overnight to enhance RNA precipitation. RNA was pelleted via centrifugation and was washed twice with cold 75% ethanol then resuspended in 10μL of RNase/DNase-free water.

Once total RNA was isolated from both cells and exosomes, DNase-free™ DNase Treatment and Removal kit (Ambion, AM1906) was used on to eliminate genomic DNA contamination. RNA quality and concentration were assessed using the NanoDrop® ND-1000 spectrophotometer (NanoDrop Technologies, USA). Total RNA absorbance of 260/280 was measured and samples with RNA purity between 1.7-2.2 were used for experiments. Samples were stored at -80°C until qRT-PCR was performed.

*Quantitative real-time PCR (*qRT-PCR)

Taqman qRT-PCR was performed on total RNA (see above) where 1μg of RNA was reverse transcribed for cells and 400ng of RNA was reverse transcribed for exosomes using qScript™cDNA supermix (Quanta Biosciences, 95047-100) as per manufacturer's instructions. cDNA was diluted to a final concentration of 10ng/rxn for cells and 20ng/rxn for exosomes and combined with 2x Ssofast™ Probe Supermix (Bio-Rad, 172-5230) and 20x Taqman Assay Mix (Applied Biosystems). The 20X Taqman Assay mix Probes (Applied Biosystems) used for this study were as follows: LIN28A (Hs00702808_s1), LIN28B (Hs01013729_m1), GAPDH (H99999905_m1), MRPS15 (Hs00229834_m1)

and TBP (Hs00427620_m1). qRT-PCR was performed using the Lightcycler 480 Real Time PCR System (Roche Applied Science). The cycling parameters were initial denaturation for 30 seconds at 95°C followed by 45 cycles of repeating denaturing at 15 seconds at 95°C and annealing for 30 seconds at 60°C with a final cooling cycle for 5 minutes at 37°C. Data was normalized using the geometric mean of GAPDH, MRPS15, and TBP and relative levels were calculated using the comparative Cp method to obtain $2^{-\Delta Ct}$ relative expression values. Each sample was run in duplicate with reverse transcriptase negative controls, non-template controls, and experiments were repeated. Statistical analysis was determined by Analysis of variance (ANOVA) followed by Tukey pairwise comparison (Minitab 17). P-values less than 0.05 were considered statistically significant.

MicroRNA qRT-PCR was performed from total RNA (see above) where 1μg of RNA was reverse transcribed for cells and 400ng of RNA was reverse transcribed for exosomes using miScript RT Kit supermix (Qiagen, 218161) as per manufacturer's instructions. cDNA was diluted to a final concentration of 1.5ng/rxn for cells and exosomes and combined with 2x QuantiTech® SYBR green PCR master mix, 10X miScript Universal Primer (miScript PCR Green PCR Kit (Qiagen, 218075). The miRNA PCR primers used for this study are listed in Table 2. qRT-PCR was performed using the Lightcycler 480 Real Time PCR System (Roche Applied Science). The cycling parameters were initial denaturation for 15 minutes at 95°C followed by 45 cycles of repeating denaturing at 15 seconds at 95°C, annealing for 30 seconds at 55°C, elongation for 30 seconds at 72°C with a final cooling cycle of 30 minutes at 40°C. Melt curves were also calculated to

ensure single miRNA amplicons were produced using the following cycling parameters: 95°C for 5 seconds and 65°C for 1 minute. Data was normalized using snRNA (U6), and relative levels were calculated using the comparative Cp method. Each sample was run in duplicate with reverse transcriptase negative controls, non-template controls, and experiments were repeated. Statistical analysis was determined by Analysis of variance (ANOVA) followed by Tukey pairwise comparison (Minitab 17). P-values less than 0.05 were considered statistically significant. When statistics were performed on miRNA levels after exosome transfer, statistical analysis was determined by a two-sided unpaired Student's t-test with $P<0.05$.

Human Epithelial to Mesenchymal Transition (EMT) RT^2 Profiler^{TM} PCR array (SABiosciences, PAHS-090G-4) was used to examine 84 genes related to EMT. Total RNA of 4 biological replicates of confluent HEK293 cells (control) and HEK293 cells exposed to IGROV1 exosomes (treatment) were isolated according to RNA isolation procedure (see above). 1ug of cDNA was made, diluted and qRT-PCR was performed as per manufacturer's instructions on the LightCycler 480 Real Time PCR System (Roche Applied Science). The cycling parameters were initial denaturation for 10 minutes at 95°C followed by 45 cycles of repeating denaturing at 15 seconds at 95°C and annealing for 1 minute at 60°C with a final cooling cycle of 5 minutes at 37°C after amplification. Melt curves were also calculated to ensure single amplicons were produced using the following cycling parameters: 95°C for 5 seconds and 65°C for 1 minute. Using SA Biosciences software, fold change analysis was utilized to determine the expression levels of genes that were upregulated following treatment.

Table 2: List of miRNA sequences. This table represents the human miRNA sequences used for qRT-PCR experiments. These sequences were obtained from miRBase program.

miRNA primers	Sequence (5'-3')
hsa-let-7a	UGAGGUAGUAGGUUGUAUAGUU
hsa-let-7b	UGAGGUAGUAGGUUGUGUGGUU
hsa-let-7c	UGAGGUAGUAGGUUGUAUGGUU
hsa-let-7d	AGAGGUAGUAGGUUGCAUAGUU
hsa-let-7e	UGAGGUAGGAGGUUGUAUAGUU
hsa-let-7f	UGAGGUAGUAGAUUGUAUAGUU
hsa-let-7g	UGAGGUAGUAGUUUGUACAGUU
hsa-let-7i	UGAGGUAGUAGUUUGUGCUGUU
hsa-let-7a-3p	CUAUACAAUCUACUGUCUUUC
hsa-let-7-f1-3p	CUAUACAAUCUAUUGCCUUCCC
hsa-miR-9	UCUUUGGUUAUCUAGCUGUAUGA
hsa-miR-17	CAAAGUGCUUACAGUGCAGGUAG
hsa-miR-18a	UAAGGUGCAUCUAGUGCAGAUAG
hsa-miR-19a	UGUGCAAAUCUAUGCAAAACUGA
hsa-miR-19b	UGUGCAAAUCCAUGCAAAACUGA
hsa-miR-20a	UAAAGUGCUUAUAGUGCAGGUAG
hsa-miR-22	AAGCUGCCAGUUGAAGAACUGU
hsa-miR-30a	UGUAAACAUCCUCGACUGGAAG
hsa-miR-30b	UGUAAACAUCCUACACUCAGCU
hsa-miR-30c	UGUAAACAUCCUACACUCUCAGC
hsa-miR-30d	UGUAAACAUCCCCGACUGGAAG
hsa-miR-30e	UGUAAACAUCCUUGACUGGAAG
hsa-miR-31	AGGCAAGAUGCUGGCAUAGCU
hsa-miR-92a	UAUUGCACUUGUCCCGGCCUGU
hsa -miR-200a	UAACACUGUCUGGUAACGAUGU
hsa-miR-200b	UAAUACUGCCUGGUAAUGAUGA
hsa-miR-200c	UAAUACUGCCGGGUAAUGAUGGA
hsa-miR-125a-3p	ACAGGUGAGGUUCUUGGGAGCC
hsa-miR-125a-5p	UCCCUGAGACCCUUUAACCUGUGA
hsa-miR-125b	UCCCUGAGACCCUAACUUGUGA
Htman t6 snRNA (U6)	CGCAAGGAUGACACGCAAAUUC

Reverse Transcriptase PCR (RT-PCR) for LIN28

RT-PCR was performed from total RNA (see above) where 1μg of RNA was reverse transcribed for cells and 400ng RNA was reverse transcribed for exosomes using qScript™cDNA supermix (Quanta Biosciences, 95047-100) as per manufacturer's instructions. Once cDNA was made, the GoTaq® DNA Polymerase kit (Promega, M3005) was used with 1200ng of cDNA and either LIN28A or LIN28B primers. These were placed in the Veriti 96-well Thermocycler with cycling parameters beginning with initial denaturation for 5 minutes at 94°C followed by 40 cycles of 15 seconds at 94°C of denaturation, 30 seconds at 60°C for annealing and 15 seconds at 72°C for elongation. The cycles ended with 3 minutes at 72°C and held at 4°C until run was ended. The samples were electrophoresed on a 2% agrose gel @190V for 30 minutes and imaged using the ChemiDoc™ MP System with the Image Lab 4.1 software. Experiments were carried out using three independent biological replicates and the experiment was repeated. The primers used were designed spanning introns. LIN28A forward primer sequence was 5'-GGCATCTGTAAGTGGTTGAACG-3' and the reverse primer sequence was 5'-CCTTCCATGTGCAGCTTACTCT-3' (118bp size) and LIN28B forward primer sequence was 5'-TAGGAAGTGAAAGAAGACCCAA-3' and the reverse primer sequence was 5'-ATGATGCTCTGACAGTAATGG-3' (151bp size).

Western Blot Analysis

Cells and exosomes were lysed in M-PER (Thermo Scientific, 78501) supplemented with Halt proteinase inhibitor cocktail (Thermo Scientific, 1:100, 87786) and phenylmethanesulfonyl fluoride solution (Boston BioProducts, 1:100, PI-120). Cells

were centrifuged at 14,000g for 5min at 4°C to remove cell debris. Protein concentration was determined using the bicinchoninic acid assay (BCA) method (Pierce™ BCA protein assay kit; Thermo Scientific, 23225). 30ug of protein from cell lysates and 40ug of protein from exosomal lysates was diluted in 6x buffer/DTT loading dye and heated to 95°C for 10min. Protein was electophoresed to 4-20% Ready Gel® Tris-HCl Precast Gels (Bio-Rad, 161-1159) at 90V for 15 min to get past the stacking gel then voltage was increased 120V for 1hr, and transferred onto a nitrocellulose membrane for 1hr at 100V on ice. The membrane was washed with 1X TBST for 5min and blocked at room temperature for 1hr with 5% dry milk in 1X TBST. The membrane was washed three times for 5 minutes in 1X TBST and incubated with the following primary antibodies: LIN28A (1:1000 rabbit polyclonal, ab63740, Abcam), LIN28B (1:1000 rabbit polyclonal, 4196S, Cell signaling technology), GAPDH (1:3000, rabbit polyclonal, ab37168) CYTO C (1:100, mouse monoclonal IgG_{2b}, sc13156, Santa Cruz Biotechnology), TSG101 (1:500, rabbit polyclonal, 14497-1-AP, Proteintech) or EPCAM (1:500, rabbit polyclonal, 21050-1-AP, Proteintech). Primary antibodies were resuspended in 5% milk 1X TBST and membrane was incubated overnight at 4°C. GAPDH was incubated on membrane for 1hr at room temperature. Membranes were washed three times for 5 minutes in 1X TBST before the secondary antibodies were applied for 1 hour at room temperature. The secondary antibodies are as follows: goat anti-rabbit IgG-HRP (1:5000, sc-2004, Santa Cruz Biotechnology) were used with LIN28A, LIN28B, and GAPDH primaries, goat anti-mouse IgG-HRP (1:2000, sc-2031, Santa Cruz Biotechnology) were used in conjugation with CYTO C primary, and goat anti-rabbit IgG-HRP (1:2000, ab6721, Abcam) were used with TSG101 and EPCAM. Membranes were washed with 1X TBST

3 times for 5 minutes and incubated for 5 minutes in ECL™ Prime Western Blotting Detection Reagent (Amersham, RPN2209) and for 1 second in SuperSignal® West Dura Extended Duration Substrate (Thermo Scientific, 34075) for chemiluminescence detection on the ChemiDoc™ MP System. Image Lab 4.1 software was used for densitometry analysis.

Experiments were carried out using at least two-three independent biological replicates and the experiments were repeated. Relative protein amounts were calculated by dividing the band volume of the gene of interest over the housekeeping gene GAPDH. Statistical analysis was determined by Analysis of variance (ANOVA) followed by Tukey pairwise comparison (Minitab 17). P-values less than 0.05 were considered statistically significant.

Exosome Transfer

IGROV1-CD63-GFP cells (1×10^6) were seeded onto 10cm cell plates (Celltreat, 229690) in complete RPMI 1640 vesicle-depleted medium and grown for 3 days. Exosomes were isolated from the culture medium using the exosome isolation procedure described above and stained with Vybrant® DiD cell-labeling solution (Invitrogen, V22887) as per manufacturer's instructions. 24 hours before exosomes were isolated, $5x10^4$ HEK293 in complete DMEM vesicle-depleted medium were grown to approximately 60-80% confluency on 4-well plates. Exosomes were resuspended in 500μL of complete DMEM vesicle-depleted medium added onto $5x10^4$ HEK293 cells for 96-hours, referred to as Exosome Transfer. The first control was 500μL of complete

DMEM vesicle-depleted medium plated onto $5x10^4$ HEK293 cells for 96-hours as a negative control. This control, (Vehicle), was used to ensure vesicle-depleted medium was not the reason for any changes seen in the HEK293 cell line. The second control was 500μL of supernatant/ExoQuick-TC™ biofluid plated onto $5x10^4$ HEK293 cells for 96-hours as a negative control. This control, (Supernatant), was used to ensure supernatant/ExoQuick-TC™ biofluid, which was in contact with the exosomes prior to addition to HEK293 cells, was not the reason for any changes in the HEK293 cells. Cells were imaged on the Olympus FSX100 Bio Imaging Navigator using the FSX100 software, or the LSM 510 Meta 405 Confocal Microscope System Zeiss. A series of images were collected at 1μm intervals and used to generate a z-stack. After 96hrs, HEK293 cells were trypsinized and snap frozen in liquid nitrogen and stored at -80°C for RNA/protein analysis or used immediately for migration and invasion assays.

Migration and Invasion Assays following Exosome Transfer

Migration and invasion assays were performed using the 24-well 8.0μm BD BioCoat™ Tumor Invasion System (BD Biosciences, 354166) and the BD Falcon™ 24-multiwell 8μm insert system (BD Biosciences, 351158) as per manufacturer's instructions. Briefly, cell monolayers were pre-treated with 10ug/mL $DiIC_{12}(3)$ in 10% FBS DMEM vesicle-depleted medium for 1 hour at 37°C. Cells were trypsinized in 0.1% FBS DMEM vesicle-depleted serum-free medium. $5x10^4$ cells were seeded onto the apical chambers. Chemoattractant of either 10% FBS DMEM vesicle-depleted medium (positive control), or 0.1% FBS DMEM vesicle-depleted serum-free medium (negative control) was added to the basal chambers. The BD BioCoat Tumor Invasion System and the uncoated BD

Falcon FluroBlok 24-Multiwell System were incubated for 48 hours at 37°C, 5% CO_2. Readings were taken every 6 hours, for 48 hours, with Syngene HT and Gen5 program using 530/25-excitation filter and 590/35-emission filter, and sensitivity set at 52. Fluorescence of invaded/migrated cells was read at wavelengths 549/565nm (Ex/Em) for detection of $DiI_{12}C$. Background fluorescence was subtracted and data reduction was performed by subtracting values for the negative from the positive control. Migration and invasion relative fluorescence units were plotted separately and experiments were carried out at least two times with three independent biological replicates.

RESULTS

LIN28A and LIN28B levels in IGROV1, OV420, and HEK293 cells

IGROV1 cells had significantly higher levels ($p<0.05$) of *LIN28A* compared to OV420 cells and HEK293 cells (Figure 9A). When *LIN28B* levels were examined, we found HEK293 cells had significantly higher levels ($p<0.05$) compared to IGROV1 and OV420 cells. (Figure 9B)

IGROV1 cells had significantly higher LIN28A protein levels ($p<0.003$) compared to OV420 cells and HEK293 cells (Figure 9C). We also demonstrated LIN28B protein was higher in HEK293 cells (Figure 9D) compared to IGROV1 and OV420 cells.

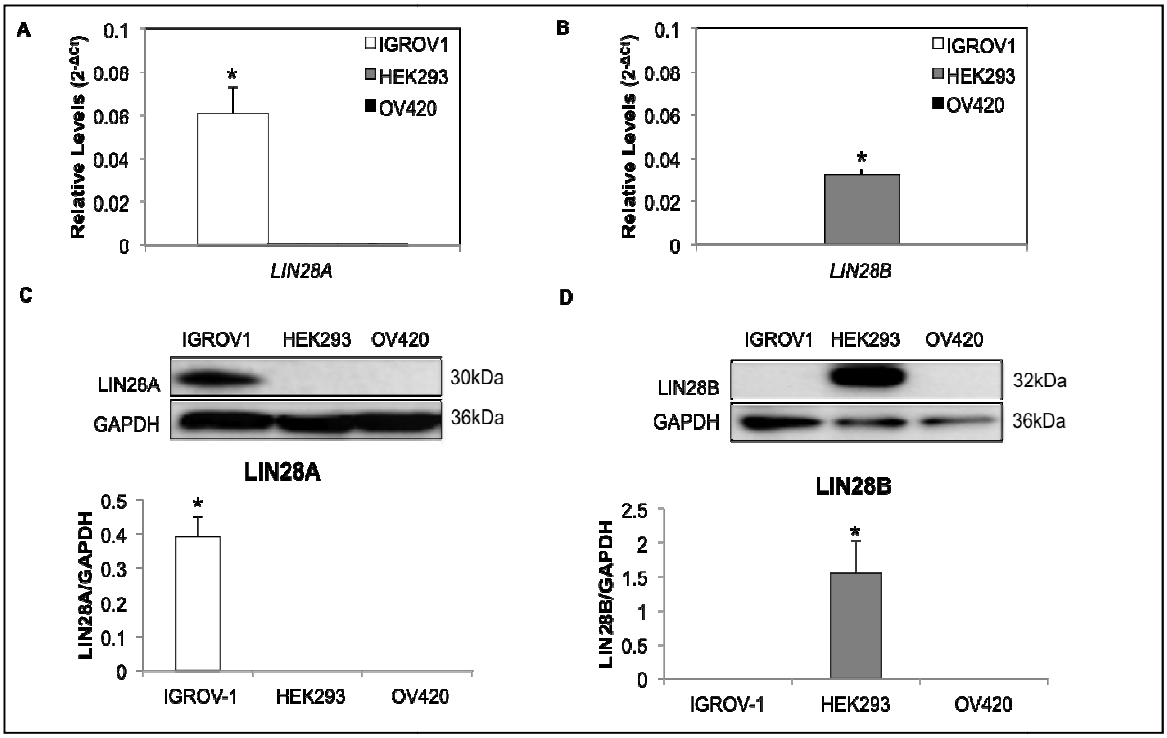

Figure 9: LIN28A and LIN28B mRNA and protein levels in IGROV1, OV420, and HEK293 cells. A) *LIN28A* mRNA levels and B) *LIN28B* mRNA levels in all three cell lines. Data was normalized against the geometric mean of GAPDH, MRPS15, and TBP. C) LIN28A protein levels and D) LIN28B protein levels in all three cell lines. Asterisks in indicates a p-value <0.05.

let-7 levels in IGROV1, OV420 and HEK293 cells

To evaluate the relative levels of miRNA *let*-7 family, (targets of LIN28), we performed qRT-PCR for all eight *let-7* isoforms (*let-7a, let-7b, let-7c, let-7d, let-7e, let-7f, let-7g,* and *let-7i)*. All eight miRNA *let-7* isoforms were significantly lower ($p<0.02$) in IGROV1 cells and HEK293 cells compared to OV420 cells (Figure 10) There were no significant differences in *let-7a, let-7b, let-7c, let-7d, let-7e, let-7f, let-7g,* and *let-7i* miRNAs in IGROV1 cells compared to HEK293 cells (Figure 10).

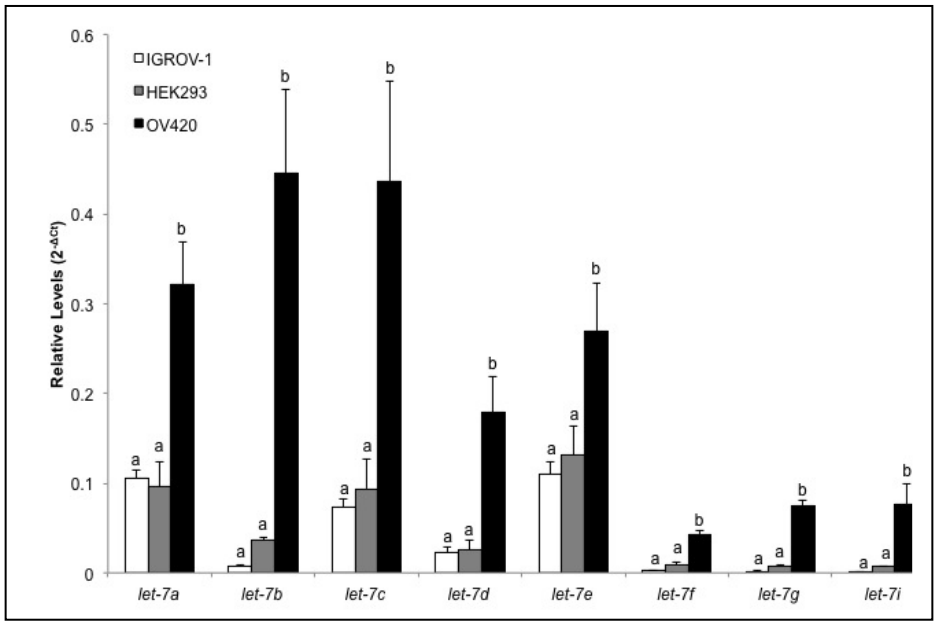

Figure 10: *let-7* miRNA levels in IGROV1, OV420 and HEK293 cells. qRT-PCR was utilized to determine the relative levels of *let-7s* in these three cell lines. Data was normalized against the U6 snRNA. Means with different superscript indicate (p-value <0.05). (p-value <0.02).

LIN28A and LIN28B levels in IGROV1, OV420 and HEK293 exosomes

We examined the relative levels of LIN28A and LIN28B in IGROV1, OV420 and HEK293 exosomes using RT-PCR. *LIN28A* was identified in exosomes from all three cell lines and *LIN28B* was only detected in HEK293 secreted exosomes (Figure 11A). Western blot performed on protein isolated from exosomes secreted by IGROV1, HEK293, and OV420 cells revealed LIN28A and LIN28B protein was not present in exosomes secreted by the three cell lines (Figure 11B).

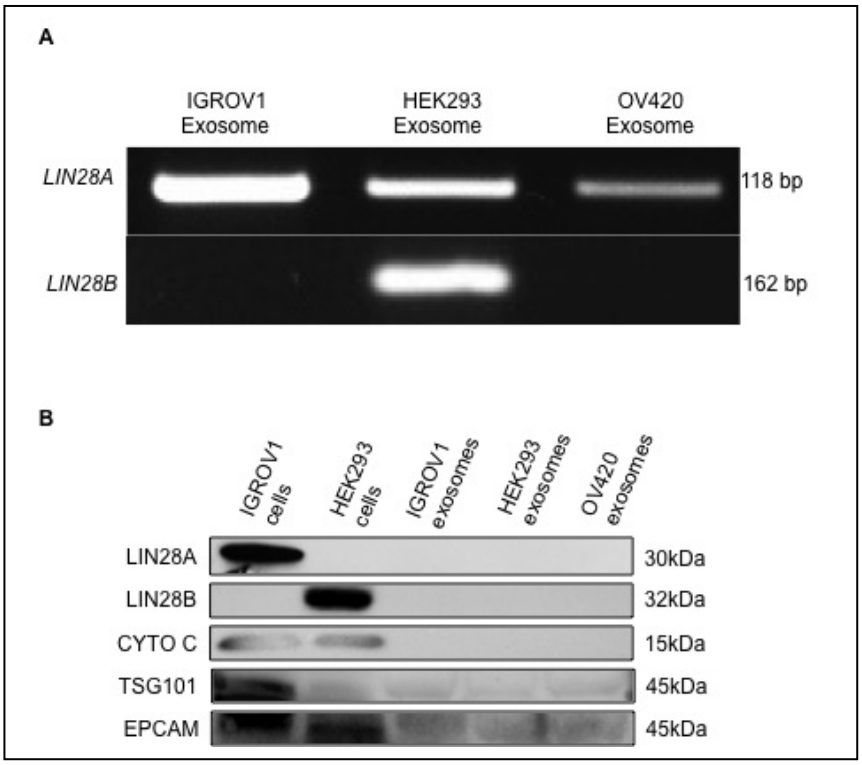

Figure 11: LIN28A and LIN28B mRNA and protein in exosomes. A) RT-PCR was performed to determine the presence of *LIN28A* and *LIN28B* in exosomes secreted from IGROV1, OV420 and HEK293 cells. B) Western blot was conducted to determine the presence of LIN28A and LIN28A protein in exosomes. Cytochrome C (CYTO C), was used as a negative control. Tumor susceptibility gene 101 (TSG101), a component of the endosomal sorting, and EPCAM (epithelial cell adhesion molecule), an exosome marker in ovarian cancer, were used as positive controls for exosomes.

let-7 levels in IGROV1, OV420 and HEK293 exosomes

To determine the relative levels of let-7 miRNAs within exosomes, qRT-PCR for all eight *let-7* isoforms (*let-7a, let-7b, let-7c, let-7d, let-7e, let-7f, let-7g,* and *let-7i)* was conducted. HEK293 and IGROV1 exosomes have significantly lower levels ($p<0.05$) of *let-7b*, *let-7c, let-7g* and *let-7i* compared to OV420 exosomes (Figure 12). There were no significant differences in *let-7a, let-7d, let-7e,* and *let-7f* miRNAs in IGROV1, HEK293 and OV420 secreted exosomes.

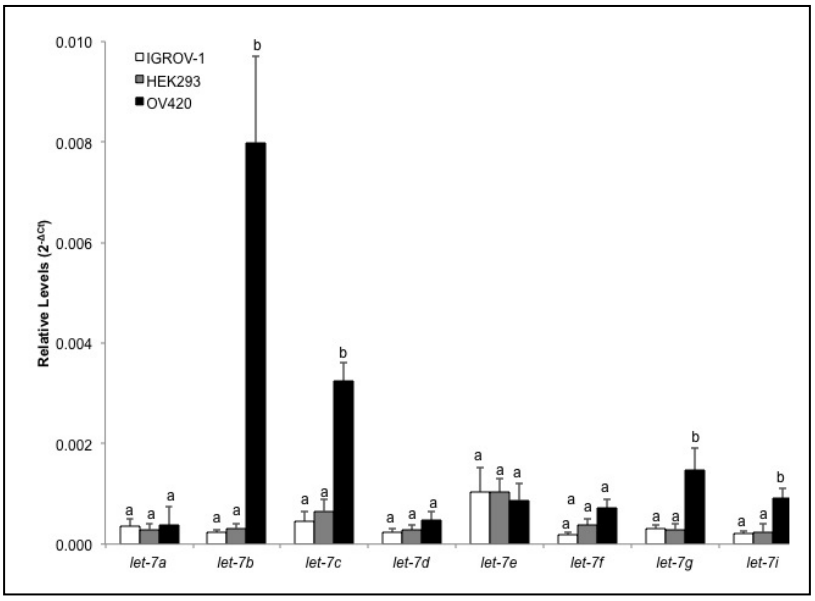

Figure 12: *let-7* miRNA levels in IGROV1, OV420 and HEK293 exosomes. qRT-PCR was used to determine the relative levels of *let-7s* in ovarian cancer cell secreted exosomes. Means with different superscript indicate (p-value <0.05).

Exosomes can be taken up by HEK293 cells

In order to determine uptake of exosomes, IGROV1 cells were transfected with CD63-GFP-cytotracer (Appendix I). CD63 positive exosomes secreted from IGROV1 cells were taken up by HEK293 cells (Figure 13A), and Z-stack confocal imaging revealed these exosomes are found within the HEK293 cells (Figure 13B). Additionally, OV420 exosomes were stained with DiD cell-labeling solution and exposed to HEK293 cells. Z-stack imaging revealed these exosomes are also found within HEK293 cells (Figure 13C).

LIN28A and LIN28B levels in HEK293 cells following IGROV1 exosome exposure

qRT-PCR was conducted to examine *LIN28A* and *LIN28B* levels after IGROV1 exosome exposure. *LIN28A* (Figure 14A) and *LIN28B* (Figure 14B) levels were not significantly higher ($p<0.05$) after 96-hour IGROV1 exosome exposure. Western blot

analysis on protein isolated from HEK293 cell after 96-hour exposure to IGROV1 exosomes and revealed LIN28A was not present in HEK293 cells after exposure of IGROV1 exosomes (Figure 14C). In addition, LIN28B was not significantly different from supernatant (negative control) in HEK293 cells exposed to IGROV1 exosomes (Figure 14D).

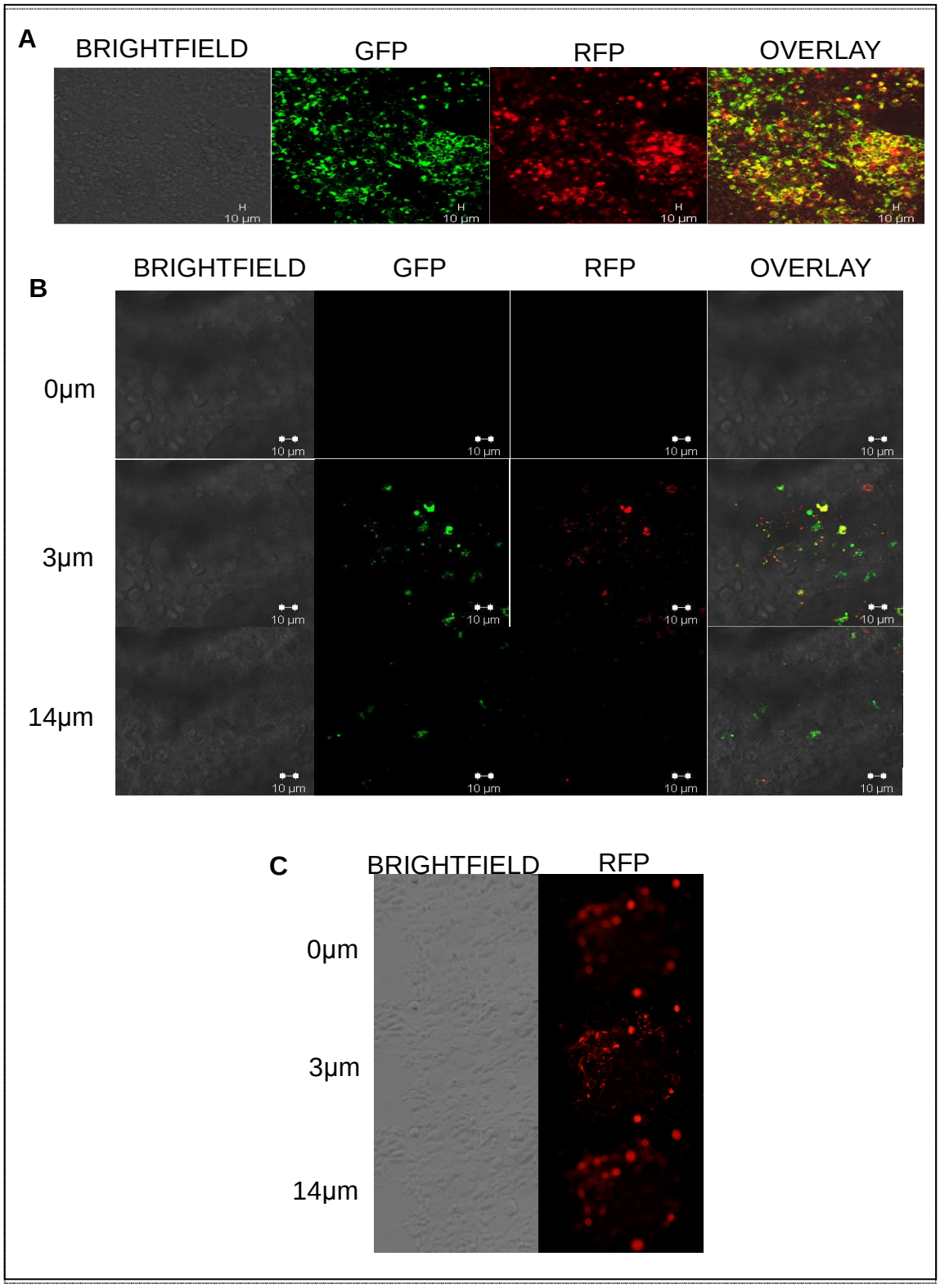
A
BRIGHTFIELD
GFP
RFP
OVERLAY
B
BRIGHTFIELD
GFP
RFP
OVERLAY
0µm
3µm
14µm
C
BRIGHTFIELD
RFP
0µm
3µm
14µm

Figure 13: Detection of IGROV1-CD63-GFP positive exosomes in HEK293 cells. A) HEK293 cells after 96-hour exposure to GFP positive IGROV1 exosomes (20X magnification) B) Z-stack image of HEK293 cells after 96-hour exposure to IGROV1-CD63-GFP exosomes. C) Z-stack image of HEK293 cells after 96hour exposure using to OV420 DID labeled exosomes (40X magnification). GFP green color indicates CD63 positive exosomal presence, RFP red color indicates DiD membrane marker.

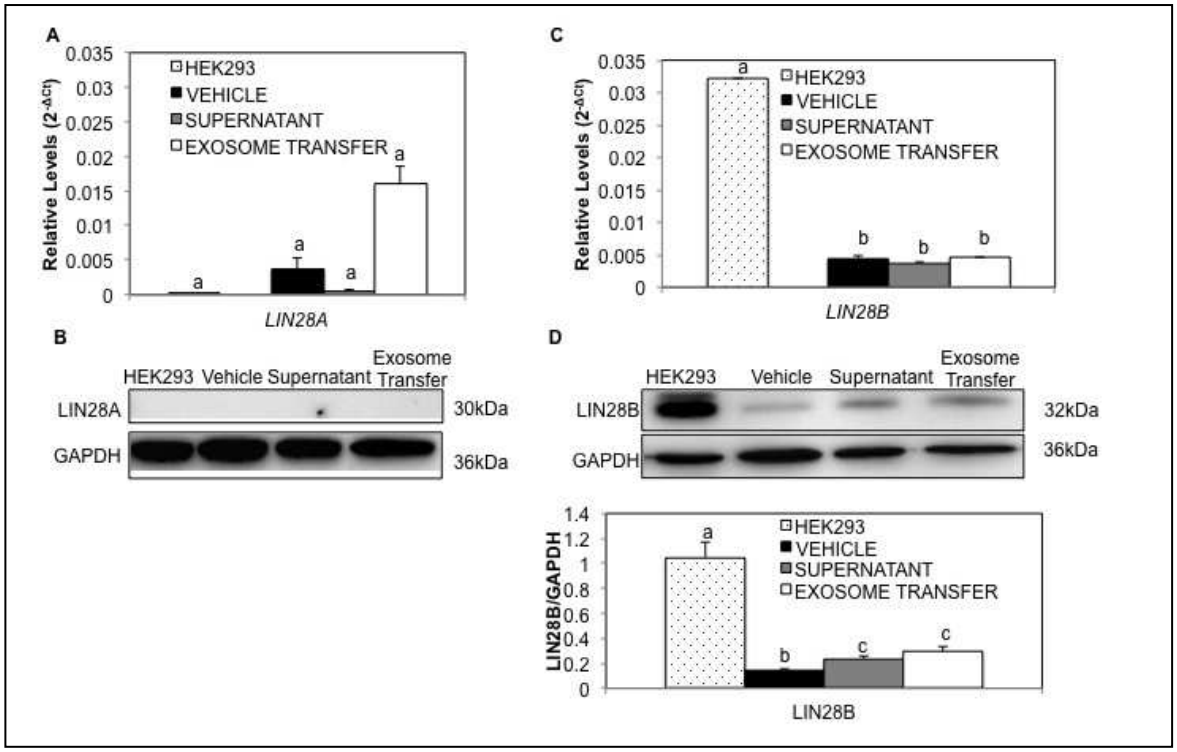

Figure 14: LIN28A and LIN28B mRNA and protein levels in HEK293 cells exposed to IGROV1 exosomes for 96-hours. HEK293 cells treated with vesicle-depleted media (vehicle), HEK293 cells treated with supernatant from exosomal pellet (supernatant), and HEK293 cells treated with exosome pellet (exosome transfer). qRT-PCR was performed to obtain mRNA levels of A) *LIN28A* and B) *LIN28B* after HEK293 cells were exposed to IGROV1 exosomes. Data was normalized against the geometric mean of GAPDH, MRPS15, and TBP. Means with different superscript indicate p-value <0.05. Western blot analysis (30μg) was performed to obtain C) LIN28A protein levels and D) LIN28B protein levels after HEK293 cells were exposed to IGROV1 exosomes. Densitometry was conducted to determined. LIN28A or LIN28B levels over GAPDH levels. Means with different superscript indicate p-value <0.05.

let-7 levels in HEK293 cells following IGROV1 exosome exposure

To determine the levels of let-7 miRNAs after HEK293 cells exposed to IGROV1 exosomes, qRT-PCR for all eight *let-7* isoforms (*let-7a, let-7b, let-7c, let-7d, let-7e, let-*

7f, let-7g, and *let-7i)* was performed. There were no significant differences in all eight miRNA *let-7* isoforms when HEK293 cells were exposed to IGROV1 exosomes compared to vehicle (Figure 15). Also, there was no significant change in additional miRNAs related to ovarian cancer (*miR-17, miR-18a, miR-19a, miR-19b, miR-20a, miR-92, miR-22, miR-200a, miR-200b, miR-200c, miR-9, miR-30a, miR-30b, miR-30c, miR-30d, miR-30e, miR31, miR-125a-3p, miR-125-5p*, and *miR-125b*), except *miR-9* miRNA, which was significantly higher ($p<0.05$) after HEK293 cells were exposed to IGROV1 exosomes (Figure 16).

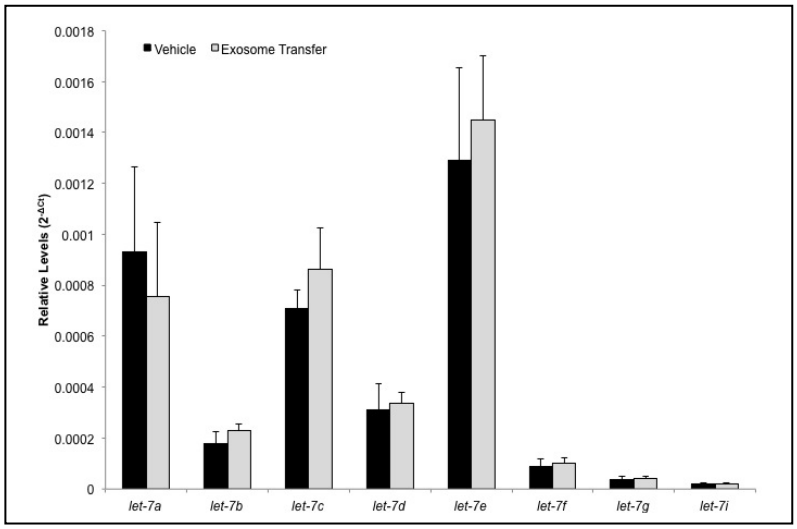

Figure 15: *let-7* miRNA levels in HEK293 cells following 96-hour IGROV1 exosome exposure. qRT-PCR was conducted to determine the relative levels of expression in ovarian cancer cell line. Data was normalized using U6 snRNA.

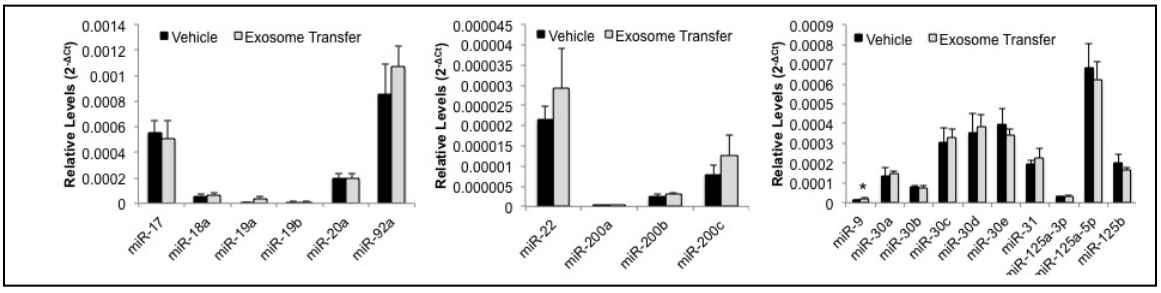

Figure 16: miRNA levels after HEK293 cells were exposed to IGROV1 exosomes for 96-hours. qRT-PCR was conducted to determine the relative levels of miRNAs in ovarian cancer cell secreted exosomes. Data was normalized using U6 snRNA. Asterisk indicates a p-value <0.05.

miRNA levels in IGROV1 and OV420 exosomes

To determine the levels of miRNAs related to ovarian cancer in exosomes (*miR-17, miR-18a, miR-19a, miR-19b, miR-20a, miR-92, miR-22, miR-200a, miR-200b, miR-200c, miR-9, miR-30a, miR-30b, miR-30c, miR-30d, miR-30e, miR31, miR-125a-3p, miR-125-5p*, and *miR-125b)* qRT-PCR was performed. *miR-200b, miR-200c, and miR-31* are lower ($p<0.05$) in IGROV1 exosomes compared to OV420 and HEK293 exosomes (Figure 17). Conversely, *miR-30a* is significantly higher in IGROV1 exosomes compared to OV420 and HEK293 exosomes (Figure 17). Additionally, *miR-30c* is significantly higher in IGROV1 exosomes compared to OV420 exosomes, but not to HEK293 exosomes (Figure 17).

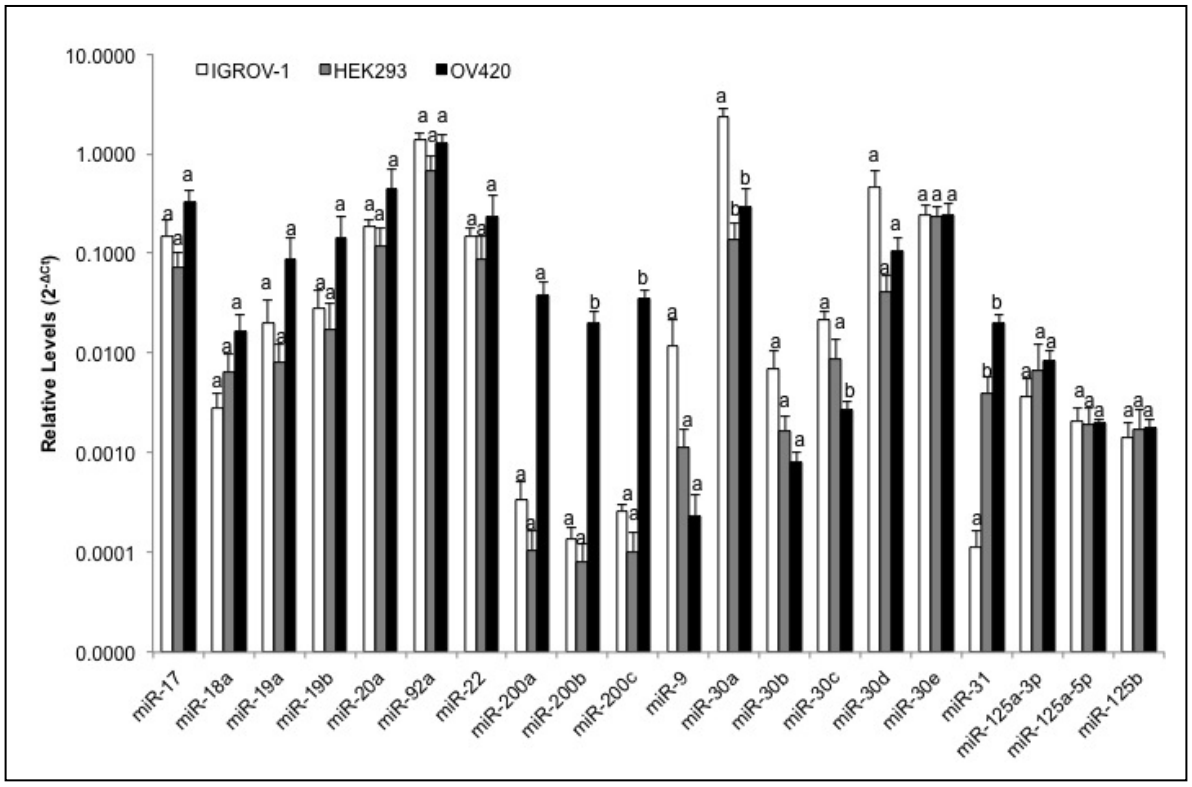

Figure 17: miRNAs levels in IGROV1, OV420, and HEK293 exosomes. qRT-PCR was used to determine the relative levels of miRNAs in IGROV1 and OV420 exosomes. Data was normalized against U6 snRNA. Means with different superscript indicate p-value <0.05.

Level of epithelial to mesenchymal transition (EMT) related genes in HEK293 cells following IGROV1 exosome exposure

To further assess the effect of IGROV1 exosomes exposure on HEK293 cells, we examined relative levels of genes related to EMT after HEK293 cells were exposed to IGROV1 exosomes. qRT-PCR analysis revealed significantly higher level in 45 EMT related genes (Table 3).

Table 3: Fold change level of EMT related genes after HEK293 cells exposed to IGROV1 exosomes.

FOLD CHANGE	GENES	FOLD CHANGE	GENES
3.03	*ZEB1*	5.24	*BMP1*
3.09	*TGFB3*	5.32	*SNAI2*
3.22	*TGFB1*	5.35	*ERBB3*
3.25	*TMEFF1*	5.39	*MMP3*
3.37	*WNT11*	5.53	*GSC*
3.80	*PLEK2*	5.70	*COL1A2*
3.81	*ILK*	6.04	*TMEM132A*
3.82	*SERPINE1*	6.32	*IL1RN*
3.86	*SPARC*	6.35	*CDH1*
3.95	*SPP1*	6.38	*NODAL*
4.00	*MMP9*	6.41	*SNAI3*
4.09	*BMP7*	6.45	*WNT5A*
4.12	*STAT3*	6.49	*JAG1*
4.14	*WNT5B*	6.58	*COL3A1*
4.19	*ITGA5*	7.13	*SOX10*
4.28	*TWIST1*	7.33	*FGFBP1*
4.29	*FZD7*	7.37	*SNAI1*
4.49	*IGFBP4*	8.32	*GNG11*
4.78	*AHNAK*	9.67	*PTP4A1*
4.82	*F11R*	10.55	*NOTCH1*
5.13	*PTK2*	10.95	*FOXC2*
5.15	*MST1R*	25.65	*TIMP1*
5.20	*KRT7*		

Effect of IGROV1 secreted exosomes on HEK293 cell migration and invasion

IGROV1 exosomes were added to HEK293 cells for 96-hours and immunofluorescence detection of stained cells that migrated or invaded was conducted every six hours for a total of 48 hours. HEK293 cells exposed to IGROV1 exosomes exhibited increased migration (Figure 18A) and invasion (Figure 19A) as early as 12 hours. In contrast, when HEK293 cells were exposed to OV420 exosomes, HEK293 cells did not demonstrate a change in migration (Figure 18B) or invasion (Figure 19B).

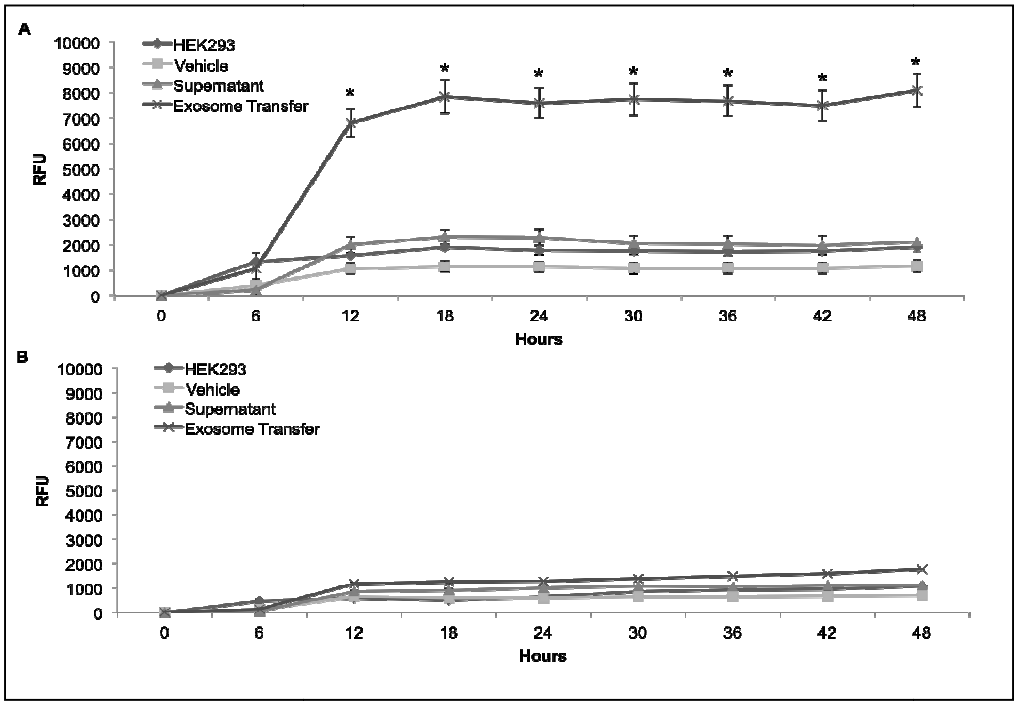

Figure 18: Migration of HEK293 cells exposed to IGROV1 or OV420 exosomes. A) 48-hour HEK293 cell migration when exposed to IGROV1 exosomes and B) 48-hour HEK293 cell migration when exposed to OV420 exosomes. Relative fluorescence units (RFU) was used to measure cells that migrated. Asterisk indicated a p-value <0.04.

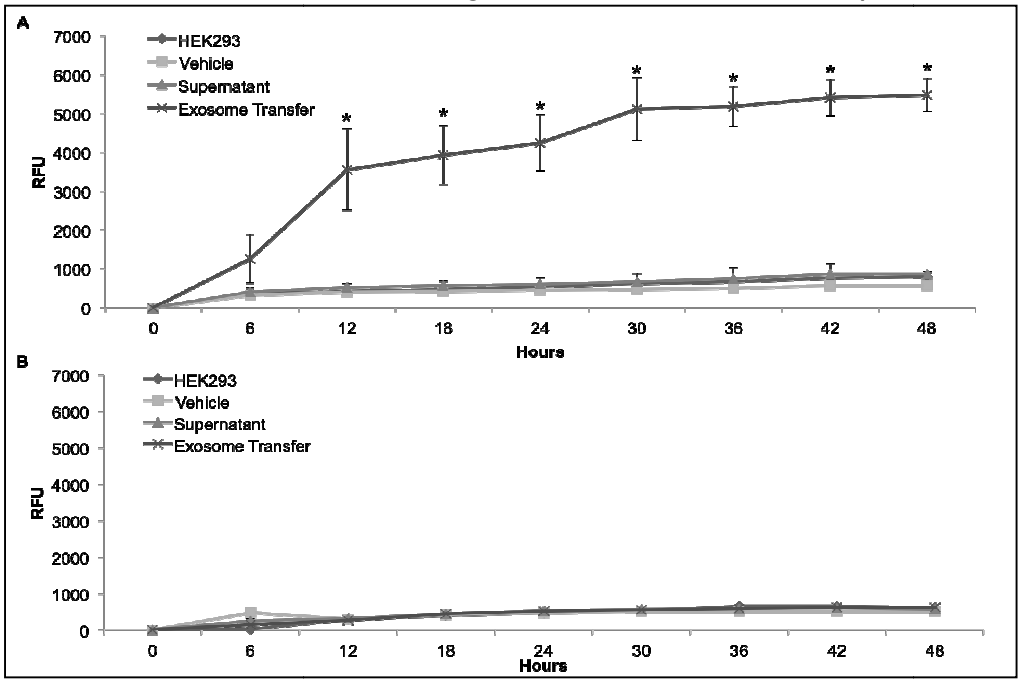

Figure 19: Invasion of HEK293 cells exposed to IGROV1 or OV420 exosomes. Invasion assay demonstrates A) HEK293 cells invaded when exposed to IGROV1 exosomes and B) HEK293 cells invaded when exposed to OV420 exosomes for 96-hours. Relative fluorescence units (RFU) were used to measure cells that invaded. Asterisk indicated a p-value <0.04.

DISCUSSION

In this study we sought to determine if exosomes from more aggressive, high LIN28 expressing cells (IGROV1), can be taken up by HEK293 cells and if exosome uptake could lead to changes in gene expression and cell phenotype. LIN28A is a RNA binding protein that interacts directly with the miRNA *let-7* family leading to a decrease in let-7 miRNAs (Heo et al., 2008; Newman, Thomson and Hammond, 2008; Rybak et al., 2008; Viswanathan, Daley and Gregory, 2008) and this relationship was also detected in ovarian cancer tumors of a more advanced malignancy (Viswanathan et al., 2009). It was recently demonstrated that IGROV1 cells have high levels of LIN28A and low levels of let-7s (Piskounova et al., 2011). They also found HEK293 cells have high LIN28B and LIN28A was not detectable (Piskounova et al., 2011). Our data corroborate this finding; additionally we determined OV420 cells contain low levels of LIN28A and LIN28B as well as high *let-7* levels.

Exosomes from ovarian cancer tumors contain miRNAs and mRNAs that are not found in healthy individuals (Taylor and Gercel-Taylor, 2008). qRT-PCR determined IGROV1, HEK293, and OV420 exosomes have *LIN28A* and HEK293 exosomes have *LIN28B.* Unfortunately, we were unable to detect LIN28A or LIN28B protein in any of the exosomes. It was recently discovered exosomes contain truncated mRNAs and compete with miRNAs and RNA-binding proteins, which could inhibit protein production (Batogov and Kurochkin et al., 2013). These findings suggest exosomal *LIN28A* may be truncated which could explain why LIN28A protein was not detected in IGROV1 exosomes.

We found that *let-7b, let-7c,* and *let-7i* are significantly lower in IGROV1 exosomes compared to OV420 exosomes. These findings are reflective of cellular expression levels. Moreover, profiling of miRNAs in epithelial ovarian tissues demonstrated *let-7s* were lower in these tissues (Iorio et al., 2007), and more importantly, lower levels of *let-7i* are found in patients resistant to chemotherapy as well as patients who are of poorer prognosis in late-stage ovarian cancer (Yang et al., 2008b). Recently a study reported that exosomal *miR-200* and *let-7* families secreted from SKOV3 cells (highly invasive) and OVCAR-3 cells (low invasive) are sequestered in exosomes of more invasive ovarian cancer cell lines (Kobayashi et al., 2014). Also, we found lower *let-7* levels in cells as well as their secreted exosomes, which was confirmed in a previous study (Taylor and Gercel-Taylor, 2008).

IGROV1 exosome exposure did not increase LIN28B mRNA or protein in HEK293 cells. IGROV1 exosomes do not contain LIN28B mRNA or protein, therefore it is not surprising that LIN28B did not significantly increase compared to supernatant control. We were also unable to detect an increase in LIN28A or LIN28B protein in HEK293 cells exposed to IGROV1 exosomes as well as lower levels of *let-7* miRNAs (*let-7b*, *let-7c, let-7g* and *let-7i*), specifically *let-7i* miRNA in IGROV1 exosomes. *Let-7i* is lower in chemoresistant patients and is associated with poor prognosis (Yang et al., 2008b).

Current studies are focused on transfer of exosomal contents into recipient cells to determine if RNAs in exosomes can be translated into functional proteins or if new proteins are expressed. Numerous studies have shown that exosomes taken up by

target cells can lead to alteration in signaling pathways, gene expression, and cell behavior, such as invasion (Valadi et al., 2007; Deregibus et al., 2007; Ratajczak et al., 2006). For example, glioblastoma tumor cell secreted exosomes in the brain are enriched with angiogenic proteins and can be taken up by brain microvascular endothelial cells to stimulate tubal formation (Skog et al., 2008). Furthermore, SKOV3 secrete exosomes that contain proteins required for exosomal uptake by the same cell line (Escrevente et al., 2011). For this study we established an IGROV1-CD63-GFP cell line to label exosomes and performed an exosome transfer experiment into target HEK293 cells. The effects of exosomes on target cells is currently being investigated to determine if cancer exosomes can reprogram target cells, leading to changes in phenotype, such as migration and invasion. It was recently described that renal cancer exosomes can increase migration and invasion as well as a decrease cell adhesion (Chen, Zhang, and Wu, 2013). Furthermore, ovarian cancer exosomes from SKOV3 and OVCAR3 cells were used to examine effects on adipose tissue derived mesenchymal stem cells, and determined each cell line could induce a myofibroblastic phenotype, often related to tumor development (Cho et al., 2011). In the current study, we demonstrate IGROV1 exosomes are capable of inducing migration and invasion in HEK293 cells and OV420 exosomes are not able to induce this response. To our knowledge, this is the first study to describe that high LIN28A, aggressive IGROV1 cells secrete exosomes that stimulate invasion and migration in target cells, contrary to low LIN28A, less aggressive OV420 ovarian cancer cells. These findings indicate a possible role for LIN28A in exosome biogenesis and/or composition.

We assessed the relative levels of genes related to epithelial mesenchymal transition (EMT) in HEK293 cells exposed to IGROV1 exosomes. EMT is an important initiation step for cancer metastasis to occur and is known to upregulate genes involved in cell adhesion and cell mobility. In a recent finding, exosomes from epithelial cancer cells stimulated A431 and DLD-1 cells to acquire an EMT-like state by activating epidermal growth factor receptor and inhibit E-Cadherin involved in invasion through the basement membrane (Garnier et al., 2012). We found IGROV1 exosome uptake by HEK293 cells led to increased level of 45 genes associated with EMT including SNAI2 and *NOTCH1*. Furthermore, *miR-9* was significantly higher in HEK293 cells after IGROV1 exosome exposure. *miR-9* regulates snail family zinc finger 2 (SNAI2) (Grimson et al., 2007; miRSearch V3.0 Exiqon), also known as *SLUG*, a necessary factor in type II tumor formation found in aggressive cancer cells. Increased levels of *miR-9* may further lead to increases in SLUG, exacerbating type II tumor formation. Furthermore, Rho GTPases family 3 (*RND3*) has recently been described as a regulator of NOTCH1 signaling (Zhu et al., 2014). *NOTCH1* is an EMT related gene upregulated in HEK293 cells upon IGROV1 exosome exposure, More studies to validate the presence of *RND3* in IGROV1 exosomes as well as a functional role of *NOTCH1* after exosome transfer could potential identify this RNA as a biomarker for cancer progression. These results would need to be confirmed, but demonstrate the dynamic role exosomal miRNAs could play in epithelial to mesenchymal transition in target cells.

In summary, our results report the more aggressive high LIN28A expressing IGROV1 cells secrete exosomes that can upregulate genes related to epithelial to mesenchymal

transition (EMT), and induce invasion and migration in HEK293 cells. Moreover, low LIN28A expressing OV420 cells secrete exosomes that do not have the ability to induce invasion and migration in HEK293 cells. Additionally, *miR-9* increased after IGROV1 exosomes exposed to HEK293 cells and can potentially target SNAI2, an EMT related gene, which was found higher in HEK293 cells after IGROV1 exosome exposure. Future experiments that elucidate molecular differences between IGROV1 exosomes and OV420 exosomes could yield a biomarker for distinguishing poor prognosis versus good prognosis. Ultimately, this study provides a better understanding of exosomal potential in ovarian cancer initiation that may influence metastatic disease.

CHAPTER V: RNA SEQUENCING OF EXOSOMES SECRETED BY IGROV1 AND OV420 CELLS

SYNOPSIS

Advances in modern medicine usually lead to a decrease in certain cancers because of new technologies leading to better diagnosis. Unfortunately, this is not the case with women diagnosed with ovarian cancer. Approximately 25% of women who develop ovarian cancer are diagnosed at an early stage, leaving approximately 75% of women being diagnosed at a late stage when the disease has already metastasized. This is due to asymptomatic disease progression and more importantly because there is no diagnostic marker to detect early stages of ovarian cancer. Genome wide deep sequencing techniques is a novel way to identify molecules that could represent a potential biomarker for detection of ovarian cancer. We previously described IGROV1 cells (more aggressive) contain high LIN28A and secrete exosomes that can increase levels of epithelial to mesenchymal transition related genes, and induce invasion and migration in HEK293 cells, whereas OV420 (less aggressive) contain low LIN28A and secreted exosomes that cannot. We hypothesized RNA signatures in ovarian cancer cell-secreted exosomes from high LIN28A expressing more aggressive cancer cells (IGROV1) versus low LIN28A expressing less aggressive cancer cells (OV420) could serve as biomarkers for detecting ovarian cancer at early stages. Using NextGen sequencing we found 320 differentially expressed RNAs. We found IGROV1 exosomes contain long non-coding RNAs. We also validated the presence of migration invasion inhibitory protein (*MIIP*) in OV420 secreted exosomes. Pathway analysis predicted amino acid metabolism, energy production, and post-translational modifications are

overrepresented among IGROV1 exosomal RNAs and embryonic development, organismal development, and tissue development are overrepresented among OV420 exosomal RNAs. This study is the first to report RNAs expressed in high LIN28A versus low LIN28A ovarian cancer cell lines, and could lead to identification of potential biomarkers in ovarian cancer.

INTRODUCTION

Approximately 90% of all ovarian cancer deaths (Seidman et al., 2004; Bell, 2005; Güth et al., 2007) are from epithelial ovarian cancer (EOC), the most aggressive and deadly form, leading to metastasis, a poorly understood process in EOC. One reason EOC is so deadly is because there is no diagnostic marker to easily detect it while it is still in early stages of progression. Many studies are focused on identifying genes that can distinguish aggressive from less aggressive EOCs to predict if patients have a poor or good prognosis. In the previous chapter, we described two EOC cell lines: IGROV1 cells, which contain high LIN28A, can induce rapid tumor formation in SCID mice (Benard et al., 1985) and OV420 cells, which do not have high levels of LIN28A, and do not form tumors in SCID mice (Lee et al., 2000). Specifically, we also have shown that exosomes secreted from IGROV1 cells can induce changes in gene expression and induce invasion and migration in HEK293 cells, whereas OV420 secreted exosomes do not (Chapter IV). It is known that exosomes secreted from tumor cells contain miRNAs, mRNA and protein signatures specific to the cell type from which they are secreted (Taylor and Gercel-Taylor , 2008). Thus there is a need to determine the RNA signatures in exosomes secreted from EOC cells to determine if these RNA signatures

could contribute to ovarian cancer progression and/or serve as biomarkers. In this study, we identified differentially expressed RNAs in IGROV1 and OV420 exosomes using NextGen sequencing analysis.

MATERIALS AND METHODS

Exosome isolation

Complete RPMI 1640 medium was ultracentrifuged (Beckman L8-80) at 100,000*g* for 16hrs at 4°C to pellet secreted membrane vesicles less than 1000nm to obtain vesicle-depleted medium. Sterile filtration was performed on vesicle-depleted medium using 0.2uM PES membranes (Thermo Scientific, 565-0020) and stored at 4°C until exosome collection.

For exosome isolation, $1x10^6$ IGROV1 and OV420 cells were seeded onto four 10cm plates (Celltreat, 229690) and cultured in either RPMI 1640 vesicle-depleted medium or DMEM vesicle-depleted medium for three days. Supernatant was collected and centrifuged at 3,000g for 15min at 4°C to remove cells and cell debris. Supernatant and ExoQuick-TC™ Exosome precipitation solution (System Biosciences, EXOTC50A-1) were combined in a 5:1 dilution, respectively and exosomes were collected as per manufacturer's instructions. Briefly, supernatant/ExoQuick-TC^{TM} biofluid was centrifuged at 1,500g for 30 minutes at 4°C; biofluid was aspirated, and centrifuged at 1,500g for 5 minutes at 4°C to remove excess biofluid without disturbance of exosome pellets. Exosome pellets were combined from four 10cm plates with $1X10^6$ cells seeded

per plate, and resuspended in 200μL of TRIzol LS Reagent (Life Technologies, 10296028) and RNA isolation was performed immediately.

RNA isolation

Total RNA was isolated from exosome isolates using TRIzol® LS Reagent (Life technologies, 10296-028). RNA isolation method was completed as per manufacturer's instructions with minor modifications. Briefly, exosomes were lysed in 200μL TRIzol LS Reagent (Life technologies, 10296-028) and homogenized with a handheld agitator for 5 minutes. Phase separation was conducted by adding 128μL of chloroform and homogenization for 5 minutes. Samples were centrifuged for 15min at 4°C to separate the RNA, DNA, and protein phases. The RNA aqueous phase was added to 400μL of cold 100% isopropanol and stored at -80°C overnight to enhance RNA precipitation. RNA was pelleted via centrifugation and was washed twice with cold 75% ethanol and resuspended in 10μL of RNase/DNase-free water.

Once total RNA was isolated from exosomes, DNase-free™ DNase Treatment and Removal kit (Ambion, AM1906) was used to eliminate genomic DNA contamination. RNA quality and concentration were assessed using the NanoDrop® ND-1000 spectrophotometer (NanoDrop Technologies, USA). Total RNA absorbance of 260/280 was measured and samples with RNA purity between 1.7-2.2 were used for experiments. Isolated RNA samples were stored at -80°C until RNA-sequencing was performed.

Library preparation for RNA-seq

The RNA collected from exosomes was tested again for purity and concentration levels using the Agilent Bioanalyzer (Agilent Technol., Palo Alto, CA) at the University of Colorado's Genomics (UCD) Genomics and Microarray Core where the cDNA libraries were constructed. Approximately 200ng of total RNA was used to generate Illumina HiSeq libraries using the TruSeq Sample Preparation RNA kit (Illumina®, RS-122-2001) according to manufacturer's instructions, and double-stranded DNA fragments were purified for clonal cluster generation. This process selects double-stranded DNA products by size-selected fragments and groups them into clonally similar clusters.

NextGen Sequencing and analysis

Sequencing was performed at the UCD's Genomics and Sequencing Core Facility using the Illumina HiSeq platform. Briefly, three lanes of flow cell for mRNA was used and sequenced to detect splice variances. Nine samples were sequenced across three lanes and were used to ensure approximately fifty million paired-end reads occurred per sample. Transcript levels were quantified in fragments per kilobase of exon per million mapped reads (FPKM). The FPKM reflects the molar concentration of a transcript in the starting sample by normalizing for gene length and for the total read number in the measurement. After quality trimming, each read generated within each sample was mapped to the Human genome by GSNAP to map genomic locations and assign them their gene/splice variant of origin. Cufflinks was used to calculate the prevalence of transcripts from each known gene based on normalized read counts and significant

isoform expression was determined using ANOVA in R. Ingenuity Pathway Analysis (IPA) was used to identify potential pathways over-represented by exosomal RNAs.

*Reverse Transcriptase PCR (*RT-PCR)

RT-PCR was performed from total RNA (see above) where 1μg of RNA was reverse transcribed for using qScript™cDNA supermix (Quanta Biosciences, 95047-100) as per manufacturer's instructions. Once cDNA was made, the GoTaq® DNA Polymerase kit (Promega, M3005) was used with 1000ng of cDNA and 10μM primer. These were placed in the Veriti 96 well Thermocycler with cycling parameters beginning with initial denaturation for 5 minutes at 94°C followed by 40 cycles of 15 seconds at 94°C of denaturation, 30 seconds at 60°C for annealing and 15 seconds at 72°C for elongation. The cycles ended with 3 minutes at 72°C and held at 4°C until run was ended. cDNA samples were electrophoresed on a 2% agrose gel @190V for 30 minutes and imaged using the ChemiDoc™ MP System with the Image Lab 4.1 software. Experiments were carried out using three independent biological replicates and the experiments were repeated. Primers for migration and invasion inhibitory protein (MIIP) were designed spanning introns to prevent amplification of gDNA. The primers sequences are listed in Table 4.

Table 4: PCR primer sequences used to amplify *MIIP*

PCR primers	Sequence (5'-3')	Base Pair Size
MIIP	F: AGGTCCATCCTGGCTCAAC R: CAATCCAGTCATAGCCCAGGTA	118bp

RESULTS

RNAs detected in IGROV1 and OV420 exosomes using NextGen Sequencing

RNA sequencing was used to construct cDNA libraries from RNA samples of IGROV1 exosomes (n=3) and OV420 exosomes (n=3) yielded a total of 149 million high-quality sequence reads. Data analysis identified 320 RNAs differentially expressed (Appendix II), based on p-values <0.05, in IGROV1 versus OV420 exosomes. Of these RNAs, 167 are higher in IGROV1 exosomes and 153 are higher in OV420 exosomes. Fold changes were used to generate a list of the top 15 exosomal RNAs present in IGROV1 (Table 5-top) and OV420 exosomes (Table 5-bottom). Of the 15 RNAs that are significantly higher in IGROV1 exosomes, we found numerous small RNAs including small nucleolar RNAs known as snoRNAs (SNORA8) and long non-coding RNAs, 7SK RNA, FRG1B, and Y RNA. We also detected adhesion molecule *CD36* and Rho family GTPase 3 (*RND3*). When assessing OV420 exosomal RNAs, we also found long non-coding RNAs, protein coding genes, and the small nuclear RNA U4.

Table 5: Top 15 RNAs in exosomes secreted by IGROV1 and OV420 exosomes

Table 5: Next Gen Sequencing Results of Exosomal RNAs				
Ensemble Gene ID	Gene Symbol	Chromosome	Description	Fold Change
Top 15 RNAs significantly (p<0.05) higher in exosomes secreted by IGROV1 compared to OV420				
ENSG000002060977	*snoRNA*	6	Small nucleolar RNA SNORA8	35.5
ENSG00000254314	*RP11-26M5-3*	8	Clone-based (Vega) Novel antisense	23.7
ENSG00000199711	*Y RNA*	17	Y RNA	23.0
ENSG00000105705	*SUGP1*	19	SURP and G patch domain containing 1	19.3
ENSG00000149531	*FRG1B*	20	FSDH region gene 1 family, member 8	18.9
ENSG00000222107	*7sK RNA*	5	7SK RNA	14.6
ENSG00000226499	*RP5-882O7.1*	1	Clone-based (Vega) Known Pseudogene	13.9
ENSG00000135218	*CD36*	7	CD36 molecule (thrombospondin receptor)	12.6
ENSG00000215467	*RPL27AP*	20	Ribosomal protein L27a pseudogene	12.1
ENSG00000252001	*RNA5SP303*	10	RNA, 5S ribosomal pseudogene 303	11.8
ENSG00000239317	*RP11-449H3.2*	5	Clone based (Vega Known pseudogene	11.8
ENSG00000249835	*VCAN-AS1*	5	VCAN antisense RNA 1	10.6
ENSG00000158321	*AUTS2*	7	Autism susceptibility candidate 2	10.1
ENSG00000146830	*GIGYF1*	7	GRB10 interacting GYF protein 1	9.1
ENSG00000115963	*RND3*	2	Rho family GTPase 3	8.9
Top 15 RNAs significantly (p<0.05) higher in exosomes secreted by OV420 compared to IGROV1				
ENSG00000235297	*FAUP1*	18	FBR-MuSV-associated ubiquitously expressed (fox derived) pseudogene 1	96.7
ENSG00000188850	*RP11-159F24.2*	5	Clone-based (Vega) Pseudogene	65.4
ENSG00000123106	*CCDC91*	12	Coiled-coil domain containing 91	65.3
ENSG00000222808	*snRNA*	17	U4 spliceosomal RNA	65.1
ENSG00000224338	*EP11-149p14.1*	1	Clone-based (Vega) Pseudogene	64.3
ENSG00000240183	*SRP RNA*	2	Metazoan signal recognition particle RNA	55.5
ENSG00000211793	*TRAV9-2*	14	T cell receptor alpha variable 9-2	53.7
ENSG00000152936	*IFLTD1*	12	Intermediate filament tail domain containing 1	49.5
ENSG00000253238	*RP11-941H19.3*	8	Clone-based (Vega Novel processed transcript	48.9
ENSG00000163746	*PLSCR2*	3	Phospholipid scramblase 2	47.0
ENSG00000239435	*KCNMB3P1*	22	Potassium large conductance calcium-activated channel, subfamily M, beta member 3	40.0
ENSG00000232874	*RP11-135A1.2*	3	Clone-based (Vega Novel antisense	38.1
ENSG00000214954	*LRRC69*	8	Leucine rich repeat containing 69	36.7
ENSG00000174407	*C20orf166*	20	Chromosome 20 open reading frame 166	36.0
ENSG00000225779	*1RP4-603I14.3*	1	Clone-based (Vega) Known pseudogene	35.1

Ingenuity Pathway Analysis (IPA)

We performed IPA using exosomal RNAs detected in IGROV1 exosomes and revealed several pathways are over-represented by 15 exosomal RNAs, including cancer, developmental disorders, cell cycle, organ morphology, amino acid metabolism, inflammatory response, and organismal injury and abnormalities (Table 6). The canonical pathways that were associated with IGROV1 exosomal RNAs were Protein Kinase A signaling, mTOR signaling, and integrin signaling. The top network identified by IPA of the top 15 RNAs contained in IGROV1 exosomes was associated with amino acid metabolism, energy production, and post-translational modification demonstrates the network pathway (Figure 20).

Table 6: Pathways associated with IGROV1 exosomal RNAs.

Pathways associated with IGROV1 exosomal RNAs		
Diseases and Disorder	**p-Value**	**Molecules**
Developmental Disorder	1.33E-04 - 4.44E-02	19
Neurological Disease	1.33E-04 - 4.05E-02	16
Organismal Injury and Abnormalities	1.33E-04 - 3.65E-02	9
Cancer	3.34E-04 - 4.05E-02	24
Inflammatory Response	1.82E-03 - 3.16E-02	8
Molecular and Cellular Functions	**p-Value**	**Molecules**
Cell Cycle	5.69E-04 - 4.05E-02	14
Amino Acid Metabolism	7.29E-04 - 4.37E-02	4
Energy Production	7.29E-04 - 3.53E-02	4
Post-Translational Modification	7.29E-04 - 9.13E-03	2
Small Molecule Biochemistry	7.29E-04 - 4.05E-02	15
Physiological System Development and Functions	**p-Value**	**Molecules**
Digestive System Development and Function	2.05E-04 - 4.05E-02	7
Hair and Skin Development and Function	5.69E-04 - 4.05E-02	9
Tissue Development	5.69E-04 - 4.05E-02	13
Nervous System Development and Function	1.56E-03 - 4.48E-02	15
Organ Morphology	1.56E-03 - 4.48E-02	17

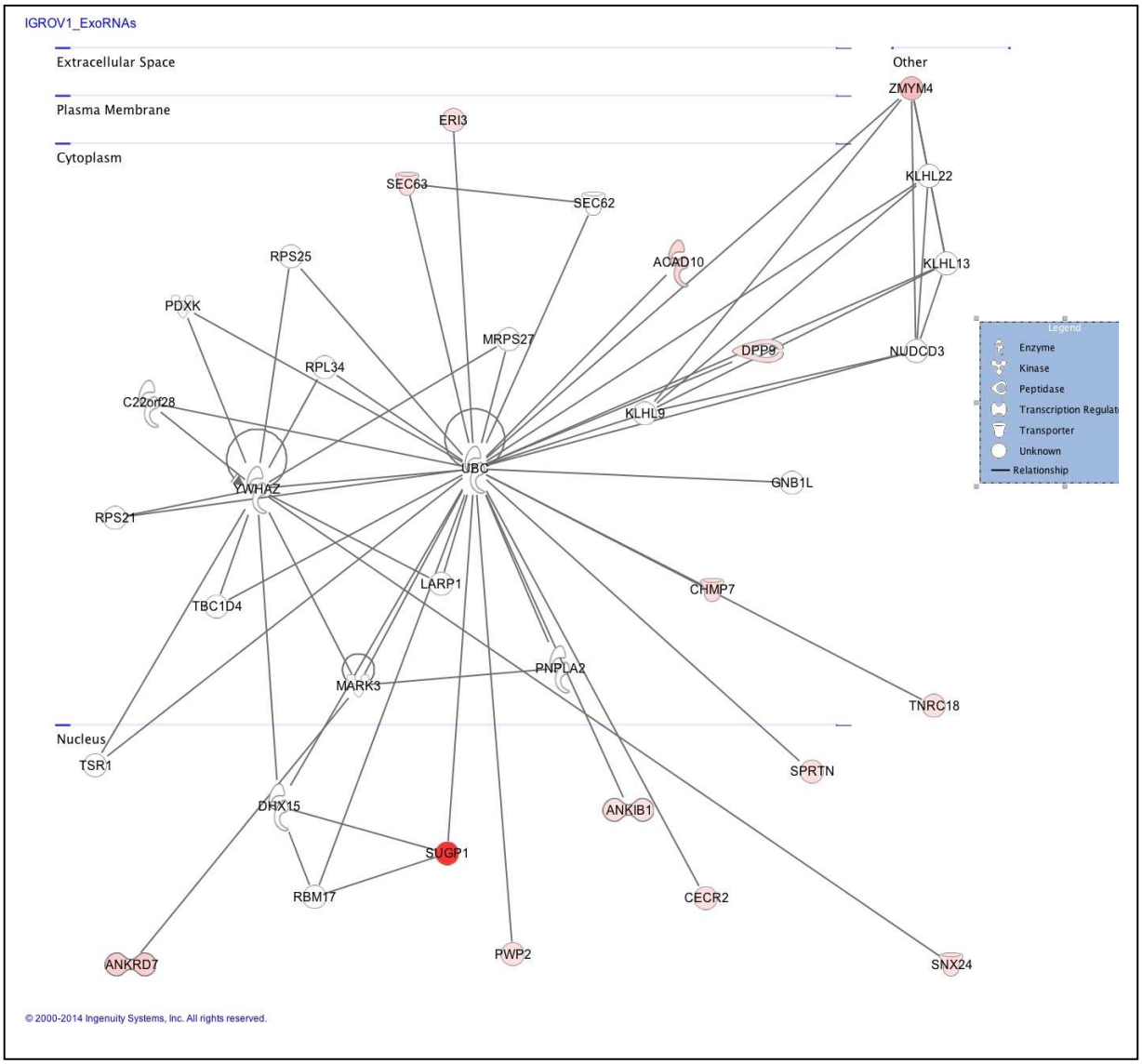

Figure 20: Top network identified by IPA of the top 15 mRNAs contained in IGROV1 exosomes was associated with amino acid metabolism, energy production, and post-translational modifications.

Additionally, we performed IPA using exosomal RNAs detected in OV420 exosomes and revealed several pathways over-represented by the 15 exosomal RNAs, including cancer, developmental disorders, cell cycle, cell-to-cell signaling and interaction, cell death and survival and DNA replication, recombination, and repair (Table 7). The top network identified by IPA of the top 15 RNAs contained in OV420 exosomes was

associated with embryonic development, organismal development, and tissue development (Figure 21).

Table 7: Pathways associated with OV420 exosomal RNAs

Pathways associated with OV420 exosomal RNAs		
Diseases and Disorder	**p-Value**	**Molecules**
Developmental Disorder	1.27E-03 - 2.05E-02	5
Renal and Urological Disease	1.27E-03 - 4.18E-02	10
Cancer	3.55E-03 - 4.86E-02	38
Connective Tissue Disorders	3.55E-03 - 1.76E-02	3
Dermatological Diseases and Conditions	3.55E-03 - 3.84E-02	2
Molecular and Cellular Functions	**p-Value**	**Molecules**
Cell-To-Cell Signaling and Interaction	3.43E-04 - 4.41E-02	9
DNA Replication, Recombination, and Repair	4.40E-04 - 4.18E-02	4
Carbohydrate Metabolism	3.55E-03 - 2.92E-02	5
Cell Cycle	3.55E-03 - 4.18E-02	6
Cell Death and Survival	3.55E-03 - 4.24E-02	9
Physiological System Development and Functions	**p-Value**	**Molecules**
Nervous System Development and Function	3.43E-04 - 4.86E-02	8
Cardiovascular System Development and Function	3.55E-03 - 4.86E-02	3
Connective Tissue Development and Function	3.55E-03 - 2.11E-02	2
Embryonic Development	3.55E-03 - 4.86E-02	9
Hair and Skin Development and Function	3.55E-03 - 3.55E-03	1

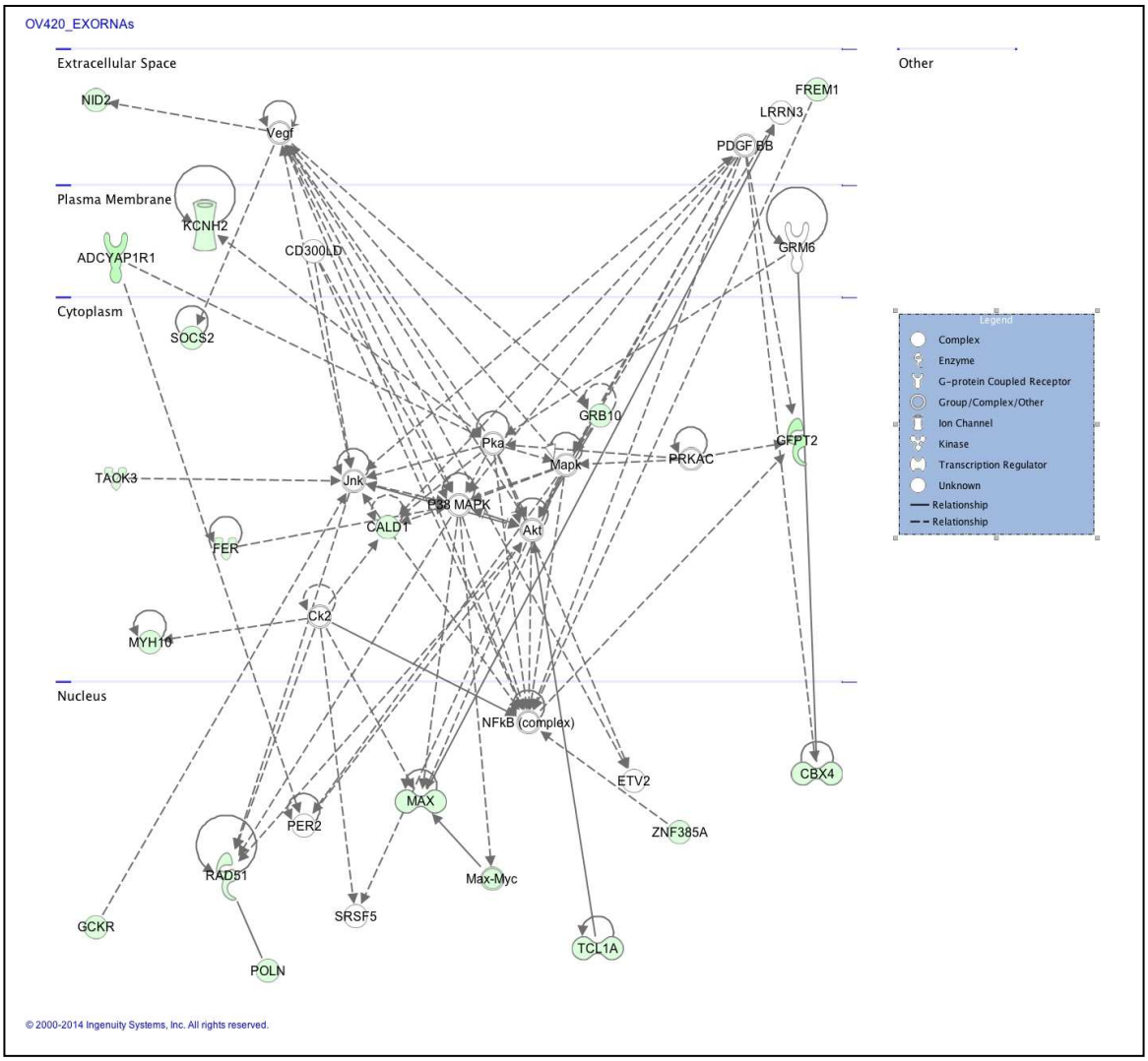

Figure 21: Top network identified by IPA of the top 15 mRNAs contained in OV420 exosomes was associated with embryonic development, organismal development, and tissue development.

MIIP in IGROV1 and OV420 cells and exosomes

In order to validate the NextGen sequencing results, we examined relative levels of migration and invasion inhibitory protein (*MIIP*), which was identified as significantly higher in OV420 exosomes, and regulates cell migration and mitosis (Wang, Wen and Zhang, 2011). RT-PCR was performed to determine the presence in IGROV1 and OV420 cells and exosomes (Figure 22). We detected the presence of *MIIP* in both

IGROV1 and OV420 cells, and were able to detect *MIIP* in OV420 exosomes but not in IGROV1 exosomes (Figure 22).

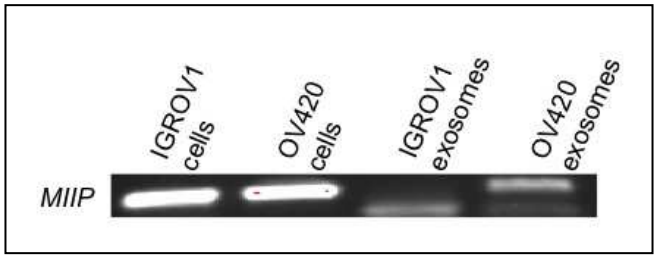

Figure 22: Detection of *MIIP* in IGROV1 and OV420 exosomes. RT-PCR was performed to determine the presence *MIIP* in OV420 exosomes to validate the NextGen sequencing results.

DISCUSSION

In this study we report differentially expressed exosomal RNAs from IGROV1 and OV420 cells and used IPA to reveal potential signaling pathways in aggressive versus less aggressive ovarian cancer cells. IGROV1 cells are more aggressive as they are capable of tumor formation upon injection of cells into SCID mice (Bernard et al., 1985) while OV420 cannot form tumors (Lee et al., 2000). It is also known that exosomes from ovarian cancer tumors contain RNAs that are not found in healthy individuals (Taylor and Gercel-Taylor, 2008) indicating RNAs in exosomes may also be found in the parent cell lines. Moreover, our previous work demonstrated IGROV1 cells contain high levels of the RNA binding protein LIN28A, whereas OV420 cells do not. Additionally, IGROV1 cell lines secrete exosomes that induce migration and invasion in HEK293 cells. We hypothesized IGROV1 and OV420 cells secrete exosomes containing differentially expressed RNAs, leading to potential identification of biomarkers for detecting ovarian cancer at early stages. NextGen sequencing of exosomal RNAs secreted from IGROV1 cells identified elevated levels of RNAs involved in cell proliferation, migration, invasion, adhesion, and tumorigenic hallmarks of cancer compared to OV420 exosomes.

We reported that 167 exosomal RNAs were significantly higher in IGROV1 exosomes and the top 15, with the greatest fold change, were used to generate a network pathway. Our study showed that among the top 15 IGROV1 exosomal RNAs were small nucleolar RNAs (snoRNAs), which are part of non-protein coded RNAs (ncRNAs) that are known to guide site specific rRNA modifications (Mattick and Makunin., 2006). Recently, twenty-two snoRNAs that were specific to tumor initiating cells (TICs) from non-small cell lung cancer (NSCLC) were found (Mannoor et al., 2014). When snoRNA42 was knocked down in TICs, tumorigenesis was decreased in mice (Mannoor et al., 2014). These finding demonstrated snoRNAs increase tumorigenesis in NSCLC. Also, snoRNAs are detected in exosomes derived from human plasma (Huang et al., 2013), but there is little to no data on exosomes derived from epithelial ovarian cancer cells. In this study we report *SNORA8* is elevated in IGROV1 secreted exosomes. To our knowledge this is the first report of snoRNA (SNORA8) in EOC exosomes and further validation and functional analyses could lead to elucidation of a role for *SNORA8s* in tumorigenesis.

Long non-coding RNAs are known regulators of chromatin remodeling, transcriptional co-activation, protein inhibition, post-transcriptional modifications, or act as decoy elements (Cheetham et al., 2013). They are involved in numerous cancers, such as prostate cancer (Kotake et al., 2011; Pasmant el al., 2011; Chung et al., 2011; de la Taille., 2007), gastric cancer (Yang et al., 2012), bladder and kidney (Martens-Uzunova et al., 2014). In this study we demonstrated lncRNA FSCH region gene 1 family

member 8 (*FRG1B)* and *7SK RNA* are higher in IGROV1 secreted exosomes. By using the genes-to-systems breast cancer database, *FRG1B* was reported as a pseudogene that is highly correlated in primary breast cancer tumors, but presence and function have yet to be revealed. In gastric cancer, knockdown of LARP7, a RNA binding protein gene that is associated with microsatellite instability, leads to decreased levels of *7SK* RNA and increases in cell migration and proliferation (Cheng et al., 2012). Conversely, LARP7 is upregulated in metastatic cervical cancer tumors, which leads to increases in *7SK* (Biewenga et al., 2008). It is possible that *7SK* has a pleiotropic function in ovarian cancer, however the role of *7SK* in ovarian cancer and their secreted exosomes has yet to be elucidated.

Another RNA that was increased in IGROV1 secreted exosomes was the cluster of differentiation 36 (*CD36*), a transmembrane glycoprotein. It is known that *CD36* is a regulator of integrin's and can sequester integrin's, such as $\alpha 3 \beta 1$ and $\alpha 6 \beta 1$, into the membrane leading to an increase in migration of MV3 melanoma cells (Thorne et al., 2000). *CD36* downregulation is associated with good prognosis (Rachidi et al., 2013) and *CD36* is upregulated in chemosensitive tumors of advanced ovarian serous adenocarcinomas (Choi et al., 2012b), suggesting it is associated with recurrent ovarian cancer progression. As our study demonstrated, IGROV1 exosomes have significantly higher levels of *CD36,* which is also involved in chemosensitivity; therefore, studying the role *CD36* in target tissues may be important in understanding ovarian cancer recurrence.

Finally, another RNA that we reported higher in IGROV1 secreted exosomes was the Rho Family GTPase 3, *RND3*. RND3 is a branch of the Rho family of GTPases that are important in regulating cytoskeleton dynamics as they control cell shape and mobility (Klein et al., 2008). *RND3* has also been implicated in transformation of epithelial cells when RAF, a proto-oncogene involved in pathways that control cell growth, proliferation, and differentiation, is activated (Hansen et al., 2000). Also, in melanoma, *RND3* is required for invasion; when RND3 is knocked down in melanoma spheroids invasion was reduced (Klein and Aplin., 2009). We demonstrated IGROV1 secreted exosomes have higher levels of RND3 suggesting cytoskeletal dynamics can be modified leading to a more invasive phenotype in ovarian cancer cells, but functional analysis is still needed to confirm this finding.

We reported that 167 RNAs are significantly higher in OV420 exosomes and the top 15, with the greatest fold change were used to identify over-represented pathways among the exosomal RNAs. The intermediate filament tail domain containing 1 (*IFLTD1)* RNA, also known as *LMNA-RS1*, is a protein-coding gene that is associated with lung adenomas. In lung tumors LNMA-RS1 was not detected, indicating this differentiation marker does not give rise to tumor formation (Manenti et al., 2004). This is important because OV420 exosomes have high levels of this RNA and their cells are less capable of inducing tumors (Lee et al., 2000). These data suggest *IFLTD1* may be an important tumor suppressor in early tumorigenesis and when altered, oncogenes could be activated but further analysis is need to confirm function.

A number of long non-coding RNA pseudogenes and antisense-RNAs are present at significantly higher levels in OV420 exosomes. Novel long non-coding RNAs found in OV420 exosomes were 1) FBR-MusV-associated ubiquitously expressed (fox derived) pseudogene 1 (FAUP1), 2) Clone based (Vega) Pseudogenes (*RP11-159F24.2, EP11-149P14.1, RP11-941H19.3, RP11-941H19.3*, and *1RP4-603I14.3*), 3) Metazoan signal recognition particle RNA (*SRP RNA*) and 4) Clone based (Vega) novel anti-sense (RP11-135A1.2). Similarly, IGROV exosomes contain two novel anti-sense RNAs, Clone-bases (Vega) novel anti-sense (RP11-26M5-3) and VCAN antisense RNA 1 *(VAN-AS1*) as well as four novel pseudogenes: 1) SURP and G patch domain contain1 (*SUGP1),* Clone based (Vega) Pseudogene *RP-883O7.1,* 3) Ribosomal protein L27a pseudogene (*RPL27AP),* and 4) RNA, 5S ribosomal pseudogene 303 (*RP11-449H3.2*). With the innovation of whole genome wide sequencing, studies have shown long non-coding RNAs in large amounts when transcriptome analyses were performed (Bertone et al., 2004; Carninci et al., 2005; Kapranov et al., 2002; Rinn et al., 2003). Recently, transcriptome analysis of exosomes also depict large amounts of long non-coding RNAs that are present (Huang et al., 2013). Additionally, long non-coding RNA pseudogene, *PTENpg1*, a *PTENpg1*-encoded antisense RNA, can regulate PTEN mRNA stability, a tumor suppressor, often decreased in cancer (Johnsson et al., 2012). Furthermore, when *PTENpg1* is inhibited the cell-cycle arrests and cells are more sensitive to the effects of doxorubicin, a cancer drug (Johnsson et al., 2012). These findings suggest long-non coding pseudogenes and anti-sense RNAs are important in cancer regulation and assessing their function and targets in ovarian cancer could lead to further

understanding of metastasis regulation in more aggressive versus less aggressive cancers.

We have demonstrated the presence of RNAs that are differentially present in IGROV1 and OV420 exosomes, but we did not reveal a functional role of exosomal RNAs. IPA revealed several pathways that are over-represented by the 15 exosomal RNAs. IPA of the top 15 mRNAs contained in IGROV1 exosomes associated with “Cell Cycle” and “Organ Morphology” and the OV420 exosomes associated with “Cell death and survival” and “DNA replication, Recombination, and Repair”. IGROV1 cells are more aggressive therefore it could be postulated that IGROV1 exosomes contain RNAs involved in changing “Organ Morphology” which could lead to EMT increases in target cells. We did reveal EMT related genes were higher in HEK293 cell exposed to IGROV1 exosomes (Chapter IV). Also, RNAs found in OV420 exosomes may have functions important for repair and cell cycle regulation of the target cells that have taken up these exosomes, which may explain why OV420 exosomes do not induce invasion or migration, but further studies are necessary to confirm function of RNAs in these signaling pathways.

IPA identified signaling pathways associated RNAs in aggressive and less aggressive ovarian cancer. In IGROV1 exosomes, “Amino acid metabolism”, “Energy Production” and “Post-Transcriptional Modifications” networks were the highest scored pathways associated with exosomal RNAs. In OV420 exosomes, “Embryonic Development”, “Organismal Development” and “Tissue development” networks were the highest scored pathways associated with exosomal RNAs. Overall, we determined potential functional

differences in exosomes secreted by aggressive versus less aggressive ovarian cancer cells, which can lead to identification of pathways activated at late and early stages in EOC development.

In order to validate the RNAs generated from NextGen sequencing results we selected migration and invasion inhibitory protein (*MIIP*), a recently discovered protein that binds to insulin-like growth factor binding protein 2 and inhibits invasion in glioma cells (Song et al., 2003). *MIIP* was significantly higher in OV420 exosomes, which are secreted from cells that are less able to produce a tumor in mice (Lee et al., 2000). Our RT-PCR results demonstrate that *MIIP* is present in OV420 exosomes and not in IGROV1 exosomes, supporting our NextGen sequencing results. Interestingly, we revealed *MIIP* was present in both IGROV1 and OV420 cells. It is unknown how RNAs are loaded into exosomes. Elucidating how RNAs are selected and loaded into exosomes can improve biomarker identification and therapeutic approaches on how to combat aggressive ovarian cancer.

Overall, this study presents new data in the field of ovarian cancer through identification of RNAs present in exosomes secreted by aggressive and less aggressive EOC cells, which has not been previously reported. Moreover, we found numerous long non-coding RNAs in both exosome populations and believe they may play an important role in ovarian cancer. Furthermore, we identified *CD36* and *RND3* protein-coding RNAs in IGROV1 exosomes, which are upregulated in tumors. IPA identified IGROV1 exosomes may influence “Organ Morphology” signaling pathways and OV420 exosomes may

influence “Cell death and survival” as well as “DNA replication, recombination, and repair” demonstrating IGROV1 exosomes could be involved in cancer progression and OV420 exosomes could be involved in preventing cancer progression. Although functional analysis was not performed in this study, we do demonstrate novel findings and further validation could lead to identification of biomarkers in early stage epithelial ovarian cancer patients.

CHAPTER VI: GENERAL DISCUSSION AND CONCLUSIONS

The overall purpose and goal of this dissertation research was to determine the role that pluripotency factors, miRNAs and cell-secreted exosomes, have on gene expression and cell phenotype in ovarian cancer. The central hypothesis tested was that ovarian cancer cell-secreted exosomes contain factors that can induce changes in gene expression and cell phenotype in target cells. In order to achieve this objective we examined pluripotency factors and miRNAs in two epithelial ovarian cancer cell lines, IGROV1 (more aggressive) and OV420 (less aggressive). We also examined LIN28 mRNA and protein levels, *let-7* miRNAs, and additional miRNAs that were associated with advanced malignancies (*miR-17, miR-18a, miR-19a, miR-19b, miR-20a, miR-92, miR-22, miR-200a, miR-200b, miR-200c, miR-9, miR-30a, miR-30b, miR-30c, miR-30d, miR-30e, miR31, miR-125a-3p, miR-125-5p*, and *miR-125b*) in both cell lines and their secreted exosomes. We determined that IGROV1 exosomes contain miRNAs that may target genes involved in EMT and revealed an increase in invasion and migration of HEK293 cells exposed to IGROV1 exosomes. We also used NextGen sequencing on IGROV1 and OV420 exosomes to identify RNAs that are differentially present. This could lead to potential identification of RNAs signatures that are higher in IGROV1 and OV420 exosomes. Ultimately, this work could lead the identification of new diagnostic and prognostic biomarkers in ovarian cancer.

In chapter III, we assessed the relative levels of *LIN28A, TFAP2C, HMGA2, POU5F1,* and *MYC* and miRNAs in our two epithelial ovarian cancer cell lines. *LIN28A, HMGA2,*

and *POU5F1* were higher in IGROV1 cells suggesting the more aggressive tumorigenic nature of these cells when injected into SCID mice possible (Benard et al., 1985) could be due to high levels of these pluripotency factors. Conversely, the less aggressive OV420 cells only had higher levels of MYC. Co-expression of LIN28A and POU5F1 is associated with cancer stem cell subpopulations of patient tumor samples (Peng et al., 2010) and our data also revealed IGROV1 cells have an increase of both *LIN28A* and *POU5F1* suggesting that aggressive EOC cancer cells may have a subpopulation of cancer stem cells. Additionally, HMGA2 was found overexpressed in individuals with high-grade serous carcinoma (Mahajan et al., 2010), and *let-7/miR-98* family is a negative regulator of HMGA2 (Malek et al., 20008). Our data confirm these results as IGROV1, more aggressive, have high *HMGA2* and lower *let-7s*. Additionally, we revealed TFAP2A and TFAP2C can bind to the promoter region of LIN28A in IGROV1 and OV420 cells and our data suggest it may be possible that TFAP2A and TFAP2C regulate LIN28A in IGROV1 and OV420 cells, but functional analysis has yet to be performed. We also found *MYC* and a subset of the *miR-17-92* cluster (*miR-17, miR-19a, miR-19b,* and *miR-92*) were higher in OV420 cells compared to IGROV1 cells. Previous studies reported C-MYC can bind to the *miR-17-92* cluster (O'Donnell et al., 2005), and positive levels of MYC is associated with 92% survival (Skirnisdottir et al., 2011). In summary, our findings suggest high levels of *LIN28A, HMGA2*, and *POU5F1* can be used to detect late stages of ovarian cancer and *MYC* can be used to detect early stages of ovarian cancer. Also our findings imply low *miR-17, miR-19a, miR-19b, miR-20a, miR92a* levels in IGROV1 cells occur because MYC is low. Furthermore, TFAP2A and TFAP2C can bind to the LIN28A promoter region in IGROV1 and OV420

cells and may regulate *LIN28A*, although that was not tested. Overall, this study may be important for determining the differences in pluripotency factors and miRNAs in regulating genes related all hallmarks of cancer: resisting cell death, sustaining proliferative signaling, evading growth suppressors, enabling replicative immortality, inducing angiogenesis and activating invasion and migration.

In Chapter IV, we determined the presence of LIN28 and *let-7* miRNAs in aggressive and less aggressive ovarian cancer cells and their secreted exosomes. Also we examined if exosomes taken up by HEK293 cells can induce changes in gene expression and cell phenotype. To assess the hypothesis that ovarian cancer cell secreted-exosomes can induce changes in gene expression and cell phenotype. We determined if *LIN28* could be transferred by exosomes to target cells. *LIN28A* was found in exosomes, but not protein. Previous studies have shown some mRNAs are truncated in exosomes and cannot be translated into functional protein. It is suggested that truncated mRNAs may instead compete with other RNA leading to regulation of mRNA stability, localization and transcriptional activity (Batogov and Kurochkin, 2013). In addition to assessing LIN28A levels, we confirmed the uptake of exosomes by target HEK293 cells, and pursued identification of gene expression changes following exosome treatments of HEK293 cells. HEK293 cells had significantly higher levels of 45 genes related to epithelial to mesenchymal transition and higher *miR-9* levels after IGROV1 exosome exposure. Interestingly, *miR-9* is a regulator of snail family zinc finger 2 *SNAI2,* also known as *SLUG* (Grimson et al., 2007; miRSearch V3.0 Exiqon). Finally, we determined HEK293 cells exposed to IGROV1 exosomes gained the ability to

migrate and invade. These results reveal that exosomes from high LIN28 expressing IGROV1 cells are capable of increasing *LIN28A* and *miR-9* in recipient cells, and more importantly can increase invasion and migration.

In Chapter V, we determined RNA signatures in ovarian cancer cell-secreted exosomes from more aggressive cancer cells (IGROV1) versus less aggressive cancer cells (OV420) to potentially identify biomarkers that can be used to detect early stage ovarian cancer. We performed NextGen sequencing and identified 320 differentially expressed exosomal RNAs from IGROV1 and OV420 exosomes. We found 167 RNAs were higher in IGROV1 exosomes and 153 were lower in OV420 exosomes. Of the 15 top RNAs we found IGROV1 exosomes had numerous small nuclear RNAs, small nucleolar RNAs, and long non-coding RNAS. Two RNAs *CD36* and *RND3* exhibit characteristics that may explain the observed increase in invasion and migration in HEK293 cells exposed to IGROV1 exosomes. When CD36 is upregulated, poor prognosis of patient often occurs (Rachidi et al., 2013) and individuals with advanced serous adenocarcinomas exhibit chemosensitive tumors (Choi et al., 2012b), suggesting *CD36* in exosomes may relay chemosensitivity to other cells. Also, *RND3* is a branch of the Rho family of GTPases that are important in regulating cytoskeleton dynamics that control cell shape and mobility (Klein et al., 2008). We demonstrated IGROV1 exosomes have higher levels of *RND3* suggesting cytoskeletal dynamics can be modified leading to a more invasive phenotype in ovarian cancer cells. Lastly, we identified OV420 exosomes had an increase in migration and invasion inhibitory protein, *MIIP*. We believe this could contribute to the suppression of migration and invasion in both OV420 cells and the

HEK293 cells after OV420 exosome exposure. These findings need to be explored further in order to understand how cell secreted exosomes induce invasion and migration, and to evaluate potential biomarker to distinguish between ovarian cancer patients with a poor prognosis versus patients with a good prognosis. We also speculate that exosome RNAs detected in our study could be used as urinary biomarkers for stage I-II and stage III-IV ovarian cancer patients, respectively.

In conclusion, this study: 1) determined the presence of pluripotency factors and miRNAs in more aggressive ovarian cancer cells versus less aggressive ovarian cancer cells, 2) determined the presence of *LIN28* and *let-7* miRNAs ovarian cancer cell-secreted exosomes, and determine if exosomes from high LIN28A expressing cells taken up by HEK293 recipient cells and can induce changes in gene expression and cell phenotype, and 3) identified RNA signatures in ovarian cancer cell-secreted exosomes from high LIN28A expressing, aggressive cancer cells (IGROV1) versus low LIN28A expressing, less aggressive cancer cells (OV420), which can potentially be used to identify biomarkers for detecting ovarian cancer at early stages. An overall summary of our findings is illustrated below (Figure 23).

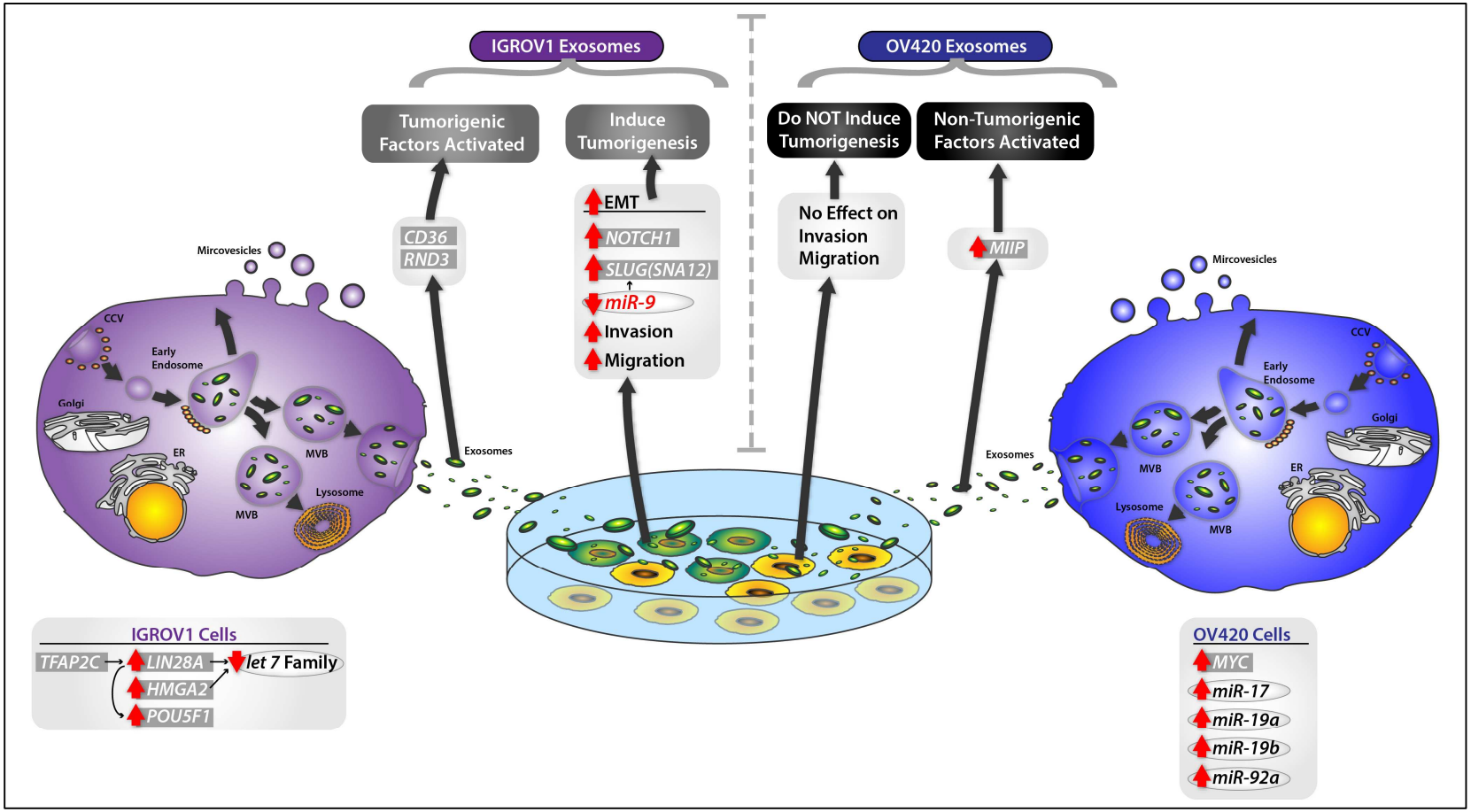

Figure 23: Summary of Major Findings

REFERENCES

Abubaker K1, Latifi A, Luwor R, Nazaretian S, Zhu H, Quinn MA, Thompson EW, Findlay JK, Ahmed N. Short-term single treatment of chemotherapy results in the enrichment of ovarian cancer stem cell-like cells leading to an increased tumor burden. Mol Cancer. 2013 Mar 27;12:24. doi: 10.1186/1476-4598-12-24.

Admyre C, Johansson SM, Oazi KR, Filen JJ, et al., Exosomes with immune modulatory features are present in human breast milk. J Immunol. 2007;179:1969–1978.

Al-Awqati Q., Proton-translocating ATPases. Ann. Rev. Cell Bioi. 1986.2:179-99

Al-Nedawi K, Meehan B, Micallef J, Lhotak V, May L, Guha A, Rak J. Intercellular transfer of the oncogenic receptor EGFRvIII by microvesicles derived from tumor cells. Nat Cell Bio l. 2008;10(5):619–624.

Altekruse SF, Kosary CL, Krapcho M, Neyman N, Aminou R, Waldron W, Ruhl J, Howlader N, Tatalovich Z, Cho H, Mariotto A, Eisner MP, Lewis DR, Cronin K, Chen HS, Feuer EJ, Stinchcomb DG, Edwards BK. Eds. 2010 SEER Cancer Statistics Review, 1975-2007. National Cancer Institute, Bethesda, MD. http://seer.cancer.gov/csr/1975_2007/.

Alvero AB, Chen R, Fu HH, Montagna M, Schwartz PE, Rutherford T, Silasi DA, Steffensen KD, Waldstrom M, Visintin I, Mor G. Molecular phenotyping of human ovarian cancer stem cells unravels the mechanisms for repair and chemoresistance. Cell Cycle. 2009 Jan 1;8(1):158-66.

Ambrosetti DC, Basilico C, Dailey L. Synergistic activation of the fibroblast growth factor 4 enhancer by Sox2 and Oct-3 depends on protein-protein interactions facilitated by a specific spatial arrangement of factor binding sites. Mol. Cell. Biol. 1997;17:6321–6329.

Andre F1, Schartz NE, Movassagh M, Flament C, Pautier P, Morice P, Pomel C, Lhomme C, Escudier B, Le Chevalier T, Tursz T, Amigorena S, Raposo G,Angevin E, Zitvogel L. Malignant effusions and immunogenic tumour-derived exosomes. Lancet. 2002 Jul 27;360(9329):295-305.

Armstron DK. Relapsed ovarian cancer: challenges and management strategies for a chronic disease. Oncologist. 2002;7 Suppl 5:20-8.

Auersperg N, Edelson MI, Mok SC, Johnson SW, Hamilton TC. The biology of ovarian cancer. Semin Oncol. 1998;25:281–304.

Baietti MF, Zhang Z, Mortier E, Melchior A, Degeest G, Geeraerts A, Ivarsson Y, Depoortere F, Coomans C, Vermeiren E, Zimmermann P, David G. Sydecan-syntenin-ALIX regulates the biogenesis of exosomes. Nat Cell Biol. 2012 Jun 3;14(7):677-85.

Bailey SM, Goodwin EH, Meyne J, Cornforth MN. CO-FISH reveals inversions associated with isochromosome formation. Mutagenesis. 1996 Mar;11(2):139-44.

Bailey SM, Williams ES, Cornforth MN, Goodwin EH. Chromosome Orientation fluorescence in situ hybridization or strand-specific FISH. Methods Mol Biol. 2010;659:173-83.

Baker SJ, Fearon ER, Nigro JM, Hamilton SR, Preisinger AC, Jessup JM, vanTuinen P, Ledbetter DH, Barker DF, Nakamura Y, White R, Vogelstein B. Chromosome 17 deletions and p53 gene mutations in colorectal carcinomas. Science. 1989 Apr 14;244(4901):217-21.

Batagov AO, Kurochkin IV. Exosomes secreted by human cells transport largely mRNA fragments that are enriched in the 3’-untranslated regions. Biol Direct. 2013 Jun 7;8:12. doi: 10.1186/1745-6150-8-12.

Batlle E1, Sancho E, Francí C, Domínguez D, Monfar M, Baulida J, García De Herreros A. The transcription factor snail is a repressor of E-cadherin gene expression in epithelial tumour cells. Nat Cell Biol. 2000;2:84–9.

Bell DA. Origins and molecular pathology of ovarian cancer. Mod Pathol. 2005;18(Suppl 2):S19 –S32.

Bénard J, Da Silva J, De Blois MC, Boyer P, Duvillard P, Chiric E, Riou G. Characterization of a human ovarian adenocarcinoma line, IGROV1, in tissue culture and in nude mice. Cancer Res. 1985 Oct;45(10):4970-9.

Bendoraite A, Knouf EC, Garg KS, Parkin RK, Kroh EM, O'Briant KC, Ventura AP, Godwin AK, Karlan BY,Berlin I, Schwartz H, Nash PD. Regulation of epidermal growth factor receptor ubiquitination and trafficking by the USP8·STAMcomplex. J Biol Chem. 20 Nov 5;285(45):34909-21. Epub 2009 Aug 24.

Berlin I1, Schwartz H, Nash PD. Regulation of epidermal growth factor receptor ubiquitination and trafficking by the USP8·STAM complex. J Biol Chem. 2010 Nov 5;285(45):34909-21. doi: 10.1074/jbc.M109.016287. Epub 2010 Aug 24.

Bertone P1, Stolc V, Royce TE, Rozowsky JS, Urban AE, Zhu X, Rinn JL, Tongprasit W, Samanta M, Weissman S, Gerstein M, Snyder M. Global identification of human transcribed sequences with genome tiling arrays. Science. 2004 Dec 24;306(5705):2242-6. Epub 2004 Nov 11.

Biewenga P1, Buist MR, Moerland PD, Ver Loren van Themaat E, van Kampen AH, ten Kate FJ, Baas F. Gene expression in early stage cervical cancer. Gynecol Oncol. 2008 Mar;108(3):520-6. doi: 10.1016/j.ygyno.2007.11.024. Epub 2008 Jan 11.

Boll W, Ohno H, Songyang Z, Rapoport I, Cantley LC, Bonifacino JS, Kirchhausen T. Sequence requirements for the recognitionof tyrosine-based endocytic signals by clathrin AP-2 complexes. EMBO J. 1996 Nov 1;15(21):5789-95.

Bolos V, Peinado H, Perez-Moreno MA, Fraga MF, Esteller M, Cano A. The transcription factor Slug represses E-cadherin expression and induces epithelial to mesenchymal transitions: a comparison with Snail and E47 repressors. J Cell Sci. 2003;116:499–511.

Bonifacino JS, Dell'Angelica EC. Molecular bases for the recognition of tyrosine-based sorting signals. J Cell Biol. 1999 May 31;145(5):923-6.

Bonnet D1, Dick JE. Human acute myeloid leukemia is organized as a hierarchy that originates from a primitive hematopoietic cell. Nat Med. 1997 Jul;3(7):730-7.

Borchert GM, Lanier W, Davidson BL. RNA polymerase III transcribes human microRNAs. Nat Struct Mol Biol. 2006 Dec;13(12):1097-101. Epub 2006 Nov 12.

Boura E, Różycki B, Chung HS, Herrick DZ, Canagarajah B, Cafiso DS, Eaton WA, Hummer G, Hurley JH. Solution structure of the ESCRT-I and -II supercomplex: implications for membrane budding and scission. Structure. 2012 May 9;20(5):874-86.

Boyer A, Lapointe E, Zheng X, Cowan RG, Li H, Quirk SM, DeMayo FJ, Richards JS, Boerboom D. WNT4 is required for normal ovarian follicle development and female fertility. FASEB J. 2010 Aug;24(8):3010-25. Epub 2010 Apr 6.

Brase JC, Johannes M, Schlomm T, Fälth M, Haese A, Steuber T, Beissbarth T, Kuner R, Sültmann H. Circulating miRNAs are correlated with tumor progression in prostate cancer. Int J Cancer. 2011 Feb 1;128(3):608-16.

Brewer S1, Jiang X, Donaldson S, Williams T, Sucov HM. Requirement for AP-2alpha in cardiac outflow tract morphogenesis. Mech Dev. 2002 Jan;110(1-2):139-49.

Brun JL, Cortez A, Lesieur B, Uzan S, Rouzier R, Daraï E. Expression of MMP-2, -7, -9, MT1-MMP and TIMP-1 and -2 has no prognostic relevance in patients with advanced epithelial ovarian cancer. Oncol Rep. 2012 Apr;27(4):1049-57. Epub 2011 Dec 22.

Bryan TM1, Englezou A, Gupta J, Bacchetti S, Reddel RR. Telomere elongation in immortal human cells without detectable telomerase activity. EMBO J. 1995 Sep 1;14(17):4240-8.

Bussing I, Slack FJ, Grosshans H. let-7 microRNAs in development, stem cells and cancer. Trends Mol Med. 2008 Sep;14(9):400-9. Epub 2008 Jul 31.

Caby MP, Lankar F, Vincendeau-Scherrer C, Raposo G, Bonnerot C. Exosomal-like vesicles are present in human blood plasma. Int. Immunol. 2005;17:879–887.

Cai Y1, Yu X, Hu S, Yu J. A brief review on the mechanisms of miRNA regulation. Genomics Proteomics Bioinformatics. 2009 Dec;7(4):147-54. doi: 10.1016/S1672-0229(08)60044-3.

Calin GA1, Croce CM. MicroRNA signatures in human cancers. Nat Rev Cancer. 2006 Nov;6(11):857-66.

Calin GA, Dumitru CD, Shimizu M, Bichi R, Zupo S, Noch E, Aldler H, Rattan S, Keating M, Rai K, Rassenti L, Kipps T, Negrini M, Bullrich F, Croce CM. Frequent deletions and down-regulation of micro-RNA genes miR15 and miR16 at 13q14 in chronic lymphocytic leukemia. Proc Natl Acad Sci USA. 2002 Nov 26;99(24):15524-9. Epub 2002 Nov 14.

Callahan MJ, Crum CP, Medeiros F, Kindelberger DW, Elvin JA, Garber JE, Feltmate CM, Berkowitz RS, Muto MG. Primary fallopian tube malignancies in BRCA-positive women undergoing surgery for ovarian cancer risk reduction. J Clin Oncol. 2007;25:3985-3990.

Campbell KH, Mcwhir J, Ritchie WA, Wilmut I. Sheep cloned by nuclear transfer from a cultured cell line. Nature. 1996;380(6569):64–66.

Cano A1, Pérez-Moreno MA, Rodrigo I, Locascio A, Blanco MJ, del Barrio MG, Portillo F, Nieto MA. The transcription factor snail controls epithelial-mesenchymal transitions by repressing E-cadherin expression. Nat Cell Biol. 2000;2:76–83.

Carninci P, Kasukawa T, Katayama S, Gough J, Frith MC, Maeda N, Oyama R, Ravasi T, Lenhard B, Wells C, Kodzius R, Shimokawa K, Bajic VB, Brenner SE,Batalov S, Forrest AR, Zavolan M, Davis MJ, Wilming LG, Aidinis V, Allen JE, Ambesi-Impiombato A, Apweiler R, Aturaliya RN, Bailey TL, Bansal M, Baxter L,Beisel KW, Bersano T, Bono H, Chalk AM, Chiu KP, Choudhary V, Christoffels A, Clutterbuck DR, Crowe ML, Dalla E, Dalrymple BP, de Bono B, Della Gatta G, di Bernardo D, Down T, Engstrom P, Fagiolini M, Faulkner G, Fletcher CF, Fukushima T, Furuno M, Futaki S, Gariboldi M, Georgii-Hemming P, Gingeras TR, Gojobori T, Green RE, Gustincich S, Harbers M, Hayashi Y, Hensch TK, Hirokawa N, Hill D, Huminiecki L, Iacono M, Ikeo K, Iwama A, Ishikawa T, Jakt M, Kanapin A,Katoh M, Kawasawa Y, Kelso J, Kitamura H, Kitano H, Kollias G, Krishnan SP, Kruger A, Kummerfeld SK, Kurochkin IV, Lareau LF, Lazarevic D, Lipovich L, Liu J,Liuni S, McWilliam S, Madan Babu M, Madera M, Marchionni L, Matsuda H, Matsuzawa S, Miki H, Mignone F, Miyake S, Morris K, Mottagui-Tabar S, Mulder N,Nakano N, Nakauchi H, Ng P, Nilsson R, Nishiguchi S, Nishikawa S, Nori F, Ohara O, Okazaki Y, Orlando V, Pang KC, Pavan WJ, Pavesi G, Pesole G, Petrovsky N, Piazza S, Reed J, Reid JF, Ring BZ, Ringwald M, Rost

B, Ruan Y, Salzberg SL, Sandelin A, Schneider C, Schönbach C, Sekiguchi K, Semple CA, Seno S,Sessa L, Sheng Y, Shibata Y, Shimada H, Shimada K, Silva D, Sinclair B, Sperling S, Stupka E, Sugiura K, Sultana R, Takenaka Y, Taki K, Tammoja K, Tan SL,Tang S, Taylor MS, Tegner J, Teichmann SA, Ueda HR, van Nimwegen E, Verardo R, Wei CL, Yagi K, Yamanishi H, Zabarovsky E, Zhu S, Zimmer A, Hide W,Bult C, Grimmond SM, Teasdale RD, Liu ET, Brusic V, Quackenbush J, Wahlestedt C, Mattick JS, Hume DA, Kai C, Sasaki D, Tomaru Y, Fukuda S, Kanamori-Katayama M, Suzuki M, Aoki J, Arakawa T, Iida J, Imamura K, Itoh M, Kato T, Kawaji H, Kawagashira N, Kawashima T, Kojima M, Kondo S, Konno H, Nakano K,Ninomiya N, Nishio T, Okada M, Plessy C, Shibata K, Shiraki T, Suzuki S, Tagami M, Waki K, Watahiki A, Okamura-Oho Y, Suzuki H, Kawai J, Hayashizaki Y;FANTOM Consortium; RIKEN Genome Exploration Research Group and Genome Science Group (Genome Network Project Core Group). The transcriptional landscape of the mammalian genome. Science. 2005 Sep 2;309(5740):1559-63.

Chambers I, Colby D, Robertson M, Nichols J, Lee S, Tweedie S, Smith A. Functional expression cloning of Nanog, a pluripotency sustaining factor in embryonic stem cells. Cell. 2003 May 30;113(5):643-55.

Chang-Ileto B, Frere SG, Chan RB, Voronov SV, Roux A, Di Paolo G. Synaptojanin 1-mediated PI(4,5)P2 hydrolysis is modulated by membrane curvature and facilitates membrane fission. Dev Cell. 2011 Feb 15;20(2):206-18.

Chang MC. The maturation of rabbit oocytes in culture and their maturation activation, fertilization and subsequent development in the Fallopian tubes. J. Exp. Zool., 1955.128: 379-405.

Chang RS. Some factors affecting the growth of normal human epithelial cell in vitro. Trans N Y Acad Sci. 1955 Jun;17(8):584-8. No abstract available.

Chappell TG, Welch WJ, Schlossman DM, Palter KB, Schlesinger MJ, Rothman JE. Uncoating ATPase is a member of the 70 kilodalton family of stress proteins. Cell. 1986 45:3–13.

Chassot AA, Gregoire EP, Lavery R, Taketo MM, de Rooij DG, Adams IR, Chaboissier MC.RSPO1/βcatenin signaling pathway regulates oogonia differentiation and entry into meiosis in the mouse fetal ovary. PLoS One. 2011;6(10):e25641. Epub 2011 Oct 3.

Chaube SK. Role of meiotic maturation regulatory factors in developmental competence of mammalian oocytes. Perspectives and Issues 2001;24(4):218-231.

Cheetham SW1, Gruhl F, Mattick JS, Dinger ME. Long noncoding RNAs and the genetics of cancer. Br J Cancer. 2013 Jun 25;108(12):2419-25. doi: 10.1038/bjc.2013.233. Epub 2013 May 9.

Chen G, Zhang Y, Wu X. 786-0 Renal cancer cell line-derived exosomes promote 786-0 cell migration and invasion in vitro. Oncol Lett. 2014 May;7(5):1576-1580. Epub 2014 Mar 11.

Cheng Y1, Jin Z, Agarwal R, Ma K, Yang J, Ibrahim S, Olaru AV, David S, Ashktorab H, Smoot DT, Duncan MD, Hutcheon DF, Abraham JM, Meltzer SJ, Mori Y. LARP7 is a potential tumor suppressor gene in gastric cancer. Lab Invest. 2012 Jul;92(7):1013-9. doi: 10.1038/labinvest.2012.59. Epub 2012 Apr 9.

Chung S1, Nakagawa H, Uemura M, Piao L, Ashikawa K, Hosono N, Takata R, Akamatsu S, Kawaguchi T, Morizono T, Tsunoda T, Daigo Y, Matsuda K, Kamatani N, Nakamura Y, Kubo M. Association of a novel long non-coding RNA in 8q24 with prostate cancer susceptibility. Cancer Sci. 2011 Jan;102(1):245-52. doi: 10.1111/j.1349-7006.2010.01737.x. Epub 2010 Sep 28.

Chi DS, Eisenhauer EL, Lang J, Huh J, Haddad L, Abu-Rustum NR, Sonoda Y, Levine DA, Hensley M, Barakat RR. What is the optimal goal of primary cytoreductive surgery for bulky stage IIIC epithelial ovarian carcinoma (EOC)? Gynecol Oncol. 2006 Nov;103(2):559-64. Epub 2006 May 22.

Chi DS1, Venkatraman ES, Masson V, Hoskins WJ. The ability of preoperative serum CA-125 to predict optimal primary tumor cytoreduction in stage III epithelial ovarian carcinoma. Gynecol Oncol. 2000;77:227–231.

Cho JA1, Park H, Lim EH, Kim KH, Choi JS, Lee JH, Shin JW, Lee KW. Exosomes from ovarian cancer cells induce adipose tissue-derived mesenchymal stem cells to acquire the physical and functional characteristics of tumor-supporting myofibroblasts. Gynecol Oncol. 2011 Nov;123(2):379-86. doi: 10.1016/j.ygyno.2011.08.005. Epub 2011 Sep 7.

Cho KR, Shih IeM. Ovarian cancer. Annu Rev Pathol. 2009;4:287-313.

Choi CH1, Choi JJ, Park YA, Lee YY, Song SY, Sung CO, Song T, Kim MK, Kim TJ, Lee JW, Kim HJ, Bae DS, Kim BG. Identification of differentially expressed genes according to chemosensitivity in advanced ovarian serous adenocarcinomas: expression of GRIA2 predicts better survival. Br J Cancer. 2012b Jun 26;107(1):91-9. doi: 10.1038/bjc.2012.217. Epub 2012 May 29.

Choi I, Carey TS, Wilson CA, Knott JG. Transcription factor AP-2γ is a core regulator of tight junction biogenesis and cavity formation during mouseearly em bryogenesis. Development. 2012a Nov 7. [Epub ahead of print]

Clark TG, Stewart ME, Altman DG, Gabra H, Smyth JF. A prognostic model for ovarian cancer. Br J Cancer 2001;85:944–52.

Clarke MF, Dick JE, Dirks PB, Eaves CJ, Jamieson CH, Jones DL, Visvader J, Weissman IL, Wahl GM. Cancer stem cells--perspectives on current status and future directions: AACR Workshop on cancer stem cells. Cancer Res. 2006 Oct 1;66(19):9339-44. Epub 2006 Sep 21.

Clayton A, Mitchell JP, Court J, Mason MD, Tabi Z. Human tumor-derived exosomes selectively impair lymphocyte responses to interleukin-2. Cancer Res. 2007;67:7458–66.

Colombo N, Parma G, Zanagnolo V, Insinga A. Management of ovarian stromal cell tumors. J Clin Oncol. 2007 Jul 10;25(20):2944-51.

Conic I, Dimov I, Tasic-Dimov D, Djordjevic B, Stefanovic V. Ovarian epithelial cancer: stem cells. ScientificWorldJournal. 2011 Jun 9;11:1243-69.

Coticchia CM, Curatolo AS, Zurakowski D, Yang J, Daniels KE, Matulonis UA, Moses MA. Urinary MMP-2 and MMP-9 predict the presence of ovarian cancer in women with normal CA-125 levels. Gynecol Oncol. 2011 Nov;123(2):295-300. Epub 2011 Sep 1.

Coticchio G, Albertini DF, De Santis L. Oogenesis. Origin, migration, and proliferation of human primordial germ cells. Book. 2013.

Cran DG, Moor RM. The development of oocytes and ovarian follicles of mammals. Sci Prog. 1980;66(263):371-83.

Creighton CJ1, Fountain MD, Yu Z, Nagaraja AK, Zhu H, Khan M, Olokpa E, Zariff A, Gunaratne PH, Matzuk MM, Anderson ML. Molecular profiling uncovers a p53-associated role for microRNA-31 in inhibiting the proliferation of serous ovarian carcinomas and other cancers. Cancer Res. 2010 Mar 1;70(5):1906-15. doi: 10.1158/0008-5472.CAN-09-3875. Epub 2010 Feb 23.

Crum CP. The female genital tract. In: Cotran RS, Kumar V, Collins T, eds. Robbins pathological basisi of disease. 6th ed. Philadelphia: W.B. Sanders Company; 1999;1066-1079.

Dahiya N1, Sherman-Baust CA, Wang TL, Davidson B, Shih IeM, Zhang Y, Wood W 3rd, Becker KG, Morin PJ. MicroRNA expression and identification of putative miRNA targets in ovarian cancer. PLoS One. 2008 Jun 18;3(6):e2436. doi: 10.1371/journal.pone.0002436.

da Silveira JC1, Veeramachaneni DN, Winger QA, Carnevale EM, Bouma GJ. Cell-secreted vesicles in equine ovarian follicular fluid contain miRNAs and proteins: a possible new form of cell communication within the ovarian follicle. Biol Reprod. 2012 Mar 19;86(3):71. doi: 10.1095/biolreprod.111.093252. Print 2012 Mar.

Dekel N, Lawrence TS, Gilula NB, Beers WH. Modulation of cell-to-cell communication in the cumulus oocyte complex and the regulation of oocyte maturation by LH. Dev Biol. 1981;86:356–362.

de Klein A, van Kessel AG, Grosveld G, Bartram CR, Hagemeijer A, Bootsma D, Spurr NK, Heisterkamp N, Groffen J, Stephenson JR. A cellular oncogene is translocated to the Philadelphia chromosome in chronic myelocytic leukaemia. Nature. 1982 Dec 23;300(5894):765-7.

de la Taille A. Progensa PCA3 test for prostate cancer detection. Expert Rev Mol Diagn. 2007 Sep;7(5):491-7.

Deregibus MC1, Cantaluppi V, Calogero R, Lo Iacono M, Tetta C, Biancone L, Bruno S, Bussolati B, Camussi G. Endothelial progenitor cell derived microvesicles activate an angiogenic program in endothelial cells by ahorizontal transfer of mRNA. Blood. 2007 Oct 1;110(7):2440-8. Epub 2007 May 29.

Dexter DL, Kowalski HM, Blazar BA, Fligiel Z, Vogel R, Heppner GH. Heterogeneity of tumor cells from a single mouse mammary tumor. Cancer Res. 1978 Oct;38(10):3174-81.

Dhahbi JM1, Spindler SR, Atamna H, Boffelli D, Mote P, Martin DI. 5'-YRNA fragments derived by processing of transcripts from specific YRNA genes and pseudogenes are abundant in human serum and plasma. Physiol Genomics. 2013 Nov 1;45(21):990-8. doi: 10.1152/physiolgenomics.00129.2013. Epub 2013 Sep 10.

Diehn M, Cho RW, Lobo NA, Kalisky T, Dorie MJ, Kulp AN, Qian D, Lam JS, Ailles LE, Wong M, Joshua B, Kaplan MJ, Wapnir I, Dirbas FM, Somlo G,Garberoglio C, Paz B, Shen J, Lau SK, Quake SR, Brown JM, Weissman IL, Clarke MF. Association of reactive oxygen species levels and radioresistance in cancer stem cells. Nature. 2009 Apr 9;458(7239):780-3.

Diniz PM, Carvalho JP, Baracat EC, Carvalho FM. Fallopian tube origin of supposed ovarian high-grade serous carcinomas. Clinics (Sao Paulo). 2011;66(1):73-6.

Donaldson JG, McPherson PS. Membrane trafficking heats up in Pavia. Golgi Meeting on Membrane Trafficking in Global Cellular Responses. EMBO Rep. 2009 Feb;10(2):132-6. Epub 2009 Jan 23. No abstract available.

Dryja TP, Rapaport JM, Joyce JM, Petersen RA. Molecular detection of deletions involving band q14 of chromosome 13 in retinoblastomas. Proc Natl Acad Sci USA 1986 83: 7391–7394.

du Bois A, Lu□ck HJ, Meier W, Adams HP, Möbus V, Costa S, Bauknecht T, Richter B, Warm M, Schröder W, Olbricht S, Nitz U, Jackisch C, Emons G, Wagner U, Kuhn W, Pfisterer J. Arbeitsgemeinschaft Gynäkologische Onkologie Ovarian Cancer Study Group. A randomized clinical trial of cisplatin/paclitaxel versus carboplatin/paclitaxel as first-line treatment of ovarian cancer., J Natl Cancer Inst. 2003 Sep 3;95(17):1320-9.

Durcova-Hills G, Tang F, Doosy G, Tooze R, Surani MA. Reprogramming primordial germ cells into pluripotent stem cells. PLoS One. 2008;3(10):e3531. doi: 10.1371/journal.pone.0003531. Epub 2008 Oct 27.

Duska LR1, Garrett A, Eltabbakh GH, Oliva E, Penson R, Fuller AF.. Paclitaxel and platinum chemotherapy for malignant mixed mullerian tumors of the ovary. Gynecol Oncol. 2002;85:459–63.

Edge SB, Compton CC., The American Joint Committee on Cancer: the 7th edition of the AJCC cancer staging manual and the future of TNM. Ann Surg Oncol. 2010 Jun;17(6):1471-4.

Edwards RG, Gates AH. Timing of the stages of the maturation divisions, ovulation, fertilization and the first cleavage of eggs of adult mice treated with gonadotrophins. J Endocrinol. 1959 May;18(3):292-304. No abstract available.

Eggan K, Jurga S, Gosden R, Min IM, Wagers AJ, Ovulated oocytes in adult mice derive from non-circulating germ cells. Nature. 2006 Jun 29;441(7097):1109-14. Epub 2006 Jun 14.

Ehrlich M, Boll W, Van Oijen A, Hariharan R, Chandran K, Nibert ML, Kirchhausen T. Endocytosis by random initiation and stabilization of clathrin-coated pits. Cell. 2004 Sep 3;118(5):591-605.

Eitan R1, Kushnir M, Lithwick-Yanai G, David MB, Hoshen M, Glezerman M, Hod M, Sabah G, Rosenwald S, Levavi H.
Tumor microRNA expression patterns associated with resistance to platinum based che motherapy andsurvival in ovarian cancer patients. Gynecol Oncol. 2009 Aug;114(2):253-9. doi: 10.1016/j.ygyno.2009.04.024. Epub 2009 May 14.

Eliyahu D, Raz A, Gruss P, Givole D, Oredn M. Participation of p53 cellular tumour antigen in transformation or normal embryonic cells. Nature. 1984 Dec 13-19;312(5995):646-9.

Escola JM, Kleijmeer MJ, Stoorvogel W, Griffith JM, Yoshie O, Geuze HJ. Selective enrichment of tetraspan proteins on the internal vesicles of multivesicular endosomes and on exosomes secreted by human B-lymphocytes. J. Biol. Chem. 1998. 273, 20121-20127.

Escrevente C1, Keller S, Altevogt P, Costa J. Interaction and uptake of exosomes by ovarian cancer cells. BMC Cancer. 2011 Mar 27;11:108. doi: 10.1186/1471-2407-11-108.

Esquela-Kerscher A1, Trang P, Wiggins JF, Patrawala L, Cheng A, Ford L, Weidhaas JB, Brown D, Bader AG, Slack FJ. The let-7 microRNA reduces tumor growth in mouse models of lung cancer. Cell Cycle. 2008 Mar 15;7(6):759-64. Epub 2008 Mar 3.

Evans MJ, Kaufman MH. Establishment in culture of pluripotential cells from mouse embryos. Nature. 1981 Jul 9;292(5819):154-6.

Evdonin AL, Martynova MG, Bystrova OA, Guzhova IV, Margulis BA, Medvedeva ND. The release of Hsp70 from A431 carcinoma cells is mediated by secretory-like granules. Eur. J. Cell Biol. 2006;(85):443-455.

Farazi TA1, Hoell JI, Morozov P, Tuschl T. MicroRNAs in human cancer. Adv Exp Med Biol. 2013;774:1-20. doi: 10.1007/978-94-007-5590-1_1.

Fathalla MF. Factors in the causation and incidence of ovarian cancer. Obstet Gynecol Surv. 1972 Nov;27(11):751-68. Review.
Featherstone C, Jackson SP. Ku, a DNA repair protein with multiple cellular functions? Mutat Res. 1999 May 14;434(1):3-15.

Ferguson SM, Raimondi A, Paradise S, Shen H, Mesaki K, Ferguson A, Destaing O, Ko G, Takasaki J, Cremona O, O' Toole E, De Camilli P. Coordinated actions of actin and BAR proteins upstream of dynamin at endocytic clathrin-coated pits. Dev Cell. 2009 Dec;17(6):811-22. Erratum in: Dev Cell. 2010 Feb 16;18(2):332. Ferguson, Shawn [corrected to Ferguson, Shawn M].

FIGO Committee on Gynecologic Oncology. Current FIGO staging for cancer of the vagina, fallopian tube, ovary, and gestational trophoblastic neoplasia. Int J Gynaecol Obstet. 2009;105(1): 3-4.

Finch A1, Beiner M, Lubinski J, Lynch HT, Moller P, Rosen B, Murphy J, Ghadirian P, Friedman E, Foulkes WD, Kim-Sing C, Wagner T, Tung N, Couch F, Stoppa-Lyonnet D, Ainsworth P, Daly M, Pasini B, Gershoni-Baruch R, Eng C, Olopade OI, McLennan J, Karlan B, Weitzel J, Sun P, Narod SA; Hereditary Ovarian Cancer Clinical Study Group. Salpingo-oophorectomy and the risk of ovarian, fallopian tube, and peritoneal cancers in women with a BRCA1 or BRCA2 Mutation. JAMA.2006a;296:185-192.

Finch A, Shaw P, Rosen B, Murphy J, Narod SA, Colgan TJ. Clinical and pathologic findings of prophylactic salpingo-oophorectomies in 159 BRCA1 and BRCA2 carriers. Gynecol Oncol. 2006b;100:58-64.

Fisher LA, Bessho M, Wakasugi M, Matsunaga T, Bessho T. Role of interaction of XPF with RPA in nucleotide excision repair. J Mol Biol. 2011 Oct 21;413(2):337-46. Epub 2011 Aug 22.

Fogh J, Fogh JM, Orfeo T. One hundred and twenty-seven cultured human tumor cell lines producing tumors in nude mice. J Natl Cancer Inst. 1977 Jul;59(1):221-6.

Fokas E, Engenhart-Cabillic R, Daniilidis K, Rose F, An HX. Metastasis: the seed and soil theory gains identity. Cancer Metastasis Rev. 2007. 2007 Dec;26(3-4):705-15.

Fox H. Pathology of early malignant change in the ovary. Int J Gynecol Pathol.1993;12:153-155.

Friel AM, Corcoran C, Crown J, O'Driscoll L. Relevance of circulating tumor cells, extracellular nucleic acids, and exosomes in breast cancer. Breast Cancer Res Treat. 2010;123:613–25.

Fromme JC, Verdine GL. Base excision repair. Adv Protein Chem. 2004;69:1-41.

Fujiwara T1, Dunn NR, Hogan BL. Bone morphogenetic protein 4 in the extraembryonic mesoderm is required for allantois development and the localization and survival of primordial germ cells in the mouse. Proc Natl Acad Sci U S A. 2001 Nov 20;98(24):13739-44. Epub 2001 Nov 13.

Garnier D1, Magnus N, Lee TH, Bentley V, Meehan B, Milsom C, Montermini L, Kislinger T, Rak J. Cancer cells induced to express mesenchymal phenotype release exosome-like extracellular vesicles carrying tissue factor. J Biol Chem. 2012 Dec 21;287(52):43565-72. doi: 10.1074/jbc.M112.401760. Epub 2012 Nov 1.

Gatti JL1, Métayer S, Belghazi M, Dacheux F, Dacheux JL. Identification, proteomic profiling, and origin of ram epididymal fluid exosome-like vesicles. Biol Reprod. 2005 Jun;72(6):1452-65. Epub 2005 Jan 5.

Gee JM1, Eloranta JJ, Ibbitt JC, Robertson JF, Ellis IO, Williams T, Nicholson RI, Hurst HC. Overexpression of TFAP2C in invasive breast cancer correlates with a poorer response to anti-hormonetherapy and reduced patient survival. J Pathol. 2009 Jan;217(1):32-41. doi: 10.1002/path.2430.

Gemer O1, Lurian M, Gdalevich M, Kapustian V, Piura E, Schneider D, Lavie O, Levy T, Fishman A, Dgani R, Levavi H, Beller U. A multicenter study of CA-125 level as a predictor of non-optimal primary cytoreduction of advanced epithelial ovarian cancer. Eur J Surg Oncol. 2005;31:1006–1010.

Ghosh S, Basu M, Roy SS. ETS-1 protein regulates vascular endothelial growth factor-induced matrix metalloproteinase-9 and matrix metalloproteinase-13 expression in human ovarian carcinoma cell line SKOV-3. J Biol Chem. 2012 Apr 27;287(18):15001-15. Epub 2012 Jan 23.

Gilbert SF. Developmental Biology. 6th edition. Sunderland (MA): Sinauer Associates; 2000. Chromosomal Sex Determination in Mammals.

Ginestier C1, Hur MH, Charafe-Jauffret E, Monville F, Dutcher J, Brown M, Jacquemier J, Viens P, Kleer CG, Liu S, Schott A, Hayes D, Birnbaum D, Wicha MS, Dontu G. ALDH1 is a marker of normal and malignant human mammary stem cells and a predictor of poor clinical outcome. Cell Stem Cell. 2007 Nov;1(5):555-67. doi: 10.1016/j.stem.2007.08.014.

Ginestra A, La Placa MD, Saladino F, Cassarà D, Nagase H, Vittorelli ML. The amount and proteolytic content of vesicles shed by human cancer cell lines correlates with their in vitro invasiveness. Anticancer Res. 1998;18:3433–37.

Gorham H1, Yoshida K, Sugino T, Marsh G, Manek S, Charnock M, Tarin D, Goodison S. Telomerase activity in human gynaecological malignancies. J Clin Pathol. 1997 Jun:50(6):501-4

Goswami S, Sahai E, E, Wyckoff JB, Cammer M, Cox D, Pixley FJ, Stanley ER, Segall JE Condeelis JS. Macrophages promote the invasion of breast carcinoma cells via a colony-stimulating factor-1/epidermal growth factor paracrine loop. Cancer Res. 2005 Jun 15;65(12):5278-83.

Golubovskaya VM, Finch R, Cance WG. Direct interaction of the N-terminal domain of focal adhesion kinase with the N-terminal transactivation domain of p53. J Biol Chem. 2005 Jul 1;280(26):25008-21. Epub 2005 Apr 25.

Gonzalez-Begn M, Lu B, Han X, Hagen FK et al. Proteomic analysis of human parotid gland exosomes by multidimensional protein identification technology (MudPIT). J. Proteome Res. 2009;8:1304–1314.

Grimson A1, Farh KK, Johnston WK, Garrett-Engele P, Lim LP, Bartel DP. MicroRNA targeting specificity in mammals: determinants beyond seed pairing. Mol Cell. 2007 Jul 6;27(1):91-105.

Guo H, Ingolia NT, Weissman JS, Bartel DP. Mammalian microRNAs predominantly act to decrease target mRNA levels. Nature. 2010 Aug 12;466(7308):835-40.

Güth U, Huang DJ, Bauer G, Stieger M, Wight E, Singer G. Metastatic patterns at autopsy in patients with ovarian carcinoma. Cancer. 2007 Sep 15;110(6):1272-80.

Hagemeijer A, van der Plas DC, Soekarman D, van Denderen J, Grosveld G. The Philadelphia translocation in CML and ALL: recent investigations, new detection methods. Nouv Rev Fr Hematol. 1990;32(1):83-6.

Hanahan D, Folkman J. Patterns and emerging mechanisms of the angiogenic switch during tumorigenesis. Cell. 1996 Aug 9;86(3):353-64.

Hanahan D, Weinberg RA. Hallmarks of cancer: the next generation. Cell. 2011 Mar 4;144(5):646-74.

Hansen SH1, Zegers MM, Woodrow M, Rodriguez-Viciana P, Chardin P, Mostov KE, McMahon M. Induced expression of Rnd3 is associated with transformation of polarized epithelial cells by the Raf-MEK-extracellular signal-regulated kinase pathway. Mol Cell Biol. 2000 Dec;20(24):9364-75.

Harding C, Heuser J, Stahl P. Receptor-mediated endocytosis of transferrin and recycling of the transferrin receptor in ratreticulocytes. J Cell Biol. 1983 Aug;97(2):329-39.

He L1, Thomson JM, Hemann MT, Hernando-Monge E, Mu D, Goodson S, Powers S, Cordon-Cardo C, Lowe SW, Hannon GJ, Hammond SM. A microRNA polycistron as a potential human oncogene. Nature. 2005 Jun 9;435(7043):828-33.

Heintz APM. Surgery in advanced ovarian carcinoma: is there proof to show the benefit? Eur. J. Surg. Oncol. 1988;14:91-99.

Helenius A, Marsh M. Endocytosis of enveloped animal viruses. Ciba Found Symp. 1982;(92):59-76.

Helland Å, Anglesio MS, George J, Cowin PA, Johnstone CN, House CM, Sheppard KE, Etemadmoghadam D, Melnyk N, Rustgi AK, Phillips WA, Johnsen H, Holm R, Kristensen GB, Birrer MJ; Australian Ovarian Cancer Study Group, Pearson RB, Børresen-Dale AL, Huntsman DG, deFazio A, Creighton CJ, Smyth GK, Bowtell DD. Deregulation of MYCN, LIN28B and LET7 in a molecular subtype of aggressive high-grade serous ovarian cancers. PLoS One. 2011 Apr 13;6(4):e18064.

Heo I1, Joo C, Cho J, Ha M, Han J, Kim VN. Lin28 mediates the terminal uridylation of let-7 precursor MicroRNA. Mol Cell. 2008 Oct 24;32(2):276-84. doi: 10.1016/j.molcel.2008.09.014.

Hermsen BB, van Diest PJ, Berkhof J, Menko FH, Gille JJ, Piek JM, Meijer S, Winters HA, Kenemans P, Mensdorff-Pouilly S, Verheijen RH. Low prevalence of (pre) malignant lesions in the breast and high prevalence in the ovary and Fallopian tube in women at hereditary high risk of breast and ovarian cancer. Int J Cancer. 2006;119:1412-1418.

Hilger-Eversheim K1, Moser M, Schorle H, Buettner R. Regulatory roles of AP-2 transcription factors in vertebrate development, apoptosis and cell-cycle control. Gene. 2000 Dec 30;260(1-2):1-12.

Hinsch KD, Hinsch E. The zona pellucida 'receptors' ZP1, ZP2 and ZP3. Andrologia. 1999 Sep:31(5):320-2.

Hirshfield AN. Development of follicles in the mammalian ovary. Int Rev Cytol. 1991;124:43-101.

Hoeben A, Landuyt B, Highley MS, Wildiers H, Van Oosterom AT, De Bruijn EA. Vascular endothelial growth factor and angiogenesis. Pharmacol Rev. 2004 Dec;56(4):549-80.

Hollstein M, Sidransky D, Vogelstein B, Harris CC. p53 mutations in human cancers. Science. 1991;253(5015):49–53.

Holstein SE, Undewiclell H, Ungecikell E. Mechanism of clatherin basket dissociation: separate function of protein domains of DNA J homologue auvilin. J Cell Bio. 1996 Nov;135(4):925-37.

Hosono S, Kajiyama H, Terauchi M, Shibata K, Ino K, Nawa A, Kikkawa F. Expression of Twist increases the risk for recurrence and for poor survival in epithelial ovarian carcinoma patients. Br J Cancer. 2007 Jan 29;96(2):314-20. Epub 2007 Jan 9.

Hossain A1, Kuo MT, Saunders GF. Mir-17-5p regulates breast cancer cell proliferation by inhibiting translation of AIB1 mRNA. Mol Cell Biol. 2006 Nov;26(21):8191-201. Epub 2006 Aug 28.

Hu X, Macdonald DM, Huettner PC, Feng Z, El Naqa IM, Schwarz JK, Mutch DG, Grigsby PW, Powell SN, Wang X. A miR-200 microRNA cluster as prognostic marker in advanced ovarian cancer. Gynecol Oncol. 2009 Sep;114(3):457-64. Epub 2009 Jun 5.

Huang X1, Yuan T, Tschannen M, Sun Z, Jacob H, Du M, Liang M, Dittmar RL, Liu Y, Liang M, Kohli M, Thibodeau SN, Boardman L, Wang L. Characterization of human plasma-derived exosomal RNAs by deep sequencing. BMC Genomics. 2013 May 10;14:319. doi: 10.1186/1471-2164-14-319.

Huffman KE1, Levene SD, Tesmer VM, Shay JW, Wright WE. Telomere shortening is proportional to the size of the G-rich telomeric 3'-overhang. J Biol Chem. 2000 Jun 30;275(26):19719-22.

Huntzinger E, Izaurralde E. Gene silencing by microRNAs: contributions of translational repression and mRNA decay. Nat Rev Genet. 2011 Feb;12(2):99-110. doi: 10.1038/nrg2936.

Huotari J, Helenius A. Endosome maturation. EMBO J. 2011 Aug 31;30(17):3481-500. doi: 10.1038/emboj.2011.286. Review.

Huret JL1, Ahmad M, Arsaban M, Bernheim A, Cigna J, Desangles F, Guignard JC, Jacquemot-Perbal MC,Labarussias M, Leberre V, Malo A, Morel-Pair C, Mossafa H, Potier JC, Texier G, Viguié F, Yau Chun Wan-Senon S, Zasadzinski A, Dessen P. Atlas of genetics and cytogenetics in oncology and haematology in 2013. Nucleic Acids Res. 2013 Jan;41(Database issue):D920-4. doi: 10.1093/nar/gks1082. Epub 2012 Nov 17.

Ichim CV, Wells RA. First among equals: the cancer cell hierarchy. Leuk Lymphoma. 2006 Oct;47(10):2017-27.

Imai T, Horiuchi A, Wang C, Oka K, Ohira S, Nikaido T, Konishi I. Hypoxia attenuates the expression of E-cadherin via up-regulation of SNAIL in ovarian carcinoma cells. Am J Pathol. 2003 Oct;163(4):1437-47.

International Federation of Gynecology and Obstetrics: Classification and staging of malignant tumours in the female pelvis. Acta Obstet Gynecol Scand. 1971;50:1–7.

Iorio MV, Visone R, Di Leva G, Donati V, Petrocca F, Casalini P, Taccioli C, Volinia S, Liu CG, Alder H, Calin GA, Ménard S, and Croce CM. MicroRNA signatures in human ovarian cancer. Cancer Res. 2007 Sep 15;67(18):8699-707.

Jackson SP. Sensing and repairing DNA double-strand breaks. Carcinogenesis. 2002 May;23(5):687-96.

Jemal A, Siegel R, Ward E, Murray T, Xu J, Smigal C, Thun MJ (2006) Cancer statistics, 2006. CA Cancer J clin 56(2):106–130

Jobanputra V, Kriplani A, Choudhry VP, Kucheria K. Detection of chromosomal abnormalities using fluorescence in situ hybridization (FISH). Natl Med J India. 1998 Nov-Dec;11(6):259-63.

Johnson CD, Esquela-Kerscher A, Stefani G, Byrom M, Kelnar K, Ovcharenko D, Wilson M, Wang X, Shelton J, Shingara J, Chin L, Brown D, Slack FJ. The let-7 microRNA represses cell proliferation pathways in human cells., Cancer Res. 2007 Aug 15;67(16):7713-22.

Johnson J, Bagley J, Skaznik-Wikiel M, Lee HJ, Adams GB, Niikura Y, Tschudy KS, Tilly JC, Cortes ML,Forkert R, Spitzer T, Iacomini J, Scadden DT, Tilly JL. Oocyte generation in adult mammalian ovaries by putative germ cells in bone marrow and peripheral blood. Cell. 2005 Jul 29;122(2):303-15.

Johnson J, Canning J, Kaneko T, Pru JK, Tilly JL. Germline stem cells and follicular renewal in the postnatalmammalian ovary. Nature. 2004 Mar 11;428(6979):145-50.

Johnson JD, Fleshner M. Releasing signals, secretory pathways, and immune function of endogenous extracellualr heat shock protein 72. J. Leuk. Biol. 2006 (79):425-434.

Johnsson P1, Ackley A, Vidarsdottir L, Lui WO, Corcoran M, Grandér D, Morris KV. A pseudogene long-noncoding-
RNA network regulates PTEN transcription and translation in human cells. Nat Struct Mol Biol. 2013 Apr;20(4):440-6. doi: 10.1038/nsmb.2516. Epub 2013 Feb 24.

Johnstone RM. Exosomes biological significance. Blood Cell Mol. Dis. 2006. (36):315-321.

Jost A. Recherches sur la differenciation sexuelle del'embryon de lapin. II. Action des androgenes synthese sur l'histogenese genitale. Archives d'Anatomie Microscopique et de Morphologie Experimentale. 1947. 36, 242-270.

Kanehisa, M. and Goto, S. KEGG: Kyoto Encyclopedia of Genes and Genomes. Nucleic Acids Res. 2000 28;27-30.

Kapranov P1, Cawley SE, Drenkow J, Bekiranov S, Strausberg RL, Fodor SP, Gingeras TR. Large-scale transcriptional activity in chromosomes 21 and 22. Science. 2002 May 3;296(5569):916-9.

Keller S, Konig AK, Marme F, Runz S, Wolterink S, Koensgen D, Mustea A, Sehouli J, Altevogt P. Systemic presence and tumor-growth promoting effect of ovarian carcinoma released exosomes. Cancer Lett. 2009;278(1):73–81.

Keller S1, Rupp C, Stoeck A, Runz S, Fogel M, Lugert S, Hager HD, Abdel-Bakky MS, Gutwein P, Altevogt P. CD24 is a marker of exosomes secreted into urine and amniotic fluid. Kidney Int. 2007 Nov;72(9):1095-102. Epub 2007 Aug 15.

Kim J, Coffey DM, Creighton CJ, Yu Z, Hawkins SM, Matzuk MM. High-grade serous ovarian cancer arises from fallopian tube in a mouse model. Proc Natl Acad Sci U S A. 2012 Mar 6;109(10):3921-6. Epub 2012 Feb 13.

Kim JJ1, Tannock IF. Repopulation of cancer cells during therapy: an important cause of treatment failure. Nat Rev Cancer. 2005 Jul;5(7):516-25.

King MC1, Marks JH, Mandell JB; New York Breast Cancer Study Group. Breast and ovarian cancer risks due to inherited mutations in BRCA1 and BRCA2. Science. 2003 Oct 24;302(5645):643-6.

Kirchhausen T. Adaptors for clathrin-mediated traffic. Annu Rev Cell Dev Biol. 1999;15:705-32. Review.
Knudson AG Jr. Mutation and cancer: statistical study of retinoblastoma. Proc Natl Acad Sci U S A. 1971 Apr;68(4):820-3.

Klein RM1, Aplin AE. Rnd3 regulation of the actin cytoskeleton promotes melanoma migration and invasive outgrowth in three dimensions. Cancer Res. 2009 Mar 15;69(6):2224-33. doi: 10.1158/0008-5472.CAN-08-3201. Epub 2009 Feb 24.

Klein RM1, Spofford LS, Abel EV, Ortiz A, Aplin AE. B-RAF regulation of Rnd3 participates in actin cytoskeletal and focal adhesion organization. Mol Biol Cell. 2008 Feb;19(2):498-508. Epub 2007 Nov 28.

Kobayashi T, Stang E, Fang KS, de Moerloose , Parton RG, Gruenberg J. A lipid associated with the antiphospholipid syndrome regulates endosome structure and function. Nature. 1998 392:193-197.

Kolter T, Sandhoff K. Principles of lysosomal membrane digestion: stimulation of sphingolipid degradation by sphingolipid activator proteins and anionic lysosomal lipids. Annu Rev Cell Dev Biol. 2005;21:81-103.

Kornfeld S, Mellman I. The biogenesis of lysosomes. Annu Rev Cell Biol. 1989;5:483-525.

Kotake Y1, Nakagawa T, Kitagawa K, Suzuki S, Liu N, Kitagawa M, Xiong Y. Long non-coding RNA ANRIL is required for the PRC2 recruitment to and silencing of p15(INK4B) tumor suppressor gene. Oncogene. 2011 Apr 21;30(16):1956-62. doi: 10.1038/onc.2010.568. Epub 2010 Dec 13.

Koutsaki M1, Spandidos DA2, Zaravinos A3. Epithelial-mesenchymal transition-associated miRNAs in ovarian carcinoma, with highlight on the miR-200 family: Prognostic value and prospective role in ovarian cancer therapeutics. Cancer Lett. 2014 Jun 18. pii: S0304-3835(14)00314-0. doi: 10.1016/j.canlet.2014.05.022. [Epub ahead of print]

Kurman RJ, Shih Ie M. The origin and pathogenesis of epithelial ovarian cancer: a proposed unifying theory. Am J Surg Pathol. 2010 Mar;34(3):433-43.

Kuroda T, Tada M, Kubota H, Kimura H, Hatano SY, Suemori H, Nakatsuji N,Tada T. Mol. Cell. Biol. 2005;25: 2475–2485

Kruchten AE, McNiven MA. Dynamin as a mover and pincher during cell migration and invasion. J Cell Sci. 2006 May 1;119(Pt 9):1683-90.

Lamb JD, Garcia RL, Goff BA, Paley PJ, Swisher EM. Predictors of occult neoplasia in women undergoing risk-reducing salpingo-oophorectomy. Am J Obstet Gynecol. 2006;194:1702-1709.

Landi D, Barale R, Gemignani F, Landi S. Prediction of the biological effect of polymorphisms within microRNA binding sites. Methods Mol Biol. 2011;676:197-210.

Lane DP. Cancer. p53, guardian of the genome. Nature. 1992 Jul 2;358(6381):15-6.

Lapidot T, Sirard C, Vormoor J, Murdoch B, Hoang T, Caceres-Cortes J, Minden M, Paterson B, Caligiuri MA, Dick JE. A cell initiating human acute myeloid leukaemia after transplantation into SCID mice. Nature. 1994 Feb 17;367(6464):645-8.

Lauchlan SC. The secondary Müllerian system. Obstet Gynecol Surv. 1972 Mar;27(3):133-46. Review. No abstract available.

Lee HC1, Chen CY, Au LC. Systemic comparison of repression activity for miRNA and siRNA associated with different types of target sequences. Biochem Biophys Res Commun. 2011 Jul 29;411(2):393-6. doi: 10.1016/j.bbrc.2011.06.159. Epub 2011 Jul 2.

Lee LF, Hellendall RP, Wang Y, Haskill JS, Mukaida N, Matsushima K, Ting JP. IL-8 reduced tumorigenicity of human ovarian cancer in vivo due to neutrophil infiltration. J Immunol. 2000 Mar 1;164(5):2769-75.

Lee R, Feinbaum R and Ambros V. The C. elegans Heterochronic Gene lin-4 Encodes Small RNAs with Antisense Complementarity to lin-14.Cell. 1993;75:843-854.
Leeper K, Garcia R, Swisher E, Goff B, Greer B, Paley P. Pathologic findings in prophylactic oophorectomy specimens in high-risk women. Gynecol Oncol. 2002;87:52-56.

Levy MZ, Allsopp RC, Futcher AB, Greider CW, Harley CB. Telomere end-replication problem and cell aging. J Mol Biol. 1992 Jun 20;225(4):951-60.

Li J1, Liang S, Yu H, Zhang J, Ma D, Lu X. An inhibitory effect of miR-22 on cell migration and invasion in ovarian cancer. Gynecol Oncol. 2010 Dec;119(3):543-8. doi: 10.1016/j.ygyno.2010.08.034. Epub 2010 Sep 24.

Li YM1, Baviello G, Vlassara H, Mitsuhashi T. Glycation products in aged thioglycollate medium enhance the elicitation of peritoneal macrophages. J Immunol Methods. 1997 Feb 28;201(2):183-8.

Lin EY, Nguyen AV, Russell RG, Pollard JW. Colony-stimulating factor 1 promotes progression of mammary tumors to malignancy. J Exp Med. 2001;193: 727–740.

Liu JP, Li H. Telomerase in the ovary. Reproduction. 2010 Aug;140(2):215-22. Epub 2010 Jun 18. Review.

Lo SH. Focal adhesions: what's new inside. Dev Biol. 2006 Jun 15;294(2):280-91. Epub 2006 Mar 30.

Lok BH and Powell SN. Molecular pathways: understanding the role of Rad52 in homologous recombination for therapeutic advancement. Clin Cancer Res. Dec 2012;18(23):6400-6. Epub 2012 Oct 15.

Lu J1, Getz G, Miska EA, Alvarez-Saavedra E, Lamb J, Peck D, Sweet-Cordero A, Ebert BL, Mak RH, Ferrando AA, Downing JR, Jacks T, Horvitz HR, Golub TR. MicroRNA expression profiles classify human cancers. Nature. 2005 Jun 9;435(7043):834-8.

Lu L, Katsaros D, Shaverdashvili K, Qian B, Wu Y, de la Longrais IA, Preti M, Menato G, Yu H. Pluripotent factor lin-28 and its homologue lin-28b in epithelial ovarian cancer and their associations with disease outcomes and expression of let-7a and IGF-II., Eur J Cancer. 2009 Aug;45(12):2212-8. Epub 2009 May 26.

Mahajan A, Lui Z, Gellert L, Zou X, Yang G, Lee P, Yang X, Wei JJ. HMGA2: a biomarker significantly overexpressed in high-grade ovarian serous carcinoma. Mod Pathol. 2010 May;23(5):673-81. doi: 10.1038/modpathol.2010.49. Epub 2010 Mar 12.

Malek A, Bakhidze E, Noske A, Sers C, Aigner A, Schäfer R, Tchernitsa O. HMGA2 gene is a promising target for ovarian cancer silencing therapy. Int J Cancer. 2008 Jul 15;123(2):348-56.

Manenti G1, Galbiati F, Giannì-Barrera R, Pettinicchio A, Acevedo A, Dragani TA. Haplotype sharing suggests that a genomic segment containing six genes accounts for the pulmonary adenoma susceptibility 1 (Pas1) locus activity in mice. Oncogene. 2004 May 27;23(25):4495-504.

Mannoor K, Shen J, Liao J, Liu Z, Jiang F1. Small nucleolar RNA signatures of lung tumor-initiating cells. Mol Cancer. 2014 May 6;13:104. doi: 10.1186/1476-4598-13-104.

Mano MS1, Rosa DD, Azambuja E, Ismael G, Braga S, D'Hondt V, Piccart M, Awada A. Current management of ovarian carcinosarcoma. Int J Gynecol Cancer. 2007;17:316–24.

Marchini S1, Cavalieri D, Fruscio R, Calura E, Garavaglia D, Fuso Nerini I, Mangioni C, Cattoretti G, Clivio L, Beltrame L, Katsaros D, Scarampi L, Menato G,Perego P, Chiorino G, Buda A, Romualdi C, D'Incalci M. Association between miR-200c and the survival of patients with stage I epithelial ovarian cancer: a retrospective study of two independent tumour tissue collections. Lancet Oncol. 2011 Mar;12(3):273-85. doi: 10.1016/S1470-2045(11)70012-2. Epub 2011 Feb 21.

Marsh M, van Meer G. Cell Biology. No ESCRTs for exosomes. Science. 2008 Feb 29;319(5867):1191-2. Doi: 10.1126/science.1155750.

Martens-Uzunova ES1, Böttcher R2, Croce CM3, Jenster G4, Visakorpi T5, Calin GA6. Long noncoding RNA in prostate, bladder, and kidney cancer. Eur Urol. 2014 Jun;65(6):1140-51. doi: 10.1016/j.eururo.2013.12.003. Epub 2013 Dec 14.

Massagué J1, Seoane J, Wotton D. Smad transcription factors. Genes Dev. 2005 Dec 1;19(23):2783-810.

Mattick JS1, Makunin IV. Non-coding RNA. Hum Mol Genet. 2006 Apr 15;15 Spec No 1:R17-29.

Mayor S, Pagano RE. Pathways of clathrin-independent endocytosis. Nat Rev Mol Cell Biol. 2007 Aug;8(8):603-12.

McCullough J, Row PE, Lorenzo O, Doherty M, Beynon R, Clague MJ, Urbé S. Activation of the endosome-associated ubiquitin isopeptidase AMSH by STAM, a component of the multivesicular body-sorting machinery. Curr Biol. 2006 Jan 24;16(2):160-5.

Memarzadeh S1, Lee SB, Berek JS, Farias-Eisner R. CA-125 levels are a weak predictor of optimal cytoreductive surgery in patients with advanced epithelial ovarian cancer. Int J Gynecol Cancer. 2003;3:120–124.

Mettlen M, Pucadyil T, Ramachandran R, Schmid SL. Dissecting dynamin's role in clathrin-mediated endocytosis. Biochem Soc Trans. 2009 Oct;37(Pt 5):1022-6. Review.

Mezzanzanica D, Bagnoli M, De Cecco L, Valeri B, Canevari S. Role of microRNAs in ovarian cancer pathogenesis and potential clinical implications. 2010 Aug;42(8):1262-72. Epub 2009 Dec 24.

miRSearch V3.0 Exiqon. NAI2 homolog 2 (ENSG00000019849) https://www.exiquon.com/ls/Pages/TPTResult.aspx?SessonPrefixKey=76ead128-60cc-4a14-845e570fe9b7952a. (assessed Jully 10, 2014).

Mitchell PS, Parkin RK, Kroh EM, Fritz BR, Wyman SK, Pogosova-Agadjanyan EL, Peterson A, Noteboom J, O'Briant KC, Allen A, Lin DW, Urban N, Drescher CW, Knudsen BS, Stirewalt DL, Gentleman R, Vessella RL, Nelson PS, Martin DB, Tewari M. Circulating microRNAs as stable blood-based markers for cancer detection. Proc Natl Acad Sci U S A. 2008 Jul 29;105(30):10513-8. Epub 2008 Jul 28.

Mitsui K, Tokuzawa Y, Itoh H, Segawa K, Murakami M, Takahashi K, Maruyama M, Maeda M, Yamanaka S. The homeoprotein Nanog is required for maintenance of pluripotency in mouse epiblast and ES cells. Cell. 2003 May 30;113(5):631-42.

Morita E. Differential requirements of mammalian ESCRTs in multivesicular body formation, virus budding and cell division. FEBS J. 2012 Apr;279(8):1399-406.

Nam EJ1, Yoon H, Kim SW, Kim H, Kim YT, Kim JH, Kim JW, Kim S. MicroRNA expression profiles in serous ovarian carcinoma. Clin Cancer Res. 2008 May 1;14(9):2690-5. doi: 10.1158/1078-0432.CCR-07-1731.

Naora H. Developmental patterning in the wrong context: the paradox of epithelial ovarian cancer. Cell Cycle. 2005;4:1033–1035.

Naslavsky N, Weigert R, Donaldson JG. Characterization of a nonclathrin endocytic pathway: membrane cargo and lipid requirements. Mol Biol Cell. 2004 Aug;15(8):3542-52. Epub 2004 May 14.

Newman MA, Thomson JM, and Hammond SM. Lin-28 interaction with the let-7 precursor loop mediates regulated microRNA processing. RNA. 2008;14:1539–1549.

Nicosia SV, Johnson JH. Surface morphology of ovarian mesothelium (surface epithelium) and of other pelvic and extrapelvic mesothelial sites in the rabbit. Int J Gynecol Pathol. 1984;3:249–260.

Nicosia SV, Nicosia RF, Neoplasms of the ovarian mesothelium. In: Azar HA, (ed). Path of Human Neoplasms. Raven Press, New York; 1998:435–486.

Nilsson EE, Skinner MK. Growth and differentiation factor-9 stimulates progression of early primary but not primordial rat ovarian follicle development. Biol Reprod. 2002 Sep;67(3):1018-24.

Niwa, H., How is pluripotency determined and maintained. Development. 2007;134(4):635-46.

Novikoff AB, Essner E, Quintana N., Golgi apparatus and lysosomes. Fed Proc. 1964 Sep-Oct;23:1010-22.

Nowell P, Hungerford D. A minute chromosome in human chronic granulocytic leukemia [abstract]. Science. 1960;132:1497.

Obeidat B, Latimer J, Crawford R. Can optimal primary cytoreduction be predicted in advanced stage epithelial ovarian cancer? Role of preoperative serum CA-125 level. Gynecol Obstet Invest. 2004;57(3):153-6. Epub 2004 Jan 15.

Oda M, Shiota K, and Tanaka S. Trophoblast stem cells. Methods Enzymol. 2006;419:38.

Odegaard E, Staff AC, Kaern J, ,Florenes VA, Kopolovic J, Trope CG, Abeler VM, Reich R, Davidson B. The AP-2gamma transcription factor is upregulated in advanced-stage ovarian carcinoma. Gynecol Oncol. 2006 Mar;100(3):462-8. Epub 2005 Oct 10.

O'Donnell KA1, Wentzel EA, Zeller KI, Dang CV, Mendell JT. c-Myc-regulated microRNAs modulate E2F1 expression. Nature. 2005 Jun 9;435(7043):839-43.

Ohno H, Stewart J, Fournier MC, Bosshart H, Rhee I, Miyatake S, Saito T, Gallusser A, Kirchhausen T, Bonifacino JS. Interaction of tyrosine-based sorting signals with clathrin-associated proteins. Science. 1995 Sep 29;269(5232):1872-5.

Olivier RI, van Beurden M, Lubsen MA, Rookus MA, Mooij TM, van de Vijver MJ, van't Veer LJ. Clinical outcome of prophylactic oophorectomy in BRCA1/BRCA2 mutation carriers and events during follow-up. Br J Cancer. 2004;90:1492-1497.

Oosterhuis JW, Stoop H, Honecker F, Looijenga LH. Why human extragonadal germ cell tumours occur in the midline of the body: old concepts, new perspectives. Int J Androl. 2007 Aug;30(4):256-63; discussion 263-4.

Pan BT, Teng K, and Wu C. Electron microscopic evidence for externalization of the transferrin receptor in vesicular form in sheep reticulocytes. Journal of Cell Biology. 1985 vol. 101, no. 3, pp. 942–948.

Pan GJ, Pei DQ. Identification of two distinct transactivation domains in the pluripotency sustaining factor nanog. Cell Res. 2003;13:499–502.

Pan G, Li J, Zhou Y, Zheng H, Pei D. A negative feedback loop of transcription factors that controls stem cell pluripotency and self-renewal. FASEB J. 2006;20:1730–1732.

Pan G, Pei D. The stem cell pluripotency factor NANOG activates transcription with two unusually potent subdomains at its C terminus. J. Biol. Chem. 2005;280:1401–1407.

Park SM1, Shell S, Radjabi AR, Schickel R, Feig C, Boyerinas B, Dinulescu DM, Lengyel E, Peter ME. Let-7 prevents early cancer progression by suppressing expression of the embryonic gene HMGA2. Cell Cycle. 2007 Nov 1;6(21):2585-90. Epub 2007 Aug 6.

Partridge E, Kreimer AR, Greenlee RT, Williams C, Xu JL, Church TR, Kessel B, Johnson CC, Weissfeld JL, Isaacs C, Andriole GL, Ogden S, Ragard LR, Buys SS; PLCO Project Team. Results from four rounds of ovarian cancer screening in a randomized trial. Obstet Gynecol. 2009 Apr;113(4):775-82.

Pasmant V, Sabbagh A, Vidaud M, Bièche I. ANRIL, a long, noncoding RNA, is an unexpected major hotspot in GWAS. FASEB J. 2011 Feb;25(2):444-8. doi: 10.1096/fj.10-172452. Epub 2010 Oct 18.

Pearce DJ1, Taussig D, Simpson C, Allen K, Rohatiner AZ, Lister TA, Bonnet D. Characterization of cells with a high aldehyde dehydrogenase activity from cord blood and acute myeloid leukemia samples. Stem Cells. 2005 Jun-Jul;23(6):752-60.

Pectasides D, Pectasides E, Kassanos D. Germ cell tumors of the ovary. Cancer Treat Rev. 2008 Aug;34(5):427-41. Epub 2008 Apr 18.

Peng S, Maihle NJ, Huang Y. Pluripotency factors Lin28 and Oct4 identify a sub-population of stem cell-like cells in ovarian cancer. Oncogene. 2010 Apr 8;29(14):2153-9. Epub 2010 Jan 25.

Pepling ME. From primordial germ cell to primordial follicle: mammalian female germ cell development. Genesis. 2006 Dec;44(12):622-32. Review.

Pepling ME, Spradling AC. Female mouse germ cells form synchronously dividing cysts. Development. 1998 Sep;125(17):3323-8.

Pepling ME, Spradling AC. Mouse ovarian germ cell cysts undergo programmed breakdown to form primordial follicles. Dev Biol. 2001 Jun 15;234(2):339-51.

Pesce M, Schöler HR. Oct-4: gatekeeper in the beginnings of mammalian development. Stem Cells. 2001;19(4):271-8. Review.

Peters H, Byskov AG, Lintern-Moore S, Faber M, Andersen M. The effect of gonadotrophin on follicle growth initiation in the neonatal mouse ovary. Journal of Reproduction and Fertility .1973;35:139–141.

Petrocca F1, Vecchione A, Croce CM. Emerging role of miR-106b-25/miR-17-92 clusters in the control of transforming growth factor beta signaling. Cancer Res. 2008 Oct 15;68(20):8191-4. doi: 10.1158/0008-5472.CAN-08-1768.

Piek JM, van Diest PJ, Zweemer RP, Jansen JW, Poort-Keesom RG, Menko FH, Gille JJ, Jongsma AP, Pals G, Kenemans P, Verheijen RH. Dyplastic changes in prophylactically removed Fallopian tubes of women predisposed to developing ovarian cancer. J Pathol. 2001 Nov;195(4):451-6.

Pirino G1, Wescott MP, Donovan PJ. Protein kinase A regulates resumption of meiosis by phosphorylation of Cdc25B in mammalian oocytes. Cell Cycle. 2009 Feb 15;8(4):665-70. Epub 2009 Feb 14.

Pisitkun, T., Shen, R. F., Knepper, M. A. Identification and proteomic profiling of exosomes in human urine. Proc. Natl. Acad. Sci. USA. 2004;101:13368–13373.

Piskounova E1, Polytarchou C, Thornton JE, LaPierre RJ, Pothoulakis C, Hagan JP, Iliopoulos D, Gregory RI. Lin28A and Lin28B inhibit let-7 microRNA biogenesis by distinct mechanisms. Cell. 2011 Nov 23;147(5):1066-79. doi: 10.1016/j.cell.2011.10.039.

Pols MS, Klumperman J. Trafficking and function of the tetraspanin CD63. Exp Cell Res. 2009 May 15;315(9):1584-92. Epub 2008 Oct 7.

Pon YL, Zhou HY, Cheung AN, Ngan HY, Wong AS. p70 S6 kinase promotes epithelial to mesenchymal transition through snail induction in ovarian cancer cells. Cancer Res. 2008 Aug 15;68(16):6524-32.

Praefcke GJ, McMahon HT. The dynamin superfamily: universal membrane tubulation and fission molecules? Nat Rev Mol Cell Biol. 2004 Feb;5(2):133-47. Review.

Prescott J, Blackburn EH, Prescott J. Telomerase RNA mutations in Saccaromyces cerevisiae alter telomerase action and reveal non processivity in vivo and in vitro. Genes Dev. 1997 Feb 15;11(4):528-40.

Priebe A, Tan L, Wahl H, Kueck A, He G, Kwok R, Opipari A, Liu JR. Glucose deprivation activates AMPK and induces cell death through modulation of Akt in ovarian cancer cells. Gynecol Oncol. 2011 Aug;122(2):389-95. Epub 2011 May 14.

Qian B, Deng Y, Im JH, Muschel RJ, Zou Y, Li J, Lang RA, Pollard JW. A distinct macrophage population mediates metastatic breast cancer cell extravasation, establishment and growth. PLoS One. 2009 Aug 10;4(8):e6562.

Qiu C, Ma Y, Peng S, Huang Y, Lin28-mediated post transcriptional regulation of Oct4 expression in human embryonic stem cells. Nucleic Acids Res. 2010 Mar;38(4):1240-8. Epub 2009 Dec 4.

Rachidi SM1, Qin T, Sun S, Zheng WJ, Li Z. Molecular profiling of multiple human cancers defines an inflammatory cancer-associated molecular pattern and uncovers KPNA2 as a uniform poor prognostic cancer marker. PLoS One. 2013;8(3):e57911. doi: 10.1371/journal.pone.0057911. Epub 2013 Mar 25.

Raiborg C, Malerød L, Pedersen NM, Stenmark H. Differential functions of Hrs and ESCRT proteins in endocytic membrane trafficking. Exp Cell Res. 2008 Feb 15;314(4):801-13. Epub 2007 Nov 26.

Rajah R, Glaser EM, Hirshfield AN. The changing architecture of the neonatal rat ovary during histogenesis. Dev Dyn. 1992 Jul;194(3):177-92.

Rana S, Zöller M. Exosome target cell selection and the importance of exosomal tetraspanins: a hypothesis. Biochem Soc Trans. 2011 Apr;39(2):559-62.

Rani S, O'Brien K, Kelleher FC, Corcoran C, Germano S, Radomski MW, Crown J, O'Driscoll L. Isolation of exosomes for subsequent mRNA, MicroRNA, and protein profiling. Methods Mol Biol. 2011;784:181-95.

Rapoport I, Boll W, Yu A, Böcking T, Kirchhausen T. A motif in the clathrin heavy chain required for the Hsc70/auxilin uncoating reaction. Mol Biol Cell. 2008 Jan;19(1):405-13. Epub 2007 Oct 31.

Raposo G, Nijman H W, Stoorvogel W, Leijendekker R, Harding CV, Melief CJ, Geuze HJ. B lymphocytes secrete antigenpresenting vesicles. J. Exp. Med. 1996 183:1161-1172.

Ratajczak J1, Miekus K, Kucia M, Zhang J, Reca R, Dvorak P, Ratajczak MZ. Embryonic stem cell-derived microvesicles reprogram hematopoietic progenitors: evidence for horizontal transfer of mRNA and protein delivery. Leukemia. 2006 May;20(5):847-56.

Rath KS, Funk HM, Bowling MC, Richards WE, Drew AF. Expression of soluble interleukin-6 receptor in malignant ovarian tissue. Am J Obstet Gynecol. 2010; 203:230.e1-8.

Rauh-Hain JA, Rodriguez N, Growdon WB, Goodman AK, Boruta DM 2nd, Horowitz NS, del Carmen MG, Schorge JO. Primary debulking surgery versus neoadjuvant chemotherapy in stage IV ovarian cancer. Ann Surg Oncol. 2012 Mar;19(3):959-65. Epub 2011 Oct 13.

Reinhart B, Slack F, Basson M, Pasquinelli A, Bettinger J, Rougvie A, Horvitz R and Ruvkun G. The 21-nucleotide let-7 RNA regulates developmental timing in Caenorhabditis elegans. Nature, 2000;403:901-906.

Reya T1, Morrison SJ, Clarke MF, Weissman IL. Stem cells, cancer, and cancer stem cells. Nature. 2001 Nov 1;414(6859):105-11.

Rink J, Ghigo E, Kalaidzidis Y, Zerial M. Rab conversion as a mechanism of progression from early to late endosomes. Cell. 2005 Sep 9;122(5):735-49.

Rinn JL1, Euskirchen G, Bertone P, Martone R, Luscombe NM, Hartman S, Harrison PM, Nelson FK, Miller P, Gerstein M, Weissman S, Snyder M. The transcriptional activity of human Chromosome 22. Genes Dev. 2003 Feb 15;17(4):529-40.

Robboy SJ, Bernhardt PF, Parmley T. Embryology of the female genital tract and disorders of abnormal sexual development. In: Kurman RJ, ed. Blaustein's pathology of the female genital tract. 4th ed. New York, NY: Springer-Verlag, 1994; 705-782.

Rodda DJ, Chew JL, Lim LH, Loh YH, Wang B, Ng HH, Robson P. Transcriptional regulation of nanog by OCT4 and SOX2. J. Biol. Chem. 2005;280:24731–24737.

Rodgers RJ, Irving-Rodgers HF. Formation of the ovarian follicular antrum and follicular fluid. Biol Reprod. 2010 Jun;82(6):1021-9. Epub 2010 Feb 17.

Romero I, Bast RC Jr. Minireview: human ovarian cancer: biology, current management, and paths to personalizing therapy. Endocrinology. 2012 Apr;153(4):1593-602. Epub 2012 Mar 13.

Rous P. A transmissible avian neoplasm. (Sarcoma of the common fowl). J Exp Med. 1910 Sep 1;12(5):696-705.

Rossant, J.; Tam, P.P. Blastocyst lineage formation, early embryonic asymmetries and axis patterning in the mouse. Development. 2009;136(5):701-13

Rowley JD. Letter: A new consistent chromosomal abnormality in chronic myelogenous leukaemia identified by quinacrine fluorescence and Giemsa staining. Nature. 1973 Jun 1;243(5405):290-3.

Ruan K, Fang X, Ouyang G. MicroRNAs: novel regulators in the hallmarks of human cancer. Cancer Lett. 2009 Nov 28;285(2):116-26 doi: 10.1016/j.canlet.2009.04.031. Epub 2009 May 22.

Rutledge TL1, Gold MA, McMeekin DS, Huh WK, Powell MA, Lewin SN, Mutch DG, Johnson GA, Walker JL, Mannel RS. Carcinosarcoma of the ovary—a case series. Gynecol Oncol. 2006;100:128–32.

Ryan KM1, Vousden KH. Characterization of structural p53 mutants, which show selective defects in apoptosis but not cell cycle arrest. Mol Cell Biol. 1998 Jul;18(7):3692-8.

Rybak A1, Fuchs H, Smirnova L, Brandt C, Pohl EE, Nitsch R, Wulczyn FG. A feedback loop comprising lin-28 and let-7 controls pre-let-7 maturation during neural stem-cell commitment. Nat Cell Biol. 2008 Aug;10(8):987-93. doi: 10.1038/ncb1759. Epub 2008 Jul 6.

Salonen J, Leminen A, Stenman UH, Butzow R, Heikinheimo M, Heikinheimo O. Tissue AP-2gamma and Oct-3/4, and serum CA-125 as diagnostic and prognostic markers of malignant ovarian germ cell tumors. Tumour Biol. 2008;29(1):50-6. Epub 2008 May 23.

Sampson VB1, Rong NH, Han J, Yang Q, Aris V, Soteropoulos P, Petrelli NJ, Dunn SP, Krueger LJ. MicroRNA let-7a down-regulates MYC and reverts MYC-induced growth in Burkitt lymphoma cells. Cancer Res. 2007 Oct 15;67(20):9762-70.

Satoh M. Histogenesis and organogenesis of the gonad in human embryos. J Anat. 1991;177:85-107.

Scheele U, Kalthoff C, Ungewickell E. Multiple interactions of auxilin 1 with clathrin and the AP-2 adaptor complex. J Biol Chem. 2001;276:36131–36138.

Schlossman DM, Schmid SL, Braell WA, Rothman JE. An enzyme that removes clathrin coats: Purification of an uncoating ATPase. J Cell Biol. 1984;99:723–733.

Schmid EM1, Ford MG, Burtey A, Praefcke GJ, Peak-Chew SY, Mills IG, Benmerah A, McMahon HT. Role of the AP2 b-appendage hub in recruiting partners for clathrin-coated vesicle assembly. PLoS Biol. 2006;4(9): e262.

Schmoll HJ. Extragonadal germ cell tumors. Ann Oncol. 2002;13 Suppl 4:265-72.

Scholer HR, Dressler GR, Balling R, Rohdewohld H, Gruss P. Oct-4: a germline-specific transcription factor mapping to the mouse t-complex. EMBO J. 1990 Jul;9(7):2185-95.

Seabrook JL, Cantlon JD, Cooney AJ, McWhorter EE, Fromme BA, Bouma, GJ, Anthony RV, Winger QA. Role of LIN28A in mouse and human trophoblast cell differentiation. Biol Reprod. 2013 Oct 24;89(4):95. doi: 10.1095/biolreprod.113.109868. Print 2013 Oct.

SEER Research Data 1973-2009 -- ASCII Text Data: Surveillance, Epidemiology, and End Results (SEER) Program (www.seer.cancer.gov) Research Data (1973-2009), National Cancer Institute, DCCPS, Surveillance Research Program, Surveillance Systems Branch, released April 2012, based on the November 2011 submission.

Seidman JD, Horkayne-Szakaly I, Haiba M, Boice CR, Kurman RJ, Ronnett BM. The histologic type and stage distribution of ovarian carcinomas of surface epithelial origin. Int J Gynecol Pathol. 2004;23:41– 44.

Selbach M, Schwanhäusser B, Thierfelder N, Fang Z, Khanin R, Rajewsky N. Widespread changes in protein synthesis induced by microRNAs. Nature. 2008 Sep 4;455(7209):58-63. Epub 2008 Jul 30.

Sever S. Dynamin and endocytosis. Curr Opin Cell Biol. 2002 Aug;14(4):463-7.

Shapira I1, Oswald M2, Lovecchio J3, Khalili H2, Menzin A3, Whyte J3, Dos Santos L3, Liang S4, Bhuiya T4, Keogh M2, Mason C2, Sultan K5, Budman D1,Gregersen PK6, Lee AT6. Circulating biomarkers for detection of ovarian cancer and predicting cancer outcomes. Br J Cancer. 2014 Feb 18;110(4):976-83. doi: 10.1038/bjc.2013.795. Epub 2013 Dec 24.

Shi Y1, Massagué J. Mechanisms of TGF-beta signaling from cell membrane to the nucleus. Cell. 2003 Jun 13;113(6):685-700.

Shibuya M. Vascular endothelial growth factor (VEGF)-Receptor2: its biological functions, major signaling pathway, and specific ligand VEGF-E. Endothelium. 2006 Mar-Apr;13(2):63-9.

Shimizu Y, Kamoi S, Amada S, Akiyama F, Silverberg SG. Toward the development of a universal grading system for ovarian epithelial carcinoma: testing of a proposed system in a series of 461 patients with uniform treatment and follow-up. Cancer. 1998 Mar 1;82(5):893-901.

Silasi DA1, Illuzzi JL, Kelly MG, Rutherford TJ, Mor G, Azodi M, Schwartz PE. Carcinosarcoma of the ovary. Int J Gynecol Cancer. 2008;18:22–9.
Skírnisdóttir IA1, Sorbe B, Lindborg K, Seidal T. Prognostic impact of p53, p27, and C-MYC on clinicopathological features and outcome in early-stage (FIGO I-II) epithelial ovarian cancer. Int J Gynecol Cancer. 2011 Feb;21(2):236-44. doi: 10.1097/IGC.0b013e31820986e5.

Skog J, Würdinger T, van Rijn S, Meijer DH, Gainche L, Sena-Esteves M, Curry WT Jr, Carter BS, Krichevsky AM, Breakefield XO. Glioblastoma microvesicles transport RNA and proteins that promote tumour growth and provide diagnostic bio- markers. Nat Cell Biol. 2008 (10):1470–76.

Skokos D, Le Panse S, Villa I, Rousselle JC, Peronet R, Namane A, David B, Mécheri S. Nonspecific B and T cell-stimulatory activity mediated by mast cells is associated with exosomes. Int Arch Allergy Immunol. 2001 Jan-Mar;124(1-3):133-6.

Smith Sehdev AE, Sehdev PS, Kurman RJ. Noninvasive and invasive micropapillary (low-grade) serous carcinoma of the ovary: a clinicopathologic analysis of 135 cases. Am J Surg Pathol . 2003;27:725–736.

Song SW1, Fuller GN, Khan A, Kong S, Shen W, Taylor E, Ramdas L, Lang FF, Zhang W. IIp45, an insulin-like growth factor binding protein 2 (IGFBP-2) binding protein, antagonizes IGFBP-2 stimulation of glioma cell invasion. Proc Natl Acad Sci U S A. 2003 Nov 25;100(24):13970-5. Epub 2003 Nov 14.

Sotelo JR, Porter KR. An electron microscope study of the rat ovum. J Biophys Biochem Cytol. 1959 Mar 25;5(2):327-42.

Sousa R, Lafer EM. Keep the traffic moving: Mechanism of the Hsp70 motor. Traffic. 2006;7:1596–1603.

Soyal SM, Amleh A, Dean J. FIGalpha, a germ cell-specific transcription factor required for ovarian follicle formation. Development. 2000 Nov;127(21):4645-54.

Sponring A, Filipiak W, Mikoviny T, Ager C, Schubert J, Miekisch W, Amann A, Troppmair J. Release of volatile organic compounds from the lung cancer cell line NCI-H2087 in vitro. Anticancer Res. 2009 Jan;29(1):419-26.

Stack MS, Ellerbroek SM, Fishman DA. The role of proteolytic enzymes in the pathology of epithelial ovarian carcinoma. Int J Oncol. 1998 Mar;12(3):569-76.

Stanford JS1, Ruderman JV. Changes in regulatory phosphorylation of Cdc25C Ser287 and Wee1 Ser549 during normal cell cycle progression and checkpoint arrests. Mol Biol Cell. 2005 Dec;16(12):5749-60. Epub 2005 Sep 29.

Stauffer ME1, Chazin WJ. Physical interaction between replication protein A and Rad51 promotes exchange on single-stranded DNA. J Biol Chem. 2004 Jun 11;279(24):25638-45. Epub 2004 Mar 31.

Sternjak A, BlaB S, Metzkow S., Jungblut P, Burmester G, Skriner SK. Immunomic analysis of syovial fluid exosomes of rheumatic diseases patients. Arthritis Res. 2002. 4 (suppl 1): 75 doi:10.1186/ar520

Stoorvogel W, Kleijmeer MJ, Geuze HJ, Raposo G. The biogenesis and functions of exosomes. Traffic. 2002 May;3(5):321-30. Review.

Takahashi K, Yamanaka S. Induction of pluripotent stem cells from mouse embryonic and adult fibroblast cultures by defined factors. Cell. 2006 Aug 25;126(4):663-76. Epub 2006 Aug 10.

Tanos B, Rodriquez-Boluan E. The epithelial polarity program: machineries involved and their hijacking by cancer. Oncogene. 2008 Nov 24;27(55):6939-57.

Takei K. Slepnev VI, Haucke V, De Camiliil P. Functional partnership between amphiphysin and dynamin in clatherin-mediated endocytosis. Nat Cell Biol. 1999 May;1(1):33-9.

Tarkowski AK. Mouse chimeras developed from fused eggs. Nature. 1961 Jun 3;190:857-60.

Tavassoli FA, Devilee P., Eds. Pathology and Genetics. Tumours of the Breast and Female Genital Organs. International Agency for Research on Cancer and World Health Organization. IARC Press. 2003. Lyon, France.

Taylor DD, Gercel-Taylor C. MicroRNA signatures of tumor-derived exosomes as diagnostic biomarkers of ovarian cancer. Gynecol Oncol. 2008 Jul;110(1):13-21.

Théry C, Boussac M, Véron P, Ricciardi-Castagnoli P, Raposo G, Garin J, Amigorena S. Proteomic analysis of dendritic cell-derived exosomes: a secreted subcellular compartment distinct from apoptotic vesicles. J Immunol. 2001 Jun 15;166(12):7309-18.

Théry C, Regnault A, Garin J, Wolfers J, Zitvogel L, Ricciardi-Castagnoli P, Raposo G, Amigorena S. Molecular characterization of dendritic cell-derived exosomes. Selective accumulation of the heat shock protein hsc73. J Cell Biol. 1999 Nov 1;147(3):599-610.

Thorne RF1, Marshall JF, Shafren DR, Gibson PG, Hart IR, Burns GF. The integrins alpha3beta1 and alpha6beta1 physically and functionally associate with CD36 in humanmelanoma cells. Requirement for the extracellular domain OF CD36. J Biol Chem. 2000 Nov 10;275(45):35264-75.

Tingen C, Kim A, Woodruff TK. The primordial pool of follicles and nest breakdown in mammalian ovaries. Mol Hum Reprod. 2009 Dec;15(12):795-803. Epub 2009 Aug 26.

Tishkoff DX1, Amin NS, Viars CS, Arden KC, Kolodner RD. Identification of a human gene encoding a homologue of Saccharomyces cerevisiae EXO1, an exonuclease implicated in mismatch repair and recombination. Cancer Res. 1998 Nov 15;58(22):5027-31.

Tomita K, van Bokhoven A, van Leenders GJ, Ruijter ET, Jansen CF, Bussemakers MJ, Schalken JA. Cadherin switching in human prostate cancer progression. Cancer Res. 2000 Jul 1;60(13):3650-4.

Tomizuka K, Horikoshi K, Kitada R, Sugawara Y, Iba Y, Kojima A, Yoshitome A, Yamawaki K, Amagai M, Inoue A, Oshima T, Kakitani M. R-spondin1 plays an essential role in ovarian development through positively regulating Wnt-4 signaling. Hum Mol Genet. 2008 May 1;17(9):1278-91. Epub 2008 Feb 4.

Torregrosa Paredes P1, Esser J, Admyre C, Nord M, Rahman QK, Lukic A, Rådmark O, Grönneberg R, Grunewald J, Eklund A, Scheynius A, Gabrielsson S. Bronchoalveolar lavage fluid exosomes contribute to cytokine and leukotriene production in allergic asthma. Allergy. 2012 Jul;67(7):911-9. doi: 10.1111/j.1398-9995.2012.02835.x. Epub 2012 May 23.

Tothill RW1, Tinker AV, George J, Brown R, Fox SB, Lade S, Johnson DS, Trivett MK, Etemadmoghadam D, Locandro B, Traficante N, Fereday S, Hung JA,Chiew YE, Haviv I; Australian Ovarian Cancer Study Group, Gertig D, DeFazio A, Bowtell DD. Novel molecular subtypes of serous and endometrioid ovarian cancer linked to clinical outcome. Clin Cancer Res. 2008 Aug 15;14(16):5198-208. doi: 10.1158/1078-0432.CCR-08-0196.

Trajkovic K, Hsu C, Chiantia S, Rajendran L, Wenzel D, Wieland F, Schwille P, Brügger B, Simons M. Ceramide triggers budding of exosome vesicles into multivesicular endosomes. Science. 2008 Feb 29;319(5867):1244-7.
Tripathi A, Kumar KV, Chaube SK. Meiotic cell cycle arrest in mammalian oocytes. J Cell Physiol. 2010 Jun;223(3):592-600.

Tsao SW, Mok SC, Fey EG, Fletcher JA, Wan TS, Chew EC, Muto MG, Knapp RC, Berkowitz RS. Characterization of human ovarian surface epithelial cells immortalized by human papilloma viral oncogenes (HPV-E6E7 ORFs). Exp Cell Res. 1995 Jun;218(2):499-507.

Vaccari S, Horner K, Mehlmann LM, Conti M. Generation of mouse oocytes defective in cAMP synthesis and degradation: endogenous cyclicAMP is essential for meiotic arrest. Dev Biol. 2008 Apr 1;316(1):124-34. Epub 2008 Jan 26.

Valadi H, Ekström K, Bossios A, Sjöstrand M, Lee JJ, Lötvall JO. Exosome- mediated transfer of mRNAs and microRNAs is a novel mechanism of genetic exchange between cells. Nat Cell Biol. 2007;9:654–59.

Valapala M, Vishwanatha JK. Lipid raft endocytosis and exosomal transport facilitate extracellular trafficking of annexin A2. J Biol Chem. 2011 Sep 2;286(35):30911-25. Epub 2011 Jul 7.

van Niel G, Raposo G, Candalh C, Boussac M, Hershberg R, Cerf-Bensussan N, Heyman M. Intestinal epithelial cells secrete exosome-like vesicles. Gastroenterology. 2001 Aug;121(2):337-49.

Van Wynsberghe PM1, Kai ZS, Massirer KB, Burton VH, Yeo GW, Pasquinelli AE. LIN-28 co-transcriptionally binds primary let-7 to regulate miRNA maturation in Caenorhabditis elegans. Nat Struct Mol Biol. 2011 Mar;18(3):302-8. doi: 10.1038/nsmb.1986. Epub 2011 Feb 6.

Villarroya-Beltri C1, Gutiérrez-Vázquez C, Sánchez-Madrid F, Mittelbrunn M. Analysis of microRNA and protein transfer by exosomes during an immune synapse. Methods Mol Biol. 2013;1024:41-51. doi: 10.1007/978-1-62703-453-1_4.

Viswanathan SR, Daley GQ, Gregory RL, Selective blockade of microRNA processing by Lin28. Science. 2008;320(5872):97–100.

Viswanathan SR, Powers JT, Einhorn W, Hoshida Y, Ng TL, Toffanin S, O'Sullivan M, Lu J, Phillips LA, Lockhart VL, Shah SP, Tanwar PS, Mermel CH,Beroukhim R, Azam M, Teixeira J, Meyerson M, Hughes TP, Llovet JM, Radich J, Mullighan CG, Golub TR, Sorensen PH, Daley GQ. Lin28 promotes transformation and is associated with advanced human malignancies. Nat Genet. 2009 Jul;41(7):843-8. Epub 2009 May 31.

Volinia S1, Calin GA, Liu CG, Ambs S, Cimmino A, Petrocca F, Visone R, Iorio M, Roldo C, Ferracin M, Prueitt RL, Yanaihara N, Lanza G, Scarpa A, Vecchione A,Negrini M, Harris CC, Croce CM. A microRNA expression signature of human solid tumors defines cancer gene targets. Proc Natl Acad Sci U S A. 2006 Feb 14;103(7):2257-61. Epub 2006 Feb 3.

Wakayama t., Perry A., Zuccotti M., Johnson KR, Yanagimachi R. Full-term development of mice from enucleated oocytes injected with cumulus cell nuclei. Nature. 1998. V. 394. № 6691. P. 369–374.

Wang Y1, Wen J, Zhang W. MIIP, a cytoskeleton regulator that blocks cell migration and invasion, delays mitosis, and suppresses tumorogenesis. Curr Protein Pept Sci. 2011 Feb;12(1):68-73.

Wassarman PM, Albertini DF. The mammalian ovum. The physiology of reproduction. In: Knobil E, Neill JD, editors. Raven Press, NY. 1994;1(2):79–122.

Watson JD. Origin of concatemeric T7 DNA. Nat New Biol. 1972 Oct 18;239(94):197-201.

Webb RJ, Marshall F, Swann K, Carroll J. Follicular-stimulating hormone induces gap junction-dependent dynamic changes in [cAMP] and protein kinase A in mammalianoocytes. Dev Biol. 2002;246: 441–454.

Weber JA, Baxter DH, Zhang S, Huang DY, Huang KH, Lee MJ, Galas DJ, Wang K. The microRNA spectrum in 12 body fluids. Clin Chem. 2010 Nov;56(11):1733-41. Epub 2010 Sep 16.

Wei X, Dombkowski D, Meirelles K, Pieretti-Vanmarcke R, Szotek PP, Chang HL, Preffer FI, Mueller PR, Teixeira J, Maclaughlin DT, Donahoe PK. Müllerian inhibiting substance preferentially inhibits stem/progenitors in human ovarian cancer cell lines compared with chemotherapeutics. Proc Natl Acad Sci USA. 2010 Nov 2;107(44):18874-9. Epub 2010 Oct 15.

Wen WH1, Reles A, Runnebaum IB, Sullivan-Halley J, Bernstein L, Jones LA, Felix JC, Kreienberg R, el-Naggar A, Press MF. p53 mutations and expression in ovarian cancers: correlation with overall survival. Int J Gynecol Pathol. 1999 Jan;18(1):29-41.

Wheelock MJ, Shintani Y, Maeda M, Fukumoto Y, Johnson KR. Cadherin switching. J Cell Sci. 2008 Mar 15;121(Pt 6):727-35.

Williamson JA, Bosher JM, Skinner A, Sheer D, Williams T, Hurst HC. Chromosomal mapping of the human and mouse homologues of two new members of the AP-2 family of transcription factors. Genomics. 1996 Jul 1;35(1):262-4.

Wilmut I, Schnieke AE, Mcwhir J, Kind AJ, Campbell KH. Viable offspring derived from fetal and adult mammalian cells. Nature. 1997;385(6619):810–813.

Winger Q1, Huang J, Auman HJ, Lewandoski M, Williams T. Analysis of transcription factor AP-2 expression and function during mouse preimplantation development. Biol Reprod. 2006 Sep;75(3):324-33. Epub 2006 May 3.

Wollert T, Wunder C, Lippincott-Schwartz J, Hurley JH. Membrane scission by the ESCRT-III complex. Nature. 2009 Mar 12;458(7235):172-7. Epub 2009 Feb 22.

Wright WE1, Shay JW. Telomere biology in aging and cancer. J Am Geriatr Soc. 2005 Sep;53(9 Suppl):S292-4.

Wu J1, Wei JJ. HMGA2 and high-grade serous ovarian carcinoma. J Mol Med (Berl). 2013 Oct;91(10):1155-65. doi: 10.1007/s00109-013-1055-8. Epub 2013 May 19.

Wubbolts R1, Fernandez-Borja M, Oomen L, Verwoerd D, Janssen H, Calafat J, Tulp A, Dusseljee S, Neefjes J. Direct vesicular transport of MHC class II molecules from lysosomal structures to the cell surface. J Cell Biol. 1996 Nov;135(3):611-22.

Wyman SK1, Parkin RK, Mitchell PS, Fritz BR, O'Briant K, Godwin AK, Urban N, Drescher CW, Knudsen BS, Tewari M. Repertoire of microRNAs in epithelial ovarian cancer as determined by next generation sequencing of small RNA cDNA libraries. PLoS One. 2009;4(4):e5311. doi: 10.1371/journal.pone.0005311. Epub 2009 Apr 23.

Xie P, Kondeti VK, Lin S, Haruna Y, Raparia K, Kanwar YS. Role of extracellular matrix renal tubule-intestitial nephritis (TINag) in cell survivial utilizing integrin (alpha)vbeta/focal adhesion (FAK)/phosphatidylinositol 3-kinase (PI3K)protein kinase B-serine/threonine kinase (AKT) signaling pathway. J Biol Chem. 2011 Sep 30;286(39):34131-46. Epub 2011 Jul 27.

Yamashiro DJ1, Maxfield FR. Acidification of morphologically distinct endosomes in mutant and wild-type Chinese hamster ovary cells. J Cell Biol. 1987 Dec;105(6 Pt 1):2723-33.

Yang F, Bi J, Xue X, Zheng L, Zhi K, Hua J, Fang G. Up-regulated long non-coding RNA H19 contributes to proliferation of gastric cancer cells. FEBS J. 2012 Sep;279(17):3159-65. doi: 10.1111/j.1742-4658.2012.08694.x. Epub 2012 Jul 31.

Yang J1, Zhou F, Xu T, Deng H, Ge YY, Zhang C, Li J, Zhuang SM. Analysis of sequence variations in 59 microRNAs in hepatocellular carcinomas. Mutat Res. 2008a Feb 1;638(1-2):205-9. Epub 2007 Aug 21.

Yang N1, Kaur S, Volinia S, Greshock J, Lassus H, Hasegawa K, Liang S, Leminen A, Deng S, Smith L, Johnstone CN, Chen XM, Liu CG, Huang Q, Katsaros D,Calin GA, Weber BL, Bützow R, Croce CM, Coukos G, Zhang L.
MicroRNA microarray identifies Let-7i as a novel biomarker and therapeutic target in human epithelial ovarian cancer. Cancer Res. 2008b Dec 15;68(24):10307-14. doi: 10.1158/0008-5472.CAN-08-1954.

Ying Y1, Liu XM, Marble A, Lawson KA, Zhao GQ. Ying Y1, Liu XM, Marble A, Lawson KA, Zhao GQ. Requirement of Bmp8b for the generation of primordial germ cells in the mouse. Mol Endocrinol. 2000 Jul;14(7):1053-63.

Yokoyama Y1, Takahashi Y, Shinohara A, Lian Z, Tamaya T. Telomerase activity in the female reproductive tract and neoplasms. Gynecol Oncol. 1998 Feb;68(2):145-9.

Yoshida N1, Mita K, Yamashita M. Function of the Mos/MAPK pathway during oocyte maturation in the Japanese brown frog Rana japonica. Mol Reprod Dev. 2000 Sep;57(1):88-98.

Yoshisa J, Horiuchi A, Kikuchi N, Hayashi A, Osada R, Ohira S, Shiozawa T, Konishi I. Changes in the expression of E-cadherin repressors, Snail, Slug, SIP1, and Twist, in the development and progression of ovarian carcinoma: the important role of Snail in ovarian tumorigenesis and progression. Med Mol Morphol. 2009 Jun;42(2):82-91. Epub 2009 Jun 18.

Yu J, Vodyanik MA, Smuga-Otto K, Antosiewicz-Bourget J, Frane JL, Tian S, Nie J, Jonsdottir GA, Ruotti V, Stewart R. Induced pluripotent stem cell lines derived from human somatic cells. Science 2007 318:1917–1920.

Yu Z1, Wang C, Wang M, Li Z, Casimiro MC, Liu M, Wu K, Whittle J, Ju X, Hyslop T, McCue P, Pestell RG. A cyclin D1/microRNA 17/20 regulatory feedback loop in control of breast cancer cell proliferation. J Cell Biol. 2008 Aug 11;182(3):509-17. doi: 10.1083/jcb.200801079.

Zhang B1, Pan X, Cobb GP, Anderson TA. microRNAs as oncogenes and tumor suppressors. Dev Biol. 2007 Feb 1;302(1):1-12. Epub 2006 Aug 16.

Zhang L, Yang N, Coukos G. MicroRNA in human cancer: one step forward in diagnosis and treatment. Adv Exp Med Biol. 2008a;622:69-78.

Zhang L1, Volinia S, Bonome T, Calin GA, Greshock J, Yang N, Liu CG, Giannakakis A, Alexiou P, Hasegawa K, Johnstone CN, Megraw MS, Adams S, Lassus H,Huang J, Kaur S, Liang S, Sethupathy P, Leminen A, Simossis VA, Sandaltzopoulos R, Naomoto Y, Katsaros D, Gimotty PA, DeMichele A, Huang Q, Bützow R,Rustgi AK, Weber BL, Birrer MJ, Hatzigeorgiou AG, Croce CM, Coukos G. Genomic and epigenetic alterations deregulate microRNA expression in human epithelial ovarian cancer. Proc Natl Acad Sci U S A. 2008b May 13;105(19):7004-9. doi: 10.1073/pnas.0801615105. Epub 2008 May 5.

Zhang S1, Balch C, Chan MW, Lai HC, Matei D, Schilder JM, Yan PS, Huang TH, Nephew KP. Identification and characterization of ovarian cancer-initiating cells from primary human tumors. Cancer Res. 2008c Jun 1;68(11):4311-20. doi: 10.1158/0008-5472.CAN-08-0364.

Zheng W, Li N, Wang J, Ulukus M, Arici A, Liang SX. Initial endometriosis showing direct morphologic evidence of metaplasia in the pathogenesis of ovarian endometriosis. Int J Gynecol Pathol. 2005 Apr;24(2):164-72.

Zhong X1, Coukos G, Zhang L. miRNAs in human cancer. Methods Mol Biol. 2012;822:295-306. doi: 10.1007/978-1-61779-427-8_21.

Zhong X, Li N, Liang S, Huang Q, Coukos G, Zhang L. Identification of microRNAs regulating reprogramming factor LIN28 in embryonic stem cells and cancer cells., J Biol Chem. 2010 Oct 14. [Epub ahead of print]

Zhu Z1, Todorova K, Lee KK, Wang J, Kwon E, Kehayov I, Kim HG, Kolev V, Dotto GP, Lee SW, Mandinova A. Small GTPase RhoE/Rnd3 is a critical regulator of Notch1 signaling. Cancer Res. 2014 Apr 1;74(7):2082-93. doi: 10.1158/0008-5472.CAN-12-0452. Epub 2014 Feb 13.

Zitvogel L, Regnault A, Lozier A, Wolfers J, Flament C, Tenza D, Ricciardi-Castagnoli P, Raposo G, Amigorena S. Eradication of established murine tumors using a novel cell-free vaccine: dendritic cell-derived exosomes. Nat Med. 1998 May;4(5):594-600.

APPENDICIES

APPENDIX I: STABLE TRANSDUCTION OF IGROV1 CELLS PRODUCE IGROV1-CD63-GFP POSITIVE LABELED EXOSOMES

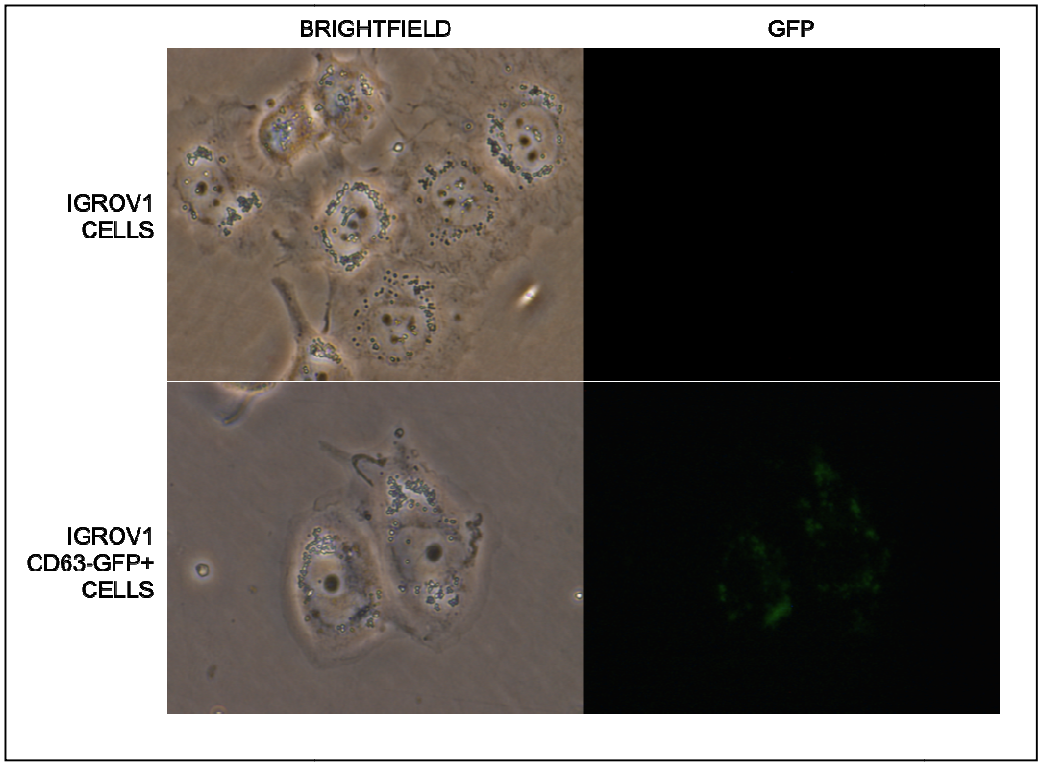

Appendix I: Stable transduction of IGROV1 cells produced IGROV-CD63-GFP positive labeled exosomes.

APPENDIX II- NEXTGEN SEQUENCING RESULTS OF 320 DIFFERENTIALLY EXPRESSED RNAS

Appendix II: NextGen sequencing results of 320 differentially expressed RNAs

ensembl_gene_id	hgnc_symbol	chromosome_name	start_position	end_position	Description	p-vaule	Fold change	GRD1	GRD2	GRD3	OV1	OV2	OV3
ENSG00000001629	*ANKIB1*	7	91875548	92030698	ankyrin repeat and IBR domain containing 1 [Source:HGNC Symbol;Acc:22215]	0.027810475	2.730760789	10.3347	13.9764	9.53029	2.26084	2.78664	7.34518
ENSG00000009335	*UBE3C*	7	156931607	157062066	ubiquitin protein ligase E3C [Source:HGNC Symbol;Acc:16803]	0.004831676	-2.466965601	1.89635	1.33505	2.66064	4.81202	5.44168	4.28176
ENSG00000010072	*SPRTN*	1	231472850	231490769	SprT-like N-terminal domain [Source:HGNC Symbol;Acc:25356]	0.01605615	2.563291569	12.2019	15.3112	15.9178	3.99597	9.39874	3.5487
ENSG00000010361	*FUZ*	19	50310126	50320633	fuzzy homolog (Drosophila) [Source:HGNC Symbol;Acc:26219]	0.030771913	2.356896011	6.25373	6.13665	3.62989	2.13143	1.66936	2.9964
ENSG00000025796	*SEC63*	6	108188960	108279393	SEC63 homolog (S. cerevisiae) [Source:HGNC Symbol;Acc:21082]	0.005496655	2.108194247	10.1308	13.9729	13.3618	6.11507	5.58623	6.07007
ENSG00000037965	*HOXC8*	12	54402832	54407570	homeobox C8 [Source:HGNC Symbol;Acc:5129]	0.029562459	1.863704992	6.91362	5.95866	4.76711	3.4688	2.10429	3.8916
ENSG00000051180	*RAD51*	15	40986972	41024354	RAD51 homolog (S. cerevisiae) [Source:HGNC Symbol;Acc:9817]	0.005672496	-7.179908683	0	0.565188	1.23119	4.30184	5.31105	3.28494
ENSG00000055118	*KCNH2*	7	150642049	150675403	potassium voltage-gated channel, subfamily H (eag-related), member 2 [Source:HGNC Symbol;Acc:6251]	0.000900303	-4.582812152	0.841836	0.885251	1.37244	4.7011	5.41298	4.09047
ENSG00000058262	*SEC61A1*	3	127770484	127790526	Sec61 alpha 1 subunit (S. cerevisiae) [Source:HGNC Symbol;Acc:18276]	0.042327986	2.443239593	5.56095	4.81284	4.40327	1.57583	0.672342	3.79997
ENSG00000064652	*SNX24*	5	122179134	122365049	sorting nexin 24 [Source:HGNC Symbol;Acc:21533]	0.035193362	1.802526016	7.62117	6.04649	5.76896	4.94284	2.48814	3.35201
ENSG00000064961	*HMG20B*	19	3572775	3579086	high mobility group 20B [Source:HGNC Symbol;Acc:5002]	0.020249121	2.490261208	8.91351	5.11593	7.17892	3.35908	2.38808	2.76936
ENSG00000065361	*ERBB3*	12	56473641	56497289	v-erb-b2 erythroblastic leukemia viral oncogene homolog 3 (avian) [Source:HGNC Symbol;Acc:3431]	0.013929435	2.439009003	17.5733	20.25	19.107	2.87509	11.5303	8.93618
ENSG00000065526	*SPEN*	1	16174359	16266955	spen homolog, transcriptional regulator (Drosophila) [Source:HGNC	0.048845367	-3.350494604	0.489505	0.833086	6.15238	10.0666	6.57438	8.40387

					Symbol;Acc:17575]								
ENSG00000066248	*NGEF*	2	233743396	233877982	neuronal guanine nucleotide exchange factor [Source:HGNC Symbol;Acc:7807]	0.01594774	-9.857851931	0.584569	1.42043	6.79702	22.1448	41.2539	23.3703
ENSG00000068745	*IP6K2*	3	48725436	48777786	inositol hexakisphosphate kinase 2 [Source:HGNC Symbol;Acc:17313]	0.01648850 7	1.6840033 9	8.79369	8.32376	10.2034	3.92837	6.11551	6.17987
ENSG00000068903	*SIRT2*	19	39369197	39390502	sirtuin 2 [Source:HGNC Symbol;Acc:10886]	0.00541781 5	5.026895354	6.93483	10.1732	10.8026	3.13449	1.08004	1.33773
ENSG00000070610	*GBA2*	9	35736863	35749983	glucosidase, beta (bile acid) 2 [Source:HGNC Symbol;Acc:18986]	0.02276257 9	4.902241976	5.59385	2.98894	3.39525	0.5598	1.51256	0.37102
ENSG00000075240	*GRAMD4*	22	46971909	47075688	GRAM domain containing 4 [Source:HGNC Symbol;Acc:29113]	0.01301748 5	1.994994242	14.9674	13.646	10.1725	6.43245	5.65216	7.357
ENSG00000078549	*ADCYAP1R1*	7	31092076	31151089	adenylate cyclase activating polypeptide 1 (pituitary) receptor type I [Source:HGNC Symbol;Acc:242]	0.04634149 5	-18.97160731	0.091659 4	0.458355	0.151807	6.73405	1.69926	4.88137
ENSG00000084734	*GCKR*	2	27719709	27746554	glucokinase (hexokinase 4) regulator [Source:HGNC Symbol;Acc:4196]	0.01763760 5	-3.907418751	1.11271	3.16702	4.66625	11.5763	15.1085	8.27089
ENSG00000085465	*OVGP1*	1	111956936	111970399	oviductal glycoprotein 1, 120kDa [Source:HGNC Symbol;Acc:8524]	0.04197383	-17.37183735	0.15472	0.598998	0.0695484	7.7644	3.64381	2.89344
ENSG00000086205	*FOLH1*	11	49168187	49230222	folate hydrolase (prostate-specific membrane antigen) 1 [Source:HGNC Symbol;Acc:3788]	0.01836511 6	4.366285643	5.71631	8.01132	4.18755	2.23309	1.11719	0.752791
ENSG00000087303	*NID2*	14	52471521	52535712	nidogen 2 (osteonidogen) [Source:HGNC Symbol;Acc:13389]	0.02507199 5	-8.685259284	0.298417	0.557456	0.512914	5.3239	4.55334	2.01103
ENSG00000090621	*PABPC4*	1	40026488	40042462	poly(A) binding protein, cytoplasmic 4 (inducible form) [Source:HGNC Symbol;Acc:8557]	0.04953074 7	2.161340335	32.5822	28.6486	47.5433	19.344	8.97965	22.0035
ENSG00000099622	*CIRBP*	19	1259384	1274879	cold inducible RNA binding protein [Source:HGNC Symbol;Acc:1982]	0.01632049 1	6.914273832	7.04821	3.60649	4.27525	1.01673	0.412234	0.73033
ENSG00000099954	*CECR2*	22	17840837	18033845	cat eye syndrome chromosome region, candidate 2 [Source:HGNC Symbol;Acc:1840]	0.03136553 6	2.556286742	4.3888	6.97011	4.00831	1.61727	2.4271	1.96717

ENSG00000100201	*DDX17*	22	38879445	38903665	DEAD (Asp-Glu-Ala-Asp) box helicase 17 [Source:HGNC Symbol;Acc:2740]	0.035592967	3.478915681	16.6809	15.431	7.91466	6.3457	3.40341	1.75636
ENSG00000100721	*TCL1A*	14	96176304	96180533	T-cell leukemia/lymphoma 1A [Source:HGNC Symbol;Acc:11648]	0.040799122	-5.095126068	0	0.620575	2.49303	6.9621	5.97501	2.9271
ENSG00000101040	*ZMYND8*	20	45837859	45985567	zinc finger, MYND-type containing 8 [Source:HGNC Symbol;Acc:9397]	0.038759187	1.471156225	4.97598	5.17495	4.59594	2.89851	2.80384	4.32165
ENSG00000101115	*SALL4*	20	50400581	50419059	sal-like 4 (Drosophila) [Source:HGNC Symbol;Acc:15924]	0.037127736	-6.659294957	0.19453	0.250382	1.90235	5.58924	2.74644	7.29543
ENSG00000101294	*HM13*	20	30102231	30157370	histocompatibility (minor) 13 [Source:HGNC Symbol;Acc:16435]	0.018376599	-3.285267137	24.9776	6.54328	17.6606	38.4117	57.146	66.0166
ENSG00000103152	*MPG*	16	127006	135852	N-methylpurine-DNA glycosylase [Source:HGNC Symbol;Acc:7211]	0.006663326	4.696790715	4.26882	6.16306	6.91543	2.02007	0.860341	0.813028
ENSG00000104299	*INTS9*	8	28625178	28747759	integrator complex subunit 9 [Source:HGNC Symbol;Acc:25592]	0.002213962	-5.013808571	1.13202	0.596024	2.01818	5.945	7.39644	5.44141
ENSG00000105705	*SUGP1*	19	19386827	19432123	SURP and G patch domain containing 1 [Source:HGNC Symbol;Acc:18643]	0.042343835	19.34214566	4.62015	10.9888	16.5858	0.384549	0.408117	0.871821
ENSG00000105929	*ATP6V0A4*	7	138391040	138484305	ATPase, H+ transporting, lysosomal V0 subunit a4 [Source:HGNC Symbol;Acc:866]	0.022562397	-2.747659852	1.98216	1.49516	1.8321	6.48595	3.64564	4.45689
ENSG00000106013	*ANKRD7*	7	117854727	117882785	ankyrin repeat domain 7 [Source:HGNC Symbol;Acc:18588]	0.037892894	4.597523993	3.02926	4.45634	5.33815	0.0815813	0.049111 8	2.65858
ENSG00000106070	*GRB10*	7	50657760	50861159	growth factor receptor-bound protein 10 [Source:HGNC Symbol;Acc:4564]	0.013638918	-3.936253947	2.98239	2.0304	5.86506	16.7878	9.77488	16.2553
ENSG00000106290	*TAF6*	7	99704693	99717464	TAF6 RNA polymerase II, TATA box binding protein (TBP)-associated factor, 80kDa [Source:HGNC Symbol;Acc:11540]	0.006278259	7.685757893	3.57282	5.32534	3.3552	0.0908043	0.507983	0.995507
ENSG00000106617	*PRKAG2*	7	151253210	151574210	protein kinase, AMP-activated, gamma 2 non-catalytic subunit [Source:HGNC Symbol;Acc:9386]	0.032403979	2.741119444	3.13559	5.4789	3.27221	1.07656	1.55695	1.70293
ENSG00000107581	*EIF3A*	10	120794356	120840396	eukaryotic translation initiation factor 3, subunit A [Source:HGNC	0.020400232	6.335578979	2.87531	2.82714	5.07105	0.288884	0.179122	1.23247

					Symbol;Acc:3271]								
ENSG00000109920	*FNBP4*	11	47738072	47788995	formin binding protein 4 [Source:HGNC Symbol;Acc:19752]	0.005415914	3.318885937	12.8162	17.0766	16.4498	3.87026	2.61637	7.47667
ENSG00000110060	*PUS3*	11	125763381	125773116	pseudouridylate synthase 3 [Source:HGNC Symbol;Acc:25461]	0.017469701	2.640289632	7.90619	8.15679	4.75074	2.80594	2.37164	2.70554
ENSG00000110436	*SLC1A2*	11	35272753	35441610	solute carrier family 1 (glial high affinity glutamate transporter), member 2 [Source:HGNC Symbol;Acc:10940]	0.047720864	3.532648039	2.30606	4.05799	5.04255	0.00767927	1.46536	1.75587
ENSG00000110713	*NUP98*	11	3692313	3819022	nucleoporin 98kDa [Source:HGNC Symbol;Acc:8068]	0.046550754	3.102837453	12.1557	10.292	5.19672	4.06587	1.67362	3.16991
ENSG00000110925	*CSRNP2*	12	51454990	51477447	cysteine-serine-rich nuclear protein 2 [Source:HGNC Symbol;Acc:16006]	8.73E-05	-5.900146155	2.52405	1.81945	1.08223	11.3486	10.5463	10.1177
ENSG00000111231	*GPN3*	12	110890289	110907019	GPN-loop GTPase 3 [Source:HGNC Symbol;Acc:30186]	0.049235293	-21.29929345	0	0.499229	1.7762	5.69263	24.2716	18.5008
ENSG00000111249	*CUX2*	12	111471828	111788358	cut-like homeobox 2 [Source:HGNC Symbol;Acc:19347]	0.027584072	-4.530358774	0.654575	0.956421	1.03694	5.62092	3.91118	2.464
ENSG00000111271	*ACAD10*	12	112123857	112194903	acyl-CoA dehydrogenase family, member 10 [Source:HGNC Symbol;Acc:21597]	0.008225727	3.604411278	5.38102	4.13709	3.29745	0.853521	1.19532	1.50668
ENSG00000111530	*CAND1*	12	67663061	67713731	cullin-associated and neddylation-dissociated 1 [Source:HGNC Symbol;Acc:30688]	0.034802399	5.133440936	17.2585	23.5453	9.91858	6.81661	2.25417	0.809996
ENSG00000112651	*MRPL2*	6	43021767	43027544	mitochondrial ribosomal protein L2 [Source:HGNC Symbol;Acc:14056]	0.003618466	3.196263988	7.68552	11.0415	8.99894	2.52708	2.54964	3.59777
ENSG00000114491	*UMPS*	3	124449213	124464040	uridine monophosphate synthetase [Source:HGNC Symbol;Acc:12563]	0.046684363	4.278735189	6.96024	4.64449	3.35001	0.510855	0.170706	2.81357
ENSG00000114770	*ABCC5*	3	183637722	183735803	ATP-binding cassette, sub-family C (CFTR/MRP), member 5 [Source:HGNC Symbol;Acc:56]	0.047454289	-3.823333714	3.08023	0.505836	2.35646	10.2429	8.38981	4.08755
ENSG00000115548	*KDM3A*	2	86667770	86719839	lysine (K)-specific demethylase 3A [Source:HGNC Symbol;Acc:20815]	0.017594365	-4.555068784	2.04045	0.0252058	2.01059	5.14783	5.14038	8.27937
ENSG00000115963	*RND3*	2	151324709	151395525	Rho family GTPase 3 [Source:HGNC Symbol;Acc:671]	0.001267252	8.931254363	13.9216	12.4328	16.9928	0.805983	0.742765	3.30468

ENSG00000116017	*ARID3A*	19	925781	975939	AT rich interactive domain 3A (BRIGHT-like) [Source:HGNC Symbol;Acc:3031]	0.036147682	2.356682714	3.46342	5.44489	3.25189	1.16385	2.04457	1.95146
ENSG00000116691	*MIIP*	1	12079523	12092102	migration and invasion inhibitory protein [Source:HGNC Symbol;Acc:25715]	0.008458951	-4.603275535	1.68148	0.410358	0.812848	3.23668	5.22847	4.90592
ENSG00000117419	*ERI3*	1	44686742	44820932	ERI1 exoribonuclease family member 3 [Source:HGNC Symbol;Acc:17276]	0.044861805	2.035938242	11.4712	20.9392	17.9331	10.1776	6.96695	7.58287
ENSG00000118473	*SGIP1*	1	66999066	67213982	SH3-domain GRB2-like (endophilin) interacting protein 1 [Source:HGNC Symbol;Acc:25412]	0.024179311	-3.731669903	4.6235	2.36891	6.01284	12.0115	14.0981	22.4217
ENSG00000120833	*SOCS2*	12	93963590	93977263	suppressor of cytokine signaling 2 [Source:HGNC Symbol;Acc:19382]	0.002967732	-5.152174835	1.82353	0.394183	1.53156	6.59437	7.52367	5.19887
ENSG00000121005	*CRISPLD1*	8	75896750	75946793	cysteine-rich secretory protein LCCL domain containing 1 [Source:HGNC Symbol;Acc:18206]	0.029552639	-3.882160953	1.98393	0.20713	1.01993	4.00176	5.57026	2.89356
ENSG00000121578	*B4GALT4*	3	118930579	118959950	UDP-Gal:betaGlcNAc beta 1,4-galactosyltransferase, polypeptide 4 [Source:HGNC Symbol;Acc:927]	0.043031364	-5.415210221	2.46127	0.442488	0	6.12428	2.77566	6.82452
ENSG00000122786	*CALD1*	7	134429003	134655479	caldesmon 1 [Source:HGNC Symbol;Acc:1441]	0.042624231	-1.951593522	59.3034	20.6881	50.2452	84.5753	98.4622	71.1316
ENSG00000123106	*CCDC91*	12	28286182	28732883	coiled-coil domain containing 91 [Source:HGNC Symbol;Acc:24855]	0.011182301	-65.34945504	1.27077	0.464039	1.26934	93.1453	58.7319	44.4423
ENSG00000124181	*PLCG1*	20	39765600	39804361	phospholipase C, gamma 1 [Source:HGNC Symbol;Acc:9065]	0.023424729	3.329824116	8.95021	11.0322	9.31266	1.26331	6.53776	0.996713
ENSG00000125952	*MAX*	14	65472892	65569413	MYC associated factor X [Source:HGNC Symbol;Acc:6913]	0.006395347	-6.686854188	3.61513	1.80473	2.04845	12.7291	21.6922	15.5182
ENSG00000127540	*UQCR11*	19	1597166	1605480	ubiquinol-cytochrome c reductase, complex III subunit XI [Source:HGNC Symbol;Acc:30862]	0.048693476	2.123880483	9.00526	8.90938	4.70165	3.3415	3.56654	3.74053
ENSG00000127914	*AKAP9*	7	91570181	91739987	A kinase (PRKA) anchor protein (yotiao) 9 [Source:HGNC Symbol;Acc:379]	0.016975696	3.390008431	8.63274	8.4304	4.93215	3.09302	1.26343	2.13182
ENSG00000129757	*CDKN1C*	11	2904443	2907111	cyclin-dependent kinase inhibitor 1C (p57, Kip2)	0.008160216	1.839684146	8.15769	8.33515	8.13308	2.94201	5.37498	5.06896

					[Source:HGNC Symbol;Acc:1786]								
ENSG00000130429	*ARPC1B*	7	98971872	98992424	actin related protein 2/3 complex, subunit 1B, 41kDa [Source:HGNC Symbol;Acc:704]	0.003394913	2.132487883	29.0339	35.644	28.0254	13.353	16.7224	13.3965
ENSG00000130997	*POLN*	4	2073645	2243848	polymerase (DNA directed) nu [Source:HGNC Symbol;Acc:18870]	0.000739667	-7.424171769	0.0516688	0.775202	2.07925	7.54493	7.45126	6.57935
ENSG00000131459	*GFPT2*	5	179727690	179780387	glutamine-fructose-6-phosphate transaminase 2 [Source:HGNC Symbol;Acc:4242]	0.029423502	-18.21684303	0.305676	0.42306	0.931903	4.3538	12.854	13.0438
ENSG00000131773	*KHDRBS3*	8	136469700	136668965	KH domain containing, RNA binding, signal transduction associated 3 [Source:HGNC Symbol;Acc:18117]	1.99E-05	-20.82252426	1.11057	7.06813	0.207776	57.7655	60.1207	56.7414
ENSG00000132256	*TRIM5*	11	5684425	5959849	tripartite motif containing 5 [Source:HGNC Symbol;Acc:16276]	0.017759151	4.328268684	8.22539	9.27335	10.622	0.299252	0.595233	5.60251
ENSG00000133026	*MYH10*	17	8377523	8534079	myosin, heavy chain 10, non-muscle [Source:HGNC Symbol;Acc:7568]	0.041312588	-7.325147944	0.516112	0.0813289	1.29454	7.13353	2.80649	3.91902
ENSG00000134256	*CD101*	1	117544382	117579167	CD101 molecule [Source:HGNC Symbol;Acc:5949]	0.013987786	-20.93575207	0.320444	0	0.909401	7.80668	12.2626	5.67845
ENSG00000134363	*FST*	5	52776239	52782964	follistatin [Source:HGNC Symbol;Acc:3971]	0.005419768	2.784706082	4.37547	6.41615	5.13158	1.71915	2.26012	1.73882
ENSG00000134697	*GNL2*	1	38032417	38061536	guanine nucleotide binding protein-like 2 (nucleolar) [Source:HGNC Symbol;Acc:29925]	0.011631609	4.697988918	6.09618	4.10255	3.94232	1.90435	0.273279	0.832393
ENSG00000135049	*AGTPBP1*	9	88161455	88356944	ATP/GTP binding protein 1 [Source:HGNC Symbol;Acc:17258]	0.025431531	2.161741116	10.9539	11.844	11.3516	8.74639	3.5872	3.46363
ENSG00000135077	*HAVCR2*	5	156512843	156569880	hepatitis A virus cellular receptor 2 [Source:HGNC Symbol;Acc:18437]	0.016372649	6.814083801	5.06606	3.16413	2.64134	0.298148	0.275132	1.02217
ENSG00000135090	*TAOK3*	12	118587606	118810750	TAO kinase 3 [Source:HGNC Symbol;Acc:18133]	0.027196687	-2.974144 21	5.69552	8.38404	3.56175	11.314	19.8929	21.2609
ENSG00000135218	*CD36*	7	79998891	80308593	CD36 molecule (thrombospondin receptor) [Source:HGNC Symbol;Acc:1663]	0.042642088	12.62035196	7.10584	2.11516	4.58068	0.475514	0.178489	0.439602
ENSG00000135253	*KCP*	7	128502505	128550773	kielin/chordin-like protein [Source:HGNC Symbol;Acc:17585]	0.038641667	2.750026033	3.07767	5.7181	6.25757	1.29164	2.5547	1.62755

ENSG00000135365	*PHF21A*	11	45950871	46142985	PHD finger protein 21A [Source:HGNC Symbol;Acc:24156]	0.038111992	-3.389348596	5.79035	2.40393	5.56447	16.1146	21.1715	9.3471
ENSG00000135749	*PCNXL2*	1	233119881	233431459	pecanex-like 2 (Drosophila) [Source:HGNC Symbol;Acc:8736]	0.007070896	2.795286566	45.4345	66.786	63.4518	22.582	14.622	25.6419
ENSG00000138796	*HADH*	4	108910870	108956331	hydroxyacyl-CoA dehydrogenase [Source:HGNC Symbol;Acc:4799]	0.032958844	2.217175731	22.9967	30.0639	22.8786	6.99442	8.624	18.632
ENSG00000139168	*ZCRB1*	12	42705880	42719920	zinc finger CCHC-type and RNA binding motif 1 [Source:HGNC Symbol;Acc:29620]	0.014265189	4.730204408	20.3432	19.6106	11.8242	5.49218	0	5.45407
ENSG00000139287	*TPH2*	12	72332626	72580398	tryptophan hydroxylase 2 [Source:HGNC Symbol;Acc:20692]	0.034195794	-4.993776345	2.66603	0.205739	1.65692	5.39944	6.16632	11.0495
ENSG00000141582	*CBX4*	17	77806955	77813228	chromobox homolog 4 [Source:HGNC Symbol;Acc:1554]	0.010463519	-5.989652817	3.07214	2.15478	0.873871	15.0127	7.98542	13.5435
ENSG00000141756	*FKBP10*	17	39968932	39979465	FK506 binding protein 10, 65 kDa [Source:HGNC Symbol;Acc:18169]	0.002360437	-3.848642672	1.59915	2.43374	2.28025	8.08918	6.65774	9.5501
ENSG00000142002	*DPP9*	19	4675246	4723855	dipeptidyl-peptidase 9 [Source:HGNC Symbol;Acc:18648]	0.018428241	1.935594556	9.5521	8.76703	6.293	4.45023	3.61374	4.65157
ENSG00000143507	*DUSP10*	1	221874766	221915518	dual specificity phosphatase 10 [Source:HGNC Symbol;Acc:3065]	0.027487146	1.846759314	10.3747	11.3079	10.677	2.99308	6.9997	7.52959
ENSG00000143740	*SNAP47*	1	227916240	227968927	synaptosomal-associated protein, 47kDa [Source:HGNC Symbol;Acc:30669]	0.040909767	-1.934888827	7.22746	6.77099	2.02493	10.7127	10.345	9.94575
ENSG00000144560	*VGLL4*	3	11597544	11762220	vestigial like 4 (Drosophila) [Source:HGNC Symbol;Acc:28966]	0.012115049	-2.824532005	2.20558	1.04828	1.90218	4.67674	3.86073	6.02593
ENSG00000145348	*TBCK*	4	106965474	107242652	TBC1 domain containing kinase [Source:HGNC Symbol;Acc:28261]	0.038489932	-2.712787905	3.5385	0.932089	4.72675	5.75731	10.1293	9.06382
ENSG00000146463	*ZMYM4*	1	35734568	35887659	zinc finger, MYM-type 4 [Source:HGNC Symbol;Acc:13055]	0.035662956	6.305835479	5.43092	1.94382	3.9382	0.738221	0.341001	0.714821
ENSG00000146677		7	44507441	44507939		0.010120888	2.421827355	18.0844	11.8679	16.6687	6.09825	5.4943	7.65779
ENSG00000146830	*GIGYF1*	7	100278172	100287071	GRB10 interacting GYF protein 1 [Source:HGNC Symbol;Acc:9126]	0.032142085	9.094920196	9.60712	3.56636	6.40273	1.57124	0.0625594	0.518634
ENSG00000147457	*CHMP7*	8	23101150	23119512	charged multivesicular body protein 7 [Source:HGNC	0.031504579	3.178581778	5.184	7.27921	9.85935	3.30149	2.97	0.751315

					Symbol;Acc:28439]								
ENSG00000147642	*SYBU*	8	110586207	110704020	syntabulin (syntaxin-interacting) [Source:HGNC Symbol;Acc:26011]	0.002705395	-3.365818238	2.46511	1.16947	1.97736	7.3885	5.88875	5.61152
ENSG00000148337	*CIZ1*	9	130928343	130966662	CDKN1A interacting zinc finger protein 1 [Source:HGNC Symbol;Acc:16744]	0.025830401	2.825257651	13.1778	13.2147	7.73746	5.53539	1.89356	4.65135
ENSG00000148700	*ADD3*	10	111756126	111895323	adducin 3 (gamma) [Source:HGNC Symbol;Acc:245]	0.042719395	4.295973283	8.39	6.02492	3.94256	0.101879	3.2803	0.891004
ENSG00000148908	*RGS10*	10	121259340	121302220	regulator of G-protein signaling 10 [Source:HGNC Symbol;Acc:9992]	0.016528647	-2.423742672	5.58908	4.02189	2.44774	7.73942	9.87459	11.6132
ENSG00000148948	*LRRC4C*	11	40135753	41481323	leucine rich repeat containing 4C [Source:HGNC Symbol;Acc:29317]	0.000577888	6.669774326	6.79917	8.31045	8.19852	0.432062	1.99571	1.06682
ENSG00000149294	*NCAM1*	11	112831997	113149158	neural cell adhesion molecule 1 [Source:HGNC Symbol;Acc:7656]	0.047891938	2.805041495	12.4856	13.3003	24.109	7.16785	5.28194	5.33779
ENSG00000149531	*FRG1B*	20	29611857	29634010	FSHD region gene 1 family, member B [Source:HGNC Symbol;Acc:15792]	0.000251208	18.86317529	4.22569	4.23874	5.16644	0	0.542584	0.180034
ENSG00000150787	*PTS*	11	112097088	112140678	6-pyruvoyltetrahydropterin synthase [Source:HGNC Symbol;Acc:9689]	0.037979613	2.314873401	24.43	15.394	15.6759	11.3272	5.40632	7.24183
ENSG00000151422	*FER*	5	108083523	108532542	fer (fps/fes related) tyrosine kinase [Source:HGNC Symbol;Acc:3655]	0.036388456	-2.709747357	2.74811	3.46975	4.46914	6.39138	12.984	9.58369
ENSG00000152936	*IFLTD1*	12	25562241	25801513	intermediate filament tail domain containing 1 [Source:HGNC Symbol;Acc:26683]	0.037771361	-49.50649164	0	0	0.291991	7.29716	5.16637	1.99192
ENSG00000154263	*ABCA10*	17	67143355	67240987	ATP-binding cassette, sub-family A (ABC1), member 10 [Source:HGNC Symbol;Acc:30]	0.006198656	-6.261297924	0.221791	10.889	2.06143	32.2876	27.8881	22.2995
ENSG00000154743	*TSEN2*	3	12525931	12581122	tRNA splicing endonuclease 2 homolog (S. cerevisiae) [Source:HGNC Symbol;Acc:28422]	0.024905942	2.538070311	9.64562	5.69237	7.18845	4.04358	2.86858	1.96326
ENSG00000155229	*MMS19*	10	99218081	99258551	MMS19 nucleotide excision repair homolog (S. cerevisiae)	0.013807523	2.401716719	13.1033	18.9934	19.3535	5.03787	6.97178	9.41261

					[Source:HGNC Symbol;Acc:13824]								
ENSG00000155629	*PIK3AP1*	10	98353069	98480271	phosphoinositide-3-kinase adaptor protein 1 [Source:HGNC Symbol;Acc:30034]	0.009083201	3.330660742	4.32563	6.61226	4.45719	1.21749	1.71023	1.69451
ENSG00000155827	*RNF20*	9	104296133	104325622	ring finger protein 20, E3 ubiquitin protein ligase [Source:HGNC Symbol;Acc:10062]	0.02976606	-7.760344485	1.09811	0.021684 9	0.270731	2.16657	5.23033	3.39406
ENSG00000156170	*NDUFAF6*	8	95907995	96128683	NADH dehydrogenase (ubiquinone) complex I, assembly factor 6 [Source:HGNC Symbol;Acc:28625]	0.007228208	-3.577475211	2.46933	1.25773	3.98915	7.3328	10.9585	9.31325
ENSG00000156427	*FGF18*	5	170846660	170884627	fibroblast growth factor 18 [Source:HGNC Symbol;Acc:3674]	0.002371141	5.228295545	10.7576	8.15882	7.38771	1.92784	1.33759	1.76568
ENSG00000157036	*EXOG*	3	38537618	38583652	endo/exonuclease (5'-3'), endonuclease G-like [Source:HGNC Symbol;Acc:3347]	0.012373313	-4.249804572	0.129065	1.8312	1.30821	5.91453	4.09126	3.88459
ENSG00000157800	*SLC37A3*	7	139993493	140104233	solute carrier family 37 (glycerol-3-phosphate transporter), member 3 [Source:HGNC Symbol;Acc:20651]	0.027057205	2.791096018	32.3263	33.2802	54.1275	9.65316	15.4558	17.7896
ENSG00000157985	*AGAP1*	2	236402733	237035198	ArfGAP with GTPase domain, ankyrin repeat and PH domain 1 [Source:HGNC Symbol;Acc:16922]	0.001239155	-3.848348221	0.753967	1.65867	1.24672	5.29489	4.12792	4.65967
ENSG00000158321	*AUTS2*	7	69063905	70258054	autism susceptibility candidate 2 [Source:HGNC Symbol;Acc:14262]	0.019212005	10.07560673	14.2227	21.4397	9.35263	0.461034	1.4489	2.55779
ENSG00000158773	*USF1*	1	161009041	161015767	upstream transcription factor 1 [Source:HGNC Symbol;Acc:12593]	0.032264294	1.778680611	10.5335	8.41289	11.5969	6.42168	7.03445	3.71575
ENSG00000161249	*DMKN*	19	35988122	36004560	dermokine [Source:HGNC Symbol;Acc:25063]	0.037064964	8.879599164	13.4889	10.5461	26.2428	1.11878	2.04469	2.4987
ENSG00000161642	*ZNF385A*	12	54762917	54785082	zinc finger protein 385A [Source:HGNC Symbol;Acc:17521]	0.009137422	-6.632517965	1.30073	0.168532	0.363897	5.21508	3.93247	3.01091
ENSG00000162419	*GMEB1*	1	28995244	29045865	glucocorticoid modulatory element binding protein 1 [Source:HGNC Symbol;Acc:4370]	0.045761802	-3.105552189	1.75706	0.249693	1.63572	5.03909	2.4415	3.8313
ENSG00000163625	*WDFY3*	4	85590704	85887544	WD repeat and FYVE domain containing 3 [Source:HGNC	0.027006728	3.527776671	5.57436	6.36874	4.873	0.338248	3.77206	0.656462

					Symbol;Acc:20751]								
ENSG00000163746	*PLSCR2*	3	146109208	146213778	phospholipid scramblase 2 [Source:HGNC Symbol;Acc:16494]	0.020850795	-46.96237535	0	0	0.322209	5.0191	7.36011	2.75249
ENSG00000164054	*SHISA5*	3	48509197	48542259	shisa homolog 5 (Xenopus laevis) [Source:HGNC Symbol;Acc:30376]	0.034891805	3.56613953	6.65471	3.44347	5.48279	1.29428	0.275302	2.79956
ENSG00000164597	*COG5*	7	106842189	107204959	component of oligomeric golgi complex 5 [Source:HGNC Symbol;Acc:14857]	0.00095993	5.039902761	11.6695	10.2267	11.4078	0.408404	3.46198	2.73768
ENSG00000164692	*COL1A2*	7	94023873	94060544	collagen, type I, alpha 2 [Source:HGNC Symbol;Acc:2198]	0.021332709	2.802755995	6.95596	4.51966	7.6637	3.43211	1.54993	1.84671
ENSG00000164778	*EN2*	7	155250824	155257526	engrailed homeobox 2 [Source:HGNC Symbol;Acc:3343]	0.024015745	3.323953899	6.87172	4.69636	3.86195	0.945301	1.2085	2.48827
ENSG00000164946	*FREM1*	9	14734664	14910993	FRAS1 related extracellular matrix 1 [Source:HGNC Symbol;Acc:23399]	0.013428445	-4.560847091	0.245691	3.30381	1.01794	5.34313	8.44408	7.04419
ENSG00000164989	*CCDC171*	9	15552895	16061661	coiled-coil domain containing 171 [Source:HGNC Symbol;Acc:29828]	0.010639941	-18.22468241	0.0439305	0.098058	0.641691	4.8003	3.05001	6.432
ENSG00000165138	*ANKS6*	9	101493611	101559247	ankyrin repeat and sterile alpha motif domain containing 6 [Source:HGNC Symbol;Acc:26724]	0.007841927	-4.633667543	0.626919	0.709625	1.81158	5.7396	5.30489	3.54287
ENSG00000165995	*CACNB2*	10	18429606	18830798	calcium channel, voltage-dependent, beta 2 subunit [Source:HGNC Symbol;Acc:1402]	0.039295851	-2.462616209	1.68134	3.18495	1.38321	6.72882	3.87146	4.78984
ENSG00000166448	*TMEM130*	7	98444111	98468394	transmembrane protein 130 [Source:HGNC Symbol;Acc:25429]	0.036634255	6.383450531	5.93146	2.06498	5.4988	0.916886	0.526476	0.670736
ENSG00000166917		10	135059982	135061395		0.007671577	-15.17649012	2.08194	0	0.00531995	14.1695	7.96919	9.53859
ENSG00000167371	*PRRT2*	16	29823177	29827201	proline-rich transmembrane protein 2 [Source:HGNC Symbol;Acc:30500]	0.008574658	1.814973936	5.53817	6.09304	5.89632	2.73379	4.25922	2.66417
ENSG00000169398	*PTK2*	8	141667999	142012315	PTK2 protein tyrosine kinase 2 [Source:HGNC Symbol;Acc:9611]	0.011880231	1.988332751	18.9802	20.6509	15.51	10.1612	6.43003	11.1411
ENSG00000169609	*C15orf40*	15	83657193	83680393	chromosome 15 open reading frame 40 [Source:HGNC Symbol;Acc:28443]	0.014447013	-10.35678283	0.251367	0.35248	1.97436	6.81525	12.6181	7.26858

ENSG00000169876	*MUC17*	7	100663353	100702020	mucin 17, cell surface associated [Source:HGNC Symbol;Acc:16800]	0.022001563	4.244298307	7.66994	7.37488	9.37405	0.554217	0.106538	5.09258
ENSG00000170190	*SLC16A5*	17	73083822	73102257	solute carrier family 16, member 5 (monocarboxylic acid transporter 6) [Source:HGNC Symbol;Acc:10926]	0.045020894	-3.580399696	3.57113	0.245632	0.423111	4.69619	6.34279	4.14146
ENSG00000173272	*MZT2A*	2	132222473	132250316	mitotic spindle organizing protein 2A [Source:HGNC Symbol;Acc:33187]	0.002034735	-12.51283553	0.037133 4	4.02115	0.424002	18.8961	15.052	22.138
ENSG00000174407	*C20orf166*	20	61147660	61167971	chromosome 20 open reading frame 166 [Source:HGNC Symbol;Acc:16159]	0.022770258	-36.02070565	0	0.146143	0.339908	2.97133	8.39569	6.14088
ENSG00000174871	*CNIH2*	11	66045661	66052772	cornichon homolog 2 (Drosophila) [Source:HGNC Symbol;Acc:28744]	0.001034148	-2.746275426	2.30805	1.83195	1.54857	5.28774	5.7145	4.62014
ENSG00000175224	*ATG13*	11	46638826	46696368	autophagy related 13 [Source:HGNC Symbol;Acc:29091]	0.042739877	5.812225724	14.3522	4.89467	13.4537	1.20898	3.12701	1.29018
ENSG00000175611	*LINC00476*	9	98520892	98638259	long intergenic non-protein coding RNA 476 [Source:HGNC Symbol;Acc:27858]	0.016467616	-1.948655331	1.97635	4.057	3.20052	5.30197	6.7482	5.94346
ENSG00000175662	*TOM1L2*	17	17746828	17875736	target of myb1-like 2 (chicken) [Source:HGNC Symbol;Acc:11984]	0.017144863	3.318764043	3.44803	5.30299	5.2931	0.819542	2.52962	0.88257
ENSG00000175806	*MSRA*	8	9911778	10286401	methionine sulfoxide reductase A [Source:HGNC Symbol;Acc:7377]	0.029469623	2.6984141 2	8.20087	10.6072	11.6203	3.28554	1.19153	6.79932
ENSG00000176571	*CNBD1*	8	87878670	88627447	cyclic nucleotide binding domain containing 1 [Source:HGNC Symbol;Acc:26663]	0.016968933	-6.150192372	0	0.137216	3.00305	5.01286	6.04539	8.25499
ENSG00000177058	*SLC38A9*	5	54921673	55069022	solute carrier family 38, member 9 [Source:HGNC Symbol;Acc:26907]	0.036530414	6.590341538	5.92952	12.157	5.70458	1.80931	0.178765	1.62192
ENSG00000177182	*CLVS1*	8	61969717	62414204	clavesin 1 [Source:HGNC Symbol;Acc:23139]	0.020464023	-4.251423593	13.0952	2.23106	1.86791	23.379	19.0443	30.6764
ENSG00000177679	*SRRM3*	7	75831216	75916605	serine/arginine repetitive matrix 3 [Source:HGNC Symbol;Acc:26729]	0.020084912	2.338166066	5.32822	3.48814	5.30953	2.43754	1.25071	2.35319
ENSG00000182095	*TNRC18*	7	5346421	5465045	trinucleotide repeat containing 18 [Source:HGNC Symbol;Acc:11962]	0.038591951	1.767663332	5.87362	4.25336	6.93661	2.76106	3.37532	3.51681
ENSG00000185864	*DMWD*	19	46286205	46296060	dystrophia myotonica,	0.016015	-	1.35971	2.68999	1.31537	3.91226	6.38828	6.40558

00					WD repeat containing [Source:HGNC Symbol;Acc:2936]	92	3.113868039						
ENSG00000185847		12	111374389	111396012		0.037268315	-3.858880473	1.35471	1.22532	7.5973	10.8104	17.8037	10.659
ENSG00000186106	*ANKRD46*	8	101521980	101572012	ankyrin repeat domain 46 [Source:HGNC Symbol;Acc:27229]	0.029320065	-3.824090432	7.59408	1.54546	7.89876	14.9693	29.8811	20.3056
ENSG00000186407	*CD300E*	17	72606026	72619897	CD300e molecule [Source:HGNC Symbol;Acc:28874]	0.009696301	-4.891344301	3.16765	2.95384	2.39394	10.2724	13.0402	18.3393
ENSG00000186431	*FCAR*	19	55385549	55401838	Fc fragment of IgA, receptor for [Source:HGNC Symbol;Acc:3608]	0.040984649	-8.658681596	0.0507779	0	1.46728	5.69412	5.48824	1.96202
ENSG00000186960	*C14orf23*	14	29241910	29282493	chromosome 14 open reading frame 23 [Source:HGNC Symbol;Acc:19828]	0.025069511	-4.427073034	0	4.68283	2.26556	13.9059	8.52373	8.3314
ENSG00000188850		5	43336266	43348818		0.005484592	-65.41031862	0	0.37098	0	10.9657	7.0236	6.27662
ENSG00000188859	*FAM78B*	1	166026674	166136206	family with sequence similarity 78, member B [Source:HGNC Symbol;Acc:13495]	0.006693677	1.532777668	8.82331	10.2295	8.9032	6.63429	5.2303	6.3742
ENSG00000196169	*KIF19*	17	72322349	72351959	kinesin family member 19 [Source:HGNC Symbol;Acc:26735]	0.043599848	-3.951713212	1.29324	1.61241	1.44026	8.56738	3.68444	4.92197
ENSG00000196233	*LCOR*	10	98592017	98740800	ligand dependent nuclear receptor corepressor [Source:HGNC Symbol;Acc:29503]	0.0374352	3.637965157	7.49451	3.9042	4.02938	1.28678	0.954167	1.99991
ENSG00000198625	*MDM4*	1	204485511	204542871	Mdm4 p53 binding protein homolog (mouse) [Source:HGNC Symbol;Acc:6974]	0.026224656	6.381786631	3.11432	5.48703	2.66706	0.159746	0.479768	1.1262
ENSG00000199426		17	56743898	56744058	U1 spliceosomal RNA [Source:RFAM;Acc:RF00003]	0.009786812	-4.048527283	0	33.4393	18.9333	59.5201	80.8772	71.6346
ENSG00000199711		7	99534233	99534334	Y RNA [Source:RFAM;Acc:RF00019]	0.033791125	5.502784367	965.559	722.436	1463.93	32.0271	28.4162	512.344
ENSG00000200102		14	21581798	21581904	U6 spliceosomal RNA [Source:RFAM;Acc:RF00026]	0.025744068	#NAME?	0	0	0	168.136	444.654	244.118
ENSG00000200179		19	36694249	36694361	Y RNA [Source:RFAM;Acc:RF00019]	0.041772483	-2.483225926	263.2	123.393	219.819	682.176	449.35	374.332
ENSG00000200356		10	75038820	75038926	U6 spliceosomal RNA [Source:RFAM;Acc:RF000	0.031831985	Inf	138.712	275.318	100.629	0	0	0

					26]								
ENSG00000201221		20	34475581	34475723	U4 spliceosomal RNA [Source:RFAM;Acc:RF00015]	0.022107974	3.187152351	344.794	387.173	295.104	12.5478	215.47	94.2357
ENSG00000201524		17	57924799	57924905	U6 spliceosomal RNA [Source:RFAM;Acc:RF00026]	0.001880442	#NAME?	0	0	0	456.043	426.401	283.408
ENSG00000202144		X	19394892	19394993	Y RNA [Source:RFAM;Acc:RF00019]	0.045477807	4.861233585	736.447	1629.28	1109.53	611.86	0	103.032
ENSG00000203520		11	63383780	63389143		0.027959761	-2.321903236	2.9795	5.28187	2.87356	8.85956	6.38757	10.6071
ENSG00000203897		1	109399839	109401146		0.008683884	#NAME?	0	0	0	3.23236	6.5454	6.82973
ENSG00000203963	*C1orf141*	1	67557859	67600639	chromosome 1 open reading frame 141 [Source:HGNC Symbol;Acc:32044]	0.035518585	-5.301682162	0.0771089	0.737854	6.70847	18.3688	12.5518	8.96625
ENSG00000206649		8	81229174	81229304	Small nucleolar RNA SNORA20 [Source:RFAM;Acc:RF00401]	0.025865446	-2.009966682	199.334	268.287	372.478	515.475	690.405	482.691
ENSG00000206697	*RNY1P8*	13	73801284	73801397	RNA, Ro-associated Y1 pseudogene 8 [Source:HGNC Symbol;Acc:42485]	0.001132127	#NAME?	0	0	0	252.261	383.153	311.065
ENSG00000206950		8	14190064	14190172	Y RNA [Source:RFAM;Acc:RF00019]	0.003766203	-4.804325118	0	55.1943	30.1028	126.321	152.509	130.965
ENSG00000206977		6	41800592	41800731	Small nucleolar RNA SNORA8 [Source:RFAM;Acc:RF00393]	0.016968114	35.53219498	92.6393	167.26	231.614	13.8329	0	0
ENSG00000207305		20	2433656	2433763	Y RNA [Source:RFAM;Acc:RF00019]	0.014445277	2.856978153	847.375	720.693	711.706	461.18	76.2299	260.557
ENSG00000207347		10	21853400	21853506	U6 spliceosomal RNA [Source:RFAM;Acc:RF00026]	0.036526052	#NAME?	0	0	0	262.512	404.359	113.066
ENSG00000207390		17	4096063	4096160	Y RNA [Source:RFAM;Acc:RF00019]	0.038797463	22.99985454	101.877	222.31	86.9239	0	0	17.8745
ENSG00000211667	*IGLV3-12*	22	23114317	23115079	immunoglobulin lambda variable 3-12 [Source:HGNC Symbol;Acc:5898]	0.010542862	-3.129977952	3.13586	2.53764	7.42049	13.8359	11.2298	15.9182
ENSG00000211793	*TRAV9-2*	14	22409313	22409848	T cell receptor alpha variable 9-2 [Source:HGNC Symbol;Acc:12154]	0.0298797	-53.67500353	0	0.523858	0	8.074	14.7043	5.33978
ENSG00000212517		20	5102063	5102185	Small nucleolar RNA SNORA26	0.047134799	-3.1274631	0	42.7712	53.2142	135.163	85.8583	79.1695

					[Source:RFAM;Acc:RF00568]		35						
ENSG00000213657		10	54148872	54149248		0.017155312	-31.48432272	0.419875	0	0	3.59545	3.08279	6.54124
ENSG00000213889	*PPM1N*	19	45992035	46005768	protein phosphatase, Mg2+/Mn2+ dependent, 1N (putative) [Source:HGNC Symbol;Acc:26845]	0.026353851	1.630568823	27.1744	19.427	24.9853	14.4108	17.1189	12.3732
ENSG00000214954	*LRRC69*	8	92114060	92231464	leucine rich repeat containing 69 [Source:HGNC Symbol;Acc:34303]	0.011450659	-36.72721753	0.273679	0.0910299	0.342801	10.1245	10.971	4.88937
ENSG00000215467	*RPL27AP*	20	42281163	42281931	ribosomal protein L27a pseudogene [Source:HGNC Symbol;Acc:16250]	0.015307704	12.09879962	3.67105	6.85853	3.97434	0	0	1.19879
ENSG00000215771	*LRRC37A14P*	22	41585731	41586192	leucine rich repeat containing 37, member A14, pseudogene [Source:HGNC Symbol;Acc:43818]	0.024583352	2.360265487	12.6212	10.9682	7.94285	6.5368	3.58515	3.23767
ENSG00000219135		6	122001118	122001605		0.003278332	4.144475026	28.1245	20.0487	20.0403	6.53231	5.16199	4.7646
ENSG00000220585	*DDX18P6*	10	92812808	92814804	DEAD (Asp-Glu-Ala-Asp) box polypeptide 18 pseudogene 6 [Source:HGNC Symbol;Acc:31126]	0.043970009	5.063311488	11.7045	6.13971	12.992	0	5.84892	0.241207
ENSG00000221923	*ZNF880*	19	52873170	52889048	zinc finger protein 880 [Source:HGNC Symbol;Acc:37249]	0.023624676	-2.511014874	3.1306	1.70351	1.01026	5.15278	5.67411	3.84841
ENSG00000222107		5	124686561	124686824	7SK RNA [Source:RFAM;Acc:RF00100]	0.029885115	14.55217339	31.0996	11.4759	35.1203	1.89584	1.87696	1.56632
ENSG00000222150	*RNA5SP239*	7	116584340	116584468	RNA, 5S ribosomal pseudogene 239 [Source:HGNC Symbol;Acc:43139]	0.036490622	-6.753811554	75.8522	16.8802	20.03	290.185	123.52	347.871
ENSG00000222395		18	29843098	29843201	Y RNA [Source:RFAM;Acc:RF00019]	0.002093491	#NAME?	0	0	0	322.06	205.855	331.679
ENSG00000222397		1	181808608	181808909	7SK RNA [Source:RFAM;Acc:RF00100]	0.017631662	#NAME?	0	0	0	16.3952	11.7019	6.22686
ENSG00000222558		9	110560025	110560128	U6 spliceosomal RNA [Source:RFAM;Acc:RF00026]	0.034753388	-9.861051852	0	124.219	0	589.234	212.048	423.648
ENSG00000222581		9	12300266	12300451	U2 spliceosomal RNA [Source:RFAM;Acc:RF00004]	0.024173134	-5.447753423	0	3.46914	3.38796	10.6093	17.6603	9.08619
ENSG00000222626		12	120942374	120942462	Y RNA	0.0419918	-	0	193.79	0	380.779	219.359	298.441

01					[Source:RFAM;Acc:RF00019]	04	4.636869808						
ENSG00000222614		19	47239569	47239676	Y RNA [Source:RFAM;Acc:RF00019]	0.017443329	-3.873195056	144.288	176.919	221.469	613.97	958.355	529.565
ENSG00000222649		6	119379045	119379139	Y RNA [Source:RFAM;Acc:RF00019]	0.048487151	-4.722458934	249.718	0	0	395.593	517.449	266.241
ENSG00000222808		17	75148643	75148756	U4 spliceosomal RNA [Source:RFAM;Acc:RF00015]	0.024148651	-65.05325943	18.0062	0	0	273.705	607.503	290.154
ENSG00000223091		17	37638739	37638843	U6 spliceosomal RNA [Source:RFAM;Acc:RF00026]	0.0128894	-31.31040363	47.7372	0	0	649.118	280.182	565.371
ENSG00000223125		17	39624208	39624398	U2 spliceosomal RNA [Source:RFAM;Acc:RF00004]	0.019266074	-18.17444786	0	0	16.7305	101.915	143.764	58.3886
ENSG00000223255		17	34216562	34216808	7SK RNA [Source:RFAM;Acc:RF00100]	0.015883661	-7.771450558	0	1.25661	3.68149	10.1278	17.8996	10.3488
ENSG00000224165	*DNAJC27-AS1*	2	25194259	25262563	DNAJC27 antisense RNA 1 [Source:HGNC Symbol;Acc:42943]	0.018342604	-8.318266891	0.514895	1.55677	0.669305	10.8496	5.06709	6.88343
ENSG00000224338		1	11485315	11485891		0.041217563	-64.32804258	0.213265	0	0	1.71764	5.1224	6.87888
ENSG00000224348		1	241468879	241469182		0.042662672	-1.648669483	16.1526	8.99147	12.7739	24.101	17.5898	20.8234
ENSG00000224935		9	12098660	12159147		0.000118499	#NAME?	0	0	0	5.71448	4.68247	4.71717
ENSG00000225131	*PSME2P2*	13	49345264	49345965	proteasome activator subunit 2 pseudogene 2 [Source:HGNC Symbol;Acc:30160]	0.021523448	-10.84179082	0.304429	0.226957	16.1424	60.058	84.5434	36.1723
ENSG00000225779		1	46836258	46836627		0.016409092	-35.07366642	0	0.558667	0	7.67971	3.40109	8.5137
ENSG00000225979		2	198176117	198177464		0.045461436	4.173042058	3.5041	5.05934	2.52417	2.13679	0.520171	0
ENSG00000226339	*RPS26P56*	X	128542359	128542598	ribosomal protein S26 pseudogene 56 [Source:HGNC Symbol;Acc:35858]	0.007526825	-1.790258246	8.42247	5.40871	7.70683	11.6875	12.8229	14.0482
ENSG00000226499		1	45309593	45309754		0.013014917	13.9094007	52.0501	114.826	103.911	0	11.0039	8.46402
ENSG00000227207		1	72767155	72767506		0.004121872	-6.741787758	1.98418	0	1.37209	8.96167	5.82791	7.83768
ENSG00000227297		20	56174751	56176256		0.024728988	1.864041045	11.9267	14.0189	11.865	9.75755	4.96842	5.55824
ENSG00000227755		22	23788785	23803020		0.005976051	#NAME?	0	0	0	6.04992	3.73912	3.42805

ENSG00000227896		10	88281702	88282443		0.044689031	-5.811733939	1.76493	4.77316	3.69445	30.0212	18.7997	10.6479
ENSG00000228399		1	101721830	101722172		0.001209265	-7.72528951	1.51929	0	1.60236	7.3944	9.3921	7.32915
ENSG00000228429		7	68105785	68106571		0.011473653	2.473448858	6.777	5.69966	7.50804	2.94449	1.32714	3.80806
ENSG00000228624		6	114290865	114792869		0.029648415	-3.176276665	3.20265	1.56709	1.44254	4.16272	7.31254	8.25666
ENSG00000229169		22	31934338	31934575		0.047379198	#NAME?	0	0	0	18.2007	8.86585	5.39284
ENSG00000229605		10	29187925	29188422		0.003503696	Inf	2.9524	5.09311	3.63754	0	0	0
ENSG00000230226		20	62133640	62136464		0.008408916	-5.988897906	7.78162	7.78761	7.42283	55.4004	52.0837	30.213
ENSG00000231054		2	45395722	45396553		0.040866626	-3.402555583	3.96876	0.682542	0.272115	4.47434	5.6551	6.62276
ENSG00000231096		17	19743439	19743828		0.037635885	-9.607323245	0.459031	4.56803	0	25.0624	11.8111	11.4231
ENSG00000231485		1	65532310	65533420		0.030497326	2.9848480 2	18.6951	21.6741	15.7786	0.956541	12.5772	5.2772
ENSG00000231712		2	30432861	30433173		0.034957199	-7.654769715	0.891052	0	6.0658	16.395	26.2076	10.6505
ENSG00000232019		7	84568665	84569561		0.002300241	-5.567558982	1.72734	0.526474	0.302308	5.32008	4.11626	4.79502
ENSG00000232271		20	7050261	7127303		0.034660668	-18.23765648	3.371	0	0	24.5401	28.3527	8.58634
ENSG00000232533		7	143076785	143077588		0.009150952	2.741562179	4.90543	5.79376	5.15326	3.02238	2.01713	0.742759
ENSG00000232778	*RPL23AP50*	6	108253004	108253458	ribosomal protein L23a pseudogene 50 [Source:HGNC Symbol;Acc:35958]	0.041865698	-25.29474351	0.27584	0	0.395235	2.99223	9.18037	4.80207
ENSG00000232874		3	193848405	193848990		0.004699	-38.06874756	0	0.248254	0.224781	7.07452	6.97676	3.95657
ENSG00000234020		1	111895897	111910031		0.049412944	-2.754818432	1.62453	4.57224	0.15073	5.32548	5.83094	6.32979
ENSG00000234022		2	15704294	15713992		0.026213451	-9.904242408	1.05267	0	0.4222	7.1516	4.54085	2.91502
ENSG00000234222		1	145486272	145508262		0.031393866	-7.287672565	3.51512	2.09065	8.78733	32.3441	51.7972	20.7509

ENSG00000234705	*HMGA1P4*	9	131425413	131425857	high mobility group AT-hook 1 pseudogene 4 [Source:HGNC Symbol;Acc:39093]	0.016785344	-4.633973283	0.589697	2.59707	0.79047	8.18273	5.465	4.78268
ENSG00000234753		6	41462591	41516359		0.035018212	-11.6121557	2.03742	0	1.90937	6.46804	19.7061	19.6566
ENSG00000234853		9	19383220	19383878		0.016479 2	-10.203988	1.87011	0	0	8.81114	4.37175	5.89969
ENSG00000235021		1	246853349	246855123		0.025086995	1.945659667	31.3276	37.7616	38.5251	21.7466	9.64343	23.9199
ENSG00000235206		9	86693892	86694300		0.012878595	2.920800703	28.6607	34.433	29.4611	2.74296	11.0276	17.9176
ENSG00000235297	*FAUP1*	18	72057119	72057532	FBR-MuSV-associated ubiquitously expressed (fox derived) pseudogene 1 [Source:HGNC Symbol;Acc:17984]	0.003927049	-96.73225243	0.42372	0	0	9.65379	13.8728	17.4608
ENSG00000235363	*SNRPGP10*	1	205320375	205320599	small nuclear ribonucleoprotein polypeptide G pseudogene 10 [Source:HGNC Symbol;Acc:39329]	0.001930126	Inf	7.05178	9.81273	6.30593	0	0	0
ENSG00000235700	*CYCSP52*	1	157098154	157098463	cytochrome c, somatic pseudogene 52 [Source:HGNC Symbol;Acc:24393]	0.046281658	-11.08370847	0.651375	0	0.828977	7.24217	7.14815	2.01747
ENSG00000235957	*COX7CP1*	13	49761615	49761806	cytochrome c oxidase subunit VIIc pseudogene 1 [Source:HGNC Symbol;Acc:2293]	0.012850 54	-15.95041472	0	0	7.17471	42.9128	48.9996	22.5272
ENSG00000235976		X	101244457	101244845		0.018345136	-4.781658449	2.20465	0.479127	1.05896	8.12517	5.37785	4.39347
ENSG00000236005		9	110296671	110297443		0.043182804	-4.963592233	0	0	5.45488	12.3482	7.12378	7.60382
ENSG00000236432		2	228085768	228189917		0.025261409	4.216995376	19.471	37.8859	24.3123	2.01896	7.83495	9.51277
ENSG00000237024		2	61079395	61079878		0.019840626	3.301046367	6.0284	11.4511	10.497	1.95867	3.05459	3.46178
ENSG00000237643		6	71104590	71109120		0.026327807	#NAME?	0	0	0	3.86962	4.42782	9.22015
ENSG00000238365	*RNU7-57P*	1	154311219	154311278	RNA, U7 small nuclear 57 pseudogene [Source:HGNC Symbol;Acc:34153]	0.011528285	6.464259953	1223.4	1628.89	1144.73	0	0	618.326
ENSG00000239026		5	174877819	174877921	Small nucleolar RNA U13 [Source:RFAM;Acc:RF01210]	0.001998681	Inf	80.1515	51.7715	83.1172	0	0	0
ENSG00000239052		2	44466707	44466800	Small nucleolar RNA U13 [Source:RFAM;Acc:RF012	0.000305403	Inf	169.195	209.328	227.703	0	0	0

					10]								
ENSG00000239122		3	195655460	195655646	U2 spliceosomal RNA [Source:RFAM;Acc:RF00004]	0.000471156	#NAME?	0	0	0	75.913	82.5701	59.2509
ENSG00000239227		3	166579732	166579898		3.31E-05	#NAME?	0	0	0	58.3132	61.3249	51.8907
ENSG00000239317		5	145518334	145518571		0.019722526	11.77288955	18.1212	35.0271	42.8137	0	0	8.1511
ENSG00000239319		1	66226743	66227035	Metazoan signal recognition particle RNA [Source:RFAM;Acc:RF00017]	0.000462042	#NAME?	0	0	0	14.4342	12.0409	10.4089
ENSG00000239435	*KCNMB3P1*	22	17061816	17063607	potassium large conductance calcium-activated channel, subfamily M, beta member 3 pseudogene 1 [Source:HGNC Symbol;Acc:6288]	0.015399838	-39.99461505	0	0	0.258127	2.86535	5.06407	2.39427
ENSG00000239917	*RPS10P16*	8	118535510	118536300	ribosomal protein S10 pseudogene 16 [Source:HGNC Symbol;Acc:36200]	0.031465074	-13.76141746	1.42872	0	0.430494	10.792	11.0598	3.73362
ENSG00000240038	*AMY2B*	1	104096437	104122156	amylase, alpha 2B (pancreatic) [Source:HGNC Symbol;Acc:478]	0.023912979	-18.34434772	1.23399	0.108004	1.10753	12.3656	9.77422	22.7951
ENSG00000240160		22	23603971	23604258	Metazoan signal recognition particle RNA [Source:RFAM;Acc:RF00017]	0.025137007	-14.02362812	0	2.22997	0	11.4244	14.4718	5.37607
ENSG00000240183		2	112687752	112688041	Metazoan signal recognition particle RNA [Source:RFAM;Acc:RF00017]	0.004722125	-55.45013062	1.57321	0	0	24.1426	39.0657	24.0264
ENSG00000240366	*RPL36AP45*	15	75478992	75479309	ribosomal protein L36a pseudogene 45 [Source:HGNC Symbol;Acc:36032]	0.017060864	-19.94494611	0.674975	0	0	5.09791	5.94074	2.42369
ENSG00000240370	*RPL13P5*	12	6982553	6993905	ribosomal protein L13 pseudogene 5 [Source:HGNC Symbol;Acc:30363]	0.011254002	-7.383585265	3.99472	0.352947	0	11.4794	7.54967	13.0723
ENSG00000240934		15	58492805	58493214		0.011320403	Inf	2.3716	3.66314	5.31491	0	0	0
ENSG00000240993		12	19329225	19329523	Metazoan signal recognition particle RNA [Source:RFAM;Acc:RF00017]	0.011113883	3.523398634	17.5809	15.0444	18.9556	6.31156	0	8.32797
ENSG00000241067	*RPL17P40*	16	16188049	16189066	ribosomal protein L17 pseudogene 40 [Source:HGNC Symbol;Acc:36672]	0.042325933	-5.156376562	0	4.32822	5.96808	24.0185	20.1115	8.9616

ENSG00000241081		14	77352720	77353093		0.007784343	-1.398349826	23.9529	18.5366	20.2069	29.3382	30.0594	28.2739
ENSG00000241170		11	74587331	74631067		0.003403017	-4.556373424	2.93519	2.10982	0.378707	9.27708	6.88481	8.55059
ENSG00000241680	*RPL31P49*	12	110898793	110899167	ribosomal protein L31 pseudogene 49 [Source:HGNC Symbol;Acc:35909]	0.020483711	-3.511430501	0	6.1422	5.83759	13.366	11.2672	17.433
ENSG00000241710		12	42636017	42636316	Metazoan signal recognition particle RNA [Source:RFAM;Acc:RF00017]	0.015188284	-7.448484509	0	0	9.29138	19.6456	18.9006	30.6605
ENSG00000241945	*PWP2*	21	45527176	45551063	PWP2 periodic tryptophan protein homolog (yeast) [Source:HGNC Symbol;Acc:9711]	0.011718014	2.336782621	7.72811	8.77539	9.89969	5.61767	3.26865	2.41263
ENSG00000242206	*RPS26P35*	8	119774095	119774440	ribosomal protein S26 pseudogene 35 [Source:HGNC Symbol;Acc:36229]	0.022269866	-11.06330386	2.91387	1.98241	4.27504	41.3915	43.1456	16.928
ENSG00000242970		8	59500979	59501323		0.023123499	#NAME?	0	0	0	6.13892	9.59508	3.43207
ENSG00000243115		9	12764762	12765054	Metazoan signal recognition particle RNA [Source:RFAM;Acc:RF00017]	0.022185419	-9.275367945	6.46976	0.845594	0	12.6095	29.9205	25.3226
ENSG00000243317	*C7orf73*	7	135347244	135378166	chromosome 7 open reading frame 73 [Source:HGNC Symbol;Acc:41909]	0.020871707	2.309361118	10.5844	15.7513	12.9851	5.17881	8.21404	3.63385
ENSG00000243389		2	113346617	113372008		0.047736551	3.304822672	4.65097	11.1979	10.0385	2.48915	3.86698	1.47708
ENSG00000243498	*UBA52P5*	8	124249092	124249302	ubiquitin A-52 residue ribosomal protein fusion product 1 pseudogene 5 [Source:HGNC Symbol;Acc:36993]	0.026560878	-5.096719428	9.56445	7.61152	0	17.0458	33.1514	37.3439
ENSG00000244053	*RPL13AP2*	14	47669778	47670307	ribosomal protein L13a pseudogene 2 [Source:HGNC Symbol;Acc:19675]	0.048751207	1.416855343	7.04923	7.42393	8.89998	5.24455	4.62451	6.62743
ENSG00000245275		5	153708997	153825410		0.000558447	6.630669849	7.47192	8.16979	9.45698	0.926244	2.07044	0.788558
ENSG00000245598	*DACT3-AS1*	19	47163621	47180704	DACT3 antisense RNA 1 [Source:HGNC Symbol;Acc:44120]	0.030084494	-7.626108717	1.39571	0	2.64838	7.95198	15.473	7.41569
ENSG00000246596		5	177046060	177099210		0.036653906	#NAME?	0	0	0	8.31072	2.8823	4.06954
ENSG00000247828	*TMEM161B-AS1*	5	87564712	87732502	TMEM161B antisense RNA 1 [Source:HGNC	0.014641534	2.110635484	28.7816	35.811	27.0189	12.3592	20.0743	10.9712

					Symbol;Acc:43839]								
ENSG00000248227		4	38368535	38387380		0.049199374	-10.09396237	0	2.26612	0	7.61968	11.6825	3.57195
ENSG00000248456		4	136034060	136044934		0.006741186	-6.509380281	0.121843	13.7149	0.131069	31.55	26.2655	33.1063
ENSG00000248840		4	3314239	3314577		0.017162968	-3.66423585	3.4833	0	3.87088	6.8326	9.51725	10.5976
ENSG00000249306		5	173763298	173959460		0.020756087	1.560578918	11.7666	15.5751	12.6967	8.97855	9.31128	7.36629
ENSG00000249550		12	114117264	114211488		0.014177045	1.952603717	7.9446	6.23056	6.05606	2.6768	4.42276	3.26159
ENSG00000249835	*VCAN-AS1*	5	82827171	82877139	VCAN antisense RNA 1 [Source:HGNC Symbol;Acc:40163]	0.041228879	10.61345748	6.31819	4.88894	1.98094	0	0	1.24258
ENSG00000250667		5	17495767	17495935		0.000135973	#NAME?	0	0	0	41.8547	34.4483	43.4662
ENSG00000251005		4	127027294	127028078		0.004895549	3.007105938	7.63319	8.03953	6.35391	3.20881	3.08638	1.02967
ENSG00000251724		5	74834423	74834483	U7 small nuclear RNA [Source:RFAM;Acc:RF00066]	0.004573582	Inf	460.9	308.062	578.521	0	0	0
ENSG00000251793		6	16148518	16148676	Small nucleolar RNA U3 [Source:RFAM;Acc:RF00012]	0.030155546	2.410156728	326.759	208.841	198.681	77.4351	126.72	100.506
ENSG00000252001	*RNA5SP303*	10	19922612	19922741	RNA, 5S ribosomal pseudogene 303 [Source:HGNC Symbol;Acc:43203]	0.006908839	11.80244664	84.7302	136.137	89.988	0	0	26.3382
ENSG00000252045		21	33910609	33910744	Small nucleolar RNA SNORA33 [Source:RFAM;Acc:RF00438]	0.000827168	#NAME?	0	0	0	17.9033	16.4603	12.19
ENSG00000252458		5	158657202	158657330	Small nucleolar RNA SNORA68 [Source:RFAM;Acc:RF00263]	0.045654273	Inf	22.2636	30.4453	67.8024	0	0	0
ENSG00000252657		17	28104637	28104762	Small nucleolar RNA SNORA70 [Source:RFAM;Acc:RF00156]	0.005794257	-26.90685199	0	15.6159	38.5173	529.298	608.173	319.083
ENSG00000252791		20	36681049	36681148	Y RNA [Source:RFAM;Acc:RF00019]	0.008458338	#NAME?	0	0	0	992.843	923.318	468.166
ENSG00000252892		2	65221880	65221994	U6 spliceosomal RNA [Source:RFAM;Acc:RF00026]	0.018749002	#NAME?	0	0	0	203.585	194.093	75.3436
ENSG00000252929		7	6097131	6097235	U6 spliceosomal RNA [Source:RFAM;Acc:RF00026]	0.006181974	5.056640448	1275.48	2007.52	1354	349.801	232.086	335.125

ENSG00000253016		12	38668250	38668351	Y RNA [Source:RFAM;Acc:RF00019]	0.003500858	6.335247822	323.46	304.44	202.466	41.5476	38.1974	51.3258
ENSG00000253238		8	81178389	81252075		0.00765536	-48.94422532	0	0	0.449774	7.54761	4.74784	9.71839
ENSG00000254126		2	107103824	107123396		9.13E-07	Inf	16.3703	15.4723	15.4046	0	0	0
ENSG00000254295		5	172381910	172384165		0.011454373	Inf	3.13257	5.35466	2.62974	0	0	0
ENSG00000254314		8	53063380	53067452		0.0190873	23.69907239	3.38675	4.77777	7.88243	0	0	0.677113
ENSG00000254394		8	83824339	83874161		0.02576682	-12.95925133	0	0.198342	1.23449	3.63676	9.15128	5.78039
ENSG00000254560		11	27068733	27241660		0.039217063	4.354237041	5.99933	5.38608	2.62622	2.02195	0	1.19598
ENSG00000254649		11	78099107	78103451		0.040409227	#NAME?	0	0	0	6.20392	6.63649	1.60172
ENSG00000254671		11	125440180	125462473		0.005566495	#NAME?	0	0	0	6.84217	4.93686	3.59177
ENSG00000256915		12	66038114	66057079		0.025642047	-33.62761568	0	0	0.304175	5.27741	2.764	2.18727
ENSG00000256923		12	22895516	22896025		0.016802584	-3.60777504	7.30208	0	6.16769	17.6254	12.423	18.5475
ENSG00000257016		12	10703865	10704134		0.008915568	6.162782443	9.73833	10.3651	8.19656	0	4.59208	0
ENSG00000257293		12	96081095	96358916		0.028556217	3.439020747	16.7403	32.3362	19.9952	4.71872	6.88285	8.48313
ENSG00000257531		12	50611445	50612126		0.041752567	2.145258916	11.3593	9.35034	6.44996	2.86378	5.64175	4.15476
ENSG00000257604		12	79893899	79894467		0.00175059	-8.929729278	5.8884	3.44849	0	22.7176	28.0881	32.5702
ENSG00000258017		12	49521565	49541652		0.04749858	2.191390045	38.0154	39.2092	21.9255	10.0829	20.6302	14.5322
ENSG00000258073		12	85333303	85333447		0.029650798	-17.51527906	0	0	10.6911	64.6036	91.4393	31.2147
ENSG00000258199		12	56556143	56584068		0.015173864	-3.292546896	1.96072	3.94783	5.17757	12.7515	15.0503	8.69977
ENSG00000258458		14	23171820	23235771		0.042094546	-15.7102585	1.48277	0	0	10.0227	10.3379	2.9341
ENSG00000259100		14	39854608	39856306		0.036225519	1.814826942	5.53412	5.77691	4.37461	1.76709	2.96024	3.91572

APPENDIX III-SELECTION OF SHRNA MEDIATED *LIN28A* KNOCKDOWN IN IGROV1 CELLS

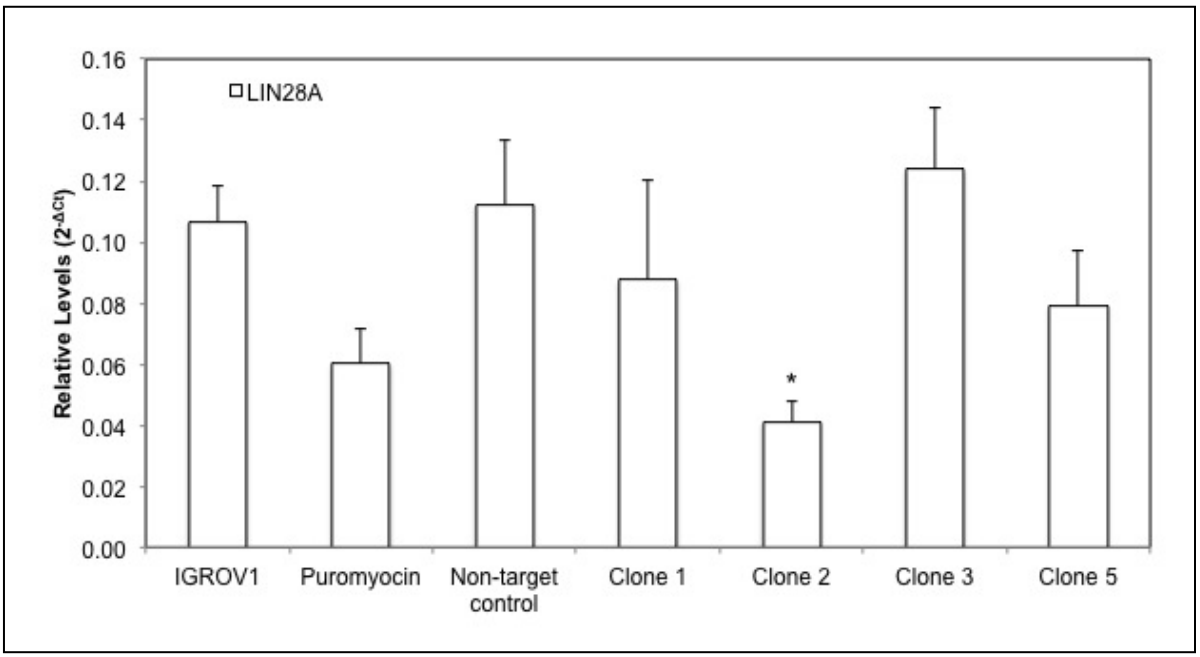

APPENDIX III: Selection of shRNA mediated LIN28A knockdown in IGROV1 cells. Asterisk indicated p-value <0.05. The IGROV1 cell line was stably transduced with Mission® shRNA lentiviral transduction particles to produce Clone2, a successful *LIN28A* Knockdown line. Protocol is described in Chapter IV.

APPENDIX IV-SHRNA MEDIATED *LIN28A* KNOCKDOWN IN IGROV1 CELLS

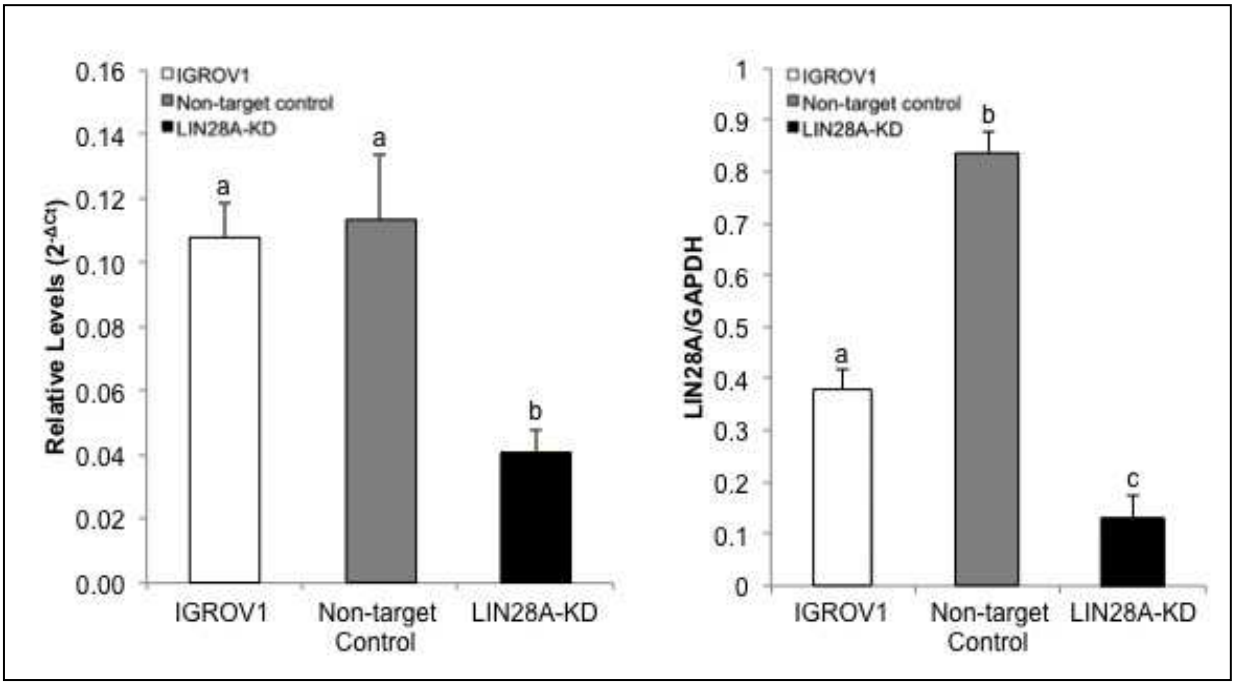

APPENDIX IV: shRNA mediated LIN28A knockdown in IGROV1 cells. LIN28A lentiviral construct, clone 2 was used to knockdown LIN28A in IGROV1 cells. A) qRT-PCR demonstrates *65% LIN28* KD when compared to Non-target control and B) Western Blot demonstrates 82% LIN28 KD when compared to Non-target control. Means with different superscript indicate (p-value <0.05). (p-value<0.05).

Protocol: To create IGROV1 LIN28A knockdown cells Mission® shRNA lentiviral transduction particles (Sigma-Aldrich, SHCLNV) were used. The Mission® shRNA lentiviral transduction particles contain a TRC1-pLOK.1-puro vector with two promoters. The first promoter, U6, drives the expression of a LIN28A target sequence and a central polypurine tract (cppt), enhancer of transduction efficiency and transgene expression. The second promoter, human phosphoglycerate kinase eukaryotic promoter (hPGK) drives expression of the puromyocin resistance gene (puroR), which was used for selection. Briefly, $1x10^3$ IGROV1 cells were seeded onto 24-well plates 24 hours before transfection to allow adhesion and were grown to approximately 60-80% confluency.

The cells were transfected with Mission® shRNA lentiviral transduction particles at a multiplicity of infection (MOI) of 200 virus particle per cell with addition of Polybrene (Millipore, TR-1003-G) at a final concentration of 2μg/mL to increase the efficiency of lipofection transfection. Cells were incubated for 24 hours to allow random virus insertion and 1-day later fresh medium was added without puromyocin for another 24 hours. Infected IGROV1 cells were selected by adding puromyocin at a final concentration of 4μg/mL to transfected cells and untreated control IGROV1 cells until control cells died.

The shRNA lentiviral transduction particles used were as follows: to knockdown LIN28A in IGROV1 cells the target sequence was CCGGCACCTTTAAGAAGTCAGCCAACTCGAGTTGGCTGACTTCTTAAAGGTGTTTT T (Sigma-Aldrich, Clone: TRCN0000021800), the non-target control sequence was CCGGGCGCGATAGCGCTAATAATTTCCTCGAGAAATTATTAGCGCTATCGCGCTTT (Sigma-Aldrich, SHC002V). Successful knockdown of LIN28A was assessed using qRT-PCR and Western blot to determine the percentage of LIN28A transcription and protein knockdown, respectively.

APPENDIX V-*MYC* AND *POUF1* LEVELS IN IGROV1, OV420, AND HEK293 CELLS

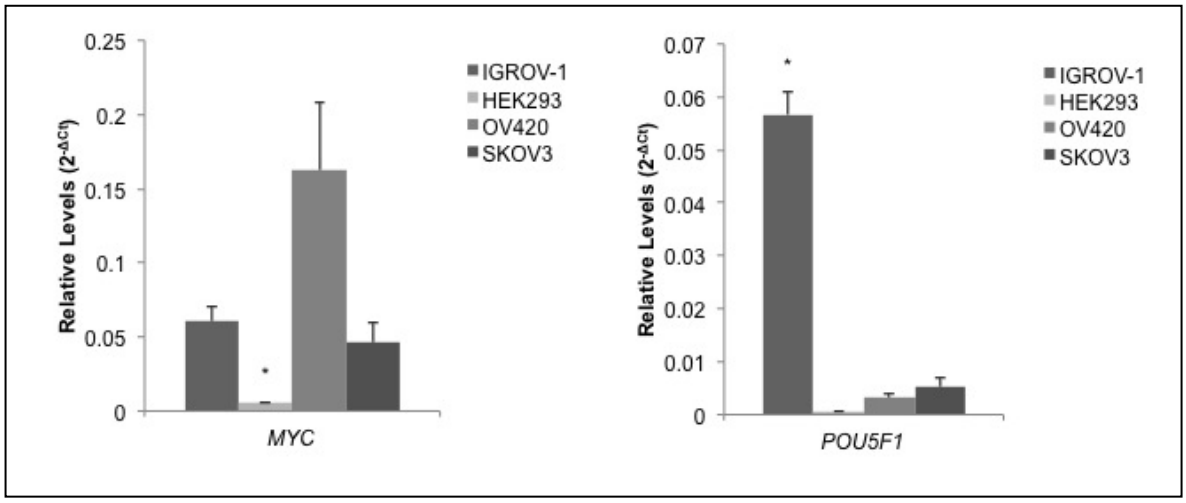

APPENDIX V: *MYC* and *POU5F1* levels in IGROV1, OV420, and HEK293 cells. qRT-PCR was performed to obtain A) *MYC* mRNA levels and B) *LIN28B* mRNA levels in all cell lines. Data was normalized against the geometric mean of GAPDH, MRPS15, and TBP. Means with different superscript indicate (p-value <0.05). (p-value<0.05). Protocol is described in Chapter IV.

APPENDIX VI-*MYC* AND *POU5F1* IN HEK293 CELLS EXPOSED TO IGROV1 EXOSOMES FOR 96-HOURS

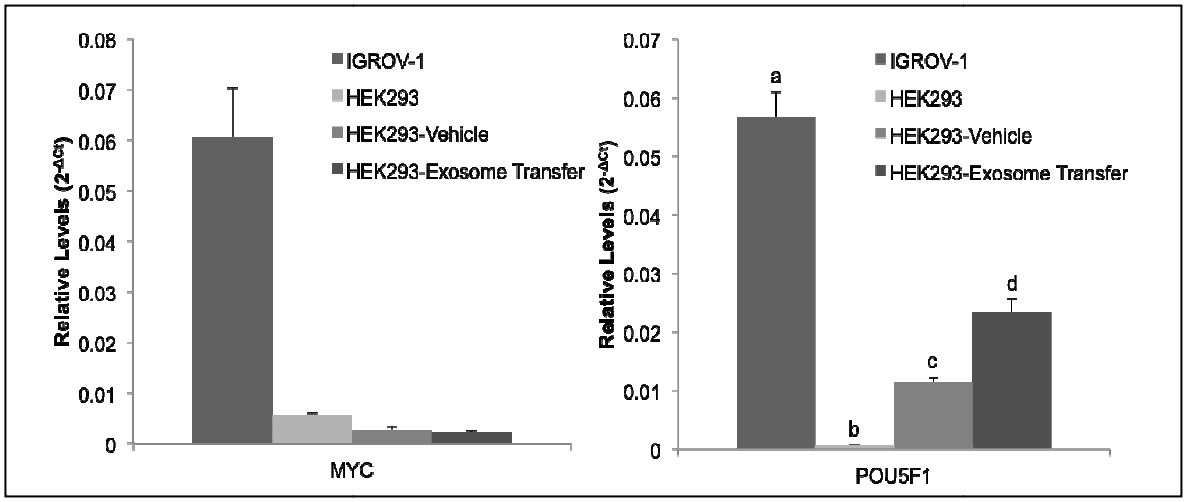

APPENDIX VI: *MYC* and *POU5F1* in HEK293 cells exposed to IGROV1 exosomes for 96-hours. HEK293 cells treated with vesicle-deplete medium (vehicle), HEK293 cells treated with supernatant from exosomal pellet (supernatant), and HEK293 cells treated with exosome pellet (exosome transfer). qRT-PCR was performed to obtain mRNA levels of and *MYC* (left side) and POU5F1 (right side) after HEK293 cells were exposed to IGROV1 exosomes. Data was normalized against the geometric mean of GAPDH, MRPS15, and TBP. Protocol described in Chapter IV. Probes were 20X Taqman Assay mix Probes (Applied Biosystems) cMYC (Hs00905030_m1) and POU5F1 (Hs00999632_g1).

APPENDIX VII- *LIN28A* LEVELS AFTER HEK293 CELLS EXPOSED TO IGROV1 EXOSOMES

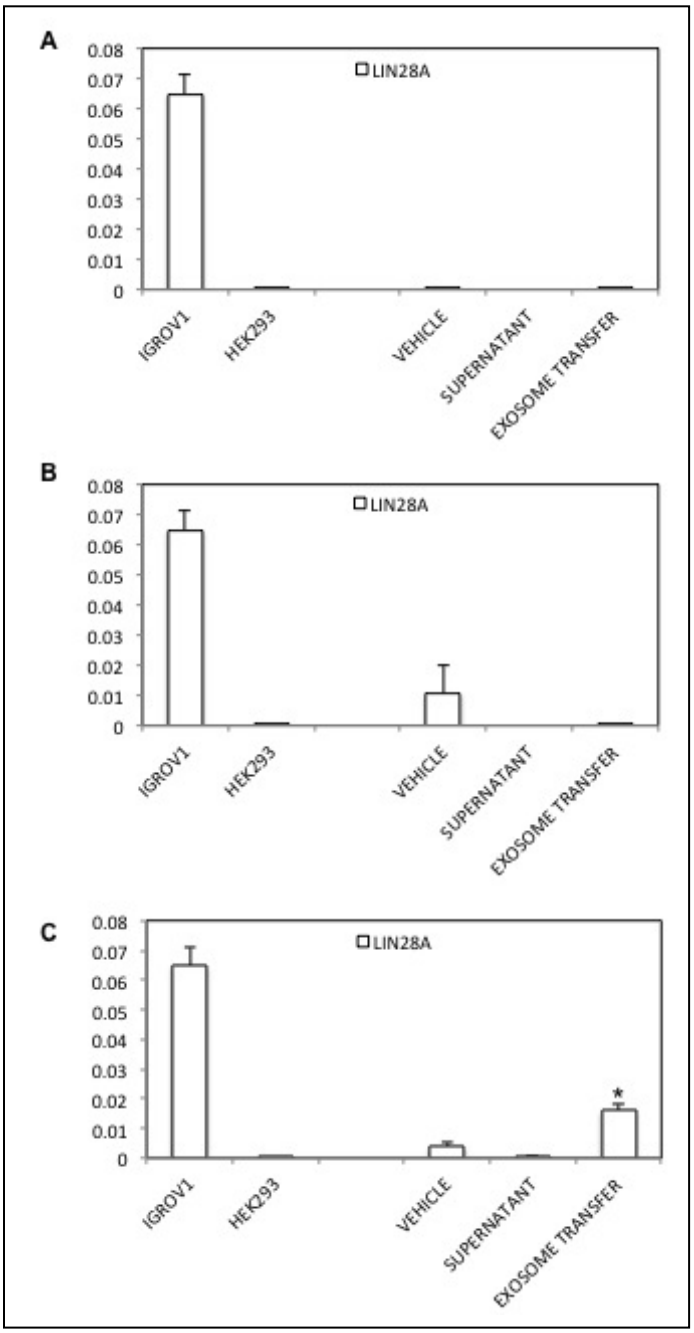

APPENDIX VII: LIN28A levels after HEK293 cells exposed to IGROV1 exosomes. HEK293 cells after A) 24-hours, B) 48-hours, and C) 96-hours after IGROV1 exposure. Asterisk indicated p-value<0.05. Optimization length of time for an effect to occur in IGROV1 exosome exposure onto HEK293 cells was performed. It was determined that

96-hours was sufficient to demonstrate LIN28A mRNA changes therefore experiments were performed for 96-hour exosome exposure.